The interplay between NAD^+, SIRT1 and circadian rhythms in cellular ageing and fibrosis

JD Henderson

PhD

The interplay between NAD^+, SIRT1 and circadian rhythms in cellular ageing and fibrosis

John David Henderson

This thesis was submitted in partial fulfilment of the requirements of the award of Doctor of Philosophy of the University of Newcastle at Northumbria

Faculty of Health and Life Sciences

January 2021

Abstract

Recently, the redox cofactor NAD^+ has been implicated as a potentially key biomolecule in the quest for healthy ageing, with its function as a rate-limiting cofactor for the deacetylase SIRT1 widely believed to be key.

Consequently, there is a heightened interest in better understanding the regulation of the NAD^+/SIRT1 axis and identifying mechanisms that increase NAD^+ levels. Within this work, the circadian regulation of NAD^+ in human PBMCs (peripheral blood monocytes) *in vivo* and NHDFs (normal human dermal fibroblasts) *in vitro* is characterised, with NAD^+ levels found to be temporally regulated by an endogenous mechanism dependent on the 'master circadian regulator' BMAL1 (brain and muscle ARNT-like 1). Importantly, this introduces the prospect of co-ordinating NAD^+ targeting interventions with the diurnal oscillations of NAD^+ - whereby timepoints associated with a daily nadir are preferentially targeted for NAD^+ enhancement.

The demonstrated efficacy of a 'multi-targeted' approach at enhancing NAD^+ titres was another important feature of this work, with the use of multiple dietary compounds targeting various steps in NAD^+ synthesis and degradation pathways shown to be effective at increasing NAD^+ both *in vitro* and within a small human cohort (n=2). At present supplementation with the NAD^+ precursor NR (nicotinamide riboside) is the most widely used intervention for the purpose of enhancing NAD^+, however the results presented here suggest a multi-targeted approach merits further investigation and may eventually offer a superior alternative to NR.

Although widely regarded as beneficial for physiological health, there are scenarios whereby increased NAD^+ may be undesirable, for example pathologies fuelled by upregulated energy metabolism pathways. It is shown herein that TGF-β (transforming growth factor beta) induced fibrotic signalling *in vitro* is accompanied by increased glycolysis, which is indispensable for the enhanced expression of the pro-fibrotic marker collagen I. Furthermore, inhibition of NAD^+ synthesis by blocking NAMPT activity via FK866 attenuated TGF-β mediated collagen I upregulation, highlighting that reducing NAD^+ levels can prevent fibrotic events *in vitro*.

Thus, this work contributes to the biogerontology field by identifying mechanisms and interventions that modulate NAD^+ levels, potentially providing the basis for new strategies with the purpose of enhancing human healthspan. Such strategies should be used with caution in diseases associated enhanced energy metabolism however, in which the role of NAD^+ requires further investigation.

Declaration

The work presented herein has not been submitted for any other award and is the work of myself. The opinions, ideas and contributions from the work of others are fully acknowledged where appropriate.

Word Count: 42,107

Acknowledgements

I extend my gratitude to Professor Dianne Ford for her expert guidance and giving me the opportunity to undertake this PhD. I also thank my co-supervisor Dr Steve O'Reilly for his technical advice and procuring the various primary derived cells and cell lines used in this work. The technicians Dr Max Brown and Sarah Wilkinson also offered experimental advice, with the latter showing me the ropes with regards to generating stable overexpressing cell lines.

A big thanks also goes to the phlebotomy team at the BPNRC who assisted with blood collection, particularly Dr Emma Sweeney and Dr Ian Walshe. Similarly, Dr Basak Aydemir also played an essential role in blood collection and training myself in venepuncture practice, whilst also helping out with the NAD^+ assays for the NR study.

Nuchido Ltd. provided the supplements used for the *in vivo* testing and came up with the idea for the pilot study, with Dr Nicola Conlon also providing a pair of hands for the NAD^+ assays relating to this work. I'm very grateful for the participants who volunteered for the pilot study, both of whom never complained, even when sitting around for 12 hours with a cannula hanging out their arm. Likewise, the contribution of the willing participants for the NR study is also greatly appreciated.

Table of Contents

Abstract iii

Declaration iv

Acknowledgements v

Table of Contents vi

List of Figures x

List of Tables xii

Chapter 1. Introduction 1

1.1 The Role of NAD^+ and NAD^+ Dependent Enzymes in Ageing 1

1.1.1 Ageing 1

1.1.2 Calorie Restriction 2

1.1.3 SIRT1 4

1.1.4 PARP1 8

1.1.5 CD38 9

1.1.6 NAD^+ 10

1.2 NAD^+ As an Anti-Ageing Therapeutic 13

1.2.1 Interventions to Increase NAD^+ 13

1.2.2 Benefits of Enhanced NAD^+ in Disease Models 15

1.2.3 NAD^+ Interventions as an Anti-Ageing Approach in Model Organisms 16

1.2.4 A darkside to NAD^+? 18

1.3 Circadian Rhythms 19

1.3.1 Circadian Regulation of Biological Processes 19

1.3.2 Circadian Rhythms and Ageing 20

1.4 MicroRNAs 22

1.4.1 Epigenetic Regulation by MicroRNAs 22

1.4.2 miR-155 23

1.5 Fibrosis 24

1.5.1 Fibrosis as an Age-Related Disease 24

1.5.2 Systemic Sclerosis 24

1.5.3 TGF-β 25

1.6 Metabolism and Disease 26

1.6.1 The Warburg Effect 26

1.6.2 Glutaminolysis and mTOR 26

1.6.3 Mitochondrial Dysfunction: Cause or Consequence of Ageing? 27

1.7 Aims and Objectives 29

Chapter 2. Materials and Methods 30

2.1 Ethics 30
2.2 Reagents 30
2.3 Cell Culture 30
2.3.1 Cell Culture Conditions 30
2.3.2 NHDFs 30
2.3.3 SSc Patient Dermal Fibroblasts 31
2.3.4 miR-155KO and Wild-Type Primary Derived Mouse Dermal and Lung Fibroblasts 31
2.3.5 *Bmal1*KO and Wild-Type Primary Derived Lung Fibroblasts 31
2.3.6 Jurkat Cell Line 31
2.3.9 Cryopreservation 32
2.3.10 Induction of Fibrosis Using TGF-β 32
2.3.11 Cell Transfection 32
2.3.12 Compounds Added to Cells *In Vitro* 33
2.4 Blood Sampling 34
2.4.1 Participant Recruitment 34
2.4.2 Blood Collection 34
2.4.3 PBMC Isolation 35
2.5 NAD^+ Measurements 35
2.5.1 NAD^+ Measurements in PBMC, Blood and Plasma Samples 35
2.5.2 NAD^+ Measurements in Primary Derived Cells and Cell Lines 36
2.6 Energy Metabolism Assays 36
2.6.1 OXPHOS – Mitochondrial Stress Assay 36
2.6.2 Glycolysis - Glycolysis Stress Assay 37
2.7 Western Blotting 38
2.7.1 Protein Extraction 38
2.7.2 SDS-PAGE 38
2.7.3 Western Blot Transfer 39
2.7.4 Immunoblotting 39
2.7.5 Re-Probing Blots 41
2.7.6 Densitometry Analysis 41
2.8 qPCR 41
2.8.1 RNA Isolation 41
2.8.2 RNA Yield Quantification 42
2.8.3 cDNA Synthesis From mRNA 42
2.8.4 cDNA Synthesis From miRNA 42
2.8.5 qPCR for mRNA Expression Analysis 43
2.8.6 qPCR for miRNA Expression Analysis 43

2.8.7 Analysis of qPCR Data 43
2.9 Cell Viability/Proliferation Assays 44
2.9.1 Alamar Blue Cell Viability Assay 44
2.9.2 XTT Cell Proliferation Assay 45
2.10 Statistical Analysis 47
Chapter 3. Interventions to Enhance NAD^+ *In Vitro* 48
3.1 Introduction 48
3.2 Aims 48
3.3 Hypotheses 49
3.4 The NAD^+ precursor NAM Enhances NHDF NAD^+ Levels 50
3.5 NHDF NAD^+ Levels in Response to Dietary Compounds 51
3.6 The Multi-Targeted Intervention NTC Increases NAD^+ in NHDFs but not Jurkat Cells 54
3.7 NAD^+ Levels are PARP1 Dependent Under Conditions of Oxidative Stress 57
3.8 Quercetin and ALA Induce Antioxidant Effects in NHDFs 60
3.9 NTC Protects Against Oxidative Stress in a PARP1 and SIRT1 Independent Manner 62
3.10 Discussion 67
Chapter 4. Circadian Regulation of NAD^+ and Its Interaction with BMAL1 71
4.1 Introduction 71
4.2 Aims 73
4.3 Hypothesis 73
4.4 NAD^+ levels Follow a Circadian Rhythm in NHDFs 74
4.5 NAD^+ Circadian Rhythmicity is Absent in *Bmal1*KO MLFs 76
4.6 miR-155 Represses *Bmal1* Expression and Circadian Rhythmicity in MDFs 77
4.7 miR-155 Regulates NAD^+ Circadian Rhythmicity 80
4.8 MiR-155KO MDFs Display a Different Metabolic Phenotype to WT MDFs 82
4.9 MiR-155KO MDFs Exhibit Enhanced Protection Against Oxidative Stress 88
4.10 *Bmal1*KO MLFs Exhibit Enhanced Proliferation but a Lowered Resistance to Oxidative Stress 89
4.11 Discussion 90
Chapter 5. Interventions to Enhance Human PBMC NAD^+ Levels *In Vivo* 94
5.1 Introduction 94
5.2 Aims 95
5.3 Hypothesis 95
5.4 Enhancement of Human PBMC NAD^+ Using NR 98
5.5 A Multi-Targeted Approach to Enhancing Human NAD^+ Titres 99
5.5.1 Human PBMC NAD^+ Exhibits a Circadian Rhythm 99
5.5.2 NCD201 Enhances PBMC NAD^+ Levels During a 16-day Treatment Phase 103

5.5.3 NCD201.2 Enhances NAD^+ But to a Lesser Extent Than NCD201 106
5.5.4 Removal of Precursor in the NCD202.1 and NCD202.2 Cocktails Reduces NAD^+ Enhancing Efficacy 107
5.5.5 NCD203: Substituting NR with NAM Maintains Cocktail Efficacy 108
5.5.6 NCD205 Failed to Effectively Enhance NAD^+ in a Female Participant 109
5.6 Variability in NAD^+ Across Different Baselines – A Notable Caveat 111
5.7 Measuring NAD^+ in PBMCs, Erythrocytes, Whole Blood and Plasma Samples 111
5.8 NAD^+ Degradation in Whole Blood and PBMCs Following Venepuncture 113
5.9 Ongoing Time+ Intervention Study 114
5.10 Discussion 118
Chapter 6. The Role of NAD^+ and SIRT1 in Skin Fibrosis 124
6.1 Introduction 124
6.2 Aims 125
6.3 Hypotheses 125
6.4 TGF-β Upregulates Aerobic Glycolysis in NHDFs 126
6.5 Blocking NAMPT Prevents the Fibrotic Phenotype 130
6.6 Resveratrol Reduces TGF-β Upregulation of Collagen I 132
6.7 NTC Suppress TGF-β Induction of Glycolysis but not Fibrotic Markers 133
6.8 Glutaminolysis Is Essential For TGF-β Induced Fibrosis Independent of mTOR 135
6.9 Glutaminase But Not Collagen Is Enhanced in SSc Patient Fibroblasts 138
6.10 Discussion 141
Chapter 7. Concluding Remarks 145
References 148

List of Figures

Figure 1.1.4.1 Cellular NAD^+ metabolism..... 10
Figure 1.1.6.1 Glycolysis, OXPHOS and the TCA cycle..... 12
Figure: 1.3.1 Circadian regulation of SIRT1 and NAD^+ 22
Figure 1.4.1 miRNA mediated gene repression..... 23
Figure 3.4.1 NHDF NAD^+ levels in response to NAM treatment..... 50
Figure 3.5.1 NHDF NAD^+ levels in response to RSV and apigenin treatment..... 53
Figure 3.5.2 NHDF NAD^+ levels in response to ALA and quercetin treatment..... 54
Figure 3.6.1 NTC treated NHDF and Jurkat NAD^+ levels..... 56
Figure 3.7.1 Rucaparib inhibits tbh7ox induced PARylation..... 58
Figure 3.7.2 Tbh7ox regulation of NHDF NAD^+ under conditions of PARP1 inhibition..... 59
Figure 3.8.1 Viability of NHDFs pre-treated with putative NAD^+ enhancers following induced oxidative stress..... 61
Figure 3.9.1 NTC protects NHDFs against oxidative stress and PARP1 inhibition 64
Figure 3.9.2 FK866 suppression of NHDF NAD^+ levels and viability..... 65
Figure 3.9.3 NHDF viability following co-treatment with tbh7ox and EX527 or FK866..... 66
Figure 4.4.1 The effect of *BMAL1* siRNA on NAD^+ levels and SIRT1, BMAL1 and NAMPT levels in NHDFs..... 74
Figure 4.4.2 NAD^+ levels in circadian synced NHDFs treated with *BMAL1* siRNA..... 76
Figure 4.5.1 NAD^+ Levels in *Bmal1*KO and WT MLFs..... 77
Figure 4.6.1 *Bmal1* expression over a 24-hour timecourse in miR-155 mimic and negative control miRNA treated MDFs..... 79
Figure 4.6.2 miR-155 expression over a 24-hour timecourse in *Bmal1* siRNA treated MDFs..... 80
Figure 4.7.1 NAD^+ levels in miR-155 mimic, *Bmal1* siRNA and scrambled siRNA treated WT and miR-155KO MDFs..... 81
Figure 4.7.2 Circadian pattern of NAD^+ in miR-155 mimic or *Bmal1* siRNA treated WT and miR-155KO MDFs..... 82
Figure 4.8.1 Proliferation rate of miR-155KO and WT MDFs..... 84
Figure 4.8.2 Mitochondrial function in low and high passage WT and miR-155KO MDFs..... 86
Figure 4.8.3 Mitochondrial function in WT and miR-155KO MDFs transfected with a miR-155 mimic or *Bmal1* siRNA..... 87
Figure 4.8.4 Glycolytic parameters of miR-155KO and WT MDFs..... 88
Figure 4.9.1 Antioxidant and anti-inflammatory features of miR-155KO MDFs 89
Figure 4.10.1 Proliferation and oxidative stress resistance in WT and *Bmal1*KO MLFs..... 90
Figure 5.4.1 PBMC NAD^+ levels during 5 days of NR supplementation..... 99

Figure 5.5.1.1 PBMC NAD^+ levels fluctuate over a 12-hour timecourse..... 101
Figure 5.5.2.1 NAD^+ titres in the PBMCs of two volunteers after 16 days consumption of NCD201.1 105
Figure 5.5.3.1 NCD201.2 increases PBMC NAD^+ levels..... 107
Figure 5.5.4.1 PBMC NAD^+ levels following consumption of NCD202.1 and NCD202.2..... 108
Figure 5.5.6.1 NAD^+ titres in a female participant in response to the NCD203 and NCD205 supplement cocktails..... 110
Figure 5.6.1 Average NAD^+ levels on 3 different baseline weeks for female participant..... 111
Figure 5.7.1 NAD^+ levels in different blood fractions..... 113
Figure 5.8.1 Degradation of NAD^+ in PBMCs and whole blood stored on ice..... 114
Figure 5.9.1 Time+ intervention study design..... 116
Figure 6.4.1 Glycolysis is an essential component of TGF-β induction of fibrotic genes in NHDFs. 128
Figure 6.4.2 Lactate levels following TGF-β stimulation..... 129
Figure 6.4.3 NHDF Viability in response to varying concentrations of 2-DG, G968 and 3PO 130
Figure 6.5.1 NAD^+ levels are key for glycolysis and fibrotic protein levels in TGF-β treated NHDFs 131
Figure 6.6.1 RSV reverses TGF-β upregulation of fibrotic markers but not glycolytic parameters..132
Figure 6.7.1 NTC attenuates TGF-β upregulation of glycolysis but not fibrotic marker levels.....134
Figure 6.8.1 Glutaminase activity is essential for TGF-β driven effects 137
Figure 6.9.1 Glycolysis and glutaminase expression in SSc patient derived dermal fibroblasts 140
Figure 6.10.1 Interaction between energy metabolism pathways and collagen synthesis.....144

List of Tables

Table 1.1.3.1 The mammalian sirtuin family..... 7
Table 2.3.11.1 Oligonucleotides used for gene knockdown studies 33
Table 2.3.12.1 Compounds used for in vitro work 33
Table 2.7.4.1 Antibodies used for western blotting 40
Table 2.8.1 Primers used for qPCR 44
Table 5.1.1 Studies using precursors to enhance human NAD^+ 96
Table 5.1.2 Key enzymes in NAD^+ synthesis and degradation pathways 97
Table 5.5.1.2 Dietary compounds targeting NAD^+ related enzymes and in vivo anti-ageing evidence 102
Table 5.9.2 Metabolites of mammalian NAD^+ metabolism 117

Abbreviations and Symbols

°C	degrees Celsius
-/-	homozygous knockout
-/-	heterozygous knockout
2-DG	2-deoxyglucose
2PY	N1-Methyl-2-pyridone-5-carboxamide
3PO	3-[3-pyridinyl]-1-[4-pyridinyl]-2-propen-1-one
AD	Alzheimer's disease
ADPR	adenosine diphosphate ribose
AMPK	adenosine monophosphate protein kinase
ANOVA	analysis of variance
APP	amyloid precursor protein
AST	aspartate transaminase
AT	ataxia telangiectasia
ATP	adenosine triphosphate
BCA	bicinchoninic assay
BMAL1	brain and muscle ARNTL-like 1
*Bmal1*KO	*Bmal1* gene knockout
BRCA1	breast cancer gene 1
BRCA2	breast cancer gene 2
C. elegans	*Caenorhabditis elegans*
C57BL/6	C57 black 6
cADPR	cyclic adenosine diphosphate ribose
CC50	50% cytotoxicity concentration
CD157	cluster of differentiation 157
CD38	cluster of differentiation 38
cDNA	complementary deoxyribonucleic acid
CI	confidence interval
Cq	quantification cycle
CR	calorie restriction
D. melanogaster	*Drosophila melanogaster*
DDR	DNA damage response
dH_2O	distilled water
DMEM	Dulbecco's Modified Eagle's Medium
DMSO	dimethyl sulphoxide
DNA	deoxyribonucleic acid
D-NAAM	*Drosophila* nicotinamidase
DNase	deoxyribonuclease
EC 50	half maximal effective concentration
ECAR	extracellular acidification rate
ECL	enhanced chemiluminescence
ECM	extracellular matrix
EDTA	ethylenediaminetetraacetic acid

EGCG	epigallocatechin gallate
ETC	electron transport chain
FBS	foetal bovine serum
FCCP	carbonyl cyanide-p-trifluoromethoxyphenylhydrazone
G968	compound 968
H_2O	water
HR	homologous repair
HRP	horseradish peroxidase
hrs	hours
IIS	insulin/IGF-1 signalling
MDF	mouse dermal fibroblast
MDM2	murine double minute 2
MELAS	mitochondrial encephalopathy, lactic acidosis, and stroke-like episodes
meNAM	methyl-nicotinamide
mg	milligram
min	minute
miR-155	microRNA-155
miR-155KO	microRNA-155 knockout
miR-191	microRNA-191
miRNA	microRNA
MLF	mouse lung fibroblast
MM	mitochondrial myopathy
mM	millimolar
mpH/min	milli-pH per minute
mRNA	messenger RNA
mtDNA	mitochondrial DNA
mTOR	mammalian/mechanistic target of rapamycin
mTORC1	mammalian/mechanistic target of rapamycin complex 1
NA	nicotinic acid
NaCl	sodium chloride
NAD^+	nicotinamide adenine dinucleotide (oxidised)
NADH	nicotinamide adenine dinucleotide (reduced)
$NADP^+$	nicotinamide adenine dinucleotide phosphate (oxidised)
NADPH	nicotinamide adenine dinucleotide phosphate (reduced)
NAMPT	nicotinamide phosphoribosyl transferase
NaN3	sodium azide
NAR	nicotinic acid riboside
NCD201-204	Nuchido cocktail 201-204
nDNA	nuclear DNA
NHDF	normal human dermal fibroblast
nM	nanomolar
NMN	nicotinamide mononucleotide
NMNAT1-3	nicotinamide mononucleotide adenyltransferase
NNMT	nicotinamide N-methyltransferase
NQO1	NAD(P)H dehydrogenase (quinone) 1
NR	nicotinamide riboside
Nrk1	nicotinamide riboside kinase 1

NTC	Nuchido Time+ cocktail
O_2	oxygen
OCR	oxygen consumption rate
OXPHOS	oxidative phosphorylation
p53	tumour protein P53
PAR	poly-ADP ribose
PARP1	poly-ADP ribose polymerase 1
PBMC	peripheral blood mononuclear cell
PBS	phosphate buffered saline
PER2	period circadian protein homolog 2
pH	power of hydrogen
pmol	picomoles
PMS	phenazine methosulphate
qPCR	quantitative polymerase chain reaction
rapa	rapamycin
RBC	red blood cell
RIPA buffer	radio-immunoprecipitation buffer
RNA	ribonucleic acid
ROS	reactive oxygen species
RPMI	Roswell Park Memorial Institute
RSV	resveratrol
RT	room temperature
ruc	rucaparib
SASP	senescence associated secretory phenotype
SD	standard deviation
SDS	sodium dodecyl sulphate
SDS-PAGE	sodium dodecyl sulphate-polyacrylamide gel
Sir2	silent information regulator 2
siRNA	small interfering RNA
SIRT1	sirtuin 1
sirtuin	silent mating type information regulation 2 homolog
SSc	systemic sclerosis
tbh7ox	tert-butylhydroperoxide
TBS	tris buffered saline
TBST	tris buffered saline with tween
TCA cycle	Tricarboxylic acid cycle
TGF-β	transforming growth factor-beta
TIFF	tagged image file format
Tris	tris(hydroxymethyl)aminomethane
Tris-HCl	tris(hydroxymethyl)aminomethane hydrochloride
Trizma	2-Amino-2-(hydroxymethyl)-1,3-propanediol
ug	microgram
uM	micromolar
VO_2max	maximal oxygen uptake during exercise
WS	Werner syndrome
WT	wild-type
XTT	2,3-bis-(2-methoxy-4-nitro-5-sulphophenyl)-2H-tetrazolium-5-carboxanilide

Chapter 1. Introduction

1.1 The Role of NAD^+ and NAD^+ Dependent Enzymes in Ageing

1.1.1 Ageing

Physiological ageing is an inevitable process that, for those who live long enough, will eventually cause mortality. The inescapable reality of ageing has fascinated humans for thousands of years and until relatively recently the underlying biological mechanisms have been a source of great mystery. As the mystique unravels, a key point of contention is whether ageing is an intentional genetically programmed process or an unintentional consequence of gradual damage accumulation.

From an evolutionary perspective, ageing as a genetically defined mechanism to induce mortality makes sense - it protects against over-population and depletion of resources, whilst it also promotes evolution of the species by ensuring a stagnant genome isn't contributing to the gene pool over multiple generations. If true, this would suggest inactivation of the pro-ageing genes or re-activation of anti-ageing genes that had been switched on or off would prevent the ageing process. The inability however to detect any such genes in model organisms however has shifted the general consensus towards a model whereby ageing is caused by 'wear and tear', i.e. gradual physical deterioration accompanied by the inability to fully repair it.

Despite this, genes that modulate lifespan and the rate of ageing have been identified in lower organisms [1-5], however their homologues in murine models generally lack this capacity. One such example is the *age-1* gene in *C. elegans,* in which mutations have been reported to increase lifespan from 1.7-fold [6, 7] to as high as almost 10-fold [8]. The *age-1* gene codes for the class-I phosphatidylinositol 3-kinase (PI3K) catalytic subunit, a key downstream target in Insulin/IGF-1 signalling (IIS) which regulates multiple cellular process such as proliferation and metabolism. The central role played by the IIS pathway in *C. elegans* longevity was re-enforced by further studies which found that mutations to the *daf-2* (homologue of the mammalian insulin like growth factor receptor 1) gene caused a 2.3-fold increase in lifespan, via a mechanism dependent on *daf-16* (homologue of the mammalian forkhead box FoxO transcription factor) activity [9]. Although not as emphatic, significant life extension by inhibition of multiple mediators within the IIS pathway was also observed within *Drosophila* [10-12], suggesting acceleration of the ageing process via IIS may be a conserved mechanism.

Typically, when applied to mouse models however, the effects of IIS inhibition on lifespan have been much more modest [13, 14], perhaps owing to the increased complexity of the IIS pathway within mammals. Notably however, overexpression of KLOTHO (an inhibitor of IIS signalling in mice)

significantly enhanced lifespan in transgenic mice, with the enhancement in average lifespan varying from 19 – 30% depending on sex and the particular transgenic allele expressed [15].

Hence, it appears that certain pathways such IIS signalling play a key role in promoting/combating ageing and their manipulation may decelerate the process – by slowing the rate at which pro-ageing molecular changes occur and/or facilitating their repair.

1.1.2 Calorie Restriction

To date, the intervention with the most repeated success at extending lifespan and delaying age-related diseases is calorie restriction (CR) – defined as a diet without malnourishment which consists of up to 60% less calories than what would be considered *ad libitum* feeding, with the extent of the calorie deficit depending on the organism. It should be noted that the terms 'calorie restriction' and 'dietary restriction' are often used interchangeably when referring to a low-calorie diet. The CR mediated enhancement of lifespan appears to be conserved across numerous eukaryotes including: yeast [16, 17], flies [18, 19], worms [20-22], rodents [23-25] and most recently rhesus macaque [26-28], although conflicting findings [29] and results interpretation [30] have been reported for the latter. The conservation across higher and lower Eukarya suggests that rather than bodyweight or percentage body fat, intracellular changes are key to the lifespan-extending CR phenotype. Importantly, both early (from birth or infant years) and late (adulthood) onset CR have extended lifespan and slowed age-related physiological decline [31-34], which is significant given the impracticality of early onset CR in humans which are required to be well fed to ensure proper development during infancy and adolescence.

Naturally, slowing the rate of energy metabolism – an obvious consequence of CR – has long been suspected as an essential component of the CR phenotype. By reducing energy precursors and therefore energy metabolism, this places less strain on mitochondria thus extending their 'shelf-life' and delaying the pro-ageing effects associated with dysfunctional mitochondria [35-37]. Aside from lowering basal levels of energy metabolism [38], other protective pathways are known to be upregulated by CR [39-42]. The development of this protective response to CR can be explained in evolutionary terms as an adaptation to times of low food availability, resulting in upregulation of stress response pathways to ensure survival during such times of hardship. This fits well with the 'disposable soma theory of ageing' [43] which posits that the energy costs of reproduction versus body maintenance/repair are in competition for the body's finite energy reserve. In times of plentiful food and hence energy the body focuses on fuelling reproduction, however in times of food shortage resources are focused on repair and maintenance mechanisms – a situation mimicked by calorie restriction.

A suspected key target of CR is mTORC1 (mechanistic target of rapamycin complex 1) [41, 44, 45], a protein complex which dictates the cellular response to multiple stimuli including nutrient availability and growth factor signalling. Indeed, gene editing approaches to inhibit mTOR signalling extended lifespan in *C. elegans* and *Drosophila*, however were unable to further extend lifespan under conditions of CR [46, 47]. Furthermore, the prototypical small molecule inhibitor of mTOR, rapamycin, has been shown to extend the lifespan of mice [48, 49], although a similar relationship between CR and mTOR signalling has yet to be verified in murine models.

It's important to acknowledge that adherence to a CR diet is impractical for many given the likely decline in physical strength and risks associated with low bodyweight, hence interventions which resemble CR at the signalling level, aka CR mimetics, are of massive interest. Although rapamycin falls into this category, it was originally developed as an immunosuppressant and thus carries potentially dangerous side effects rendering it unsuitable as an anti-ageing therapeutic. Promisingly, a number of rapalogues (compounds designed to mimic rapamycin) have been developed as anti-cancer agents ([50, 51] to combat certain cancers which depend on MTORC1 to upregulate biosynthetic pathways and promote proliferation. The efficacy of other rapalogues at replicating the lifespan extending effects of rapamycin has yet to be demonstrated, however this remains an emerging avenue of ageing research [52].

In addition to MTORC1, there is growing evidence that the benefits of CR are mediated through NAD^+ and SIRT1. Moroz *et al*. showed that the activity of the NAD^+ salvage pathway was essential for CR mediated lifespan extension in *C. elegans*, whereby although the benefit of CR was reduced in both *sir-2.1* (*C. elegans* homologue of SIRT1) and *pnc-1* (NAD^+ salvage pathway enzyme) overexpressing mutants [53], it was attenuated more so in the *pnc-1* overexpressors - suggesting that CR benefits mediated through NAD^+ may have mechanisms supplementary to SIRT1 activation. Furthermore, a mouse strain overexpressing the NADH dehydrogenases NQO1 and CYB5R3 (which yield NAD^+ as a catalytic byproduct) was reported to resemble the CR phenotype [54].

The link between SIR2/SIRT1 and CR has been extensively investigated, with a particularly notable study by Rogina *et al*. demonstrating that CR was unable to further extend lifespan in the long living *Sir2* overexpressing flies, whilst also being unable to induce any enhancement of longevity in mutants with low Sir2 activity [55]. In rodents, the developmental impairment that occurs in *Sirt1* heterozygous knockout mice makes the dependency of CR on SIRT1 harder to assess, however for those that survive development, no benefit in response to CR for the *Sirt1-/-* mutants has been reported [56]. Furthermore, mice genetically engineered to constitutively overexpress *Sirt1*

metabolically resemble WT mice fed a CR diet, whilst also exhibiting the same enhanced glucose tolerance and reduced insulin level which is characteristic of a CR regimens [57].

1.1.3 SIRT1

The sirtuin (silent mating type information regulation 2 homolog) family of enzymes (Table 1.1.3.1) are the mammalian homologues of yeast Sir2, with its orthologue SIRT1 in particular attracting significant attention for its purported role as a potential regulator of the ageing process. This attention began when it was discovered that the SIR2 gene extended lifespan in yeast [58] and was essential for the lifespan enhancing effects of CR [16]. The excitement surrounding SIRT1 was further amplified when overexpression of SIR2 orthologs in *Drosophila* [55, 59], *C. elegans* [2] and mouse neurons [60] resulted in significant lifespan extension. Furthermore, the discovery of small molecule SIRT1/Sir2 activators which also mediated lifespan extension in the same model organisms [61-64] gave hope that SIRT1 could be pharmacologically targeted with similar effects in humans. Alternatively, a number of studies refuted the central importance of SIRT1/Sir2 as regulators of longevity, whereby upregulation of their expression failed to enhance lifespan [65-67]. Hence, just how important SIRT1 is in human ageing remains a point of contention in the biogerontology field.

SIRT1, similar to the majority of the sirtuins, functions as a deacetylase which targets acetylated residues on histones and other protein substrates, allowing it to modulate a wide array of cellular processes. The deacetylation is a hydrolytic reaction requiring NAD^+, with O-acetyl-ADP-ribose and nicotinamide yielded as by-products. *In vitro*, nicotinamide functions as a non-competitive inhibitor of SIRT1 [68] and thus prevents overactivation of SIRT1 via a negative feedback loop - potentially a mechanism to prevent rapid depletion of NAD^+ reserves via excessive SIRT1 activity. It should be noted however that the inhibitory effects of nicotinamide on SIRT1 activity have yet to be demonstrated *in vivo*.

Importantly, NAD^+ is the rate-limiting cofactor for SIRT1 activity, with the age-dependent decrease in NAD^+ believed to drive the impaired SIRT1 activity that also occurs with increasing age [69, 70]. Given SIRT1 exerts regulatory control of glycolysis [71, 72] and OXPHOS (oxidative phosphorylation) [56, 73] (the two metabolic processes which are key determinants of the redox status of the cellular NAD^+ pool), it appears plausible that NAD^+ levels represent the fulcrum point in a bidirectional relationship between SIRT1 activity and energy metabolism.

As mentioned already a key substrate of SIRT1 are acetylated histone residues, with H4 lysine 16 (H4K16), H3 lysine 9 (H3K9), H3 lysine 14 (H3K14) and H1 lysine 26 (H1K26) particularly prominent targets [74-76]. By inducing histone deacetylation this allows tighter packing of DNA, thus impairing

the accessibility of promoter regions to transcription factors. Consequently, SIRT1 generally functions as a transcriptional repressor.

The cellular acetylation profile or 'acetylome' is another example of the bidirectional relationship between SIRT1 activity and energy metabolism, not just via NAD^+-fuelled deacetylation but also in this instance the availability of acetyl CoA which is the acetyl group donor for most acetyltransferases and thus SIRT1 antagonists [77]. During what would be considered a well-fed physiological state (no calorie deficit), acetyl CoA accumulates via glycolysis and is subsequently utilised for lipid synthesis in the cytoplasm or histone acetylation in the nucleus. Such conditions are also associated with lower NAD^+ and therefore lower SIRT1 activity, further promoting higher levels of acetylation. Conversely, the activation of starvation mode via calorie restriction forces energy metabolism to attain optimal efficiency [78] – hence higher levels of OXPHOS at the expense of glycolysis. This increases the shuttling of acetyl CoA into the TCA (tricarboxylic acid) cycle within the mitochondria, in turn yielding more intermediates that can be used for respiration. As a consequence, cytoplasmic and nuclear acetyl CoA levels are significantly reduced thus impairing histone acetylation, an effect exacerbated by increased NAD^+ from elevated OXPHOS, which consequently enhances SIRT1 activity and thus further histone deacetylation.

In addition to histones, a number of transcription factors are important targets of SIRT1 which underpins its ability modulate such a large range of pathways [79-81]. One substrate of particular interest is the critical tumour suppressor protein P53 (tumour protein P53), often referred to as 'the guardian of the genome'. This is a reference to its prominent role in co-ordinating the response to DNA damaging stimuli, during which it initiates cell cycle arrest and activation of the DDR (DNA damage response) pathway [82]. Furthermore, P53 represents a vital obstacle to tumour development: not only does it stall the cell cycle to facilitate DNA repair, but it also activates apoptosis when the DNA damage is too severe, thus preventing the proliferation of potentially pro-tumourigenic cells. Indeed, its importance as a tumour suppressor is highlighted by the presence of *P53* mutations in over 50% of cancers [83].

Under normal circumstances, the expression of *P53* is kept at very low levels to ensure its activation of cell cycle arrest and apoptotic pathways only occurs when absolutely necessary, with this control largely exerted by MDM2 (murine double minute 2) which binds P53 and signals for its degradation via ubiquitination [84, 85]. However, in response to DNA damaging stimuli the MDM2 mediated inhibition is relieved and P53 levels rapidly accumulate in the nucleus, with other post-translational modifications taking the place of MDM2 in eliciting tight control of P53 activity. Multiple lysine residues on P53 can become acetylated in response to stressors, resulting in increased stability by

preventing the addition of degradation signalling ubiquitin chains whilst also causing a conformational change which enhances its DNA binding affinity – hence acetylation strongly promotes P53 activation [86, 87].

CBP/P300 [88], TIP60 [87] and hMOF [89] are well established acetyltransferases that target P53, whereas SIRT1 [90, 91] and the PID/HDAC complex [92] are the known deacetylases. Thus, at face value it would seem likely that SIRT1 represses P53 induced apoptosis, and whilst largely true, this isn't always the case. Under conditions of increased intracellular ROS (reactive oxygen species), SIRT1 deacetylation of P53 prevents P53 localisation to the nucleus [93] and hence prevents transcriptional upregulation of pro-apoptotic factors. On the other hand, SIRT1 activity in the presence of persistently high intracellular ROS leads to an accumulation of cytoplasmic P53 which can eventually result in P53 translocation into the mitochondria, inducing apoptosis via mitochondrial membrane depolarisation [93].

The inhibitory effects of SIRT1 on P53 are somewhat of a double-edged sword however, with increased *SIRT1* expression or dependency on SIRT1 activity identified in a number of cancers [94-99] – possibly due to its antagonism of P53 activity. The potential pro-tumourigenic effects of SIRT1 are further emphasised by the efficacy of the specific SIRT1 inhibitor Sirtinol at inducing growth arrest in both breast and lung cancer cells *in vitro* [100]. It is important to acknowledge that SIRT1 has also been widely implicated as being anti-tumourigenic [101-104], highlighting the extremely complex nature of SIRT1 signalling.

Table 1.1.3.1 The mammalian sirtuin family.

Sirtuin	Subcellular Localisation	Enzymatic Activity	Substrates	Key Roles	Ref.
SIRT1	Nucleus, Cytoplasm	Deacetylase	PGC-1α↑, BMAL1↑, FOXO1↑, FOXO3a↑, HMGCS1↑, AceCS1↑, H3K9↓, H4K16↓, NF-Kβ↓, P53↓	Regulates energy metabolism and can activate antioxidant defence systems as well as suppress inflammation in response to physiological stress. Also an important mediator of P53 activity.	[105-111]
SIRT2	Cytoplasm, Nucleus	Deacetylase	FOXO1↑, FOXO3a↑, GKRP↑, H4 K16↓	Prevents chromosome condensation during mitotic stress and regulates glucose uptake.	[112, 113]
SIRT3	Mitochondria	Deacetylase	Ku70↑, AceCS2↑, HMGCS2↑, SOD2↑	Upregulates mitochondrial antioxidants, may also regulate OXPHOS.	[114-116]
SIRT4	Mitochondria	Weak ADP-ribosyltransferase, weak delipoylase and demethylglutarylase.	GLDH↓, MCD↓	Inhibits PDH and GLUD1, thus regulating the TCA cycle and glutamine metabolism respectively.	[117-119]
SIRT5	Mitochondria	Weak histone deacetylase, desuccinylase, demalonylase and deglutarylase.	CPS1↑, SOD1↑, PKM2↑, IDH2↑, G6PD↑	Activates CPS1 which modulates ammonia levels during starvation and promotes ketogenesis by desuccinylation of HMGCS2.	[120, 121]
SIRT6	Nucleus	ADP ribosyltransferase and deacetylase	DNA polyβ↑, PKM2↓, H3K9Ac↓, H3K56Ac↓, NF-Kβ↓	Deacetylates H3K9Ac and H3K56Ac, allowing downregulation of certain NF-Kβ target genes. Inhibits glycolytic genes by repressing HIF-1α.	[122-125]
SIRT7	Nucleolus	Deacetylase	H3K18Ac↓, H3K36Ac↓	Strong preference for deacetylation of H3K18Ac. Found at high concentration in the nucleolus where it deacetylates and activates RNA Pol I.	[126-128]

1.1.4 PARP1

Like SIRT1, PARP1 (poly-ADP ribose polymerase 1) requires NAD^+ for its enzymatic activity, however it utilises NAD^+ to synthesis ADP ribose subunits which it adds to protein substrates as a multi-subunit poly-(ADP ribose) (PAR) chain [129]. Its primary function is the recruitment of DNA repair enzymes to sites of single strand DNA breaks, facilitating both BER (base excision repair) and NER (nucleotide excision repair) [130]. Indeed, the central role for PARP1 in the repair of single strand breaks has been exploited to treat BRCA1 and BRCA2 deficient breast cancer tumours which have impaired repair of double strand breaks via homologous recombination (HR). By inhibiting PARP1, single strand breaks become double strand breaks which cannot be repaired properly within the tumour tissue due to the impaired BRCA1/BRCA2 function, thus killing the cancer cells, whereas healthy cells are protected due to their possession of a functional BRCA dependent HR pathway [131].

Given that every day a typical mammalian cell experiences thousands of DNA lesions, PARP1 plays an integral role in supporting the maintenance of genomic stability. Upon detection of a single strand break via its zinc finger, PARP1 undergoes auto ADP-ribosylation which recruits repair enzymes such as the scaffold protein XRCC1 and ligase III to the site of the damage and thus initiates the repair process [132]. The DNA damage checkpoint protein ATM is also recruited by the presence of PAR chains, thus inducing cell cycle arrest and initiating the DDR pathway. To prevent unnecessary cell cycle arrest/DDR activation PAR subunits are rapidly degraded by PARG (Poly ADP-ribose glycohydrolase) [133], thus returning PARP1 to its regular conformation such that it can carry on surveying the genome for other DNA lesions.

As an NAD^+ dependent enzyme however, it has been theorised that PARP1 and other NAD^+ consumers such as SIRT1 are competing with each other for a limited supply of NAD^+, hence an increase in the activity of PARP1 could reduce the activity of SIRT1, or at least its potential to function at maximum capacity. Similarly, the opposite would hold true – excessive SIRT1 activity would limit the NAD^+ availability for PARP1 activity. This hypothetical competition between PARP1 and SIRT1 would become further intensified with increasing age given the age-related decline in NAD^+ and increase in DNA damage [134-136].

If PARP1 and SIRT1 do indeed exist in an NAD^+-dependent equilibrium, then this suggests another mechanism by which age related accumulation of DNA damage could contribute to ageing: overactivation of PARP1 which hinders the activity of SIRT1. Given both enzymes perform essential functions (Figure 1.1.4.1), from a healthspan-promoting perspective it would be hard to justify inhibition of PARP1 for the purpose of enhancing SIRT1 activity or vice versa. This therefore suggests the optimal approach would be to ensure maintenance of high cellular NAD^+ levels, such that

upregulated PARP1 and SIRT1 activity can both be supported without compromising the capacity of the other.

1.1.5 CD38

CD38 (Cluster of differentiation 38) is a cell surface molecule which although ubiquitous [137], is particularly highly expressed in immune cells where it functions as a cyclic ADP ribose hydrolase. The major reaction catalysed by CD38 is the hydrolysis of NAD^+ to yield ADPR and nicotinamide, although it also converts a small amount of ADPR to cyclic-ADPR via a cyclase reaction [138]. Additionally, CD38 can also catalyse the production of NAADP from NADP and nicotinic acid (NA), which like cADPR and ADPR plays an important role as a second messenger in calcium signalling.

CD38 catalysis is renowned for being highly inefficient, requiring approximately 100 molecules of NAD^+ per molecule of ADPR generated [139], hence it has been widely posited that inhibition of CD38 could be an attractive intervention to enhance NAD^+ levels. Its ability to activate calcium signalling is known, however although thought to be related to immune regulation, the exact physiological role CD38 fulfils is poorly understood. The idea that its function may be dispensable is largely borne out of the observed improvement in the mitochondrial function of *CD38-/-* mice without any reported adverse effects [140]. Moreover, Camacho-Pereira *et al*. also show that *CD38* expression drastically increases in multiple mouse tissues with age, which combined with their observation that *CD38-/-* mice are protected from age-related NAD^+ decline [140] frames CD38 as a potentially key driver of decreasing NAD^+ levels. Additionally, these findings are corroborated by a study whereby mice were treated with the specific CD38 inhibitor 78c [141] which enhanced NAD^+ in multiple tissues.

It's worth noting that the CD38 homologue CD157 is also likely to contribute to NAD^+ degradation, however whilst it exhibits NAD^+ hydrolysis it has a much higher affinity for NR (nicotinamide riboside) as a substrate which it converts to nicotinic acid riboside (NAR) [142]. Hence, it may be that high levels of CD157 lower NAD^+ levels by depriving NR from entering the salvage pathway rather than hydrolysing NAD^+. An inhibitor of CD157 has been characterised [143], however to date there has been no investigation into the efficacy of inhibiting CD157 *in vivo* as an intervention to increase NAD^+ or improve metabolic function.

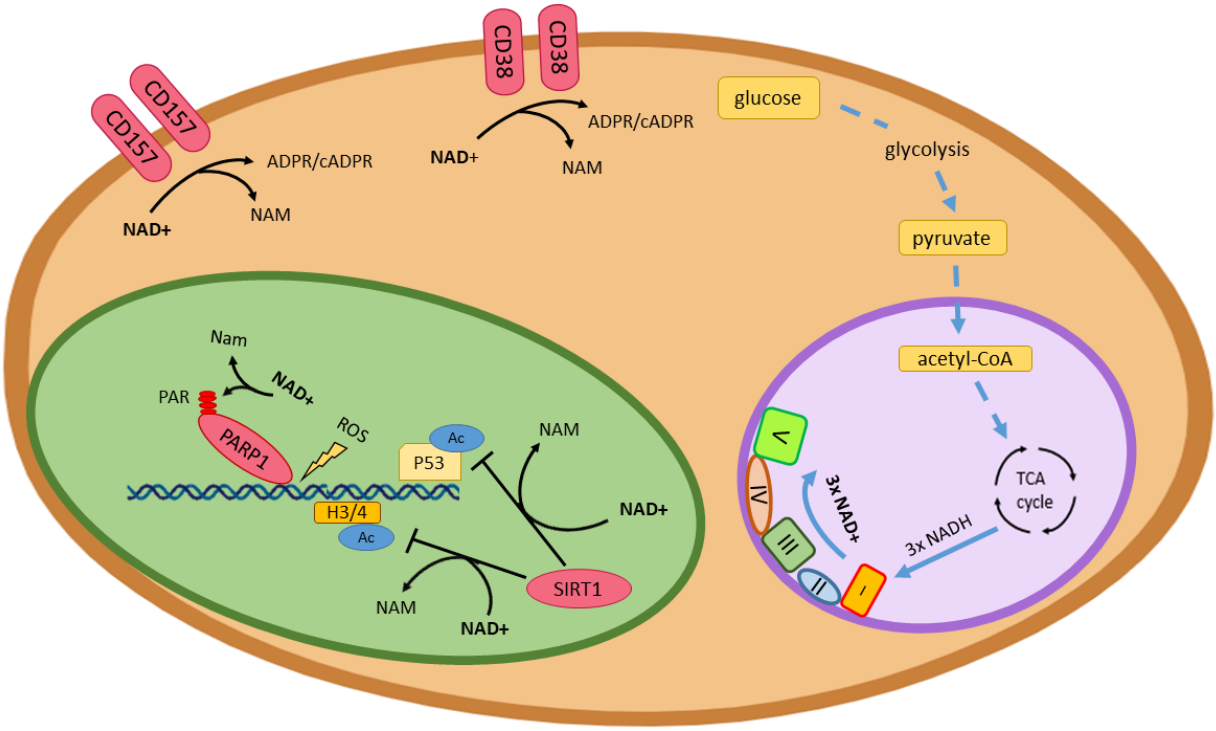

Figure 1.1.4.1 Cellular NAD⁺ metabolism.
NAD⁺ homeostasis is controlled by multiple intracellular processes. The intermembrane proteins CD157 and CD38 utilise NAD⁺ for ADPR synthesis in the cytoplasm, whilst it is regenerated by complex I during mitochondrial respiration (purple compartment). In the nucleus (green compartment) NAD⁺ is an essential cofactor for SIRT1, a deacetylase responsible for regulation of P53 stability and transcription via the acetylation status of histones H3 and H4. Additionally, nuclear NAD⁺ facilitates PARP1 auto-poly(ADPR)-ribosylation, a key step in activating repair of DNA damage in response to lesions induced by ROS.

Abbreviations: I, II, III, IV and V – complexes I, II, III, IV and V, ADPR – adenosine phosphate ribose, H3/4 – histone 3 and histone 4, NAM – nicotinamide, ROS – reactive oxygen species.

1.1.6 NAD⁺

NAD⁺ is best known for its role as an essential intermediate in energy metabolism where it functions as a substrate for glycolysis and the TCA cycle, undergoing reduction to NADH such that it can then transport electrons to complex I in the electron transport chain (ETC) and become oxidised back to NAD⁺ (Figure 1.1.6.1). Consequently, the ratio of NAD⁺/NADH generally reflects the balance between the two main energy producing pathways glycolysis and OXPHOS, with comparatively higher levels of OXPHOS generating more NAD⁺, whereas a shift towards glycolysis and away from OXPHOS driven energy production increases the conversion of NAD⁺ to NADH. With regards to their efficiency at producing ATP, OXPHOS is far more optimal – generating 30-36 ATP molecules per cycle, compared to glycolysis' net gain of 2 molecules per cycle. This enhanced efficiency means under typical conditions approximately 95% of cellular energy is yielded by OXPHOS. However, this places a

significant burden on the enzymes which facilitate OXPHOS as part of the ETC, found embedded within the inner mitochondrial membrane. It has been well established that analogous to a car engine, with increasing age damage accumulation causes a reduction in the power output of mitochondria and thus their ability to generate ATP in an efficient manner is weakened. This is reflected by decreased NAD^+ and increased NADH levels, with reduced OXPHOS driving the equilibrium back towards glycolysis [144], thus increasing the dependency on an inferior ATP producing pathway which manifests as an age-related decline in ATP.

It seems probable that in addition to functional impairments in elderly mitochondria, other age-related processes also contribute to NAD^+ depletion, thus exacerbating the problem of reduced mitochondrial function by depriving it of its key energy precursor. This therefore has become a central area of focus within biogerontology – how can the age-related decline in mitochondrial function be protected against or even reversed? Whilst enhanced NAD^+ levels would seem a beneficial approach, this only addresses one aspect of the problem, akin to providing an improved fuel source to an engine that is still old and rusty. Indeed, this reflects the sobering reality of the quest for genuine anti-ageing interventions, which will need to target multiple cellular pathways in order to be truly effective.

As already discussed, in addition to its role as an essential energy intermediate, NAD^+ is also a cofactor for a number of enzymes: namely PARP1-2, the sirtuins and CD38. Similar to OXPHOS, in the context of ageing their collective relationship with NAD^+ is bidirectional in the sense that reduced NAD^+ impairs the activity of SIRT1, thus impairing antioxidant defence systems and creating an environment more susceptible to DNA damage, resulting in PARP1 activation and further NAD^+ depletion.

As a consequence of this dual role as both an energy intermediate and an enzyme cofactor it links the two together: activity of the NAD^+ dependent enzymes is affected by energy metabolism via its regulation of the NAD^+/NADH balance, whilst NAD^+ dependent enzymes also influence energy metabolism through their consumption of NAD^+ reserves and hence NAD^+/NADH availability for OXPHOS/glycolysis.

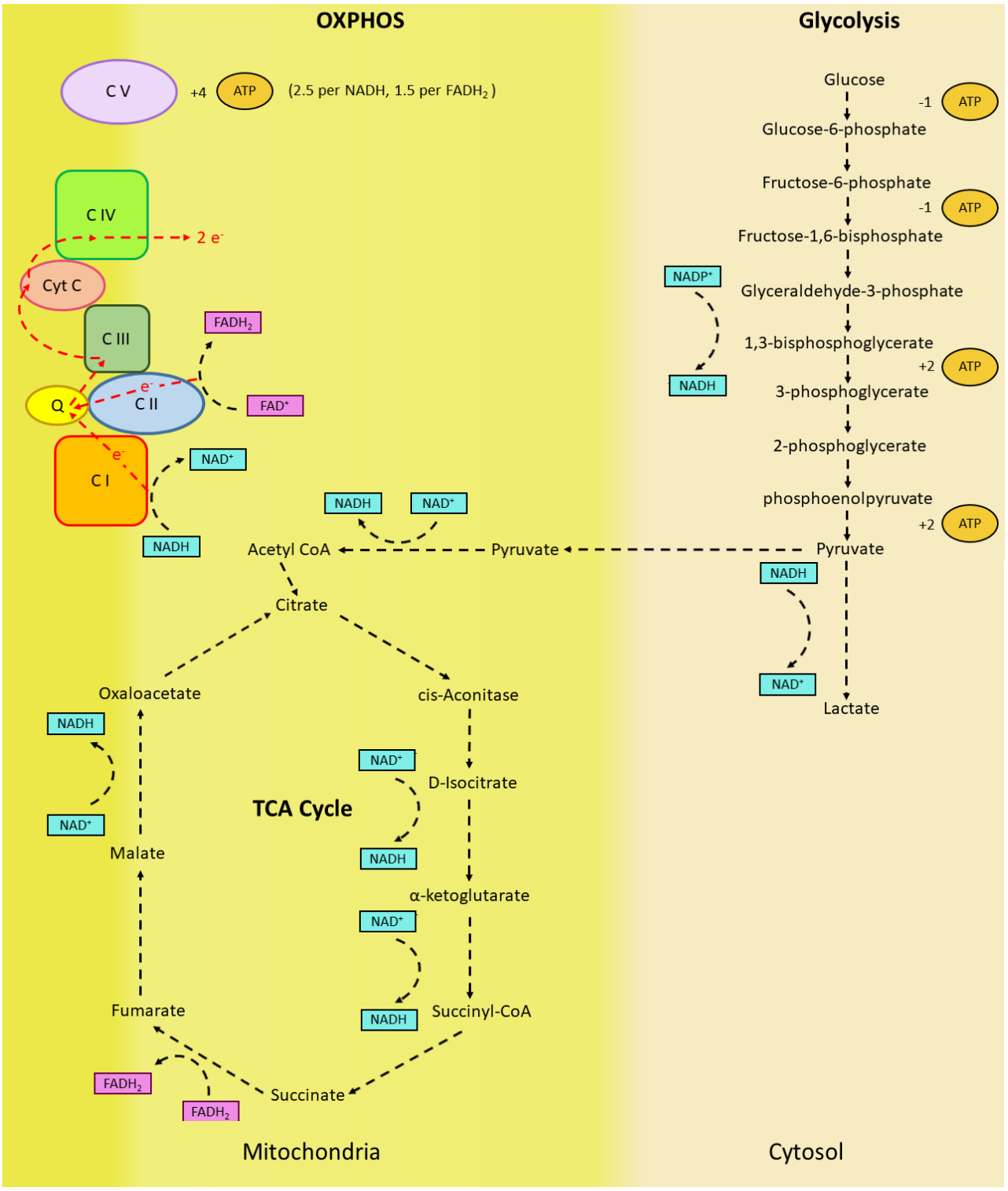

Figure 1.1.6.1 Glycolysis, OXPHOS and the TCA cycle.
The 3 main ATP producing pathways within eukaryotes are depicted. Every molecule of glucose that undergoes glycolysis yields 2 molecules of pyruvate. During aerobic respiration, i.e. when pyruvate is converted to acetyl CoA as opposed to lactate, the successive breakdown of glucose by glycolysis and then 2 molecules of pyruvate via the TCA cycle produces a net gain of 9 NADH and 2 $FADH_2$ per glucose. These can then donate electrons to the electron transport chain (ETC) which induce transient conformational changes as they pass through the complexes, creating an electrochemical gradient. The electrochemical gradient drives the catalytic activity of complex V (C V) which then produces ATP. Via this mechanism, each NADH and $FADH_2$ yield 2.5 and 1.5 molecules of ATP respectively, resulting in an approximate net gain of 28 ATP per glucose molecule metabolised by glycolysis and the TCA cycle.

1.2 NAD^+ As an Anti-Ageing Therapeutic

1.2.1 Interventions to Increase NAD^+

Given the inability of NAD^+ to cross the plasma membrane due to its bulky size, efforts to increase cellular NAD^+ in human studies have focused on the use of precursors. It should be noted, that whilst it is generally accepted that circulating NAD^+ is unable to enter cells, there may be some tissue dependent exceptions – e.g. the finding that NAD^+ was able to cross the blood brain barrier and enter neurons via a mechanism dependent on the transmembrane protein connexin-43 [145].

Nicotinamide riboside (NR) and nicotinamide mononucleotide (NMN) are the precursors that have been most widely investigated for their ability to enhance NAD^+, with both currently marketed as commercially available 'anti-ageing' treatments. Intensified by the apparent commercial value of effective NAD^+ enhancers, which precursor represents the superior option is a hot topic of debate.

Ratajczak *et al*. found that NMN was unable to enhance NAD^+ levels in mice lacking the *Nrk1* gene which converts NR to NMN [146], suggesting that NMN must first be converted to NR extracellularly prior to entering cells. This was further supported in the same study by *in vitro* radiolabelling experiments which found that treating HepG2 cells with labelled NMN caused a sudden spike in extracellular NR containing the label, suggesting that an extracellular protein must be converting NMN to NR before uptake. The authors implicate CD73, an enzyme previously shown to hydrolyse NMN to NR and adenosine. Recently this was countered however by Grozio *et al*. who discovered an NMN transporter in mouse cells and tissue named *Slc12a8* [147]. Although a human homologue exists its expression hasn't been characterised for different human tissues, hence it may be that NMN is directly taken up by some cell types whereas others first require its conversion to NR.

Outside the focus on NR/NMN, the alternative NAD^+ precursors nicotinic acid (NA) and nicotinamide (NAM) have both also shown an excellent ability to enhance NAD^+ in human studies [148-151], however as a side effect the former causes severe flushing hence is only recommended in the treatment of pellagra (a disorder caused by vitamin B_3 deficiency) and dyslipidemia. Indeed, 8 weeks taking 100mg of daily NA supplementation accounts for the largest published increase in human NAD^+ within a healthy multiple person cohort, reported at 575% of the baseline value [148]. Interestingly, this study also found that NAD^+ levels gradually increased over the 8-week treatment period, which is surprising given the expectation that the NAD^+ synthesis and recycling pathways would become less efficient by way of de-sensitisation to the increasing precursor availability. It's worth noting only 2 participants were used however and a later study found that the same daily dosage of NA only mildly enhanced NAD^+ [149], an effect limited to participants who began the study with low NAD^+ levels. The latter study only measured NAD^+ before and after a 14-week period, hence

it is possible that the less emphatic results were due to de-sensitisation to the NA over this much longer treatment period.

The largest human increase in NAD^+ reported for NR is approximately 217% [152], significantly less than that for NA, although the caveats concerning this study have been discussed. On the other hand, no data on the efficacy of NMN at enhancing NAD^+ in humans has been reported, however it has been shown to be effective at raising NAD^+ in mice, with increases as high as 3-fold reported in mouse aorta [153]. Recently, the novel precursor dihydronicotinamide riboside (NRH) was tested for its ability to enhance NAD^+, producing remarkable results in mice. 48 hours after an intraperitoneal injection of NRH dissolved in PBS, NAD^+ levels rose 2.4 fold in blood, 2.2-fold in the brain and 5.4 fold in liver tissue [154]. By comparison, injections of NR and NMN only increased liver NAD^+ 1.3 and 1.5-fold respectively in the same study [154].

Another novel compound recently emerging as a potential NAD^+ enhancer is the hypolipidemic treatment acipimox, which is a derivative of NA that lacks the flushing as a side effect. Although the authors made no mention of its effect on NAD^+ levels *in vivo*, acipimox was shown to increase ATP content, ETC protein levels and the expression of a number of genes downstream of NAD^+ metabolism in muscle tissues from type 2A diabetes patients receiving the treatment [155]. Additionally, they also showed that acipimox enhanced NAD^+ levels in cultured C2C12 myoblasts. These promising results provided the stimulus for an ongoing clinical trial investigating the efficacy of acipimox at improving muscle symptoms in a subset of mitochondrial disease patients (AIMM - Acipimox in Mitochondrial Myopathy Study).

Being such a prominent and inefficient NAD^+ consumer, it is surprising that inhibition of CD38 as a strategy to increase NAD^+ has received relatively modest attention compared to precursor supplementation. Notable findings thus far include the ability of the CD38 inhibitor apigenin to approximately double NAD^+ in liver tissue from mice fed a high fat diet [156]. Additionally, as already discussed, 78c is a pharmacological CD38 inhibitor which has been shown to significantly enhance NAD^+ in mouse liver, skeletal muscle and spleen tissue [141]. Hence, an intervention combining both CD38 inhibition and precursor supplementation would appear to represent a promising multi-targeting strategy to increase NAD^+ enhancements.

Indeed, one problem with an approach taken to increase NAD^+ that solely focuses on precursors is that it neglects the underlying mechanisms which have caused NAD^+ depletion. Consequently, therapeutics that target CD38 driven depletion, aberrant energy metabolism and dysregulation of the NAD^+ synthesis/recycling pathways should theoretically represent a superior alternative as they tackle the root causes of decreased NAD^+, rather than looking for a quick fix. If it is the altered levels

of specific proteins that is driving decreased NAD^+ it is likely these will also limit the efficacy of precursor supplementation, perhaps explaining why the likes of NR and NMN have failed to induce the kind of increases that would restore the NAD^+ levels of a 60 year-old to say that of a 20 year-old. As a result, the utility of a multi-targeted approach is becomingly increasingly appreciated and may pave the way for interventions with an enhanced ability to restore cellular NAD^+ to optimal levels.

1.2.2 Benefits of Enhanced NAD^+ in Disease Models

Given the widespread focus of NAD^+ enhancement is to promote healthy ageing, combating age-related diseases also pertains to this objective. To this end, NAD^+ targeted interventions have been implemented in a wide range of age-related disease models. In particular, the increasing incidence of Alzheimer's disease (AD) in western societies has placed a strong emphasis on investigating the disease-modifying properties of NAD^+ enhancement in AD and other models characterised by progressive cognitive decline [157-162].

One mutant which demonstrates the possible benefit of enhanced NAD^+ in the context of neurological disease is the remarkable spontaneous *Wld*^{s} mouse mutant, which due to a tandem DNA triplication overexpresses a chimeric protein containing the first 70 amino acids of the ubiquitination protein UBE4B linked to the full NMNAT1 protein [163, 164]. Transection of neurons derived from *Wld*^{s} mice in vitro exhibit a large delay to the development of axonopathy compared to wild-type mouse neurons, with a mutation introduced into the NMNAT1 portion of the *WLD*^{s} chimeric protein ablating the delayed axonopathy. Furthermore, NA, NAM and NR have all been shown to delay axonopathy induced *in vitro*, although the former two required the concomitant overexpression of NAD^+ salvage pathway genes [165].

NAD^+ precursor supplementation has also been shown to improve neurological function in a number of AD models, with oral and nanoparticle-mediated delivery of NAM able to profoundly reverse cognitive and histopathological markers of AD [166-168]. In transgenic mice overexpressing amyloid precursor protein (APP), supplementation with NMN attenuated changes to the levels of mitochondrial fusion/fission proteins, reduced APP levels and improved mitochondrial function in brain tissue homogenates [169]. In the same model, a different study found NMN potently reduced hippocampal and cortical amyloid beta levels, prevented the appearance of diffuse plaques and improved the performance of the transgenic mice at memory tests [162]. NR supplementation had a similar outcome in the *Tg2576* mice AD model, with 3 months consumption found to reduce amyloid beta fibrils, improve synaptic plasticity and promote mitochondrial gene expression [170]. Hence, evidence is accumulating that NAD^+ precursors can prevent the defining features of AD pathology in rodent models.

Aside from AD mice, the benefits of increased NAD^+ for mitochondrial function is further highlighted by the ability of NMN to enhance lifespan by 90% in a mouse mitochondrial disease model of Leigh Syndrome [171], although it's important to note that NAD^+ levels were only enhanced in cardiac and skeletal muscle and not brain tissue. Additionally, the murine *Sco2*^{KOKI} mitochondrial disease model showed improvements in motor performance, ETC gene expression and skeletal muscle NAD^+ levels in response to supplementation with NR, whilst PARP1 inhibition also improved motor performance and mitochondrial function in skeletal muscle [172]. Deletor mice resemble adult-onset mitochondrial myopathy (MM) and thus exhibit progressive muscle dysfunction, which occurs due to the accumulation of mtDNA (mitochondrial DNA) deletions resulting from a mutation present in the mitochondrial replicative helicase Twinkle. These mice were also shown to benefit from NR treatment as a result of rejuvenated mitochondrial function [173], whereby the accumulation of mtDNA deletions and morphologically abnormal mitochondria was inhibited. On the back of these promising results the same group conducted a recently completed clinical trial using NAM in MM patients [151], with another trial once again using NAM in an MM cohort currently ongoing (NCT04538521).

NR has also displayed an impressive ability to preserve hepatic function in mice with diet induced liver fibrosis [174, 175]. Particularly noteworthy was the discovery that in mice fed ethanol daily, NR was able to attenuate multiple markers of liver damage, increase liver NAD^+ levels by over 300% and restore both mtDNA and SIRT1 levels to those in the non-ethanol treated littermates [176]. NR also exerted a similarly protective effect against age related liver pathology in elderly mice, significantly reducing levels of the liver damage marker AST (aspartate transaminase) whilst also dramatically improving steatosis scores [177]. Thus, from the findings in various animal models it appears the protection against age-related pathologies via enhanced NAD^+ extends to multiple different tissues.

1.2.3 NAD^+ Interventions as an Anti-Ageing Approach in Model Organisms

In a number of organisms there is mounting evidence that both manipulating enzymes involved in NAD^+ metabolism and precursor supplementation can extend lifespan and healthspan. Although *Drosophila* lack a homologue of NAMPT, D-NAAM (*Drosophila* nicotinamidase) is an enzyme which converts NAM to NA, a critical step in *Drosophila* NAD^+ synthesis. In addition to increasing the NAD^+/NADH ratio, overexpression of D-NAAM also increased lifespan by 30% [178]. This increase was absent in *Sir2* mutants, hence implying increased Sir2 activity via enhanced NAD^+ is fuelling the long-lived phenotype.

Further evidence for SIRT1/Sir2 mediated lifespan extension via increased NAD^+ is provided by *C. elegans* fed with NR and NAM or treated with pharmacological PARP inhibitors. Both interventions

enhanced NAD^+ levels and longevity in *C. elegans,* however the lifespan extension was once again absent in *sir-2.1* mutants [179].

In contrast, there is no evidence for significant lifespan extension in healthy mammalian organisms chronically supplemented with NAD^+ precursors, which has been sparsely investigated aside from one study noting a 5% lifespan increase in mice consuming NR [180]. However, this study also found 6 weeks of NR treatment improved physical endurance, mitochondrial function and replenished muscle stem cell levels in elderly mice – highlighting a positive effect of NR supplementation on healthspan, if not longevity. 1 week of ingesting NMN was also shown to have a similar effect in aged mice by reducing muscle atrophy, upregulating mitochondrial biogenesis and stimulating OXPHOS [181].

Furthermore, a longer term 12-month NMN supplementation regime in mice beginning at 5 months resulted in a remarkable attenuation of all age-related physiological changes measured, including: energy metabolism, serum lipid profile, weight gain, insulin sensitivity, mineral bone density and skeletal muscle mitochondrial respiration [182].

NMN was also found to induce remarkable improvements to the exercise capacity of elderly mice, with two months of NMN supplementation restoring the capillary density of 20-month old mice to that of 6-month old mice, whilst also resulting in a 56-80% increase in the distance covered by the elderly mice on a treadmill when running to exhaustion [183]. Moreover, these benefits of NMN supplementation were absent in *Sirt-/-* mice, suggesting NMN is mediating these effects through increased SIRT1 activity. The recent literature therefore implies that NMN can improve the muscular and vascular capacity of elderly mice by restoring mitochondrial function – indicative of enhanced healthspan.

Accelerated ageing models resembling the human diseases ataxia telangiectasia (AT) and Werner syndrome (WS) provide a useful tool for testing the efficacy of potential anti-ageing interventions. Both AT and WS are genetic disorders resulting from mutations to key DNA repair genes [184, 185], thus resulting in a faster rate of DNA damage accumulation which translates to an accelerated ageing phenotype. NR and NMN were both able to restore lifespan in *C. elegans* AT and WS models to wild-type levels [186, 187], with 14 days of NR treatment also able to dramatically improve lifespan in an AT mouse model [187]. Lymphoma is over-represented in AT patients [188], thus it would be useful to determine how NAD^+ mediated lifespan increase in AT mice influences lymphoma incidence.

Aside from precursor supplementation, pharmacologically targeting CD38 activity has also proven successful at attenuating various ageing biomarkers in elderly mice using the specific

thiazoloquin(az)olin(on)e CD38 inhibitor 78c. As well as increasing NAD^+ in multiple tissues, 78c improved glucose tolerance, lowered insulin and improved various exercise parameters. In skeletal muscle from the aged mice the authors found that 78c reduced DNA damage, dampened the expression of various genes associated with fibrosis and inflammation and increased lysine acetylation, a marker of SIRT1 activity [141]. The efficacy of 78c is a particularly useful development given the other known CD38 inhibitors apigenin and quercetin are undermined by low bioavailability.

1.2.4 A darkside to NAD^+?

Whilst the efforts to identify NAD^+ enhancing strategies intensifies, it's important to consider the potential drawbacks of increased NAD^+ under certain circumstances: highlighted by the elevated NAD^+ levels found in various cancer cells due to increased expression of the rate-limiting NAD^+ salvage pathway enzyme *NAMPT* [189, 190].

Regarding NAD^+ synthesis/recycling pathways, *NAMPT* in particular has garnered attention for its pro-tumourigenic function, with its expression shown to negatively correlate with survival in multiple different cancers [189, 191, 192]. Moreover, targeting NAMPT with the small molecule inhibitor FK866 has shown potent anti-cancer effects in both *in vitro* and *in vivo* models [193-196], prompting its use in phase I and II clinical trials [197, 198] albeit without a favourable outcome despite being well-tolerated. One mechanism by which NAMPT inhibition was shown to specifically kill breast cancer cells lines was the stabilisation of the SIRT1 target p73, due to an increase in its acetylation [199]. It has also been suggested that impairment of antioxidant defence systems due to depleted NAD^+ may make cancer cells highly susceptible to the abundance of ROS they produce [200], outlining another reason cancer cells require an adequate supply of NAD^+.

On the other hand, some studies implicate an anti-tumorigenic role for increased NAD^+, for example the finding that increased SIRT1 activity suppressed tumour formation in a mouse model of colon cancer via downregulated β-catenin signalling [104]. Additionally, mitochondria specific increases in NAD^+ impaired the clonogenicity and thus the tumour forming potential of glioblastoma tumour-initiating cells, which the authors speculated may be due to increased SIRT3 activity [201].

NAMPT has also been framed as a driver of cellular senescence, with oncogene induced senescence in IMR90 cells shown to coincide with increased *NAMPT* expression and NAD^+ levels [202]. NAMPT inhibition using FK866 or shRNA knockdown suppressed development of the SASP (senescence associated secretory phenotype) in this model, with the downstream upregulation of OXPHOS and glycolysis shown to be key to NAMPT's pro-senescent effects. NAMPT can also be found extracellularly where it's suspected to primarily function as a cytokine, often referred to as visfatin

or eNAMPT (extracellular NAMPT). Villalobos *et al.* showed that the presence of elevated eNAMPT in culture media potently induces senescence in human umbilical vein endothelial cells (HUVEC) in a dose-dependent manner [203]. Interestingly, they found FK866 attenuated these effects whereas NMN (the product of NAMPT activity) also promoted senescence. This implies eNAMPT must either become intracellular to elicit pro-senescent effects or perhaps does so via the extracellular conversion of NAM to NMN.

The notion that NAMPT is pro-senescent is controversial however, with other studies presenting contrasting findings. For example, FK866 was shown to induce senescence in young mesenchymal stem cells (MSCs) [204, 205], whilst overexpression of NAMPT using a lentiviral vector protected MSCs derived from old mice against senescence [204]. FK866 was also shown to induce senescence in human vascular smooth muscle cells (SMCs) [206], with induced overexpression of NAMPT once again found to suppress replicative senescence. Consequently, the jury is still out on the role of NAMPT and NAD^+ levels in the development of senescence which is likely to be nuanced and tissue dependent. It should be noted that all the studies referenced have only investigated the role of NAMPT in senescence using *in vitro* models, hence results from *in vivo* studies are needed to better characterise the involvement of NAMPT and NAD^+ in senescent pathways.

Although enhanced NAD^+ would generally be considered beneficial for physical performance via improved mitochondrial function, one study found that NR supplementation decreased exercise performance in rats [207]. Furthermore, the NR treated rats had higher levels of the oxidative stress marker F_2-isoprostane, combined with lowered levels of a number of antioxidant enzymes [208]. The authors attributed these adverse effects of NR to their use of young healthy rats, suggesting that supplementation with NAD^+ precursors should be reserved for the elderly. Contrastingly, Canto *et al.* found that consumption of NR resulted in a small but non-significant increase in VO_2max (maximal oxygen uptake during exercise) of young mice [89]. They did find however that NR significantly improved the VO_2max in mice fed a high fat diet, therefore re-iterating that the beneficial effects of enhanced NAD^+ may be limited to ageing/disease conditions.

1.3 Circadian Rhythms

1.3.1 Circadian Regulation of Biological Processes

In order to utilise physiological resources more efficiently, mammals have developed a regulatory system whereby certain pathways follow a 24-hour pattern of varying levels of activity. The classical example is circulating levels of the sleep promoting hormone melatonin, which for someone with a typical sleep wake cycle is present at very low levels around the usual waking hours, before gradually increasing in the late afternoon and reaching a peak around bed-time [209]. Thus, circadian control

means the sleep promoting effects of melatonin are only experienced around the time sleep is required, whereas they're absent when the body needs to be awake and alert. Furthermore, melatonin can regulate multiple cellular pathways throughout the body by binding to melatonin receptors, thus allowing physiological processes like blood pressure, thermoregulation and metabolism to be co-ordinated to the light-dark cycle and by extension our daily routine.

This rhythmicity of melatonin release and indeed other hormones which follow a 24-hour pattern is controlled by the suprachiasmatic nucleus (SCN), a tiny structure within the hypothalamus which receives direct input from optic nerves. This input of photosensory information allows entrainment of the SCN such that it uses the 24-hour light dark cycle as a compass for the 24-hour period. This also allows it to be 're-calibrated', for example if moving to a different timezone. In addition to melatonin, there is evidence that the SCN regulates the daily fluctuations of other hormones such as leptin, ghrelin, cortisol, growth hormone and insulin [210]. The circulating levels of these hormones can then themselves regulate processes within peripheral cells, therefore acting as an intermediary by which circadian control is transmitted from the SCN to other tissues.

In addition to input from the SCN, it appears most cells have an endogenous regulatory clock which is synchronised by signalling from the SCN – in a similar way to how the SCN is calibrated by the external light-dark cycle. At the molecular level, the clock in both SCN cells and those in the periphery is regulated by a core group of enzymes: BMAL1, CLOCK, PER1, PER2, CRY1, CRY2, REV-ERBα and REV-ERBβ [211-214]. These comprise a feedback loop in which BMAL1 and CLOCK form a transcriptionally active dimer which can promote transcription of genes with an E-box containing promoter [215]. Amongst the genes whose expression is upregulated are *PER1/2* and *CRY1/2* which function as transcriptional repressors of *BMAL1* and *CLOCK* [216], thus completing a negative feedback loop which underpins the rhythmicity of all genes under circadian control.

1.3.2 Circadian Rhythms and Ageing

It's well established that circadian rhythms change with age, which explains the shift in sleep patterns of the elderly who tend to sleep and wake at earlier times [217, 218]. Additionally, the oscillations of core body temperature [219, 220], time of optimal cognitive performance [221-223] and circulating cortisol [224, 225] have also been shown to change with age, emphasising the widespread effects of altering the circadian cycle. In mice ablation of the *Bmal1* gene [226] or mutations in *Clock* [227] and *Per2* [228] were capable of promoting a pro-ageing phenotype, whilst in humans irregular sleeping patterns caused by shift work have been associated with an increased risk for age-related illnesses such as cancer [229-231] and cardiovascular disease [232].

At the molecular level, a number of genes implicated within the ageing process are known to be under circadian control, including *SIRT1, PARP1* and *NAMPT* [233]. The circadian regulation of NAMPT has been shown in mouse liver tissue to result in a daily oscillation of intracellular NAD^+ [234], hence SIRT1 and PARP1 activity would be expected to mirror this oscillation under conditions of rate-limiting NAD^+. Consequently, the ability of cells to initiate an anti-inflammatory, antioxidant or DNA damage response via SIRT1 or PARP1 may be affected by the time of day, especially in the elderly.

As well as being under circadian control, SIRT1 itself has been implicated as a key regulator of the circadian clock through its ability to promote BMAL1 activity via deacetylation which prevents the binding repressors like PER2 and CRY1/2 [234]. Ramsey *et al.* also showed that the BMAL1:CLOCK dimer upregulated *NAMPT* expression in mouse liver samples and MEFs [234], thus identifying a positive feedback loop whereby BMAL:CLOCK enhance NAD^+ through NAMPT which increases SIRT1 activity, subsequently increasing BMAL1:CLOCK promoter binding and completing the loop (Figure 1.3.1).

This provides a molecular basis for a putative mechanism by which declining NAD^+ levels could modify circadian rhythms with age. Of course, if BMAL1 and NAD^+ comprise a feedback loop then the reverse may also be true if *BMAL1* expression decreases with age, as has been suggested by the finding that white blood cell *BMAL1* mRNA levels decreased with age in healthy females [235]. At the endocrine level the ability of the pineal gland to synthesise and secrete melatonin may be impaired with age [236], thus representing another physiological change which could drive age associated alterations to circadian rhythms. Given melatonin has been shown to modulate SIRT1 activity [237, 238], the ability of the SCN to regulate peripheral circadian clocks via melatonin may very well be dependent on SIRT1. Hence, NAD^+ and SIRT1 appear to be key players in circadian rhythms via multiple interactions.

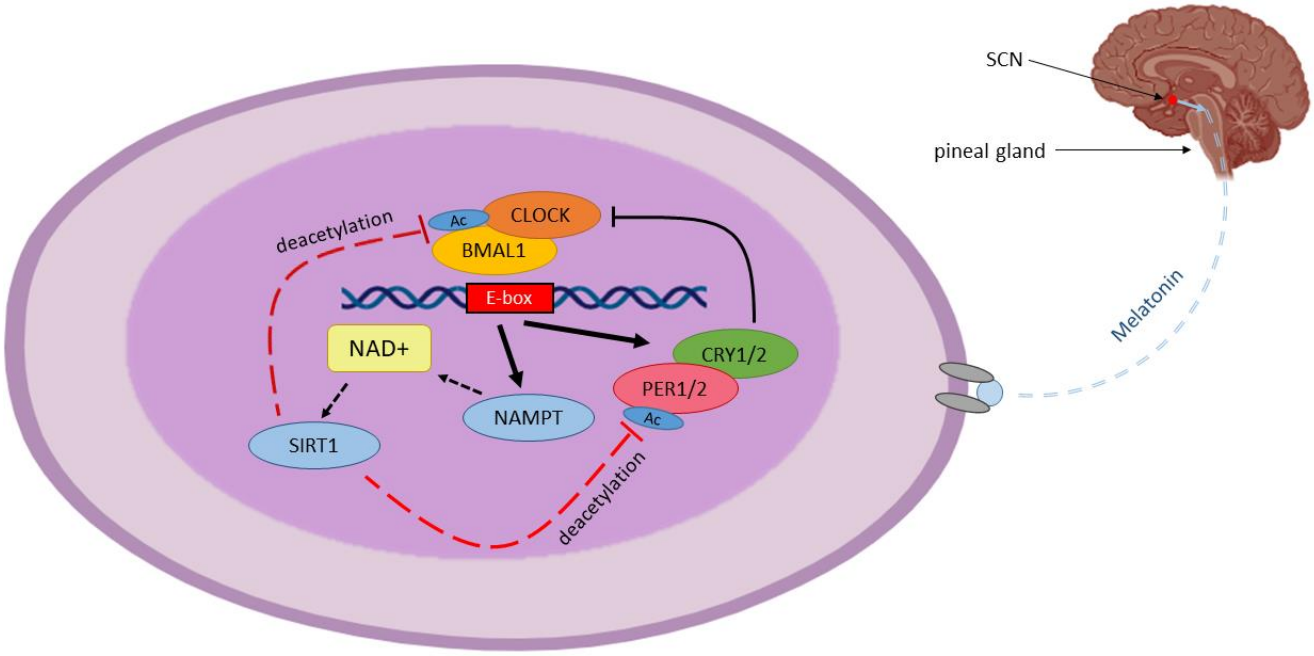

Figure: 1.3.1 Circadian regulation of SIRT1 and NAD$^+$.
The SCN can regulate circadian rhythms in peripheral cells by controlling the secretion of hormones such as melatonin from the pineal gland. At the intracellular level, the CLOCK:BMAL1 heterodimer can bind the E-box region in the *NAMPT* promoter which upregulates its expression. NAMPT can then increase NAD$^+$ synthesis which in turn promotes SIRT1 activity. SIRT1 mediated deacetylation of BMAL1 subsequently creates a positive feedback loop by preventing the binding of the BMAL1 repressors CRY1/2 to the BMAL1:CLOCK heterodimer. SIRT1 further promotes BMAL1:CLOCK activity by deacetylating PER2, another repressor of the BMAL1:CLOCK. SIRT1 mediated deacetylation of PER2 promotes its degradation by the proteasome, thus preventing it from interacting with BMAL1:CLOCK. A negative feedback arm exists in the system however due to the ability BMAL1:CLOCK to bind the *PER1/2* and *CRY1/2* promoters and increase their expression. Consequently, these positive and negative feedback arms create the temporal oscillations in BMAL1 activity which constitute circadian rhythmicity at the molecular level.

1.4 MicroRNAs

1.4.1 Epigenetic Regulation by MicroRNAs

In addition to DNA and histone modifications, microRNAs (miRNAs) represent another omnipresent epigenetic mechanism that regulates gene expression (Figure 1.4.1). miRNAs are very short oligonucleotides (20-25 nucleotides in length) which bind to the 3' UTR of mRNAs (also the 5'UTR in rare instances), creating an RNA duplex that gets degraded by the endonuclease activity of the RISC:Dicer complex [239]. The genes for miRNAs are usually located in introns and are transcribed to yield a pri-miRNA molecule which undergoes further processing to form the 70-nucleotide pre-miRNA duplex, before being exported to the cytoplasm. Once in the cytoplasm the pre-miRNA undergoes unwinding and cleavage mediated by Dicer to create the 20-25 nucleotide mature miRNA, after which it associates with the RISC complex. The miRNA can subsequently bind target mRNAs

which aren't always perfectly complementary – allowing a single miRNA to repress many different genes.

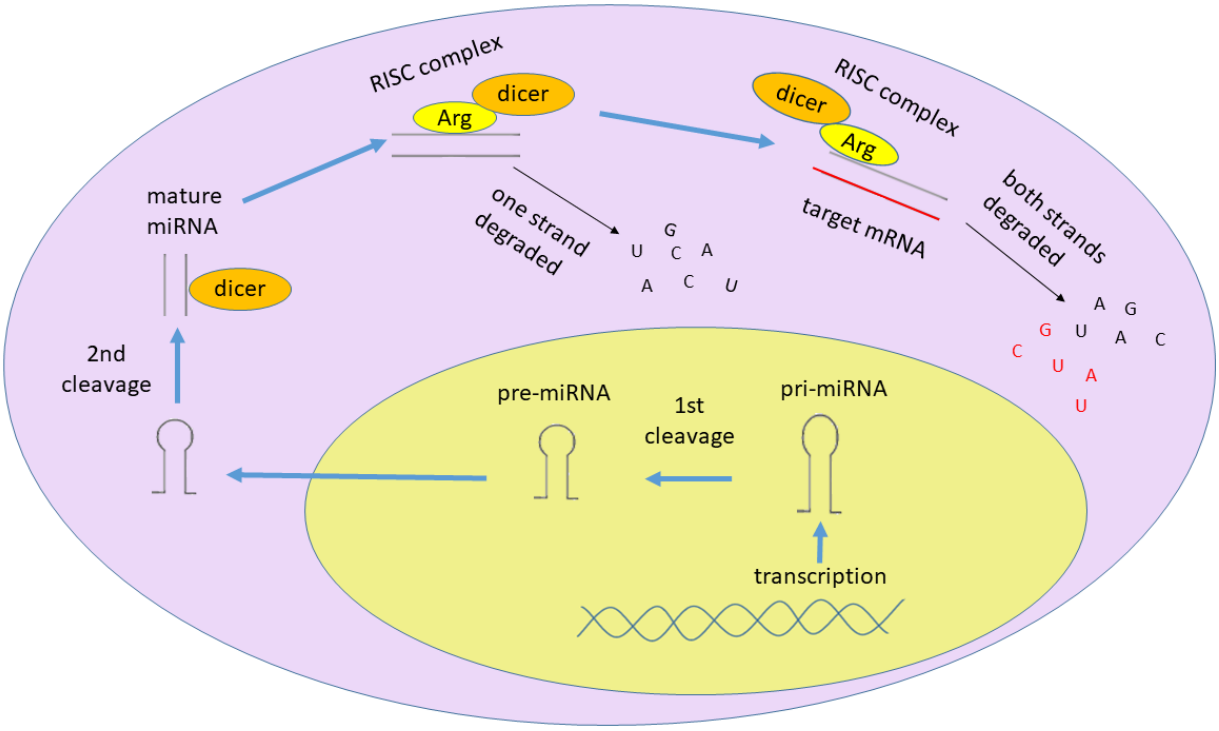

Figure 1.4.1 miRNA mediated gene repression.
Following transcription pri-miRNA is cleaved into pre-miRNA before being exported to the cytoplasm where it interacts with Dicer and undergoes further cleavage during which the stem-loop is removed. The RISC complex is then formed, with the guide strand which is complementary to the target mRNA bound by Argonaute. This allows degradation of the passenger strand by the RISC complex, whilst the guide strand remains intact. The guide strand can then bind its target mRNAs, culminating in the destruction of both strands by the RISC complex which results in gene repression.

1.4.2 miR-155

At present approximately 2578 different mature miRNAs have been identified (http://www.mirbase.org/), emphasising the extensive regulation of gene expression commanded by the miRNA pool. Regarding their contribution to disease there has been a particular focus on their role in cancer, with cancer promoting miRNAs aptly labelled 'oncomiRs'. Of the oncomiRs identified to date, miR-155 is one of the most prominent, found to be upregulated in multiple different tumour types [240-243]. Its tumour promoting activity is thought to be multifaceted, with upregulation of glycolysis via hexokinase II, inhibition of apoptotic gene expression and activation of the β-catenin/Wnt pathway all pro-tumourigenic mechanisms attributed to miR-155 [243]. Additionally, its status as a pro-inflammatory mediator has been augmented by its elevation in inflammatory disorders such as Crohn's disease [244] and rheumatoid arthritis [245], whilst it's also been shown

to be critical for the disease pathogenesis in mouse models of multiple sclerosis [246, 247]. Relating to circadian rhythms, Curtis *et al.* demonstrated in mice that *Bmal1* transcripts contain two binding sites to which mir-155 binds in response to a pro-inflammatory stimulus [248] and thus exerts regulation over circadian rhythm. The effects of miRNAs are known to be cell dependent therefore it isn't known how ubiquitous this mechanism throughout different tissues is and indeed even whether it is also conserved in humans.

1.5 Fibrosis

1.5.1 Fibrosis as an Age-Related Disease

Fibrosis is the process which causes the formation of scar tissue, often as a result of physical trauma or a prolonged inflammatory response. Many organs can be affected by fibrosis, ultimately resulting in tissue dysfunction. The 'scar' is a result of the excessive differentiation of fibroblasts into myofibroblasts and their abundant secretion of collagen and other extracellular matrix ECM proteins in response to a pro-fibrotic stimulus such as TGF-β or various other cytokines. Where fibrosis is modest, the scar tissue will often be replaced with new healthy tissue, however as we get older the body's ability to replace the scar tissue is impaired – likely due to depletion of the stem cell reserve [249], the growing presence of senescent cells [250] and persistent low-level inflammation [251].

The accumulation of fibrotic lesions and the body's dwindling ability to repair them with age is a particular concern with regards to cardiac tissue, with heart failure a leading cause of hospitalisation for those over the age of 65 [252-254]. Idiopathic pulmonary fibrosis (IPF) is another prominent cause of disability for elderly populations, with age a significant risk factor [255, 256]. Additionally, renal fibrosis and liver fibrosis are also over-represented in those over the age of 50 [257, 258] – highlighting that an increased risk for fibrosis in multiple organs is an important and often overlooked aspect of the ageing phenotype.

Consequently, preventing the development of fibrosis or mediating its repair is a key goal in the quest for healthy ageing. Although there are differences to the fibroblasts resident in different tissues, the mechanism by which they instigate fibrosis is largely the same: an inflammatory response provoking excessive ECM secretion. Hence a better understanding of fibrosis in an organ such as skin could also translate to an improved understanding of fibrosis in other tissues.

1.5.2 Systemic Sclerosis

A condition characterised by skin fibrosis, and thus a useful model for understanding the molecular mechanisms which drive fibrosis is systemic sclerosis (SSc). SSc is an idiopathic autoimmune disease in which fibrosis first appears in the skin, before progressing to internal organs in approximately half

of the patients. Internal organ involvement is what differentiates the two subsets of SSc: limited SSC (lSSc) is localised to the skin, whereas the much more aggressive diffuse SSc (dSSc) begins with a more severe skin fibrosis followed by pulmonary, renal and cardiac involvement which eventually causes mortality. The aetiology is unknown, however the pro-fibrotic cytokine TGF-β is strongly implicated as playing a key role [259, 260]. Additionally, epigenetic mechanisms including histone acetylation are becoming increasingly suspected as important features of SSc pathogenesis, as has been reviewed previously [261]. Thus, if histone acetylation is a central modulator of fibrotic pathways this suggests a possible role for the histone deacetylase SIRT1.

1.5.3 TGF-β

TGF-β is a potent inducer of the fibroblast to myofibroblast transition and subsequent upregulation of pro-fibrotic genes, hence its use as the quintessential *in vitro* inducer of fibrosis. Although usually regarded as a pro-fibrotic and pro-inflammatory cytokine, TGF-β embodies the term pleiotropic – able to both promote and inhibit processes like inflammation and proliferation depending on the extracellular environment and the cell type it binds to.

In the context of fibroblasts, TGF-β stimulates proliferation, fibroblast to myofibroblast differentiation, ECM synthesis and impaired secretion of matrix proteases – combining to create the perfect storm for the development of fibrosis. Under healthy conditions these effects constitute the wound healing response which is an essential mechanism for tissue repair following damage, however persistent TGF-β signalling will begin to have a counter-productive outcome. In many ways, this resembles the chronic inflammatory response underlying diseases such as osteoarthritis, multiple sclerosis, and rheumatoid arthritis, whereby a protective mechanism becomes damaging if overactivated.

The TGF-β family contains three distinct isoforms which exist as homodimers – TGF-β1, TGF-β2 and TGF-β3. Being cytokines they function extracellularly, binding to the TGFβR1 (TGF-β1 receptor 1) which then recruits and phosphorylates TGFβR2 (TGF-β1 receptor 2), initiating a signalling cascade. TGF-β signalling is generally categorised as either SMAD-dependent or SMAD-independent [262, 263], reflecting the prominent role SMAD proteins play in transducing TGF-β driven effects. Of particular importance are SMAD2 and SMAD3 which are phosphorylated by TGFβR1, resulting in the formation of a complex containing SMAD2, SMAD3 and SMAD4 which translocates to the nucleus and transcriptionally upregulates profibrotic genes, whilst also indirectly downregulating antifibrotic targets [264]. The master control TGF-β has over fibrotic pathways is facilitated by the wide range of genes targeted by the SMAD complex including ECM proteins, profibrotic miRNAs, tissue inhibitor

of matrix metalloproteinases (TIMPs) and inhibitors of antifibrotic miRNA transcription [261, 265, 266].

1.6 Metabolism and Disease

Terms such as 'metabolic re-modelling' and 'metabolic re-programming' have become something of a recent trend owing to the increasing acceptance that metabolic changes are pivotal in a number of non-metabolic diseases (by classical definition) [267-270]. Indeed, the existence of a wide range of illnesses resulting from impairment of various metabolic pathways (termed metabolic disorders) highlights the importance of maintaining the correct function of these pathways. Included in these metabolic disorders are a number of conditions caused by mutations in TCA cycle genes which are characterised by symptoms including neurodegeneration and developmental delay [271-273], whilst a wide range of mitochondrial disorders occur due to mutations in both mtDNA and nDNA mitochondrial genes [274].

1.6.1 The Warburg Effect

The most notorious and indeed original example of metabolic re-programming is cancer and the 'Warburg effect' [275]. The Warburg effect is the seemingly counter-intuitive upregulation of glycolysis in cancer cells even in the presence of adequate oxygen for OXPHOS, thus is also more informatively termed 'aerobic glycolysis'. Given glycolysis is a far less efficient pathway for ATP production compared to OXPHOS – producing approximately 2 ATP per round in contrast to OXPHOS' 30-36 ATP – the massively enhanced levels in cancer cells of the former seems odd, especially given their high demand for ATP due to rapid growth. The prevailing theory explaining this is that it's the biosynthetic intermediates that are produced as byproducts in the glycolytic chain that are important, providing the building blocks for the abundant macromolecule synthesis that supports tumourigenicity. It is also a common misconception that the Warburg effect involves glycolysis being enhanced at the expense of OXPHOS: this isn't necessarily the case. Many cancer cells also have high levels of OXPHOS to support their high ATP demand [276], augmenting the idea that the importance of glycolysis in cancer is the generation of biosynthetic intermediates rather than ATP production. Rather than viewing glycolysis and OXPHOS as two alternative pathways for ATP synthesis between which an equilibrium exists, it is important to remember that they're intrinsically linked via the TCA cycle.

1.6.2 Glutaminolysis and mTOR

Aside from glycolysis and OXPHOS, another key metabolic pathway implicated in multiple diseases is glutaminolysis: a 2-step process whereby glutamine is converted to α-ketoglutarate via glutamate.

α-Ketoglutarate is an essential metabolite under growth conditions, functioning as a key precursor for amino acid synthesis and lipid metabolism, whilst also supporting energy production by feeding into step four of the TCA cycle. Additionally, the transamination of glutamine to glutamate which constitutes the initial step in glutaminolysis provides nitrogen required for amino acid synthesis, with glutamate itself also able to be funnelled as a substrate into amino acid synthesis pathways.

Given it performs a very similar role in facilitating rapid growth, it is perhaps unsurprising that like glycolysis, glutaminolysis is also regarded as a critical component of cancer development [277]. Similarly, a spike in glutamine metabolism occurs during T cell activation suggesting it may also be important in autoimmunity [278, 279].

One anabolic mechanism thought to be promoted by glutaminolysis but not glycolysis is activation of the mTORC1 complex [280]. mTORC1 is a multi-subunit complex which contains mTOR as its key catalytic subunit: a serine/threonine kinase regarded as the 'master regulator' of intracellular anabolic pathways [281]. The relationship between glutaminolysis and mTOR is bidirectional with α-ketoglutarate activating mTOR via prolyl hydroxylases, whilst the subsequent mTOR mediated enhancement of nutrient uptake facilitates glutaminolysis through increased glutamine availability. mTOR is also known to enhance glycolysis via HIF-1α [282] and thus this represents yet another pathway through which α-ketoglutarate promotes growth.

Importantly, as mentioned previously mTOR activity can be attenuated by the immunosuppressant rapamycin. Indeed, the use of rapamycin has proven to be effective at blocking disease pathogenesis in a number of tumour containing mice [283-285] and pro-fibrotic rodent models [286-289].

1.6.3 Mitochondrial Dysfunction: Cause or Consequence of Ageing?

Mitochondria are a focal point of many theories regarding the molecular basis for ageing, hence it stands to reason that mitochondrial driven metabolism may also be key. The first mitochondrial ageing theory to gain widespread support was the 'mitochondrial free radical theory of aging' (MFRTA) which posits that mtROS (mitochondrial ROS), which are unavoidable byproducts of the ETC, cause the intracellular damage underpinning physiological decline [290]. Complexes I and III in the ETC produce the superoxide anion which via fenton chemistry is eventually converted to the hydroxyl radical, a highly reactive ROS that oxidises proteins, lipids and DNA. The MFRTA proposes that mitochondrial function declines with age due to the accumulation of mutations within the mitochondrial genome, resulting in less efficient electron transfer and more mtROS production. This forms a vicious cycle whereby mtROS induce mtDNA damage, which in turn induces higher mtROS

production and more mtDNA damage, augmented by the cell's impaired antioxidant capacity due to mtROS damage to proteins and nuclear DNA.

Since then however, mitochondrial theories of ageing have undergone various refinements and doubts have been raised about the contribution of mtROS to ageing: upregulation of mitochondrial antioxidants failed to increase lifespan in mice [291], whilst reduced levels of the mitochondrial antioxidant SOD2 in heterozygous *Sod2*$^{+/-}$ mice increased oxidative stress yet failed to reduce lifespan [292]. Most recently, the role of mitochondria in ageing has focused on its relationship with inflammation and senescence, with mitochondrial dysfunction found to be essential for the development of the SASP [35, 293]. The mechanisms proposed differ however, with activation of the SASP via a persistent DDR induced by mtROS oxidation of nuclear DNA one model [35, 294]. Alternatively, it has also been shown that mitochondrial induced senescence is dependent on a lowered NAD^+/NADH, which drives senescence via P53 stabilisation downstream of AMPK activation [293].

There is also evidence which suggests dysfunctional mitochondria trigger the SASP by activating the cGAS-STING pathway, a mediator of innate immunity. cGAS is a sensor for cytoplasmic double stranded DNA (dsDNA), thought to have primarily evolved to detect infiltrating viruses, which upon sensing dsDNA activates the transcriptional activator STING which in turn increases transcription of a number pro-inflammatory genes [295]. Damaged mitochondria release mtDNA fragments which can increase inflammation via NLRP3 inflammasome activation [296] and also bind to cGAS [297], thus stimulating an immune response. Whilst cytoplasmic mtDNA binding constitutes a neat mechanism of cGAS activation downstream of mitochondrial dysfunction, Vizioli *et al.* found that it was actually nDNA fragments resulting from aberrant mitochondria to nucleus retrograde signalling that caused cGAS-STING induced senescence [298]. It therefore appears likely that mitochondria are heavily implicated in senescent pathways, however more clarity on the dominant mechanisms is required.

1.7 Aims and Objectives

The important role of NAD^+ and SIRT1 in healthy ageing is becoming increasingly accepted, however the influence of factors such as circadian rhythms, NAD^+ precursor supplementation and the activity other NAD^+ consuming enzymes on NAD^+ homeostasis and SIRT1 activity requires further investigation. By better understanding these interactions, this will provide valuable information on how to optimise NAD^+ focused strategies for the purpose of enhancing SIRT1 activity therapeutically – with the ultimate goal of extending human healthspan.

Specific questions to address:

1. Can PARP1 inhibition enhance SIRT1 activity via increased availability of NAD^+?
2. Do NAD^+ levels follow a circadian rhythm in dermal fibroblasts and how does this impact SIRT1 activity?
3. Can naturally occurring compounds targeting enzymes involved in NAD^+ metabolism enhance NAD^+ levels and protect cells against oxidative stress *in vitro*?
4. What is the efficacy of these compounds at enhancing human PBMC NAD^+ levels if implemented as a dietary supplement *in vivo*?
5. Does the NAD^+/SIRT1 axis interact with pro-fibrotic signalling in dermal fibroblasts?

Chapter 2. Materials and Methods

2.1 Ethics

Full ethical approval was obtained from the Northumbria University ethics committee for all work reported within this thesis (internal submission references 743 and 9040).

2.2 Reagents

All reagents and plasticware (Greiner) used were purchased from Sigma-Aldrich unless otherwise stated.

2.3 Cell Culture

2.3.1 Cell Culture Conditions

Unless otherwise stated, cells were grown in high glucose Dulbecco's Modified Eagle's Medium (DMEM) (Gibco cat no. 21969035, Thermo Fisher Scientific, Paisley, Scotland, UK) supplemented with 10% fetal bovine serum (FBS), 1% penicillin/streptomycin, and 2mM L-glutamine (all Gibco, Thermo Fisher Scientific, Paisley, Scotland, UK) and kept in an incubator (Heracell VIOS 160i, Thermo) at a temperature of 37°C and with an atmosphere of 5% CO_2.

For adherent cells, culturing was performed by detaching the cells using a 0.05% w/v Trypsin 0.02% v/v EDTA solution (Gibco, Thermo Fisher Scientific, Paisley, UK), before collecting a cell pellet by centrifugation and then adding the re-suspended cells to the new flask(s). For suspension cells, these were passaged by adding the suspension to new flasks containing media using the appropriate dilution factor.

When passaging or harvesting cells for downstream experimental analysis (where cytotoxicity wouldn’t be expected), viability was assessed by mixing 10-20ul of cell suspension with an equal volume of 0.4% trypan blue solution (Gibco, Thermo Fisher Scientific, Paisley, UK). Cells were then added to a haemocytometer (Hawksley, Lancing, Sussex, UK) and visualised using a bright-field microscope at 10x magnification to determine the presence of cell death in the form of cells stained blue.

2.3.2 NHDFs

Primary derived NHDFs (normal human dermal fibroblasts) (n=3) were received as gifts from Dr Nicola Fullard (Durham University, UK), Dr Julie Worrell (Newcastle University, UK) and Dr Richard Stratton (UCL, UK). NHDFs were routinely passaged every 5-7 days (typically a 1:3 split) and used at

passage number <25. NHDFs were typically seeded down at a density of 2,000 cells/well for 96-well plates, 8,000 cells/well for 24-well plates and 60,000 cells/well for 6-well plates during experiments.

2.3.3 SSc Patient Dermal Fibroblasts

Dermal fibroblasts derived from skin lesions of SSc patients (n=4) and dermal fibroblasts from age/gender matched controls (n=3) were obtained as a gift from Dr Richard Stratton (UCL, UK). These were grown and passaged/seeded down for experiments following the same conditions as NHDFs and were used at passage number 4–9.

2.3.4 miR-155KO and Wild-Type Primary Derived Mouse Dermal and Lung Fibroblasts

Skin and lung tissue explants from *miR-155*$^{-/-}$ C57BL/6 and wild-type C57BL/6 mouse littermates (n=5 for each genotype) were received as a gift from Dr Mariola Kurowska-Stolarska (Glasgow University, UK). On arrival the explants were minced up using a sterile scalpel and embedded onto the surface of a 6-well plate which had been scratched several times with the scalpel. The plates were then incubated under standard culturing conditions and the media were replaced every 2 - 3 days. Once the fibroblasts had extensively migrated from the tissue as determined by visualising under a bright-field microscope, the remaining pieces of tissue were discarded and the fibroblasts cultured into a T25 flask. The cells were then used for experiments after reaching passage 5 with the same seeding densities as used for NHDFs. An n=4 for each genotype is used for experiments involving these fibroblasts due to failure of the fibroblasts to migrate from the skin explant for 1 miR-155KO and 1 WT explant.

2.3.5 *Bmal1*KO and Wild-Type Primary Derived Lung Fibroblasts

Mouse lung fibroblasts (MLFs) derived from *Bmal1*$^{-/-}$ and wild-type C57BL/6 mice littermates (n=2) were provided as a gift from Dr Steven O'Reilly (Durham University, UK). These were grown under standard conditions and used for experiments between passage numbers 16 and 25, with the same seeding densities as NHDFs.

2.3.6 Jurkat Cell Line

These cells were grown in suspension in Roswell Park Memorial Institute (RPMI) 1640 Medium (cat no. 21875034, Thermo Fisher Scientific, Paisley, UK) supplemented with 10% foetal bovine serum (FBS), 1% penicillin/streptomycin, and 2mM L-glutamine (all Gibco, Thermo Fisher Scientific, Paisley, UK) and kept at a temperature of 37°C in an atmosphere of 5% CO_2. Cells were split at a confluency of 2-3 million cells/ml whereby they were seeded down and used for experiments at a density of 200,000-300,000 cells/ml.

2.3.9 Cryopreservation

All cells were cryopreserved after reaching 70-80% confluency. Following trypsinisation for adherent cells, the pellets were re-suspended in the appropriate culture media at a concentration of approximately 1 million cells/ml and chilled on ice. DMSO (cat no. D2650, Sigma-Aldrich, Gillingham, UK) was then slowly added dropwise onto the cells to a final concentration of 10% v/v, before the cells were added to cryovials and placed in a pre-cooled (4°C) Mr Frosty (Nalgene) container at -80°C overnight. The next day the cryovials were transferred to a -150°C freezer for long term storage.

2.3.10 Induction of Fibrosis Using TGF-β

The standard method used to induce fibrosis *in vitro* is treating cells with TGF-β. Due to the potential presence of TGF-β in FBS, NHDFs were serum starved (media lacking FBS) overnight prior to the addition of 10ng/ml TGF-β (stored as a 10ug/ml stock in filter sterilised dH_2O). Before adding the TGF-β, the culture media were replaced with fresh media containing reduced FBS (0.1%). Afterwards, no further media changes were made for the duration of the experiment. Although low serum may be an unnatural environment for cells, this was found to yield the most reproducible results and didn't induce any cytotoxic effects as determined by staining cells with trypan blue, whereby the presence of cells stained blue by the trypan blue dye would indicate a porous plasma membrane and thus cell death.

2.3.11 Cell Transfection

Gene knockdown studies were performed by transfecting cells with siRNA or miRNA mimic oligonucleotides using a 'forward transfection' protocol. Cells were seeded down in a 24-well plate at 30-40% confluency and left to adhere overnight. The next day HiPerFect transfection reagent (Qiagen, Manchester, UK) ((no of wells + 1) x 0.8ul) and the siRNA/miRNA mimic (4x final concentration) were added to FBS and antibiotic free DMEM ((no of wells + 1) x 15ul), before being left for 15 minutes at RT (room temperature) to allow transfection complex formation. During this time, the media in the 24-well plate were removed and replaced with 45ul of culture media containing no antibiotic. 15ul of the transfection reagent/oligonucleotide mix was then added dropwise into each well and the media replaced 8 hours later with regular antibiotic-containing culture media. The efficacy of the *BMAL1* siRNA (human), *Bmal1* siRNA (mouse) and miR-155 mimic at knocking down their targets was confirmed by western blotting and qPCR for a range of concentrations (typically 25nM, 50nM, 75nM, 100nM and 125nM) after 48 and 72 hours, which informed of the optimal concentration and treatment duration for each gene silencer used.

Table 2.3.11.1 Oligonucleotides used for gene silencing studies.

Oligonucleotide	Manufacturer	Working Concentration
BMAL1 siRNA (Human)	Qiagen (cat no. SI00023016)	100nM
Bmal1 siRNA (Mouse)	Invitrogen (cat no. 4390771)	75nM
Silencer™ Negative Control No. 1 siRNA	Sigma (cat no. SIC OO1)	(100nM human, 75nM mouse)
miR-155 mimic (Mouse)	Qiagen (cat no. 219600)	50nM
miRIDIAN miRNA Negative Control #1	Dharmacon (cat no. HMC0002)	50nM

2.3.12 Compounds Added to Cells *In Vitro*

All compounds (Table 2.3.10.1) used in the cell culture work presented within this thesis were dissolved in either DMSO (Sigma-Aldrich, Gillingham, UK), sterile filtered molecular grade ethanol (Fisher) or sterile filtered dH_2O. Optimal doses for viability assays were determined by titrating over a range of doses, with the appropriate dose range determined from the literature.

Table 2.3.12.1 Compounds used for *in vitro* work

Compound	Supplier (cat no.)	Solvent	Working concentration
2-deoxyglucose (2-DG)	Sigma-Aldrich (D3179)	dH_2O	10 - 50mM
3PO	Selleck Chemicals (SML1343-5MG)	DMSO	8uM
α-lipoic acid (ALA)	Nuchido Ltd.	DMSO	20 - 100uM
Antimycin A	Sigma-Aldrich (A8674-25MG)	DMSO	0.5uM
Apigenin	Selleck Chemicals (S2262)	DMSO	10 - 100uM
Compound 968 (G968)	Sigma-Aldrich (352010)	DMSO	10uM
Dexamethasone	Sigma-Aldrich (D4902)	DMSO	100nM
EGCG	Nuchido Ltd.	DMSO	4uM
EX527	Selleck Chemicals (S1541)	DMSO	40uM
FCCP	Sigma-Aldrich (C2920-10MG)	ethanol	1uM
FK866	Selleck Chemicals (S2799)	DMSO	2 - 200nM
Glucose	Sigma-Aldrich (G7021)	dH_2O	10mM
Nicotinamide (NAM)	Sigma-Aldrich (N0636)	dH_2O	100uM - 1mM
Oligomycin	Sigma-Aldrich (O4876)	DMSO	1uM
Quercetin	Selleck Chemicals (S2391)	DMSO	18 - 89uM
Rapamycin	Selleck Chemicals (S1039)	DMSO	500nM
Resazurin	Santa Cruz Biotechnology (sc-206037)	1x PBS	0.02% w/v
Resveratrol (RSV)	Selleck Chemicals (S3168)	DMSO	60uM, 100uM
Rotenone	Sigma-Aldrich (R8875-1G)	DMSO	0.5uM
Rucaparib	Selleck Chemicals (S4948)	DMSO	1-10uM
Rutin	Nuchido Ltd.	DMSO	4 - 74uM
Sodium Pyruvate	Sigma-Aldrich (P5280)	dH_2O	1mM
(tert-butyl hydroperoxide) tbh7ox	Sigma-Aldrich (458139)	-	20 – 140uM

2.4 Blood Sampling

2.4.1 Participant Recruitment

For the experiments investigating human *in vivo* NAD^+ levels in response to NR and the NCD cocktails, participants were recruited by word of mouth before they were screened for their eligibility to take part. The exclusion criteria for participation was:

- Regular consumption of supplements containing niacin (vitamin B3), niacinamide nicotinamide riboside or nicotinamide mononucleotide
- Food allergies or sensitivities
- Currently taking blood pressure medication
- Currently taking blood thinning medication (e.g. aspirin, warfarin, heparin)
- History or current diagnosis of drug/alcohol abuse
- History of kidney or liver disease, or other severe diseases of the gastrointestinal tract (e.g. iron accumulation, iron utilization disorders, hypercalcaemia, hypercalcaemia), that are likely to interfere with metabolism/absorption/secretion of the product under investigation
- History of neurological or psychiatric illness (excluding depressive illness and anxiety)
- Blood disorders (e.g. anaemia, haemophilia, thrombocytosis)
- Heart disorder, or vascular illness
- Chronic gastrointestinal problems (e.g. Inflammatory Bowel Disease, Irritable Bowel Syndrome, celiac disease)
- Any known active infections
- Diagnosed with or may be at risk of having syphilis, hepatitis, the Human T - lymphotropic virus, the Human Immunodeficiency Virus or any other infectious blood-borne disease (due to the health risk this poses to the phlebotomist)
- Health condition that would prevent fulfilment of the study requirements
- Currently participating in or in the past 3 weeks participated in other clinical or nutrition intervention studies

2.4.2 Blood Collection

All blood samples for the NR study were obtained by venepuncture from the basilic, cephalic or median cubital vein. 8ml of blood was drawn into a vacutainer (sodium heparin, BD), inverted 2-3 times and then immediately placed on ice. For the NCD cocktail studies the baseline and full treatment day blood samples were taken every 2 hours over a 12-hour period (8am – 8pm) by cannulation. All other samples for the NCD cocktail work were collected by venepuncture as for the NR study.

2.4.3 PBMC Isolation

PBMCs (peripheral blood mononuclear cells) were isolated from whole blood immediately following collection of the sample, with the blood and the subsequently isolated PBMCs kept on ice throughout the entire process, unless being centrifuged at 3ºC. 15ml of lymphoprep (Stemcell technologies, Cambridge, UK) was added to a 50ml falcon tube and 8ml of blood gently mixed with 16ml of sterile 1x PBS 2% FBS solution was then carefully layered on top of the lymphoprep, ensuring minimal mixing between the lymphoprep and the diluted blood interface. When the blood obtained was less than 8ml, the process was the same but with the volume of 1x PBS 2% FBS solution added equal to twice the volume of blood.

The lymphoprep/blood containing tube was then centrifuged at 1000xg, 12 minutes, 3°C, with the deceleration set to 0. The PBMCs were then visible as a cloudy layer between the plasma and lymphoprep fractions, allowing them to be extracted by pipetting into a 15ml tube containing 12ml of ice-cold 1x PBS 2% FBS. Plasma was also removed and immediately stored in cryovials at -80°C. The PBMC suspension was then centrifuged at 500xg, 8 minutes, 3°C, with the deceleration returned to the maximum. The subsequent pellet was re-suspended in 400ul 100% FBS and mixed before the addition of an equal volume of 80% FBS 20% DMSO, with the PBMCs then added to a cryovial and placed in a Mr Frosty in the -80°C overnight. The next day the cells were transferred to the -150°C.

2.5 NAD^+ Measurements

NAD^+ measurements were performed following an optimised protocol using a commercially available kit (NAD/NADH Glo, Promega, Southampton, UK). For *in vivo* measurements, 1 human sample from each study visit was assayed as technical duplicates. For *in vitro* measurements, 3 culture plate technical replicates for each condition were assayed in duplicate. The experiment was repeated and the average of the experimental means was used to give the data presented herein.

2.5.1 NAD^+ Measurements in PBMC, Blood and Plasma Samples

For *in vivo* measurements, PBMCs were thawed on ice and then added to 20ml ice cold 1x PBS before being centrifuged at 600xg, 8 minutes, 3°C. The pellet was then resuspended in 200ul of 1x PBS, before 10ul of this suspension was then added to 90ul 1x PBS, giving a final concentration of 200,000-400,000 cells/ml. In a white, flat-bottomed 96-well plate 20ul of each biological sample was then added to a well containing 20ul of 0.2M NaOH 1% Dodecyltrimethylammonium bromide before 20ul of 0.4M HCl was added. The plate was sealed with parafilm and then incubated at 60°C for 15 minutes, before being allowed to cool for 10 minutes at RT after which 20ul of 0.5M Trizma was added to each well. 40ul of each well was then added to the adjacent well leaving a total volume of

40ul in all wells, to which 40ul of freshly prepared 'glo reagent' (made up using reagents provided with the kit) was added. The plate was kept in the dark at room temperature for 30-45 minutes before luminescence was read using a luminometer (Spark 10M, Tecan, Mannedorf, Switzerland) with an integration time of 1 second per well. An NAD^+ standard curve containing concentrations from 5nM – 400nM made by diluting lyophilised NAD^+ in 1x PBS was also added to the plate alongside the samples, allowing the concentration of NAD^+ for each sample to be calculated. Subsequently, a BCA (bicinchoninic assay) assay was performed so that NAD^+ could be normalised to protein concentration.

To prepare samples for protein quantification, 10x RIPA (radio-immunoprecipitation) buffer (100 mM Tris-Cl pH 8.0, 1% sodium deoxycholate, 1% SDS, 10% Triton X-100, 1.4M NaCl) was then added to the remaining cell suspensions which were vigorously vortexed and then left on ice to lyse for 30 minutes. The supernatant was then collected and the pellet discarded after centrifuging at 12,000xg, 12 minutes, 3°C. After diluting the supernatant 3-fold in 1x PBS, a micro-BCA assay (micro-BCA assay kit, Thermo Fisher Scientific, Paisley, UK) was performed at 37°C for 2-6 hours and the absorbance at 562nm read using a plate reader (FLUOstar Omega, BMG Labtech, Aylesbury, England). The ng NAD^+/ml for each sample was then divided by the ug/ml total protein such that the NAD^+ levels were subsequently expressed as ng NAD^+/ug protein.

2.5.2 NAD^+ Measurements in Primary Derived Cells and Cell Lines

For the *in vitro* NAD^+ measurements, adherent cells were washed 3 times in the well-plate using ice cold 1x PBS before being scraped off in 1x PBS, collected in an Eppendorf tube and then immediately frozen at -80°C. For the Jurkat cell line, the cells were collected by centrifugation at 300xg for 5 minutes, re-suspended in 1x PBS and once again pelleted by centrifugation. The cells were then re-suspended in 200ul of 1x PBS and frozen at -80°C. On the day of the assay, cells were thawed on ice and the protocol conducted as for the *in vivo* measurements. For NHDFs cells were diluted in 100ul 1x PBS to a final concentration of 50,000-100,000 cells/ml whereas they were diluted to 200,000-400,000 for the Jurkats.

2.6 Energy Metabolism Assays

2.6.1 OXPHOS – Mitochondrial Stress Assay

Parameters of OXPHOS were assessed using the 'Seahorse XF cell mito stress test' programme on the Seahorse XFp Analyser (Agilent, Stockport, UK), whereby OXPHOS activity is measured by the change in O_2 concentration (pmol O_2/min) within the cell media. Cells were seeded down in a 6-well or 24-well plate and the experimental conditions set up accordingly. 24 hours before the assay, cells

in the 6-well or 24-well plate were trypsinised and seeded down in a seahorse miniplate at a concentration of 2000-3000 cells/well before being centrifuged at 600xg for 2 minutes to promote adherence. The remaining cells were re-plated onto a 6-well/24-well plate. Experimental conditions in the seahorse miniplate were set up to replicate those of the 6-well and 24-well plates, whilst the seahorse cartridge was hydrated in XF calibrant (Agilent, Stockport, UK) overnight. On the day of the assay, the cells in the miniplate were washed twice with seahorse XF base media (Agilent, Stockport, UK) and incubated at 37°C, no CO_2 in seahorse base media supplemented with 10mM D-glucose, 2mM L-glutamine and 1mM sodium pyruvate.

10x stocks of 10uM oligomycin, 10uM FCCP (carbonyl cyanide-p-trifluoromethoxyphenylhydrazone) and 5uM rotenone/antimycin A were freshly prepared in the seahorse base media and then loaded into the seahorse cartridge such that oligomycin would first be added to the wells, followed by FCCP and finally rotenone/antimycin A. The assay was then run under the machine programme 'mito stress test'. The cells in the 6-well/24-well plate with identical experimental conditions in parallel were then lysed in 1x RIPA buffer in preparation to be used for western blotting.

After completion of the mitochondrial stress test, the cells in the seahorse miniplate were washed twice in ice cold 1x PBS and then lysed in 1x RIPA buffer for 30 minutes, before the supernatant was collected and the pellet discarded. The supernatant was then diluted 6-fold in 1x PBS, allowing a micro BCA assay to then be performed to determine the protein content within each sample. Once the protein content was calculated, the OCR (oxygen consumption rate) values generated by the mitochondrial stress test were divided by the total protein such that the results were expressed as OCR/ug protein.

'Basal respiration' was then calculated by subtracting the OCR/ug protein after oligomycin treatment from the OCR/ug protein after the addition of rotenone/antimycin A. The difference in OCR/ug following the FCCP treatment and antimycin A/rotenone treatments constituted 'maximal respiration', whilst 'respiratory reserve' was the difference in the basal and post FCCP addition OCR/ug. Finally, ATP production was determined by calculating the difference between the basal and post oligomycin OCR/ug protein.

2.6.2 Glycolysis - Glycolysis Stress Assay

Parameters of glycolysis were measured using the 'Seahorse XF glycolysis stress test' protocol on the Seahorse XFp Analyser. Experiments were set up in a seahorse miniplate using the same protocol as the OXPHOS assays, however the media used was seahorse base media supplemented with only 2mM L-glutamine. 10x stocks of 100mM D-glucose, 10uM oligomycin and 500mM 2-DG (2-

deoxyglucose) were freshly prepared in seahorse media and added to the sensor cartridge such that during the assay D-glucose would be added first to the wells, followed by oligomycin and then 2-DG. The XFp analyser then measured the basal ECAR (extracellular acidification rate – mpH/min) and the ECAR following the addition of the compounds mentioned for each well in the miniplate.

As for the OXPHOS assays, protein content was calculated for each miniplate well by performing a micro BCA assay, allowing glycolytic parameters to be expressed as ECAR/ug protein. Levels of 'basal glycolysis' were calculated by subtracting the ECAR following 2-DG treatment from the ECAR after glucose addition. 'Glycolytic capacity' was the difference in the ECAR/ug protein` following 2-DG and oligomycin addition, whilst 'glycolytic reserve' was the difference in the ECAR/ug protein between the glucose and oligomycin treatments.

2.7 Western Blotting

2.7.1 Protein Extraction

Well plates containing cells were transferred to ice and the cells were washed twice in ice cold 1x PBS before 1x RIPA buffer (10 mM Tris-Cl pH 8.0, 0.1% sodium deoxycholate, 0.1% SDS, 1% Triton X-100, 140mM NaCl) was added to each well (24 well plate – 40ul, 12 well plate – 60ul, 6-well plate – 100ul). The cells were then scraped from the plate and collected in 500ul Eppendorf tubes before being kept on ice for 30 minutes to promote cell lysis. The lysates were then centrifuged at 12,000xg, 12 minutes, 3°C and the supernatant was added to a fresh tube whilst the pellet of debris was discarded. A 10ul sample of the supernatant was used to perform a BCA assay (Pierce BCA assay kit, Thermo Fisher Scientific, Paisley, UK) to determine protein concentration, which was read at an absorbance of 562nm using a plate reader (FLUOstar Omega, BMG Labtech, Aylesbury, UK). The amount of each sample required to load 20ug protein was then calculated and 6x laemmli buffer (375 mM tris-HCl pH 6.8, 6% SDS, 4.8% glycerol, 9% 2-mercaptoethanol, 0.03% bromophenol blue) added to a final concentration of 1x, before samples were then stored at -20°C for <6 months prior to western blotting.

2.7.2 SDS-PAGE

On the day of running the SDS-PAGE gel, the lysates in laemmli were thawed on ice before being boiled at 90°C for 5 minutes using a heating block. For 10 and 15-well assays, samples were run on a 10% acrylamide gel with a 6% acrylamide stacking gel at a constant voltage of 100V in 1x running buffer (25Mm Tris, 192mM glycine, 0.1% SDS) until the dye front reached the bottom of the gel. For 16-24 well assays, samples were run on precast 26-well gels (cat no. 5671085, Bio-Rad, Watford, UK) at a constant voltage of 185V, once again until the dye front reached the bottom of the gel.

2.7.3 Western Blot Transfer

After completion of the SDS-PAGE, the gel was rinsed in dH_2O and the protein was then transferred to a nitrocellulose membrane (0.45um cat no. 1620115, Bio-Rad, Watford, UK) in 1x transfer buffer (25mM Tris, 192mM glycine, 20% MeOH) at a constant voltage of 30V for 19 hours at 4°C. For regular size gels, a Mini Trans Blot-Cell (cat no. 1703935, Bio-Rad, Watford, UK) was used, whereas the Trans-Blot Cell (cat no. 1703939, Bio-Rad, Watford, UK) was used for 26-well gels.

2.7.4 Immunoblotting

The blot was then rinsed in dH_2O and left to air dry for 45-60 minutes before loading and transfer quality was inspected by incubating the blot in ponceau red solution (0.1% Ponceau S, 0.5% acetic acid) on a rocker for 5-10 minutes and then washing off background staining by rinsing 2-3 times in dH_2O. Images of the ponceau staining were then taken using a printer scanner after wrapping the blot in clingfilm. The blot was then repeatedly washed in 1x TBST (50mM Tris, 125mM NaCl, 0.1% tween 20) until no ponceau stain was visible. Next, the blot was blocked in 5% milk (skimmed milk powder, Tesco) diluted in 1x TBST for 1 hour at RT, before being incubated in the primary antibody on a roller at 4°C, overnight. All primary antibodies were diluted in 5% milk and used at the concentrations specified in Table 2.7.4.1.

After staining in the primary antibody, blots were washed on a rocker for 5 minutes 3 times in 1x TBST and then incubated in the appropriate secondary antibody, diluted in 5% milk (see table 1 for concentrations) for 1-2 hours on a roller at RT. Blots were then once again washed for 5 minutes, 3 times in 1x TBST before being imaged using either ECL Western Blotting Detection Reagent (cat no. 10754557, GE Healthcare, Chalfont St Giles, UK) or Pierce Super Signal West Dura (cat no. 34075, Thermo Fisher Scientific, Paisley, UK) on an imaging platform (Chemi G:Box, Syngene, Cambridge, UK).

Table 2.7.4.1 Antibodies used for western blotting.

Primary antibody target	Manufacturer (cat no.)	Concentration (epitope species)	Secondary antibody (concentration/species)
Acetylated H3 (Ac-H3)	Sigma (06-942)	1.3000 (human), 1.5000 (mouse)	1.3000 anti-rabbit HRP
Acetylated P53 (Ac-P53)	Cell Signalling Technology (2570)	1.500 (human), 1.1000 (mouse)	1.1000 anti-rabbit HRP
α-tubulin	Abcam (ab4074)	1.5000 (human, mouse)	1.2000 anti-rabbit HRP
α-SMA	Abcam (ab5694)	1.3000 (human, mouse)	1.2000 anti-rabbit HRP
β-catenin	Santa Cruz (H-102)	1.2000 (human, mouse)	1.2000 anti-rabbit HRP
BMAL1	Abcam (ab93806)	1.3000 (human)	1.3000 anti-rabbit HRP
BMAL1	Gift from Imperial College London	1.2000 (mouse)	1.2000 anti-mouse HRP
Collagen I	Abcam (ab138492)	1.2000 (human, mouse)	1.2000 anti-rabbit HRP
Glutaminase C/KGA	Proteintech (12855-1-AP)	1.1000 (human)	1.2000 anti-rabbit HRP
Hexokinase II	Abcam (ab104836)	1.1000 (human)	1.2000 anti-mouse HRP
Histone H3	Abcam (ab1791)	1.6000 (human, mouse)	1.5000 anti-rabbit HRP
NAMPT	Proteintech (11776-1-AP)	1.1000 (human, mouse)	1.2000 anti-rabbit HRP
NRF2	Abcam (ab137550)	1.500 (human)	1.1000 anti-rabbit HRP
PARP1	Bio-Rad (VMA00016)	1.2000 (human, mouse)	1.2000 anti-mouse HRP
PAR	Trevigen (4336-BPC-100)	1.2000 (human)	1.2000 anti-rabbit HRP
PGC-1α	Calbiochem (AB3242)	1.1000 (human)	1.2000 anti-rabbit HRP
P53	Cell Signalling Technology (1C12)	1.500 (mouse)	1.2000 anti-mouse HRP
P53	Proteintech (10442-1-AP)	1.1000 (human)	1.1000 anti-rabbit HRP
SIRT1	Abcam (ab32441)	1.2000 (human, mouse)	1.2000 anti-rabbit HRP
SIRT3	Santa-Cruz (F-10)	1.500 (human) 1.400 (mouse)	1.2000 anti-mouse HRP

2.7.5 Re-Probing Blots

Blots were stripped for re-probing where necessary by two methods. When preparing to probe using a primary of different species to the one used previously, the HRP (horseradish peroxidase) bound to the previous antibody was inactivated by incubating overnight in 10% NaN_3, 1x TBS solution before being washed 6 times for 5 minutes in 1x TBST and then blocked in 5% milk, 1x TBST. Alternatively, the blot was incubated in 'harsh stripping buffer' (62.5mM Tris-HCl pH 6.8, 2% w/v SDS, 0.8% 2-mercaptothanol) at 60ºC for 40 minutes with gentle shaking of the blot container every 5 minutes. The blot was then left under running tap water for 5 minutes before being washed 6 times for 5 minutes in 1x TBST to remove all traces of 2-mercaptoethanol and SDS, thus allowing the blocking step to begin in preparation for the next primary antibody to be used.

2.7.6 Densitometry Analysis

Where a fully quantitative analysis of western blots was required, densitometry was performed on the specific bands of interest. The protein ladder was used as a reference to determine the bands of interest on blots where non-specific bands were present. Images saved as TIF files were then opened using ImageJ software (downloaded from imagej.nih.gov/ij/). The images were converted to greyscale and a rectangular box drawn such that it covered the first sample lane on the blot. A duplicate of this box was then copied onto all the other lanes on the blot, with each separate box numerically labelled. Using the 'straight line' tool, a line was drawn above the background signal for the peak corresponding to the band of interest within each lane when opening the 'plot lanes' profile. The 'wand' tool was then selected and used to click on these peaks within the plot lanes window. After selecting 'label peaks', a value for the relative density of all peaks is provided, whereby the density of each peak is expressed as a % of the density of all peaks combined.

2.8 qPCR

2.8.1 RNA Isolation

Prior to and during the RNA extraction procedure pipettes, bench top, fumehood and gloves were cleaned using RNaseZap (Invitrogen, Thermo Fisher Scientific, Paisley, UK). All gene expression assays were performed on cells grown in 6-well plates so that a sufficient yield of RNA could be obtained. The cells were washed in ice cold 1x PBS before 1ml of TRIzol (Invitrogen, Thermo Fisher Scientific, Paisley, UK) was added to each well and the cells scraped from the surface of the plate. The cell suspension in TRIzol was then frozen at -80ºC before further processing. Upon thawing, 200ul of chloroform (molecular grade, MP Biomedicals, Fisher Scientific, Loughborough, UK) was added and after 3 minutes the tubes were centrifuged for 15 minutes, at 12000xg, 4ºC. The clear upper phase in the tube was then carefully removed into a new low-binding Eppendorf tube and

incubated for 10 minutes after 500ul of isopropanol (molecular grade, Fisher Scientific, Loughborough, UK) was added. After another 15-minute, 12000xg, 4°C spin the resulting pellet was re-suspended in 1ml 75% ethanol (molecular grade, Fisher Scientific, Loughborough, UK), briefly vortexed and centrifuged for 5 minutes at 7,500xg, 4°C. The supernatant was then removed and the RNA pellet allowed to air dry in a pre-sterilised biosafety cabinet under laminar flow, before another re-suspension in 1ml 75% ethanol and spin for 5 minutes at 7,500xg, 4°C. After air-drying the pellet was re-suspended in 40ul of nuclease free H_2O (IDT, Leuven, Belgium) and placed on ice.

For downstream miRNA analysis DNA was removed by mixing 1ul of extracted RNA with 1ul 10x DNase reaction buffer, 1ul DNase I (both cat no. 18068015, Thermo Fisher Scientific, Paisley, UK) and 7ul nuclease free H_2O. The tubes were then incubated for 15 minutes at RT and then 5ul 25mM EDTA was added to the tube which was incubated at 65°C for 10 minutes to deactivate the DNase.

2.8.2 RNA Yield Quantification

The concentration and purity of RNA samples was assessed by measuring the absorbance at wavelengths of 230nm, 260nm and 280nm on a NanoDrop spectrophotometer (ND-1000, NanoDrop). First, a 1ul aliquot of the RNA sample was diluted by adding to 9ul of nuclease free H_2O and vortexed. 1ul of this dilution was added to the nanodrop and the A260/A230 and A260/A280 ratios were calculated. Only samples with a A260/A230 >1.85 and A260/A280 >2 were subsequently used for cDNA synthesis. The A260 value was multiplied by 40 to determine the concentration of RNA in ug/ml.

2.8.3 cDNA Synthesis From mRNA

The Maxima First Strand cDNA Synthesis Kit (cat no. K1671, Thermo Fisher Scientific, Paisley, UK) was used to convert RNA to cDNA, with 200 – 600ng of RNA typically used as a template for the reaction. The template RNA, 10x dsDNase buffer and nuclease-free H_2O were added to a low binding Eppendorf tube, centrifuged at 200xg, 30 seconds and incubated at 37°C for 3 minutes. The 5x reaction mix, RT enzyme mix and nuclease-free water were then added and the tubes incubated in a thermocycler with a 10 min 25°C first step, followed by 15min at 50°C and finally 5 min at 85°C. The cDNA product was then immediately used for qPCR with the remaining cDNA stored at -80°C.

2.8.4 cDNA Synthesis From miRNA

cDNA synthesis for miRNA expression assays were performed using the TaqMan™ MicroRNA Reverse Transcription Kit (cat no. 4366596, Thermo Fisher Scientific, Paisley, UK). Prior to reverse transcription, RNA samples were diluted into the 200ng/ml – 2ug/ml range using nuclease free H_2O. 5ul RNA was then mixed with the RT reaction mix and the reverse transcription performed in a

thermocycler under the following conditions: 30 minutes at 16°C, 30 minutes at 42°C and finally 5 minutes at 85°C. The resulting cDNA was then diluted 10-fold in nuclease free H_2O and used immediately for qPCR, with left over sample stored at -80°C.

2.8.5 qPCR for Gene Expression Analysis

Primers for mRNA targets were re-constituted in 0.1x TE buffer at 20x working concentration and kept at -80°C, before use at a final concentration indicated in Table 2.6.5.1. In a semi-skirted PCR plate (cat no. HSL9645, Bio-Rad, Watford, UK) the primer pairs were added along with mastermix (PrecisionPLUS qPCR mastermix with SYBR, Primerdesign, Camberley, UK), nuclease-free H_2O and cDNA (20-80ng). All samples used were biological triplicates and run as technical duplicates. The plate was sealed with an optical adhesive seal (cat no. 4360954, Thermo Fisher Scientific, Paisley, UK) and briefly centrifuged at 100xg to collect the mix at the bottom of the wells. Using a Bio-Rad CFX96 thermocycler, qPCR was then performed under the following conditions: 2 minutes at 95°C 1x cycle, then 10 seconds 95°C and 60 seconds 60°C for 40x cycles, with fluorescence detection using the FAM channel.

2.8.6 qPCR for miRNA Expression Analysis

The miR-155 or miR-191 (housekeeping miRNA gene) primers (Table 2.6.5.1) were added to wells of an optical PCR plate (cat no. 4346907, Thermo Fisher Scientific, Paisley, UK), before mastermix (TaqMan™ Fast Advanced Master Mix with ROX, Thermo Fisher Scientific, Paisley, UK), nuclease free H_2O and cDNA (diluted 20-fold) were also added. All samples used were biological triplicates and run as technical duplicates. The plate was sealed with an optical adhesive (Thermo Fisher Scientific, Paisley, UK) and briefly centrifuged to collect the mix at the bottom of the wells. The qPCR was then performed on a qPCR thermocycler (StepOne Plus, Applied Biosystems, Carlsbad, USA) under the following conditions: 2 minutes at 50°C for 1x cycle, 20 seconds at 95°C 1x cycle, then 3 seconds at 95°C and 30 seconds at 60°C for 40x cycles, with fluorescence measured through the ROX channel. Prior to analysis of the data the threshold value of the amplification plot was adjusted to 0.2 and the C_q values of the no template control wells checked for non-specific amplification.

2.8.7 Analysis of qPCR Data

qPCR data for mRNA and miRNA levels was analysed by the '$2^{-\Delta\Delta Ct}$ method' [299]. After calculating the $2^{-\Delta\Delta Ct}$ values, these were converted back to the linear scale by taking the log2 of each value.

Table 2.8.1 Primers used for qPCR.

Primer	Forward Sequence (5'-3')	Reverse Sequence (5'-3')	Working Concentration
ARNTL1 (human)	GGAAAAATAGGCCGAATGAT	GAGCCTGGCCTGATAGTAG	250nM
18S rRNA (human)	AGGAATTGACGGAAGGGGACCAC	GTGCAGCCCCGGACATCTAAGG	200nM
ARNTL1 (mouse)	GCCTACTATCAGGCCAGGCTCA	AGCCATTGCTGCCTCATCATTAC	400nM
18S rRNA (mouse)	GTCCTGGGTTCTGCATGATG	CATTAAGGGCGTGGCGCGG	250nM
miR-155 (mouse)	Unknown (ID 002571, Thermo)	-	500nM
MiR-191 (mouse)	Unknown (ID 002576, Thermo)	-	500nM

2.9 Cell Viability/Proliferation Assays

2.9.1 Alamar Blue Cell Viability Assay

Cell viability was quantified by the alamar blue assay, which involves incubating cells in a solution containing 0.02% resazurin (Santa Cruz Biotechnology). Resazurin is a non-toxic, cell permeable dye which can be irreversibly reduced to the highly fluorescent resorufin in the presence of the reducing agents NADH and NADPH. Consequently, the accumulation of resorufin and the fluorescence it emits corresponds to the presence of NADH and NADPH, which themselves correlate with metabolically active cells and hence provide a readout of viability. It should be noted that resorufin induced fluorescence doesn't allow quantification of total NADH and NADPH per se, but rather reflects their rate of turnover – as occurs during metabolism.

All alamar blue assays were set up in 96-well plates under normal culture conditions. 4 hours prior to the measurement of fluorescence, 90% of the wells' media volume was discarded and then replaced with fresh media, which was repeated once more. 10% of the wells' volume was then discarded and replaced with 0.2% resazurin solution, thus giving a final concentration of 0.02% resazurin. The 0.2% resazurin was made fresh on the day of the assay by diluting a 2% resazurin 1x PBS stock 10-fold in culture media. The plate was then returned to the incubator for approximately 4 hours after which the fluorescence was then read on a plate reader (Spark 10M, Tecan, Mannedorf, Switzerland) at an excitation wavelength of 560nm and emission wavelength of 590nm. After subtracting the blank average (wells with just media and no cells) fluorescence from all wells on the plate, the fluorescence for each well was expressed as a percentage of the untreated control (each column on the well plate has its own individual untreated control), which was taken as a readout for viability.

All viability analysis involved the use of technical triplicates, with the mean % viability of the untreated control calculated by averaging the means of two separate biological experiments. Because of the day to day variability that can occur when using tbh7ox, the replicate biological experiments using tbh7ox were performed simultaneously, using different flasks of NHDFs for each experiment (different by <5 passages) and different diluted stocks of tbh7ox.

2.9.2 XTT Cell Proliferation Assay

The XTT (2,3-bis-(2-methoxy-4-nitro-5-sulphophenyl)-2H-tetrazolium-5-carboxanilide) assay operates on the same principle as alamar blue, functioning as a readout of metabolically active cells. Similar to resazurin, XTT is reduced by reductants such as NADH and NADPH, however this occurs at the plasma membrane given XTT isn't cell permeable. To overcome this, PMS (phenazine methosulfate) or menadione is used as an electron-carrier intermediate within XTT assays to transfer electrons from NADH or NADPH to XTT, resulting in the conversion of XTT to the orange-coloured dye formazan. In the context of cell proliferation, changes in absorbance due to formazan build up correspond to the extent of cell proliferation, given more proliferation results in more metabolically active cells and hence more XTT reduction. Hence XTT and alamar blue assays can be used for both cytotoxicity and proliferation analysis.

The XTT assay was found to be more sensitive and consistent than the alamar blue assay, however the cost of this assay was far more expensive than using alamar blue. Therefore, as a compromise alamar blue was used exclusively for the cytotoxicity assays which constituted a much greater volume of work, whereas XTT was used for cell proliferation analysis.

To perform the assay, XTT (Sigma-Aldrich, Gillingham, UK) was diluted in DMEM (no phenol red, Gibco, Thermo Fisher Scientific, Paisley, UK) to a final concentration of 1mg/ml, whilst a 950ng/ml PMS (Sigma-Aldrich, Gillingham, UK) 1x PBS solution was also added to the same tube at a final concentration of 9.5ng/ml, constituting a 5x XTT working reagent. This working reagent was stored as single use aliquots at -20°C and thawed at 56°C on the day of the assay.

4 hours prior to the assay, cells were split and seeded down in a 96-well plate at a density of 4,000 cells/well, before being centrifuged at 300xg for 30 seconds to promote adherence. 6 hours later, in the well-plate 90% of the wells' media volume was discarded and then replaced with fresh media, with this step repeated once more. 20% of the well volume was then discarded and replaced with the XTT working reagent, after which the plates were returned to the incubator.

After 24, 48 or 72 hours the absorbance was read on a plate reader ((FLUOstar Omega, BMG Labtech, Aylesbury, UK) at wavelengths of 450nm and 690nm. The absorbance at 690nm was subtracted from

the 450nm absorbance for each well, and the blank (media with no cells) average (n=3) was then subtracted from all wells on the plate. By comparing the absorbances measured at different timepoints, the relative change in absorbance between the same timepoints indicates relative cell proliferation, which distinguishes this assay from regular viability analysis where only one measurement is made.

2.9.3 CC50 Calculations

CC50 (50% cytotoxic concentration) calculations for the cell viability analysis of NHDFs treated with tbh7ox and/or other compounds was performed using nonlinear regression within the GraphPad Prism software (GraphPad Software, San Diego, USA). The treatment compound concentrations were log transformed and a best curve was generated by the software using the equation: Y=Bottom + (Top - Bottom)/(1 + (IC50/X)^HillSlope). The curve fitting was performed using least squares regression without any weighting. Asymptotic confidence intervals for the CC50 values were calculated using the Prism software at a confidence level of 95%.

2.10 Lactate Assay

Measurement of lactate released into the culture media of TGF-β treated and untreated NHDFs was performed using a commercial L-lactate assay kit (cat no. 8308, Sciencecell, Carlsbad, USA). NHDFs were first seeded in a 24-well plate at a density of 8,000 cells/well and the following day were treated with or without 10ng/ml TGF-β as detailed in section 2.3.10, using DMEM without phenol red (Gibco, Thermo Fisher Scientific, Paisley, UK). 24, 48, 72 and 96-hours following addition of the TGF-β the supernatants in each well (approximately 500ul) were collected and stored at -20°C until the day of the assay.

On the day of the assay, 50ul of each sample (in triplicate) was added to 200ul of the kit assay buffer in a 96-well plate. Additionally, the L-lactate standard provided with the kit was diluted in assay buffer at concentrations ranging from 0.0625 – 2mM, with 50ul of each standard added to 200ul assay buffer (in duplicate) in the 96-well plate along with two blanks (blank 1 - 250ul assay buffer, blank 2 – 50ul no phenol red DMEM and 200ul assay buffer). 2ul of the kit enzyme mix and 50ul of substrate mix was then added to each well and the absorbance at 490nm measured 20 minutes later using a plate reader ((FLUOstar Omega, BMG Labtech, Aylesbury, UK).

The absorbance value of blank 1 was then subtracted from all standards on the assay plate and the absorbance of blank 2 subtracted from the NHDF supernatants on the plate. Using the equation produced by the standard curve the lactate concentration in the supernatants from the TGF-β treated/untreated NHDFs was then calculated.

2.11 Statistical Analysis

All data presented within this thesis is shown as the mean +/- SD (standard deviation). *In vitro* experiments involving NHDFs were performed using either 2 or 3 biological replicates and typically repeated once or twice (as stated in figure legends). *In vitro* experiments using the miR-155KO and matched WT derived cells were performed using 3 or 4 biological replicates and were repeated once or twice (as stated in figure legends). 4 SSc dermal fibroblasts and 2 or 3 matched control dermal fibroblasts were used for *in vitro* experiments reported in Chapter 6, with these experiments repeated once or twice (as indicated in the figure legend). The mean and SD reported for all in vitro work is calculated from the means of the separate biological experiments (n=2 or n=3), thus the SD is the variability between the separate experiments.

For the *in vivo* work in Chapter 5, one biological sample was collected for each participant study day. Unless otherwise stated, for the treatment days error bars represent the error of two technical replicates, whereas the baseline is the mean and error are calculated from 2 or 3 biological replicates, as indicated in the text.

Student's independent t-tests were used to test for significance when analysing two datasets. In all instances where used, t-tests were two-tailed. For comparison of 3 or more datasets 1-way ANOVA was used, typically followed by a Dunnett's post hoc test where significance between the control group versus all other groups was tested. In some instances where indicated, a Bonferroni post hoc test was performed to compare the means of all experimental groups. In Chapter 5, comparisons were made between datasets of different size, hence repeated measures ANOVA was used to account for this variability.

For timecourse experiments multiple comparisons 2-way ANOVA was performed to test for significance between the experimental groups, timepoints and to identify any interaction between the experimental conditions and time. The 2-way ANOVA was also usually followed by a Dunnett's post hoc test to compare experimental conditions against the control group.

CC50 (50% cytotoxic concentration) calculations were also performed for viability experiments involving treatment with tbh7ox or inhibitors as described in section 2.9.3.

All statistical tests were carried out using the software GraphPad Prism v5 (GraphPad Software, San Diego, USA).

Chapter 3. Interventions to Enhance NAD^+ *In Vitro*

3.1 Introduction

Although renowned for almost a century for its role as an essential cofactor in cellular redox reactions, more recently NAD^+ has gained increasing attention for its participation in other reactions – particularly those implicated in cellular ageing. SIRT1 and PARP1 are enzymes that require NAD^+ for deacetylation and ADP-ribosylation of their substrates respectively, with both these activities thought to combat processes which promote ageing.

SIRT1 is known to upregulate antioxidant defence systems [300-302], stimulate mitochondrial biogenesis [303-305] and dampen inflammation [306-308], whilst PARP1 detects and activates the repair of single strand DNA breaks [309]. Thus, under conditions of reduced NAD^+ as would be expected to occur during ageing [70], it's possible that the capacity of these enzymes would be impaired. Additionally, the accumulation of oxidative damage with age increases PARP1 activity, hence in the presence of lowered NAD^+ this may come at the expense of SIRT1 activity thus exacerbating the decline in cellular function and perpetuating the ageing process. To further investigate this the contribution of PARP1 activity towards NAD^+ depletion in NHDFs was probed, both under basal conditions and also during induced oxidative stress.

Due to the heightened interest around NAD^+'s function as a potentially key biomolecule in ageing, there is an intense search to identify compounds which can enhance NAD^+ levels. At present, supplementation with NAD^+ precursors have proven effective at achieving this goal [152, 310, 311], however in the context of age-related NAD^+ decline precursor accessibility isn't a driving force behind NAD^+ depletion, hence additionally targeting the pathways facilitating the decline would seem the optimal approach. A number of naturally occurring polyphenols (e.g. resveratrol, apigenin) are known to target various enzymes involved in NAD^+ metabolism and pathways affected by ageing, therefore represent leading candidates as potential NAD^+ enhancers. This chapter will explore the capacity of these compounds to enhance NAD^+ levels and improve resistance to oxidative stress – both individually and as a combination.

3.2 Aims

This chapter sets out to assess the ability of compounds targeting important pathways in NAD^+ metabolism to modify NAD^+ levels *in vitro* and whether a multi-compound approach is optimal for the purpose of maximum NAD^+ enhancement. Additionally, identifying whether oxidative stress depletes NAD^+ and if PARP1 can be manipulated to enhance NAD^+ under such conditions is also addressed.

3.3 Hypotheses

The combination of multiple NAD^+ targeting compounds will result in a superior enhancement of NAD^+ compared to the single compound approach. It is expected NAD^+ levels will be downregulated under conditions of oxidative stress, an outcome attenuated in the presence of pharmacological PARP1 inhibition.

3.4 The NAD^+ precursor NAM Enhances NHDF NAD^+ Levels

First it was sought to determine the efficacy of nicotinamide (NAM) at modulating NAD^+ levels in NHDFs. Over a 36-hour timecourse using varying doses of NAM (Figure 3.4.1), the maximal enhancement of NAD^+ levels (measured using an NAD^+ cycling assay) achieved was a 294% increase after 12 hours with 100uM NAM, which failed to achieve statistical significance via 1-way ANOVA due to the high standard deviation (SD) between replicates (SD – 248%). It should be noted that outlier testing using the ROUT (robust regression and outlier removal) method [312] did identify the 100uM dose at 12 hours as the sole outlier in the data set, however the NAD^+ increase recorded for the two individual experiments performed was 470% and 118%, suggesting that despite the high error across the two experiments these conditions do still promote a substantial increase in NAD^+.

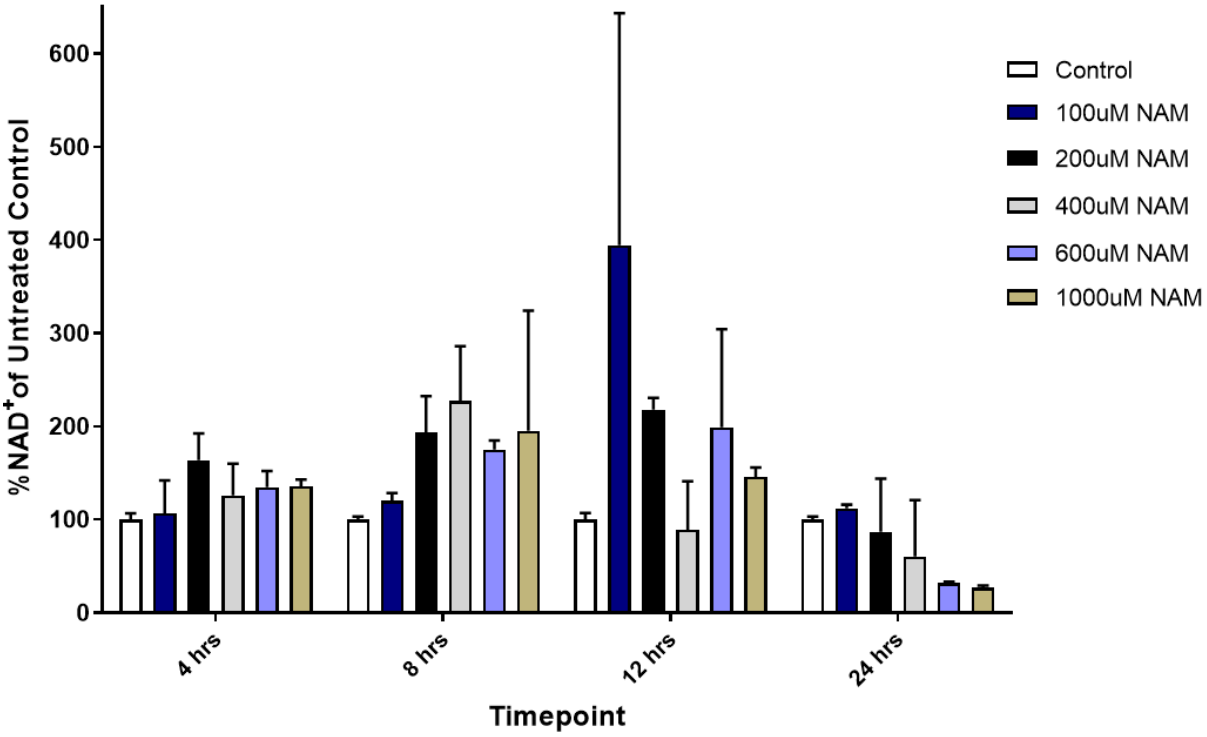

Figure 3.4.1 NHDF NAD^+ levels in response to NAM treatment.
NHDFs were treated with 0, 100, 200, 400, 600 or 100uM NAM for 4, 8, 12, 24 or 36 hours (n=3 technical replicates for all conditions). NAD^+ levels were measured by an NAD^+ cycling assay and normalised to total protein measured via a BCA assay. NAD^+ levels are expressed as the % of the untreated control for each timepoint. 1-way ANOVA was performed for each timepoint and a Dunnett's post hoc test was used to test for significance against the untreated control for each timepoint control. Error bars represent +/- SD. Data shown is the average for 2 separate biological experiments (n=2).

On average, the different doses of NAM increased NAD^+ by 33% after 4 hours, by 82% after 8 hours, 109% after 12 hours and 29% after 48 hours. Additionally, after 24 hours, on average the different NAM doses reduced NAD^+ levels by 36%. 2-way ANOVA found that the NAD^+ levels in response to NAM are both highly time and concentration dependent ($p<0.001$ for both), emphasising the likely

need to optimise dose and concentration when taking a precursor approach to increasing NAD^+ titres.

3.5 NHDF NAD^+ Levels in Response to Dietary Compounds

Resveratrol (RSV) is a polyphenol which previously attracted attention in the ageing field due to a number of studies highlighting its ability to attenuate age-related markers [63, 164, 313, 314], with activation of SIRT1 believed to be the dominant mechanism. How it activates SIRT1 remains controversial, with some suggestions it occurs via increased NAD^+ [315], whilst other studies endorse increased *SIRT1* transcription [316] or direct protein binding [317] as the mechanisms responsible. Apigenin is another polyphenol which has demonstrated a capacity to enhance NAD^+ [156] courtesy of its ability to inhibit CD38: a highly inefficient consumer of NAD^+ whose activity is upregulated with age [318].

To determine whether they were capable of increasing NAD^+ in NHDFs, RSV was added to NHDFs at doses of 60uM and 100uM and apigenin at doses of 10uM, 20uM and 50uM for 12, 24 and 48 hours (Figure 3.5.1). These doses were determined to constitute the appropriate range given previous experiments performed using RSV and apigenin within the former research group of Prof Dianne Ford and the other studies which have used these compounds in vitro [319-323]. It should be noted however that these doses are higher than what could ever be achieved in vivo, which is a limitation of this work.

RSV was unable to induce any significant enhancement in NAD^+, with a 34% decrease ($p<0.05$) at 100uM after 24 hours the only notable difference. 50uM apigenin was able to significantly enhance NAD^+ after 12 hours (56% increase, $p<0.05$), with non-significant increases of 23% after 24 hours and 20% after 48 hours also recorded for this dose.

Two other dietary compounds which previous studies have shown to be key regulators of metabolic and NAD^+ related pathways are alpha lipoic acid (ALA) [324, 325] and quercetin [156, 326]. ALA primarily functions as an antioxidant which can also promote mitochondrial biogenesis and OXPHOS [327], hence would be expected to modulate NAD^+ via the latter. There is also evidence that quercetin may increase mitochondrial function via the upstream activation of AMPK [328], which combined with its previously demonstrated ability to inhibit the NADases CD38 [156] and CD73 [329] implies there are multiple mechanisms by which it could potentially upregulate NHDF NAD^+ levels.

It was therefore surprising to find that 100uM ALA significantly decreased NAD^+ after 4 hours (58% decrease, $p<0.001$), 8 hours (25% decrease, $p<0.05$) and 16 hours (23% decrease, $p<0.01$), before rising just above basal levels after 24 hours (16% increase, non-significant) (Figure 3.5.2 A). Interestingly, for the first 3 timepoints NAD^+ levels also appear to somewhat decrease in a dose dependent manner. Contrastingly, quercetin was able to significantly enhance NHDF NAD^+ levels (Figure 3.5.2 B), however this was limited to doses of 27uM (27% increase, $p<0.01$) and 89uM (23% increase, $p<0.05$) after 8 hours of treatment. Consequently, quercetin mediated upregulation of NHDF NAD^+ levels is short-lived, showing similarity to apigenin which is especially noteworthy given they both share CD38 as a prominent target.

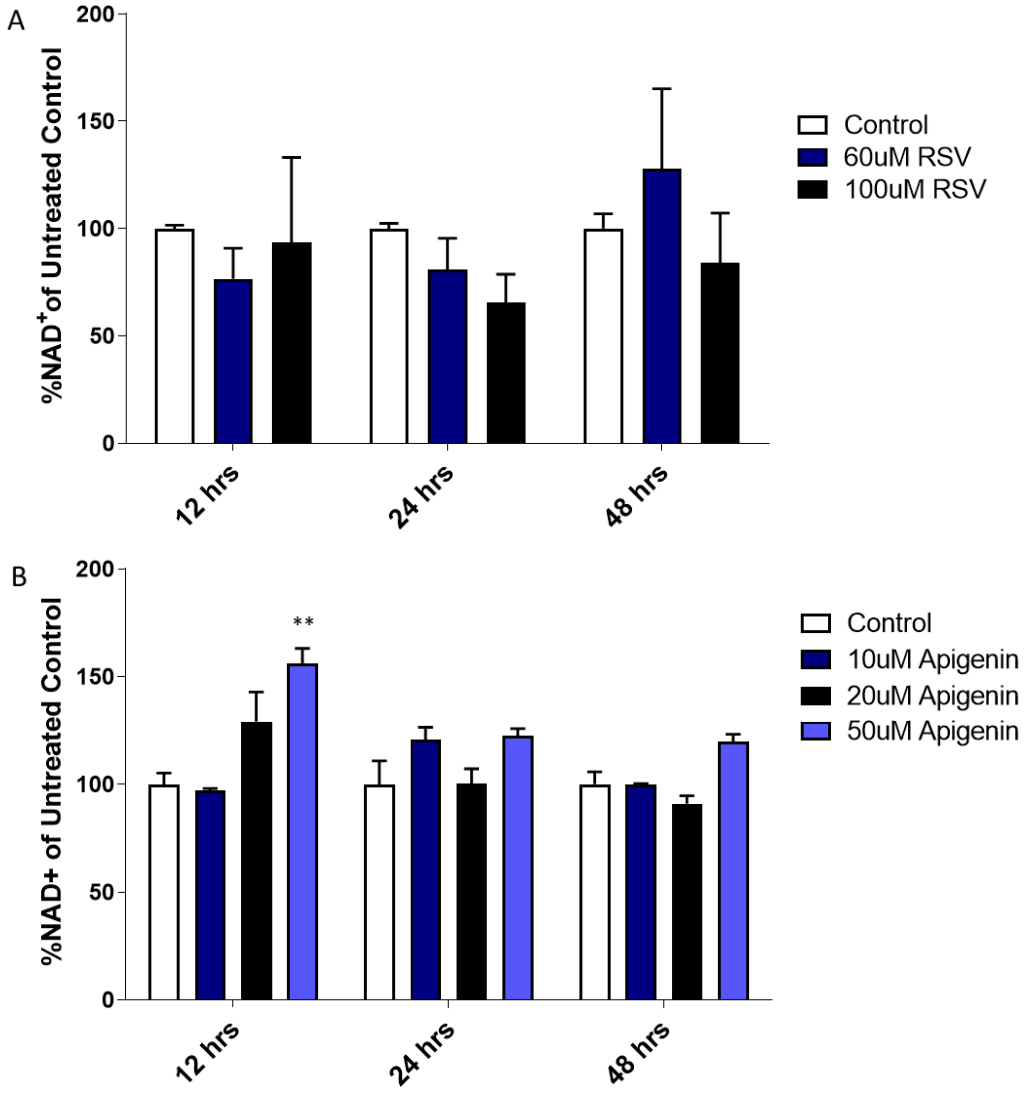

Figure 3.5.1 NHDF NAD^+ levels in response to RSV and apigenin treatment.
(A) NHDFs were treated with 60uM RSV, 100uM RSV or 0.1% DMSO for 12, 24 and 48 hours (n=3 technical replicates for all conditions). (B) NHDFs were treated with 10uM, 20uM or 50uM apigenin or 0.05% DMSO for 12, 24 and 48 hours. NAD^+ levels were measured by a cycling assay and normalised to protein via a BCA assay. NAD^+ levels are expressed as the % NAD^+ of the DMSO treated control for each timepoint. 1-way ANOVA was performed for each timepoint and a Dunnett's post hoc test was used to test for significance against the DMSO control. Error bars represent +/- SD. Data shown is the average for 2 separate experiments (n=2).

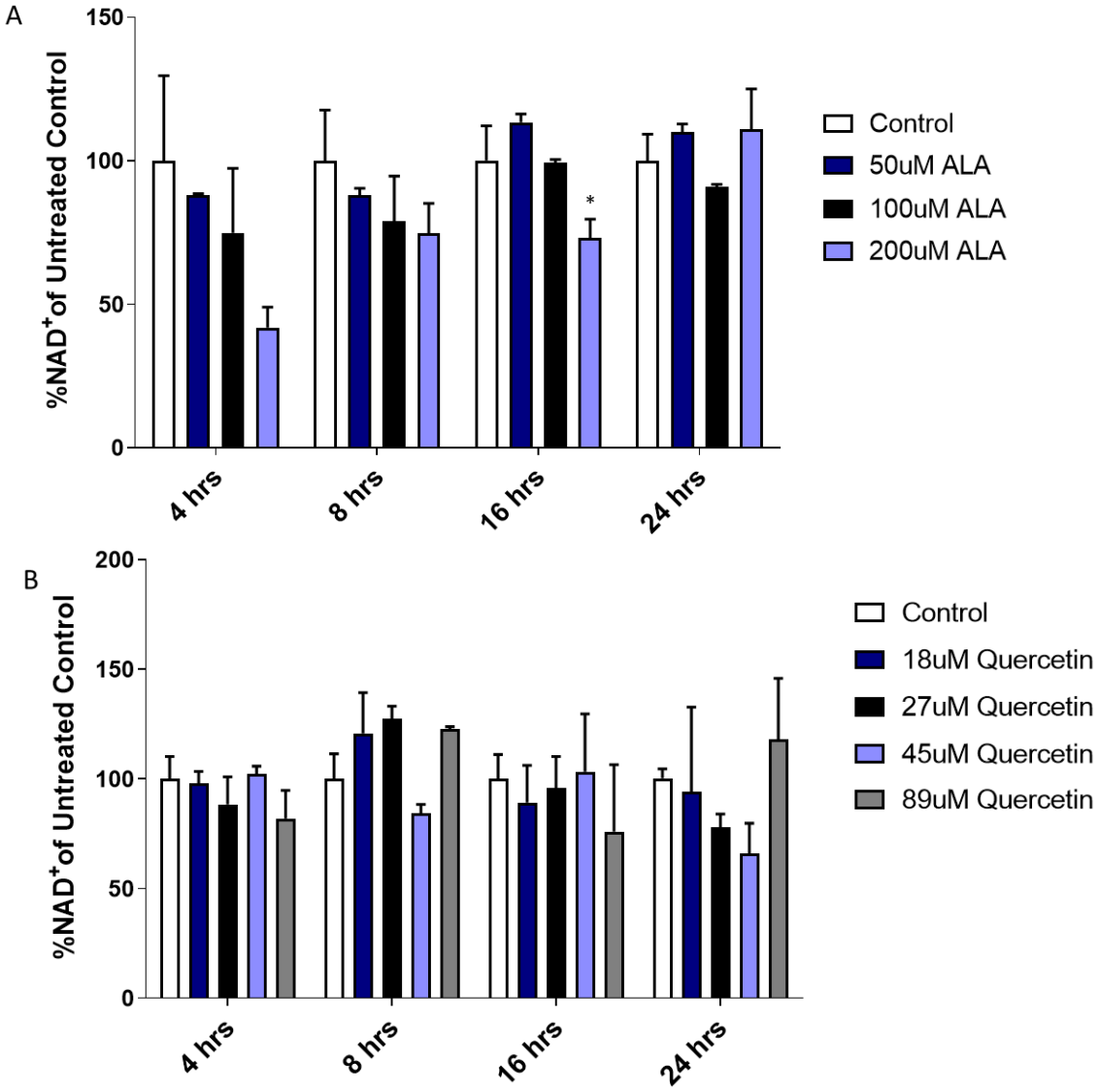

Figure 3.5.2 NHDF NAD⁺ levels in response to ALA and quercetin treatment.
(A) NHDFs were treated with the ALA (A) and quercetin (B) doses indicated along with 0.1% DMSO (only for quercetin) for 4, 8, 16 and 24 hours (n=3 technical replicates for all conditions). NAD⁺ levels were measured by a cycling assay and normalised to protein via a BCA assay, shown here as % NAD⁺ of the 0.1% DMSO/untreated control for each timepoint. 1-way ANOVA was performed for each timepoint and a Dunnett's post hoc test was used to test for significance against the untreated/DMSO control. Error bars represent +/- SD. Data shown is the average for 2 separate biological experiments (n=2).

3.6 The Multi-Targeted Intervention NTC Increases NAD⁺ in NHDFs but not Jurkat Cells

Next, a combination of dietary compounds including those tested thus far was used to explore whether a multi-targeted supplement approach could offer superior enhancement of NAD⁺ levels *in vitro*, as hypothesised. The combination (Table 3.6.1) used was based on a formulation developed by an industry collaborator Nuchido Ltd. and is credited to them, hence is termed NTC (Nuchido Time⁺ Cocktail). The ultimate goal was to test the cocktail in human participants, however as a proof of concept it was deemed of use to also assess its efficacy *in vitro*. The Jurkat T lymphocyte cell line was used due to these being a type of PBMC (peripheral blood monocyte) which were the blood cells

planned to be used for the *in vivo* testing. Additionally, NHDFs were also used so that the efficacy of the cocktail could be compared to the results previously obtained for the compounds tested individually.

Compared to NHDFs treated with 0.23% DMSO (the same DMSO concentration as NTC) for each timepoint, the NTC treatment increased NAD^+ levels in the NHDFs by 53% (unpaired student's t-test, p=0.016) after 12 hours and 51% (unpaired student's t-test, p=0.023) after 24 hours, with a 3% decrease at the 48-hour timepoint (Figure 3.6.1 A). Hence, NTC was effective at increasing NAD^+ for 24 hours before losing its potency by 48 hours.

Table 3.6.1 NTC components

Compound	Concentration	Target
Alpha-lipoic Acid (ALA)	100Um	NQO1
Apigenin	50Um	NQO1, CD38
Ascorbic Acid	100uM	-
Epigallocatechin Gallate (EGCG)	2uM	NNMT
Quercetin	18uM	CD73, CD38, NAMPT
Resveratrol (RSV)	20uM	NRK1/2, NMNAT1
Rutin	4uM	NAMPT

Abbreviations: NQO1 - NAD(P)H dehydrogenase (quinone) 1, NNMT - nicotinamide N-methyltransferase, NAMPT - nicotinamide phosphoribosyl transferase, NRK1/2 – nicotinamide riboside kinase 1/2, NMNAT - nicotinamide mononucleotide adenylyl transferase.

In contrast, for the Jurkats no statistically significant increases in NAD^+ tested for by 1-way ANOVA were recorded during the same time interval when comparing NTC and 0.23% DMSO treated cells (Figure 3.6.1 B). Additionally, Jurkats were also treated with 100uM NAM + 0.23% DMSO to compare the NTC combination against a solitary precursor, which also failed to induce any significant NAD^+ enhancement compared to the DMSO treated controls. There was however a 73% increase in NAD^+ for the NTC treated cells after 12 hours, whereas the NAD^+ in the NAM treated Jurkats only increased by 25%.

The favourable effects of the cocktail being limited to the NHDFs was surprising given their lower basal metabolic rate and anticipated lower expression of CD38 being a non-immune cell type, one of the key targets of the cocktail. This does however highlight that a multi-supplement approach will very likely have varying degrees of effectiveness in different cell and thus tissue types when applied *in vivo*.

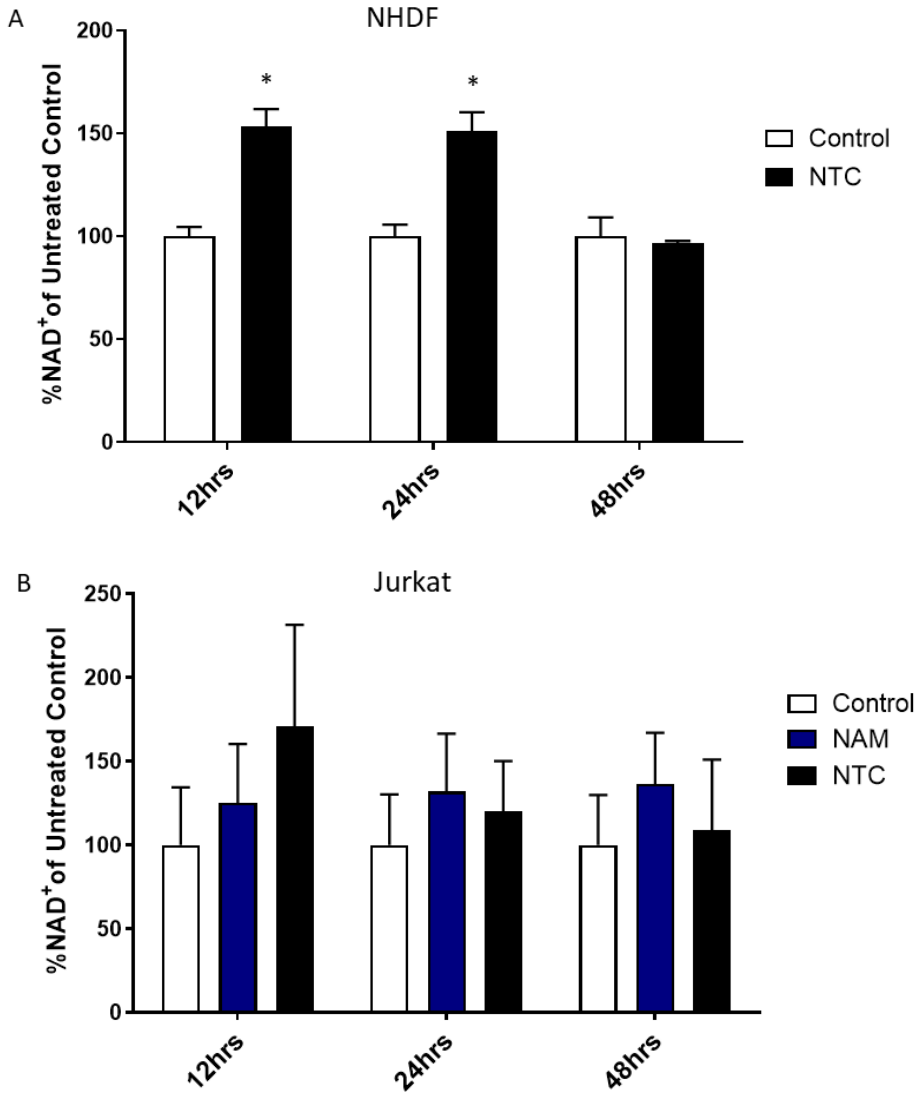

Figure 3.6.1 NTC treated NHDF and Jurkat NAD^+ levels.
(A) NHDFs were treated for 12, 24 and 48 hours with NTC or 0.23% DMSO. (B) Jurkat cells were treated for 12, 24 and 48 hours with NTC, 0.23% DMSO or 0.23% DMSO and 100uM NAM (n=3 technical replicates for all conditions). NAD^+ levels were measured via a cycling assay before being normalised to protein concentration quantified by a BCA assay. Data is shown as % NAD^+ of the DMSO treated control for each timepoint, error bars represent +/- SD. Statistical significance was tested for by an unpaired Student's t-test for panel A and by 1-way ANOVA followed by a Dunnett's post hoc test for all conditions at each timepoint for panel B. *$p<0.05$. Data shown is the average for 2 separate biological experiments (n=2).

3.7 NAD^+ Levels are PARP1 Dependent Under Conditions of Oxidative Stress

To test the hypothesis that PARP1 activity is a key determinant of cellular NAD^+ levels, NHDFs were treated with the specific PARP1 inhibitor rucaparib (AG014699) [330] for 12, 24 and 48 hours (Figure 3.7.2 A). The largest increases were recorded for 1uM and 5uM rucaparib doses after 12 hours, resulting in NAD^+ increases of 32% and 20% respectively compared to the DMSO treated control, without achieving statistical significance.

Although DNA damage is perpetual and thus PARP1 is constitutively active, its activity is easier to assess under conditions of induced DNA damage. The oxidising agent tbh7ox (tert-butyl hydroperoxide) can be used for this purpose by promoting extensive oxidative damage to DNA [331, 332], resembling the type of damage which accumulates during ageing but on a drastically amplified scale. The easiest way to assess PARP1 activity is by measuring levels of poly(ADP-ribosyl) (PAR) which is the moiety PARP1 adds to its substrates in the form of a multi-branched polymer. By measuring protein PARylation via western blotting, a 30-minute incubation in the presence of 40uM tbh7ox is shown to increase PAR levels which is attenuated in NHDFs pre-treated for 24 hours with varying concentrations of rucaparib (Figure 3.7.1 A).

The 10uM rucaparib dose was most effective at reducing PAR levels and thus PARP1 activity, however although statistically insignificant there was small decrease in NHDF viability (5%) for the 10uM rucaparib treatment after 48 hours (Figure 3.7.1 B), hence it was decided 5uM rucaparib was the optimal concentration to use for further PARP1 inhibition experiments.

To determine whether PARP1 inhibition could alter NAD^+ levels under conditions of oxidative stress, NHDFs were treated with a low dose (40uM) or high dose (100uM) of tbh7ox following a 24-hour incubation with 5uM rucaparib or 0.1% DMSO. The cells were then harvested at various timepoints following the tbh7ox insult and NAD^+ levels subsequently measured, before being expressed as a % of the non-tbh7ox treated control at each timepoint (Figure 3.7.2 B and C). Interestingly, as determined by 2-way ANOVA rucaparib was able to significantly increase NAD^+ following the low dose of tbh7ox ($p<0.05$), with this effect greatest after 24 hours where the NAD^+ levels were 90% higher in the rucaparib treated NHDFs ($p<0.05$).

Contrastingly, the NAD^+ levels were reduced in response to rucaparib following treatment with 100uM tbh7ox, with significant differences recorded for 60-minute and 120-minute tbh7ox incubations (both $p<0.01$) as measured by 2-way ANOVA. This was likely due to the visibly increased presence of dead floating cells that occurred within the rucaparib treated NHDFs due to their inability to repair extensive oxidative DNA lesions under conditions of PARP1 inhibition. Hence, it

appears that lower levels of oxidative stress induce NAD^+ depletion via increased PARP1 activity, however under conditions of high oxidative stress PARP1 inhibition fails to reverse this decrease due to the cytotoxic effect of combining PARP1 inhibition and severe oxidative damage: thus depleting NAD^+ via cell death.

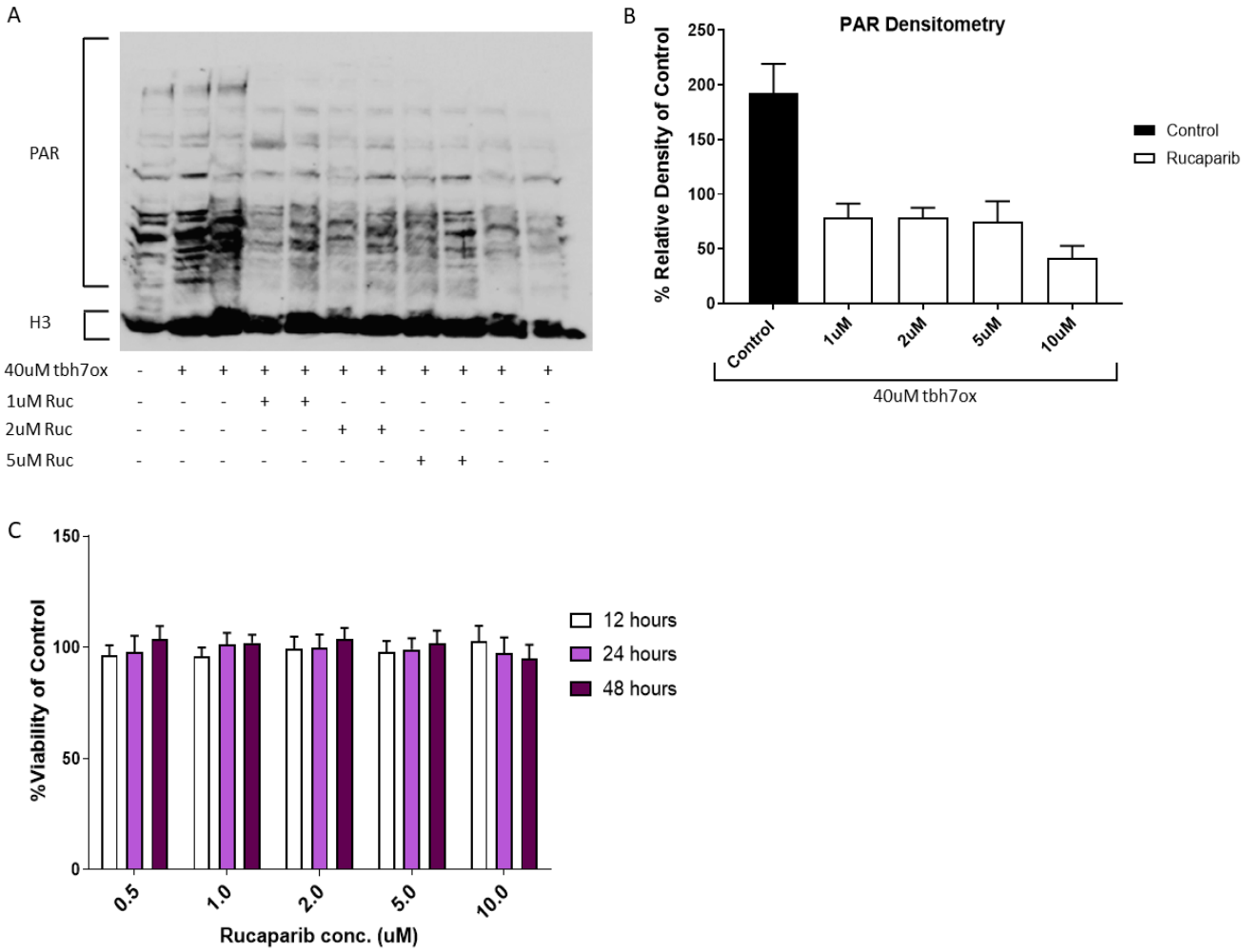

Figure 3.7.1 Rucaparib inhibits tbh7ox induced PARylation.
(A) NHDFs were treated for 24 hours with the concentrations of rucaparib indicated, after which 40uM tbh7ox was added for 30 minutes. The NHDFs were collected and the extent of PARylation was probed by western blotting using an anti-PAR antibody and H3 as a loading control. The image shown is representative of 3 separate biological experiments. (B) Densitometry analysis was performed for the blots (n=3) using ImageJ software, with PAR staining density for all conditions treated with tbh7ox expressed as a % of the PAR staining density for NHDFs treated without tbh7ox or rucaparib. Error bars represent +/- SD. (C) The viability of NHDFs in response to various concentrations of rucaparib for 12, 24 and 48 hours was assessed using an alamar blue assay (n=3 technical replicates for each concentration). Data is shown as % viability of the DMSO treated control, error bars represent +/- SD. The data in panel B is the average of two separate biological experiments (n=2).

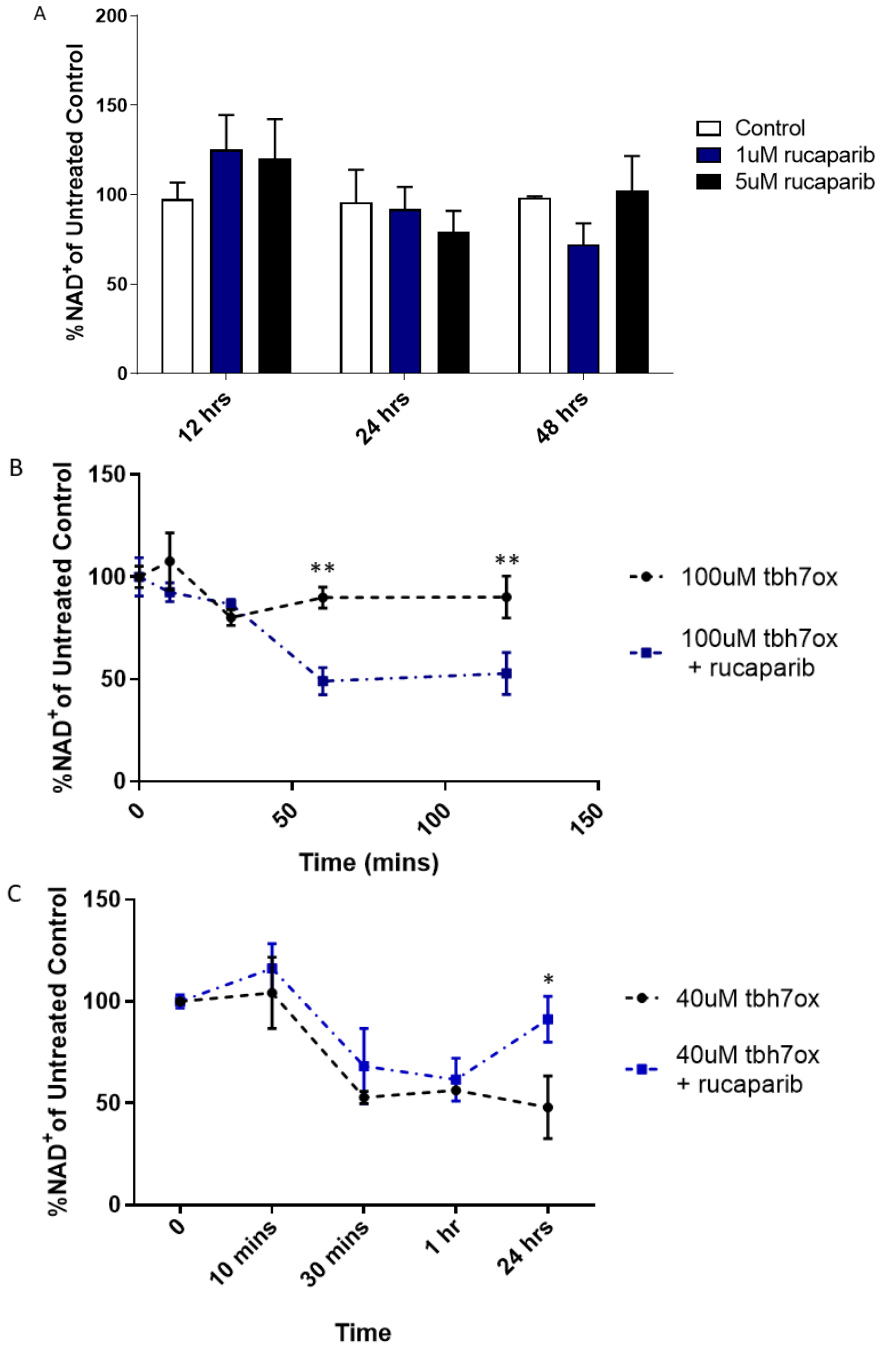

Figure 3.7.2 Tbh7ox regulation of NHDF NAD⁺ under conditions of PARP1 inhibition.
(A) NHDFs were treated with 1uM or 5uM rucaparib or 0.1% DMSO and harvested after 12, 24 and 48-hour incubations so that NAD⁺ could be measured by an NAD⁺ cycling assay (n=3 technical replicates for all conditions). Protein levels were then quantified by a BCA assay and the NAD⁺ levels were expressed as % ng NAD⁺/ug protein of the DMSO treated control for each timepoint. NHDFs were also pre-treated with 5uM rucaparib or 0.1% DMSO for 24 hours, after which (B) 100uM of tbh7ox was added to the media and cells were harvested 10, 30, 60 and 120 minutes later, or (C) 40uM was added and cells harvested 10 minutes, 30 minutes, 60 minutes and 24 hours later (n=3 technical replicates for all conditions). NAD⁺ levels were measured and expressed as done for panel A. Data is presented as % ng NAD⁺/ug protein of the DMSO treated control, error bars represent +/-SD. Significance was tested for by 1-way ANOVA for panel A and by 2-way ANOVA with a Dunnett's post hoc test for panels B and C. *p<0.05, **p<0.01. The results shown are the average of 2 separate biological experiments (n=2).

3.8 Quercetin and ALA Induce Antioxidant Effects in NHDFs

The compounds previously tested for their ability to increase NAD^+ levels were also tested for their capacity to protect against oxidative stress induced by tbh7ox. NAM, ALA, apigenin, RSV and quercetin have all previously been shown to elicit antioxidant effects *in vitro* [333-337] and *in vivo* [338-343], therefore it was of interest to determine if these effects were also present in NHDFs.

NHDFs were treated with the compounds (apart from NAM) for 24 hours, before 40uM tbh7ox containing media was added to the cells for 1 hour. For NAM a 12-hour pre-treatment was used given this was the point of maximal NAD^+ enhancement previously recorded (Figure 3.4.1), with tbh7ox then added for 1-hour as for the other compounds. Following this incubation, the media were replaced with fresh media once again containing the compounds used for the pre-treatment but without tbh7ox, with viability then assessed using a 4-hour incubation in 0.02% alamar blue solution 20 hours post tbh7ox exposure.

A significant reduction in tbh7ox induced cytotoxicity across a range of concentrations was only observed for ALA and quercetin, with NAM, apigenin and RSV unable to offer any protection against the oxidative stress (Figure 3.8.1). The efficacy of quercetin was particularly impressive, with 45uM quercetin increasing the raw viability (minus the blank) by 81% compared to the 0.2% DMSO (DMSO concentration used for all NHDFs) control when pre-treated with 40uM tbh7ox ($p<0.001$). The smallest increase in viability recorded for quercetin and tbh7ox treated cells compared to the tbh7ox control was 46% ($p<0.01$), which was at 9uM quercetin, the lowest concentration used.

ALA was also capable of protection against the tbh7ox insult, with concentrations of 20uM and 50uM increasing viability by 79% ($p<0.01$) and 76% ($p<0.01$) compared to the tbh7ox treated control respectively. Surprisingly, the higher doses of 67uM, 200uM and 400uM improved viability post tbh7ox treatment, but failed to achieve statistical significance. The viability in the non-tbh7ox treated NHDFs at these higher concentrations did show a small decline (9% decrease 200uM, 12% decrease 400uM, non-significant) however, suggesting there may be some toxic effects of ALA in NHDFs at these higher doses. Nonlinear regression analysis to calculate EC50 (half maximal effective concentration) was performed for the experiments using quercetin and ALA, however complete confidence intervals (at 95% confidence level) were undefined, thus EC50 values are unable to be accurately calculated from this data.

For the NAM treated NHDFs, no significant increase in viability was recorded across a 10-800uM concentration range, suggesting solely increasing NAD^+ isn't sufficient to protect against tbh7ox-induced oxidative stress.

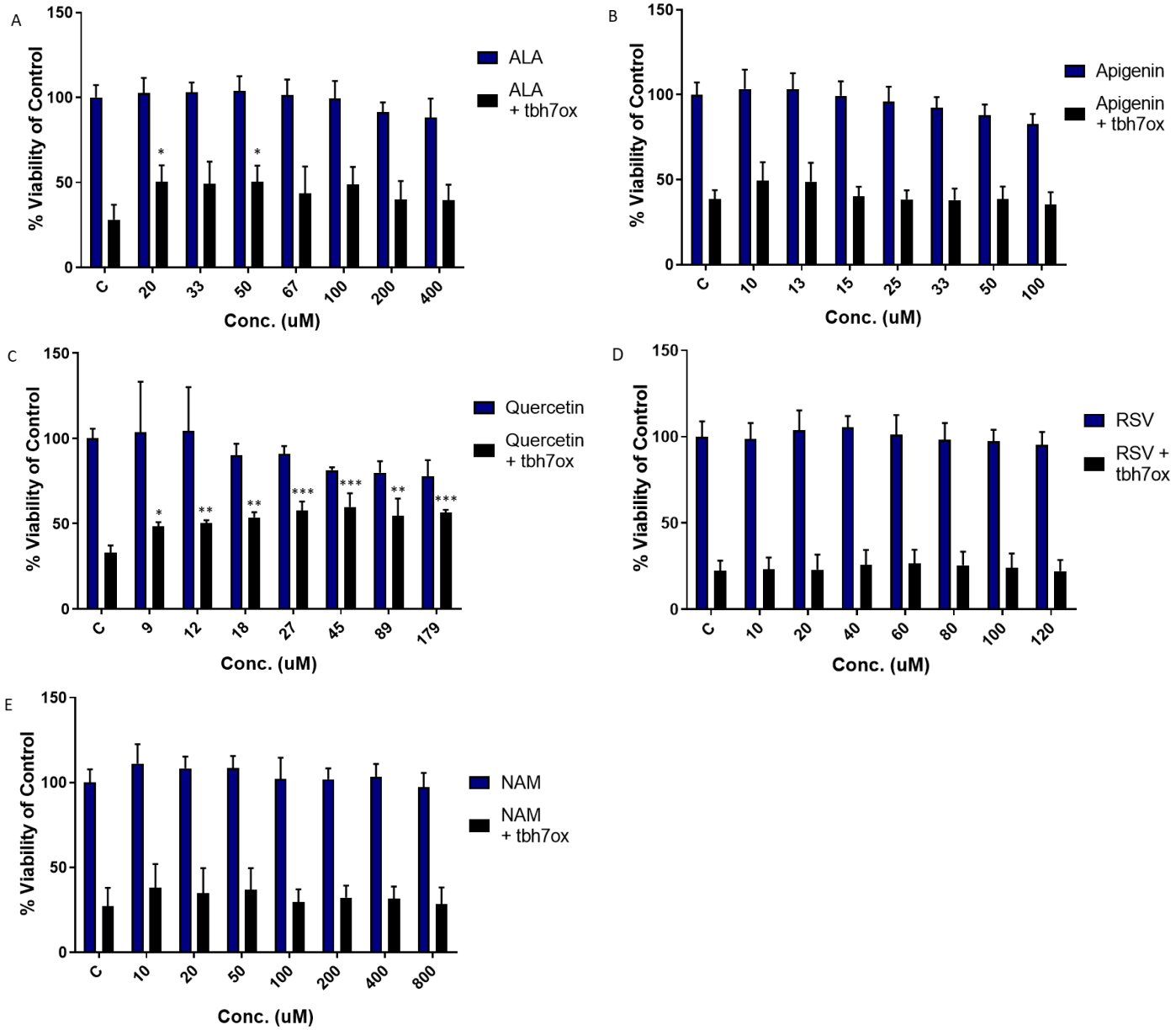

Figure 3.8.1 Viability of NHDFs pre-treated with putative NAD^+ enhancers following induced oxidative stress.

NHDFs were pre-treated with (A) ALA, (B) apigenin, (C) quercetin and (D) RSV for 24 hours as well as (E) NAM for 12 hours at the concentrations indicated (n=6 technical replicates for all conditions). 40uM tbh7ox was then added for 1 hour to half the wells (n=3) for all conditions, before the media was replaced with fresh media containing the same compounds as prior to the tbh7ox addition. Viability was then assessed 20 hours later by incubating the cells for 4 hours in 0.02% alamar blue solution, after which fluorescence was quantified using a fluorometer. The fluorescent values were then expressed as a % of the non-tbh7ox treated control as shown here. Error bars represent +/-SD. Significance was tested for in both the tbh7ox and non-tbh7ox groups by 1-way ANOVA, followed by a Dunnett's post hoc test. The data shown is the average of 2 separate biological experiments (n=2).

3.9 NTC Protects Against Oxidative Stress in a PARP1 and SIRT1 Independent Manner

The NTC supplement combination was next tested for any potential antioxidant capacity in NHDFs treated with tbh7ox. As done previously, the cells were treated with NTC for 24 hours before a 1-hour incubation in the presence of 60uM tbh7ox, after which the cells were returned to the normal NTC containing media and viability assessed 24 hours later. A higher concentration of tbh7ox was used compared to previous experiments due to a noticeable decrease in the cytotoxicity tbh7ox, possibly as a consequence of long-term storage. NHDFs were also pre-treated for 12 hours with NAM, to compare NTC to an NAD^+ precursor only approach.

NTC was able to completely protect the NHDFs against any tbh7ox induced cytotoxicity, in contrast to the NAM treated cells (Figure 3.9.1 A). Surprisingly, the protective effects of NTC showed no attenuation when NTC was added along with 5uM rucaparib, suggesting NTC combats oxidative stress in a PARP1-independent manner. As would be expected, inhibition of the DNA repair enzyme PARP1 using rucaparib does result in sensitisation of the NHDFs to tbh7ox, with tbh7ox concentrations of 60uM and 80uM found by multiple comparisons 2-way ANOVA to significantly reduce NHDF viability when combined 5uM rucaparib (both $p<0.001$).

Pre-treatment with NTC (Figure 3.9.1 B) was able to partially attenuate the sensitisation to tbh7ox induced by rucaparib, as evidenced at tbh7ox doses of 100uM and 140uM whereby NHDF viability was significantly increased (2-way ANOVA, $p<0.001$) when NTC was also added to cells treated with tbh7ox and rucaparib. This therefore implies that instead of enhancing PARP1 facilitated DNA repair, NTC is protecting against tbh7ox in a mechanism dependent on neutralising the damaging ROS (reactive oxygen species).

The CC50 (50% cytotoxic concentration) and CI (confidence intervals) values for curves generated using nonlinear regression were: tbh7ox - 90.6, 95% CI (85.0, 96.2); tbh7ox with rucaparib - 73.8, 95% CI (57.2, 90.4) and tbh7ox with rucaparib and NTC - 144.5, 95% CI (0.0, 356.5). Although pre-treatment with rucaparib reduced the CC50 following the tbh7ox insult, there was no statistically significant difference between the CC50 values as tested by 1-way ANOVA, emphasising that the sensitisation to tbh7ox via PARP1 inhibition is only limited to higher tbh7ox concentrations. Likewise, the CC50s for NHDFs treated with tbh7ox, rucaparib and NTC showed no significant difference to the other conditions, however this comparison was hindered by the large 95% CI (0.0, 356.5).

Next, a similar approach was used whereby rucaparib was substituted with the small-molecule SIRT1 inhibitor EX527 [344]. Pre-treatment with 40uM EX527 failed to enhance tbh7ox induced cytotoxicity at all tbh7ox concentrations (2-way ANOVA), suggesting SIRT1 plays a minimal role

protecting NHDFs against acute oxidative stress (Figure 3.9.2). Nonlinear regression analysis was used to plot a curve of tbh7ox concentrations for the different conditions against viability, with the CC50 of tbh7ox for treatment of cells with just tbh7ox 72.1 (CI – 68.6 – 75.5) versus a CC50 of 94.8 (CI – 88.7 – 100.0) for tbh7ox and an NTC pre-treatment ($p<0.05$, 1-way ANOVA).

Co-incubating NTC treated NHDFs with EX527 failed to ameliorate the protective effects of NTC following tbh7ox exposure, as determined across all tbh7ox concentrations by 2-way ANOVA. Furthermore, the CC50 of tbh7ox in EX527 and NTC treated NHDFs was 93.3 (CI – 83.8 – 139.0), compared to 94.8 (CI – 88.7 – 100.0) for just the NTC pre-treatment, with no significant difference as determined by comparing the CC50s via 1-way ANOVA**.** Hence, it appears SIRT1 activity has no beneficial role in NTC-mediated protection against tbh7ox.

The failure of PARP1 or SIRT1 inhibition to abrogate the capacity of NTC to neutralise oxidative stress was surprising, hence it was next investigated whether the unknown mechanism responsible was dependent on adequate NAD^+ availability by using the NAMPT inhibitor FK866 [345]. Initially, to characterise FK866's ability to deplete NAD^+ in NHDFs, NAD^+ levels were measured following 24, 48 and 72-hour treatments with 5, 10, 20 or 50nM of FK866 (Figure 3.9.3 A). Notable downregulation of NAD^+ didn't occur until the 48-hour timepoint at which 5uM FK866 reduced NAD^+ by 48% compared to untreated NHDFs, whilst the other concentrations induced an 81-84% depletion. Further depletion occurred by the 72-hour timepoint, where the reduction ranged from 91-96% NAD^+. 2-way ANOVA found a significant difference between the different timepoints ($p<0.001$) but not FK866 concentrations, although there was a significant interaction between timepoint and FK866 concentration ($p<0.001$).

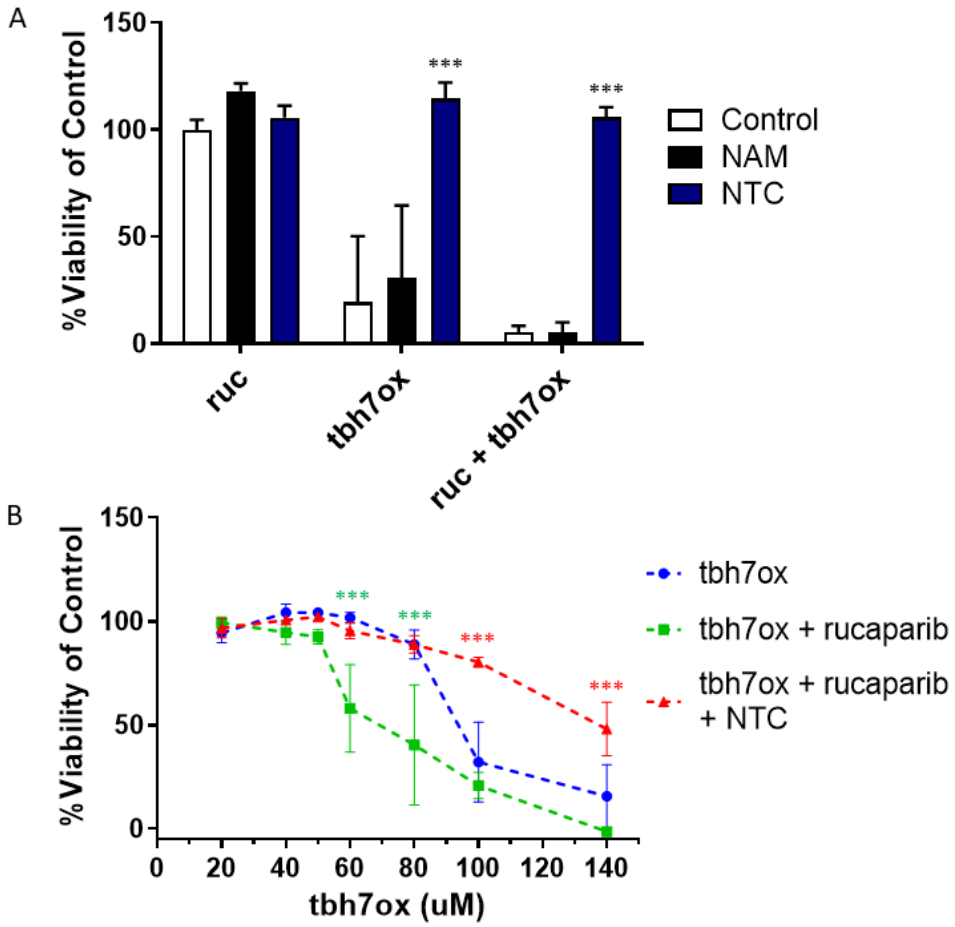

Figure 3.9.1 NTC protects NHDFs against oxidative stress and PARP1 inhibition.
(A) NHDFs were treated for 24 hours with 5uM rucaparib (ruc) or DMSO control with/without NTC or 100uM NAM. The wells indicated were incubated for 1 hour with tbh7ox after which they were returned to normal media containing the compounds previously added (n=3 technical replicates for all conditions). After 20 hours cell viability was assessed via a 4-hour incubation in 0.02% alamar blue solution. Data is expressed for each condition as the percentage viability of untreated NHDFs, shown as the average of 2 separate biological experiments. (B) NHDFs were treated for 24 hours with 5uM rucaparib or DMSO control with/without NTC. Concentrations of 0, 20, 40, 50, 60, 80, 100 and 140uM tbh7ox were then added to the wells for 1 hour. The media was then replaced with fresh media with/without 10uM rucaparib/NTC/DMSO. After 20 hours the cell viability was assessed using 0.02% alamar blue solution. Statistical significance in panel A was tested for by 1-way ANOVA with a Dunnett's post hoc test. In panel B significance was tested for by 2-way ANOVA, with a Dunnett's post hoc test where the tbh7ox group is designated as the control. The results shown are the average of two separate biological experiments (n=2).

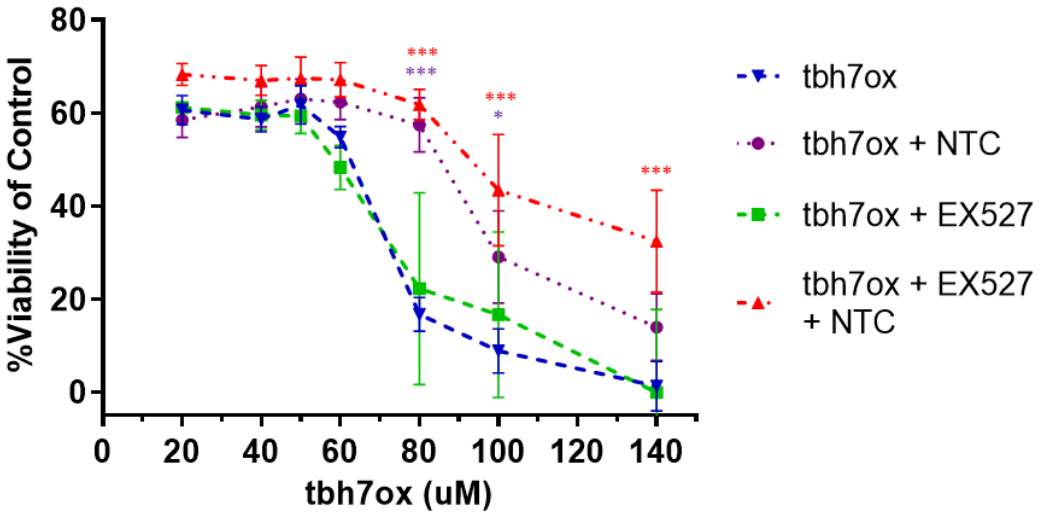

Figure 3.9.2 NHDF viability following co-treatment with tbh7ox and EX527.
NHDFs were treated for 48 hours with 40uM EX527 and/or NTC for 24 hours. The cells were then treated with concentrations of 0, 20, 40, 50, 60, 80, 100 and 140uM tbh7ox for 1 hour (n=3 technical replicates for all conditions). Afterwards fresh media containing EX527 and/or NTC was added, replicating conditions before the tbh7ox stimulus. After 20 hours cell viability was assessed via a 4-hour incubation in 0.02% alamar blue solution and the subsequent measurement of fluorescence. Data is represented the % viability of the DMSO treated control, shown as the average of two separate biological experiments (n=2). Error bars represent +/- SD. Statistical significance was assessed by 2-way ANOVA followed by a Bonferroni post hoc test. **p<0.01, ***p<0.001.

As discussed already, severe NAD^+ depletion will likely have deleterious consequences, hence cell viability was also assessed in response to various FK866 concentrations (1, 5, 10, 20, 50, 100 and 200nM) after 48, 72 and 96-hour treatments using an alamar blue assay (Figure 3.9.3 B). Once again 2-way ANOVA found a significant difference between the different timepoints ($p<0.001$), however this time there was also a significant difference between the varying FK866 concentrations ($p<0.001$), hence NHDF viability in response to FK866 is both time and concentration dependent. None of the FK866 concentrations induced a significant loss of viability 48 hours post-treatment despite all doses >10nM reducing NAD^+ >80% at this timepoint, therefore the adverse effects of NAD^+ depletion aren't immediately translated to decreased cell viability.

Taken together, the data for the NAD^+ and cell viability analysis finds that a 48-hour treatment with 10nM FK866 causes an 84% decrease in NAD^+ without any notable loss in cell viability (98.4% viability of the control), hence these were the conditions chosen to pharmacologically induce NAD^+ depletion for further experiments.

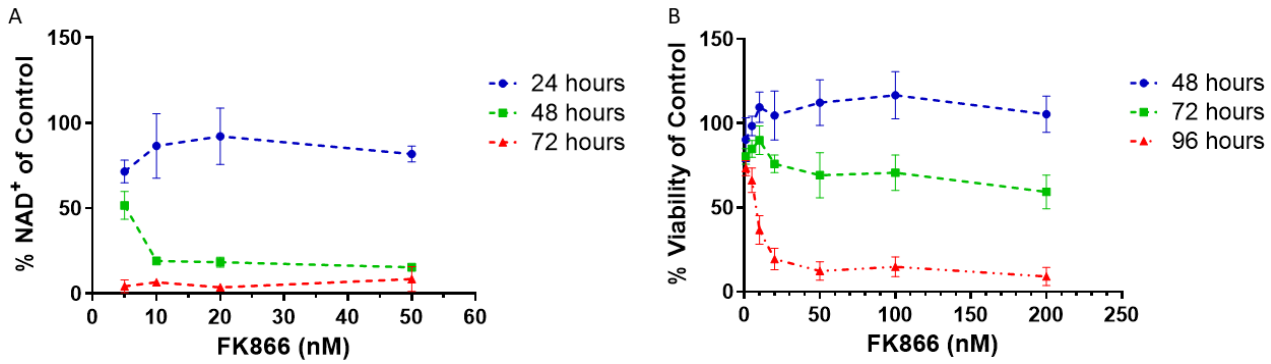

Figure 3.9.3 FK866 suppression of NHDF NAD⁺ levels and viability.
(A) NHDFs were treated with 5, 10, 20 or 50nM FK866 for the incubation times indicated (n=3 technical replicates) and NAD⁺ levels were measured by an NAD⁺ cycling assay before being normalised to protein levels via a BCA assay. The data is expressed as % NAD⁺/ug protein of the untreated NHDFs for each timepoint. (B) NHDFs were treated with 1, 5, 10, 20, 50, 100 and 200nM FK866 for the incubation times indicated. 4 hours before the end of the incubation period the cells were treated with 0.02% alamar blue solution and viability was assessed by measuring fluorescence. The viability for each FK866 concentration is expressed as the % viability of the untreated control NHDFs for each timepoint. Error bars represent +/-SD. All data points shown are the average from 2 separate biological experiments (n=2).

To test the effect of NAD⁺ depletion on viability in the presence of tbh7ox and whether reduced NAD⁺ reverses the protective effects of NTC against oxidative stress NHDFs were treated for 48 hours with/without 10nM FK866 and/or NTC, along with a 1-hour tbh7ox incubation 24 hours before viability was assessed.

Compared to NHDFs treated with just tbh7ox, those which were also incubated with FK866 had significantly reduced viability for all tbh7ox concentrations used (multiple comparisons 2-way ANOVA, $p<0.001$ for all concentrations) (Figure 3.9.4).

Moreover, the protective effects of NTC against tbh7ox were completely lost when it was added to NHDFs in combination with FK866, with the viability of cells treated with NTC, FK866 and tbh7ox significantly lower than those treated with just tbh7ox for tbh7ox concentrations of 20, 40, 50, 60, 80 and 100uM (multiple comparisons 2-way ANOVA).

Nonlinear regression analysis of the viability data was used to generate CC50 values for all conditions as follows: tbh7ox CC50 - 65.8, 95% CI (58.1, 80.5); tbh7ox with NTC CC50 - 96.2, 95% CI (80.7, 389.9); tbh7ox with FK866 CC50 - 11.53, 95% CI (0.0 – 103.5); tbh7ox with NTC and FK866 CC50 – 0.3, 95% CI (0.0 – 183.4). Hence, once again the beneficial effect of treating NHDFs with NTC before and after

the tbh7ox incubation is observed, with FK866 nullifying these effects. It should be noted that due to the potent reduction of viability induced by FK866 even at the lowest tbh7ox concentration (20uM), the CC50 couldn't be accurately estimated for curves generated for FK866 treated NHDFs.

Nonetheless, in contrast to rucaparib and EX527, it is apparent FK866 attenuates the protective effects of NTC against tbh7ox, thus it appears that NTC requires NAMPT activity to support its antioxidant capabilities.

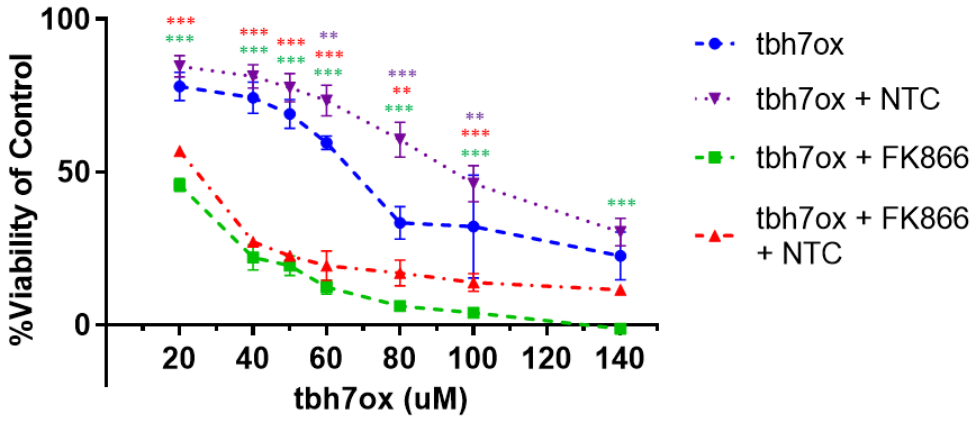

Figure 3.9.4 NHDF viability following co-treatment with tbh7ox and FK866.
(B) NHDFs were treated for 48 hours with 10nM FK866 and/or NTC for 24 hours. The NHDFs were treated for 1 hour with tbh7ox concentrations of 0, 20, 40, 50, 60, 80, 100 and 140uM (n=3 technical replicates). Viability was subsequently assessed 20 hours later by incubating the cells for 4 hours in 0.02% alamar blue solution and then measuring fluorescence. Data is presented as the % viability of the DMSO treated control, shown as the average of two separate biological experiments (n=2). Error bars represent +/-SD. Statistical significance was assessed by 2-way ANOVA followed by a Bonferroni post hoc test. **p<0.01, ***p<0.001.

3.10 Discussion

Of the individual compounds tested, apigenin and quercetin were both found to be effective at enhancing NHDF NAD^+ levels, however this was restricted to 12 hours post-treatment for apigenin and 8 hours post-treatment for quercetin, suggesting limited efficacy. This is particularly problematic in the context of a therapeutic intervention where a sustained enhancement of NAD^+ would be desirable. The precursor NAM was also capable of temporarily increasing NAD^+, however by 24 hours NAD^+ had decreased at the NAM higher doses, suggesting there may be a negative feedback mechanism at play. The presence of some sort of negative feedback is further supported by failure of the larger NAM doses to significantly increase NAD^+, with a significant decrease recorded for the two highest doses after 24 hours.

This problem was partially bypassed by using a multi-compound approach, whereby numerous enzymes involved in NAD^+ homeostasis are targeted with the intention of upregulating NAD^+ synthesis and recycling pathways, whilst also reducing NAD^+ degradation. NTC is a combination of compounds fulfilling this criteria, which was able to significantly increase NAD^+ in NHDFs 12 hours and 24 hours post-treatment. Its effectiveness was however diminished by the 48-hour timepoint, suggesting sensitisation to the treatment may also be an issue for the multi-targeted approach.

Furthermore, although NTC also enhanced NAD^+ in Jurkat cells at 12 and 24-hours post-treatment, this failed to achieve statistical significance, undermining the efficacy of NTC in this specific cell type. This highlights that the success of interventions with the intent of enhancing NAD^+ will likely vary between different cells and tissues due to the heterogenous nature of NAD^+ homeostasis across different cell types [346], linked to the cellular metabolic phenotype which itself is dictated by the energy demands of the cell. Additionally, some of the enzymes targeted by NTC such as CD38 and NAMPT are expressed differently across tissue types [137, 347]. Hence, the concentration of the constituents of NTC would need to be optimised for different cell types to achieve maximal upregulation of NAD^+, an approach which in retrospect should've been undertaken within this work for the Jurkat cell line.

It was also interesting to find that oxidative stress induced by tbh7ox depletes NAD^+, with this depletion partially reversible under conditions of PARP1 inhibition - provided the levels of oxidative stress are below a threshold. Indeed, the paradoxical decrease in NAD^+ at higher concentrations of tbh7ox in the presence of the PARP1 inhibitor rucaparib was a consequence of extensive decrease in cell viability determined by trypan blue staining (data not shown), emphasising the double-edge sword that accompanies inhibition of PARP1. Hence, although PARP1 inhibition may increase NAD^+ levels under specific conditions *in vitro*, this isn't a feasible approach for this purpose at the organismal level due to the deleterious effects of PARP1 inhibition in the presence of high levels of DNA damage. The use of rucaparib as a chemotherapeutic for the treatment of BRCA-deficient cancers is an obvious exception [348], given the therapeutic value PARP1 inhibition has in this context as a treatment for a life-threatening illness.

It is important to consider however, that the rate limiting enzyme of the pentose phosphate pathway within the endoplasmic reticulum H6PD (hexose-6-phosphate dehydrogenase) has been identified as a non-specific target of rucaparib [349]. Consequently, PARP1 inhibition using rucaparib may be accompanied by metabolic stress within the endoplasmic reticulum via H6PD inhibition, which could influence cell viability measurements in a PARP1-independent manner. Consequently, the relevance of the effects of rucaparib on intracellular NHDF NAD^+ levels and viability with regards to PARP1

inhibition should be verified by repeating these experiments with siRNA/shRNA silencing of PARP1 in place of rucaparib treatment.

NTC was able to increase the antioxidant capabilities of NHDFs in the presence of tbh7ox, however it was surprising to find that this increased antioxidant capacity was independent of PARP1 and SIRT1 activity. It should be noted however, due to lack of a bona fide SIRT1 activity biomarker and the reported inconsistency of commercial SIRT1 activity assays the inhibitory effect of EX527 on SIRT1 was never independently validated.

It had been posited that increasing NAD^+ could be a combative strategy against oxidative stress by supporting PARP1 mediated DNA damage repair, however treatment with NAM fails to offer any protection against tbh7ox cytotoxicity suggesting increasing NAD^+ by itself is insufficient for this purpose. This outcome, combined with the redundant impact of PARP1 inhibition in NHDFs co-treated with NTC and tbh7ox implies that NTC is eliciting an antioxidant effect by preventing oxidative damage from occurring, rather than enhancing its repair. Thus, useful experiments in the future would be to use enzymatic activity or probe-based cell sorting assays that measure markers such as protein carbonylation, DNA oxidation and lipid peroxidation to verify whether NTC protects against oxidative damage in the presence of tbh7ox.

Interestingly, co-treatment with the NAMPT inhibitor FK866 showed that the effects of NTC are dependent on an adequate NAD^+ supply or functional NAMPT, hence an unknown NAD^+ requiring mechanism must be supporting the antioxidant capacity of NTC. It is possible this effect could be mediated via other sirtuins, for example SIRT3 which is localised to mitochondria where it combats oxidative damage via upregulation of the ROS scavenger SOD2 [350]. Indeed, SIRT3 has previously been shown to be responsible for protection against tbh7ox in cell lines via an SOD2 dependent mechanism [351, 352]. Hence, treating NHDFs with NTC, tbh7ox and an inhibitor of SIRT3 such as SDX-437 [353] or *SIRT3* siRNA would be one possible approach to test this theory.

With regards to the viability data for cells treated with various tbh7ox concentrations, only having replicate experimental data values for all conditions is a notable drawback, increasing the statistical uncertainty within the data. Likewise, experiments measuring NHDF NAD^+ levels were only performed twice, thus it has to be acknowledged that this is a serious weakness within this work which gives less weight to these findings.

Although subsidiary to the main scope of this chapter, the remarkable capacity of quercetin to neutralise induced oxidative stress in NHDFs was a notable discovery. ROS are important intermediates in various cell signalling pathways, however their aberrant overproduction (often a

result of mitochondrial dysfunction) results in oxidative stress, which when chronic may promote the pathogenesis of age-related illnesses such as Alzheimer's disease [354-356], Parkinson's disease [357-359], cardiovascular disease [360-362] and physiological ageing itself [294, 363, 364]. Hence, independent of NAD^+, quercetin represents an exciting compound which merits further investigation as a potential intervention in pathologies associated with increased oxidative stress. As is the case for many polyphenols, its therapeutic application has been hindered by low bioavailability, however delivery strategies utilising liposome or nanoparticle loaded quercetin have been shown to enhance *in vivo* potency [365-368]. Therefore, to replicate the NAD^+ enhancing and antioxidant properties of NTC *in vivo* may require the polyphenol components to be administered via a liposomal/nanoparticle delivery system.

Chapter 4. Circadian Regulation of NAD^+ and Its Interaction with BMAL1

4.1 Introduction

Circadian rhythms are diurnal oscillations of biological processes, a product of evolution to allow tailoring of physiological functions to the time of day, or more specifically sunlight hours. The most obvious example is the fluctuating levels of the sleep promoting hormone melatonin, which is low during the day before steadily increasing throughout the evening. A key co-ordinator of circadian rhythms throughout the human body is the hypothalamic structure known as the suprachiasmatic nucleus (SCN), which processes environmental cues (e.g. sunlight) and releases circulating factors to synchronise circadian processes occurring in the periphery. At the intracellular level, a core group of enzymes including BMAL1 and CLOCK are particularly key [369]: integrating signalling from the SCN and other molecular events to establish circadian rhythmicity of numerous pathways.

Although the circadian regulation of genes relating to sleep and feeding are well understood, a multitude of other enzymes unrelated to these processes are also under circadian control. One such enzyme is SIRT1, which evidence suggests is regulated by the 'master controller of circadian rhythms' BMAL1 as part of a bidirectional relationship [105]. The exact mechanism by which SIRT1 activity is regulated by BMAL1 however remains unclear. Direct binding of the BMAL1:CLOCK dimer to the SIRT1 promoter has been suggested, however it's also been shown that BMAL1 regulates NAMPT expression [233, 234], thus modulation of NAD^+ levels via NAMPT fluctuations represents another mechanism by which BMAL1 may control SIRT1 activity. Furthermore, there have been reports that the ability of BMAL1 to dimerise with CLOCK is promoted by SIRT1-mediated deacetylation of PER2 (period circadian protein homolog 2), another key regulatory protein of circadian rhythms [370-372]. PER2 interacts with the BMAL1:CLOCK dimer and represses its ability to bind target promoters, however the stability of PER2 and its import into the nucleus is impaired by deacetylation via SIRT1 [105] – laying the foundation for a positive feedback loop between BMAL1 and SIRT1.

Dysregulation of circadian rhythms, primarily due to insufficient sleep, is widely accepted as being a factor promoting ill-health [373, 374]. The disrupted sleeping patterns of nightshift workers provides somewhat of a human model to study the importance of circadian rhythms regarding physiological health, with a number of chronic diseases found to be over-represented in these workers [375-377]. The likelihood to succumb to certain diseases is also related to time of day and thus under circadian influence, whilst outcome following surgery also appears time-dependent [378], although other human factors may explain the latter. As we enter an era where therapeutic interventions tailored to an individual's genome is on the horizon, it would seem beneficial to also tailor treatments to circadian rhythms. For example, if a protective protein against a disease is particularly low at one

daily timepoint, this would identify the optimal timepoint for a therapeutic boosting its levels to be active.

An interesting phenomenon relating to circadian biology in humans is the existence of 'morning' and 'evening' chronotypes [379], describing those who prefer waking and being active early in the day and vice versa. These two chronotypes are genetically defined [380-382] with a subsidiary layer of regulation at the environmental level [383, 384], manifesting as two distinct circadian rhythm profiles whereby the timing of the daily rise and fall in melatonin differs. Furthermore, a shift towards earlier sleeping and waking times is experienced by people as they age such that they become more likely to be a 'morning' type [217, 385], strongly suggesting that circadian rhythms are altered with age and hence may be a component of age-related physiological decline. What causes this, is it tissue-specific and whether it is a consequence of molecular aberrations or changes to the hypothalamic structure are key questions that need to be addressed in order to better understand the relationship between ageing and circadian rhythms.

The potential importance of BMAL1 in biological ageing is highlighted by the short-lived *Bma1*$^{-/-}$ mice which were found to have an average lifespan of 37 weeks, in contrast to the wild-type and heterozygous genotypes which all survived to the end of a 52-week duration study [226]. Moreover, in addition to premature mortality the *Bmal1*$^{-/-}$ mice also exhibit an accelerated appearance of age-related pathologies including sarcopenia, organ shrinkage and increased ROS production [226]. Interestingly, a separate study found that activity of the nutrient sensor mTOR was enhanced in *Bmal*$^{-/-}$ mice and that inhibiting mTOR was able to significantly extend their lifespan [386]. Thus it may be that mTOR is under circadian control and impaired BMAL1 signalling elicits a pro-ageing effect via increased mTOR activity: a well-characterised mediator of age-related molecular changes [387].

Given circadian rhythms have been tailored to physiological functions, it's highly likely that they vary for different tissues, thus it isn't clear how prominent diurnal rhythmic oscillations will be in dermal fibroblasts, in which circadian rhythms have been sparsely characterised. From an experimental perspective, it is also relevant to consider the absence *in vitro* of the hormonal control exerted by the SCN. Hence, it is important to acknowledge that the *in vitro* work presented within this chapter is limited to examining the endogenous system of circadian regulation in dermal and lung fibroblasts, which *in vivo* is likely to synergise with upstream signalling from the SCN.

4.2 Aims

The work within this chapter aims to identify whether BMAL1 regulates NAD^+ levels in dermal fibroblasts and by extension whether NAD^+ levels follow a circadian rhythm. An insight into the wider effects of elevated/repressed *BMAL1* expression on energy metabolism is also explored.

4.3 Hypothesis

It is proposed that NAD^+ levels are under endogenous circadian control mediated by BMAL1. Specifically, enhanced BMAL1 levels are expected to increase NAD^+ levels via upregulation of NAMPT and vice versa when BMAL1 is downregulated.

4.4 NAD^+ levels Follow a Circadian Rhythm in NHDFs

Initially, to test whether BMAL1 is a regulator of NAD^+ in NHDFs, *BMAL1* expression was downregulated using siRNA (small interfering RNA). A pool of 4 different siRNAs was used, which theoretically should increase the chances of efficient knockdown by targeting multiple sites in the target mRNA transcript. The previously shown ability of BMAL1 to regulate NAD^+ in other cell types led to the hypothesis that knockdown of *BMAL1* would reduce NAD^+ levels due to the role BMAL1 plays as a transcriptional activator of NAMPT [234]. The siRNA was able to reduce *BMAL1* expression as shown by the protein levels of BMAL1 72 hours post-transfection (Figure 4.4.1 A), but only resulted in a small and non-significant decrease in NAD^+ (8.12 ng NAD^+/ug protein for scrambled siRNA treated vs 6.98 ng NAD^+/ug protein for *BMAL1* siRNA treated) (Figure 4.4.1 B). The levels of NAMPT and SIRT1 in response to the siRNA mediated knockdown of *BMAL1* showed little change despite the decrease in *BMAL1* mRNA, thus the existence of a regulatory role for BMAL1 in NHDF NAMPT levels is questionable.

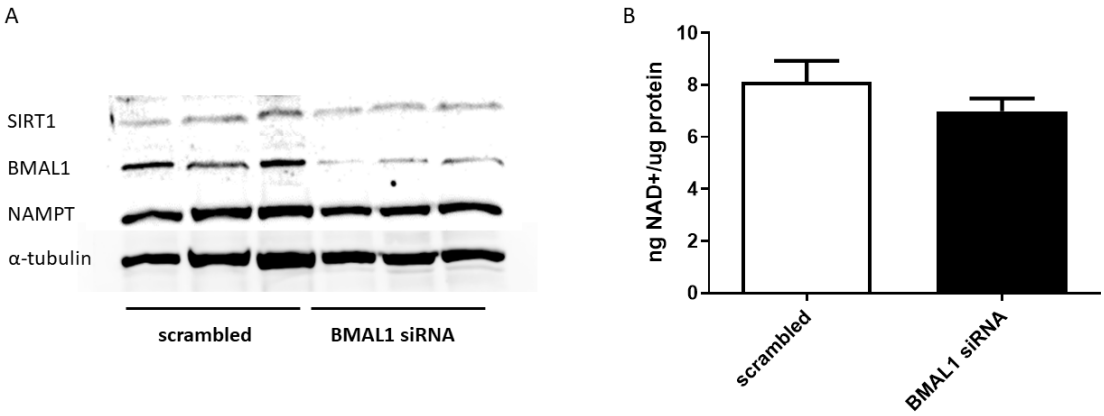

Figure 4.4.1 The effect of *BMAL1* siRNA on NAD^+ levels and SIRT1, BMAL1 and NAMPT levels in NHDFs.
(A) NHDFs were transfected with 100nM scrambled siRNA or 100nM *BMAL1* siRNA and after 72 hours cells were harvested and lysed. The proteins indicated were analysed by western blotting, with the blot shown representative of 3 individual experiments. (B) NHDFs were once again transfected with 100nM scrambled siRNA or 100nM *BMAL1* siRNA for 72 hours (n=3 technical replicates). NAD^+ levels were then quantified using an NAD^+ cycling assay and then normalised to total protein via a BCA assay. Data is shown as mean ng NAD^+/ug protein for two separate biological experiments and error bars represent +/- SD. Significance testing was performed using an unpaired Student's t-test.

It has already been established that NAD^+ levels exhibit some degree of circadian regulation in blood [388], however this has yet to be established in dermal fibroblasts. *In vitro* cells lack both the hormonal input from the SCN and environmental stimuli such as sunlight and temperature. Consequently, the circadian rhythm of cultured fibroblasts would be expected to be 'out of sync' given the absence of these external inputs. In order to synchronise circadian rhythms under *in vitro* conditions cells can be pre-treated with dexamethasone [389], a corticosteroid previously used for this purpose in a number of other studies [390-392].

To test for the presence of an NAD^+ circadian rhythm in NHDFs, cells were treated with 100nM dexamethasone for 2 hours before the dexamethasone was removed and the cells returned to normal culture media. The NHDFs were then harvested and immediately frozen at -80ºC every 4 hours, allowing NAD^+ to be subsequently quantified for the entirety of a 24-hour timecourse (the standard diurnal period). Prior to the dexamethasone treatment, half the NHDFs were transfected with 100nM scrambled siRNA and the other half transfected with 100nM *BMAL1* siRNA for 72 hours. This was to test if any observed rhythmicity of NAD^+ in the scramble treated cells was a genuine consequence of an endogenous circadian rhythm, given this would inevitably be perturbed by *BMAL1* repression in the *BMAL1* siRNA treated cells.

The scrambled siRNA treated NHDFs exhibit variable NAD^+ levels over the 24-hour timecourse, with the levels gradually increasing up until 12 hours post dexamethasone incubation before plateauing (Figure 4.4.2). Contrastingly, this early increase is absent in the *BMAL1* siRNA treated NHDFs which remain relatively consistent throughout with no obvious rhythmic pattern. Given the significant difference in the 24-hour NAD^+ profile for the scrambled and *BMAL1* siRNA treated NHDFs (2-way ANOVA, $p<0.001$), this suggests that the NAD^+ pattern observed for the scrambled treated cells is indeed dependent upon BMAL1 regulation, rather than a consequence of another mechanism induced by the dexamethasone pre-treatment. This data therefore provides evidence for the existence of endogenous circadian regulation of NAD^+ in NHDFs.

It should be noted however that despite finding an overall significant difference between the scrambled and *BMAL1* siRNA treatments, there wasn't a significant difference at any of the individual timepoints. Furthermore, 2-way ANOVA also revealed a significant difference in NAD^+ levels between the individual timepoints ($p<0.05$), highlighting NAD^+ levels in NHDFs are time-dependent following the dexamethasone incubation.

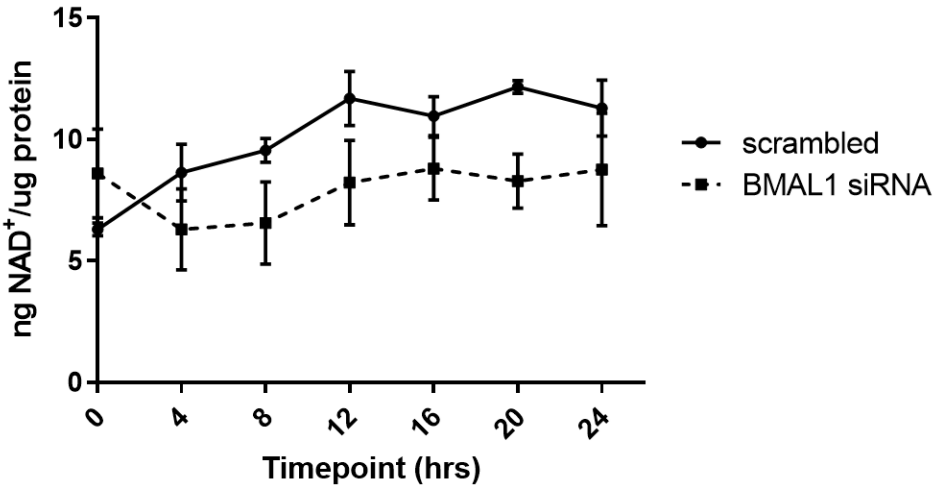

Figure 4.4.2 NAD$^+$ levels in circadian synchronised NHDFs treated with BMAL1 siRNA.
NHDFs were transfected with 100nM scrambled siRNA or 100nM BMAL1 siRNA (n=3 technical replicates) and after 72 hours the cells were then incubated for 2 hours in media containing 100nM dexamethasone to induce synchronisation of circadian rhythms. The cells were returned to regular media and then harvested and frozen at -80ºC every 4 hours over a 24-hour timecourse. NAD$^+$ levels were subsequently quantified by an NAD$^+$ cycling assay and then normalised to total protein via a BCA assay. Significance was tested for by multiple comparisons 2-way ANOVA. Data is shown as mean ng NAD$^+$/ug protein of 2 separate biological experiments (n=2) and error bars represent +/- SD.

4.5 NAD$^+$ Circadian Rhythmicity is Absent in *Bmal1*KO MLFs

An important consideration when using siRNA to examine the effects of knockdown of *BMAL1* on NAD$^+$ levels is the only partial reduction of gene expression that can be achieved using siRNA, particularly in difficult to transfect cells like NHDFs. On the other hand, it's also necessary to consider the unlikelihood that *BMAL1* expression would ever be completely lost under *in viv*o conditions, hence it can be argued that it provides a more realistic model than the complete ablation of *BMAL1* gene function. Nonetheless, the effects of complete loss of *BMAL1* expression on NAD$^+$ levels was a pertinent question that remained to be answered.

To investigate this, NAD$^+$ levels were compared in primary MLFs (mouse lung fibroblasts) derived from *Bmal1*$^{-/-}$ (*Bmal1*KO) and WT littermate MLFs. Given the small decrease in NHDF NAD$^+$ following *BMAL1* siRNA treatment it was very surprising to find that the *Bmal1*KO MLFs had significantly higher NAD$^+$ levels compared to the WT MLFs (WT 0.67 ng NAD$^+$/ug protein vs *Bmal1*KO 1.06 ng NAD$^+$/ug protein, $p<0.002$) (Figure 4.5.1 A). Of course, this could reflect differences in the mouse and human genome which may alter regulation of NAD$^+$ metabolism. Additionally, as already alluded to, gene knockout doesn't resemble the less severe perturbations that may occur to gene expression due to processes such as physiological ageing. Hence, the loss of BMAL1 may also be impacting other pathways which alter NAD$^+$ irrespective of the BMAL1-NAMPT-NAD$^+$ axis.

However, the regulation BMAL1 elicits is much more relevant under conditions of circadian rhythmicity to better replicate the situation occurring *in vivo*. Hence, the *Bmal1*KO and WT MLFs were synchronised using the standard 2-hour 100nM dexamethasone pre-treatment and NAD^+ was subsequently measured at 4-hour intervals over a 24-hour period, as done previously (Figure 4.5.1 B). NAD^+ levels in the WT cells somewhat resembled a typical circadian pattern, starting at a nadir before gradually rising, although they were yet to show a downward trend towards the end of the timecourse as would be typical of a circadian oscillation. On the other hand, the *Bmal1*KO MLFs showed no discernible pattern, with the NAD^+ levels remaining relatively stable for the duration of the timecourse. This therefore does suggest that BMAL1 plays a role in regulating NAD^+ levels *in vitro* – albeit one which is dependent on the establishment of an underlying circadian rhythm.

It should be noted that 2-way ANOVA found no significant difference between the WT and *Bmal1*KO NAD^+ levels over the timecourse, however there was a significant interaction between genotype and timepoint, reflecting the static nature of WT NAD^+ versus the ascending values for the *Bmal1KO* fibroblasts.

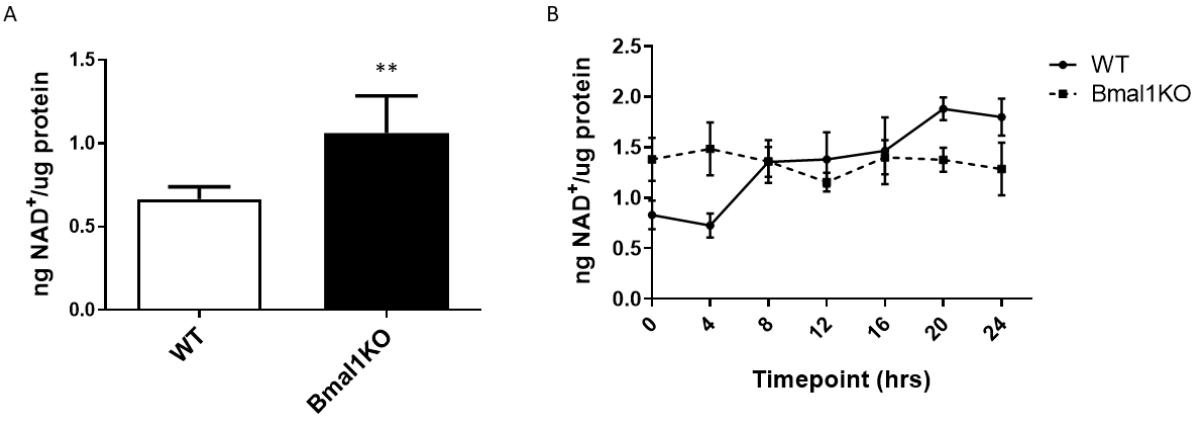

Figure 4.5.1 NAD^+ Levels in *Bmal1*KO and WT MLFs.
NAD^+ levels were measured in (A) unsynchronised WT and *Bmal1*KO MLFs (n=2 biological replicates for each genotype) and (B) WT and *Bmal1*KO MLFs (n=2 biological replicates for each genotype) synchronised with 100nM dexamethasone. After removal of the dexamethasone, cells were harvested every 4 hours over a 24-hour timecourse (n=3 technical repeats for each condition). NAD^+ was measured for both A and B via an NAD^+ cycling assay before being normalised to total protein after performing a BCA assay. Data is shown as mean ng NAD^+/ug protein and error bars represent +/-SD. Significance was tested for (A) using an unpaired Student's t-test and (B) by 2-way ANOVA. **p<0.01.

4.6 miR-155 Represses BMAL1 Expression and Circadian Rhythmicity in MDFs

Additionally, the effects of increased *BMAL1* on NAD^+ titres and rhythmicity was also of interest. To investigate the consequence of *BMAL1* overexpression, a *BMAL1* overexpressing NHDF cell line was generated by inserting an extra copy of the *BMAL1* gene into NHDFs using a lentiviral vector.

However, due to delays experienced generating the cell line, other options were explored, one being modulation of *BMAL1* expression via miRNAs.

Using TargetScan, a database which identifies putative gene targets of known miRNAs [393, 394], miRNAs predicted to bind *Bmal1* mRNA were identified. miR-155 was one such example, which in mice is predicted to bind at position 235-241 of the *Bmal1* transcript 3' UTR. By using primary mouse dermal fibroblasts (MDFs) from mice lacking the miR-155 gene (miR-155KO) and WT littermates, it was first sought to determine whether loss of miR-155 did indeed increase BMAL1 levels by removing its repressive effect. Western blotting using lysates from the WT and miR-155KO cells showed that under basal conditions (without any synchronisation of circadian rhythms) BMAL1 protein levels were strongly enhanced in the miR-155KO cells (Figure 4.1 A).

Next, the efficacy of an miR-155 mimic (synthetically generated miR-155 oligonucleotide) at inhibiting *Bmal1* gene expression in the WT MDFs was investigated. The optimal treatment conditions for miR-155 mimic mediated attenuation of *Bmal1* transcription was found to be 48 hours post transfection at a concentration of 50nM, resulting in a 41% decrease in *Bmal1* mRNA levels compared to MDFs transfected with 50nM of a negative control miRNA mimic. By comparison, in MDFs treated with *Bmal1* or scrambled siRNA, the *Bmal1* siRNA was able to reduce *Bmal1* gene expression by 59%. Thus, this substantiated the prediction made by TargetScan that miR-155 is a post-transcriptional repressor of *Bmal1* in mouse cells.

The effect of the miR-155KO genotype on *Bmal1* gene expression under conditions of circadian rhythmicity was subsequently probed by performing qPCR for cells pre-treated with 100nM dexamethasone as done for previous experiments (Figure 4.6.1 B). Additionally, prior to the dexamethasone treatment WT and miR-155KO cells were treated with 50nM of the miR-155 mimic or 50nM negative control miRNA mimic for 48 hours.

Bmal1 mRNA levels exhibited a different circadian profile for the miR-155KO and WT MDFs treated with the negative control miRNA whereby the *Bmal1* mRNA was higher in the miR-155KO cells for 5 out of the 7 timepoints, with an average increase of 1.7-fold (SD - 2.8-fold).

Convincing evidence for the inhibitory effect of miR-155 on *Bmal1* was observed in the miR-155 mimic treated cells, where *Bmal1* mRNA levels were strongly downregulated in both the WT and miR-155KO cells (Figure 4.1 A and C). 6 out of 7 of the timepoints for the miR-155 mimic treated WT cells had reduced *Bmal1* mRNA levels compared to the negative miRNA treated WT cells, which was on average 2.9-fold lower (SD - 2.3-fold). The mimic treated miR-155KO cells on average had a 3.7-fold reduction in *Bmal1* expression (SD - 1.1-fold) compared to the negative control miRNA treated

miR-155KO cells, with all 7 timepoints showing reduced *Bmal1* mRNA levels. Hence, the miR-155 mimic was effective at reducing *Bmal1* expression under conditions of circadian rhythmicity.

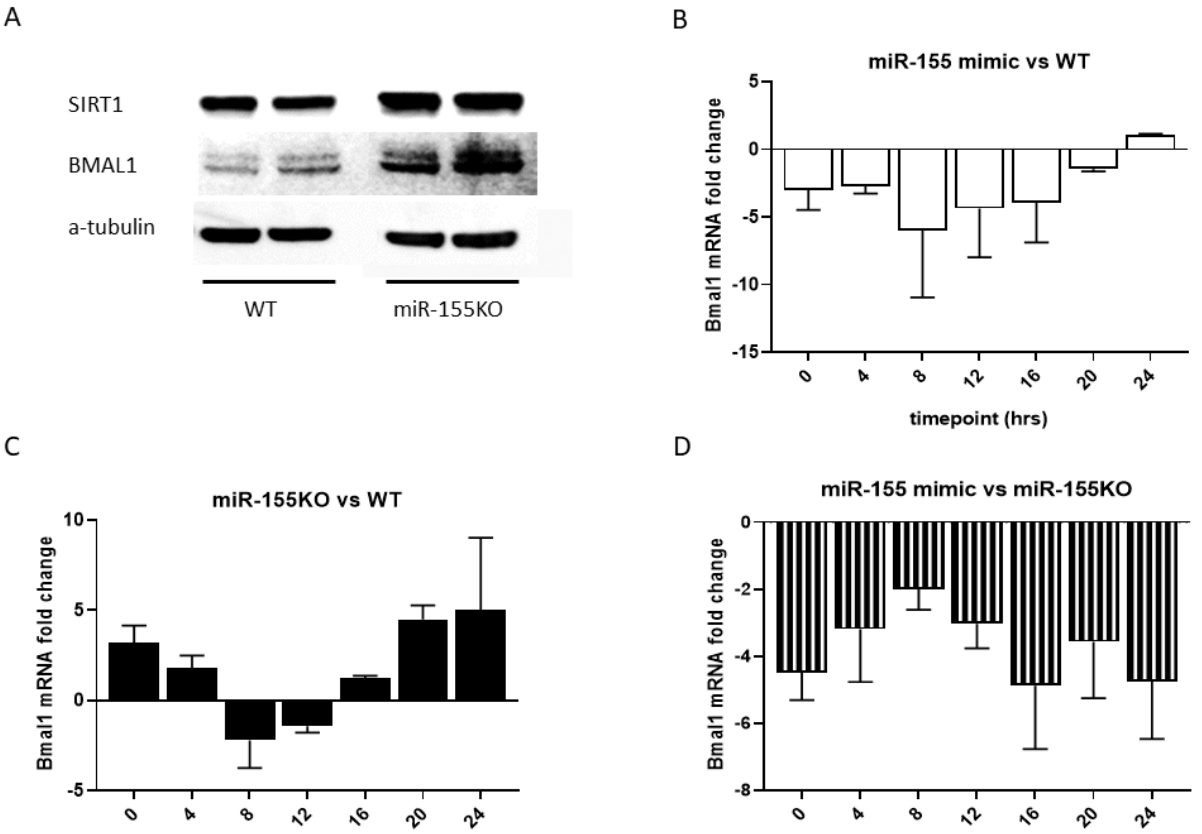

Figure 4.6.1 *Bmal1* expression over a 24-hour timecourse in miR-155 mimic and negative control miRNA treated MDFs.

(A) Sirt1, Bmal1 and α-tubulin protein levels in WT and miR-155KO MDFs were measured by western blotting. The blot shown is presentative of 3 independent experiments. (B-D) WT and miR-155KO MDFs (n=4 biological replicates for both genotypes) were incubated with 50nM negative control miRNA or 50nM miR-155 mimic for 48 hours. Circadian rhythms were then synchronised by a 2-hour incubation in 100nM dexamethasone. After removing the dexamethasone from the media, cells were harvested at 4-hour intervals over a 24-hour timecourse and *Bmal1* mRNA and 18S rRNA expression was then measured by qPCR, with expression of *Bmal1* relative to 18S calculated using the $2^{-\Delta\Delta Ct}$ method with the negative miRNA control treated WT 0-hour timepoint (B and C) and the negative miRNA control treated miR-155KO cells 0-hour timepoint (D) used as the control averages respectively. (A) Bmal1 expression in miR-155 mimic treated WT MDFs is shown relative to the expression of the negative control miRNA treated MDFs at each timepoint. (C) Bmal1 expression in negative control miRNA treated miR-155KO MDFs is shown relative to the expression of the negative control miRNA treated MDFs at each timepoint. (D) Bmal1 expression in miR-155 mimic treated miR-155ko MDFs is shown relative to the expression of the negative control miRNA treated miR-155KO MDFs at each timepoint. Data is presented as the mean fold-change in mRNA levels, with error bars indicating +/- SD.

It's ability to negatively regulate *Bmal1* introduces the possibility that miR-155 may function as a circadian regulator, hence it was next investigated whether the expression of *MIR155* itself follows a circadian rhythm and whether Bmal1 regulates it as part of a negative feedback loop. To do this, WT MDFs were treated with scrambled siRNA or *Bmal1* siRNA for 48 hours, after which the cells were synchronised using 100nM dexamethasone as done for previous experiments. There wasn't a noticeable oscillatory pattern to the miR-155 levels with or without the *Bmal1* siRNA, however the average expression of miR155 over the timecourse was less for the siRNA treated cells (1.5-fold reduction, SD - 2.1-fold), without reaching statistical significance when tested by 2-way ANOVA.

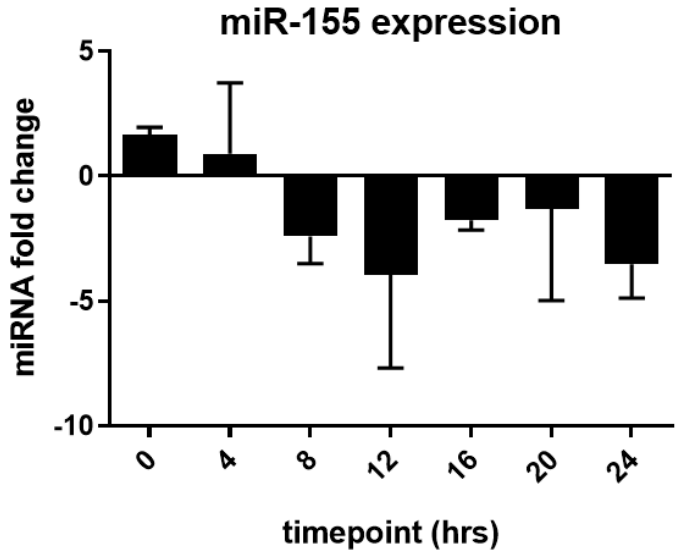

Figure 4.6.2 miR-155 expression over a 24-hour timecourse in *Bmal1* siRNA treated MDFs.
MDFs were pre-treated with 75nm scrambled siRNA or 75nm *Bmal1* siRNA for 48 hours before beginning the timecourse (n=4 biological replicates for all conditions). Circadian rhythm was then synchronised by a 2-hour incubation in 100nM dexamethasone. After removing the dexamethasone from the media, cells were then harvested at 4-hour intervals over a 24-hour timecourse. miR-155 and miR-191 gene expression was then measured by qPCR, with expression of miR-155 relative to miR-191 calculated using the $2^{-\Delta\Delta Ct}$ method with the 0-hour timepoint for the scrambled RNA treated MDFs used as the control average. The miR-155 levels in the *Bmal1* siRNA treated NHDFs was then expressed as fold-change relative to the miR-155 levels in the scrambled siRNA treated MDFs at each timepoint. Data points represent the mean fold change (n=4 biological replicates), with error bars indicating +/-SD.

4.7 miR-155 Regulates NAD^+ Circadian Rhythmicity

Given the established role of BMAL1 in regulating cellular NAD^+ levels and the repressive control miR-155 exerts on *Bmal1* expression, it was postulated that the enhanced BMAL1 levels in miR-155KO cells under basal conditions would result in higher levels of NAD^+. Additionally, over a 24-hour timecourse it was hypothesised that the NAD^+ fluctuations in the miR-155KO cells would mirror their pattern of *Bmal1* expression, whereby there is a delay in the rise and fall of the NAD^+ levels compared to the WT cells.

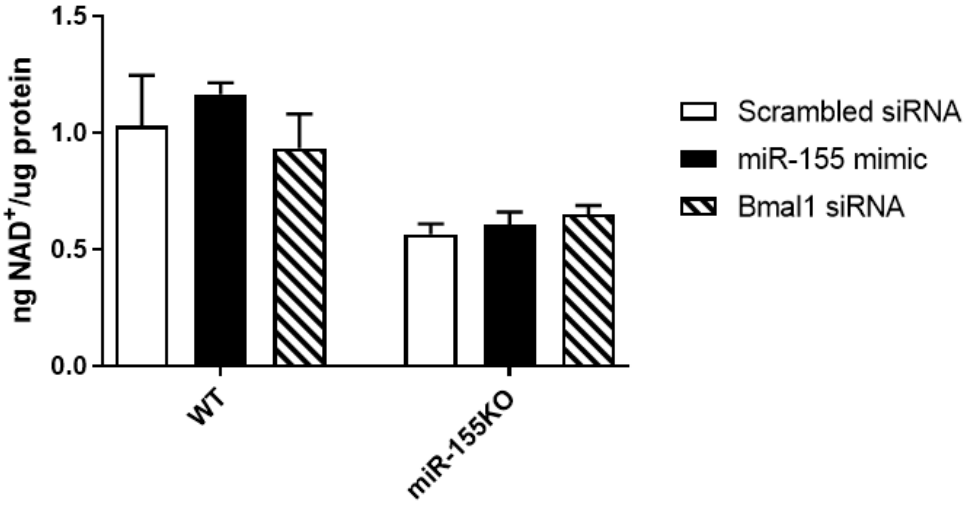

Figure 4.7.1 NAD$^+$ levels in miR-155 mimic, *Bmal1* siRNA and scrambled siRNA treated WT and miR-155KO MDFs.
WT and miR-155KO MDFs were transfected with 50nM miR-155 mimic, 75nM *Bmal1* siRNA or 75nM scrambled siRNA and cells were harvested 72 hours later (n=4 biological replicates for all conditions). NAD$^+$ levels were then measured by an NAD$^+$ cycling assay before being normalised to total protein quantified by a BCA assay. Data is shown as mean ng NAD$^+$/ug protein of two separate biological experiments (n=2) and error bars represent +/- SD. Significance differences were tested for in the WT and miR-155KO groups separately by 1-way ANOVA and a Dunnet's post hoc test, whereby the scrambled treated WT or miR-155KO cells were used as the control.

Under basal conditions lacking any synchronisation of circadian rhythms, the miR-155KO cells showed significantly lower NAD$^+$ levels compared to the WT cells as determined by multiple comparisons 2-way ANOVA for all conditions (scrambled siRNA $p<0.001$, miR-155 mimic $p<0.001$, *Bmal1* siRNA $p<0.05$) (Figure 4.7.1), surprising given their characteristic high BMAL1 levels. The 72-hour pre-treatment with either the miR-155 mimic or *Bmal1* siRNA failed to significantly change the basal NAD$^+$ titres in both the WT and miR-155KO groups however, as tested by 1-way ANOVA.

The effect of *Bmal1* siRNA on NAD$^+$ levels in NHDFs was found to be dependent on circadian synchronisation to induce any noticeable effect, hence it stood to reason that a similar situation may exist in MDFs. To test this, WT and miR-155KO MDFs were transfected with the miR-155 mimic, *Bmal1* siRNA or scrambled siRNA for 72 hours. Immediately prior to the timecourse all cells then underwent a 2-hour incubation in 100nM dexamethasone to synchronise circadian rhythms.

The 24-hour NAD$^+$ profiles for the scrambled siRNA treated WT and miR-155KO cells failed to show any resemblance to the 24-hour oscillation of *Bmal1* mRNA as had been hypothesised (Figure 4.7.2 A). Instead, the miR-155KO NAD$^+$ remained relatively stable aside from a sharp peak at the 4-hour timepoint where NAD$^+$ levels rose from 0.58 ng NAD$^+$/ug protein (0 hours) to 4.8 ng NAD$^+$/ug protein (4 hours) and then back to 0.95 ng NAD$^+$/ug protein (8 hours). In contrast, the WT NAD$^+$ levels exhibited a slight and steady increase over the timecourse, with 1.07 ng NAD$^+$/ug protein measured for the 0 hr timepoint and 2.13 ng NAD$^+$/ug protein for the 24-hour timepoint.

Surprisingly, the miR-155 mimic enhanced the 4-hour peak (scrambled - 4.8 ng NAD^+/ug protein vs mimic – 8.8 ng NAD^+/ug protein), an unexpected finding given the presence of the miR-155 mimic would be expected to reverse the effects of miR-155 knockout rather than exacerbate them. Furthermore, treatment with *Bmal1* siRNA reduced the peak (miR-155KO - 4.8 ng NAD^+/ug protein vs miR-155KO + siRNA – 1.28 ng NAD^+/ug protein), hence it appears its presence is a consequence of altered Bmal1 expression.

It is acknowledged that the use of scrambled siRNA as a negative control for cells treated with the miR-155 mimic is against common practice, however given both scrambled siRNA and negative control miRNA are 20–25 nucleotides long duplex RNA sequences processed by the RISC:Dicer complex, a different relevant biological outcome of using these interchangeably is extremely unlikely.

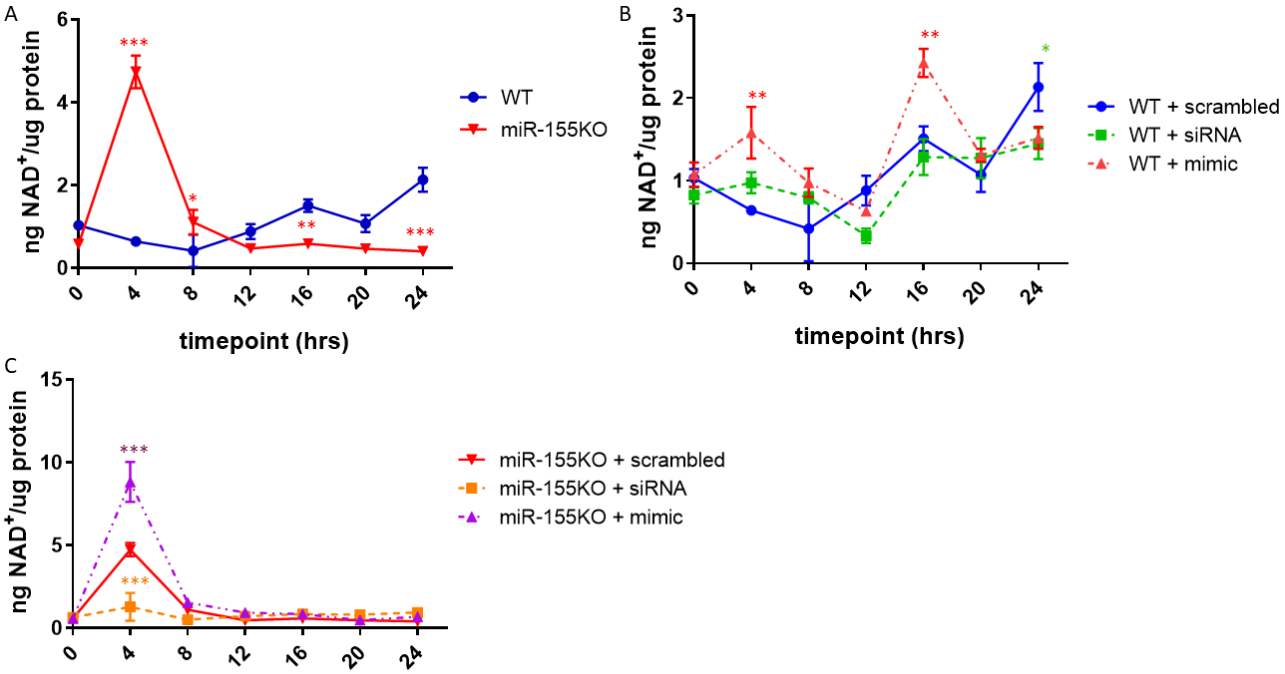

Figure 4.7.2 Circadian pattern of NAD^+ in miR-155 mimic, *Bmal1* siRNA and scrambled siRNA treated WT and miR-155KO MDFs.
WT and miR-155KO MDFs were transfected with a 50nM miR-155 mimic, 75nM *Bmal1* siRNA or 75nM scrambled siRNA for 72 hours (n=4 biological replicates for all conditions). The circadian rhythm in all cells was then synchronised by a 2-hour incubation in 100nM dexamethasone and the cells were harvested every 4 hours over a 24-hour timecourse. For each timepoint NAD^+ levels were measured by an NAD^+ cycling assay before being normalised to total protein quantified by a BCA assay. NAD^+ levels are presented as the mean ng NAD^+/ug protein for 2 separate biological experiments (n=2) for (A) scrambled siRNA treated WT and miR-155KO MDFs, (B) scramble RNA, *Bmal1* siRNA and miR-155 mimic treated WT MDFs and (C) scrambled siRNA, *Bmal1* siRNA and miR-155 mimic treated miR-155KO MDFs. Error bars represent +/- SD.

4.8 miR-155KO MDFs Display a Different Metabolic Phenotype to WT MDFs

A notable feature of the miR-155KO MDFs compared to the WT MDFs is a vastly enhanced proliferation rate, highlighted by the higher optical density change in the media of the miR-155KO

cells when treated with XTT and PMS (phenazine methosulphate) for 24, 48 and 72 hours (Figure 4.8.1). In a reaction facilitated by an electron donor like PMS, the XTT undergoes reduction to formazan in the presence of cellular reductants such as NADH, resulting in a colour and optical density change due to the accumulation of formazan in the media. Hence, the increased optical density in the media of miR-155KO cells is a consequence of a net increase in metabolic activity - corresponding to increased proliferation and cell number.

Given the very different proliferation phenotypes of the miR-155KO and WT cells it was deemed of interest to investigate the potential metabolic changes induced by knockout of miR-155. Furthermore, it was posited that an altered metabolic profile may explain why despite enhanced Bmal1 expression the miR-155KO cells have significantly reduced NAD^+ levels compared to the WT cells.

Initially, mitochondrial function was probed by performing a 'Seahorse XF cell mitochondrial stress assay', which allows the oxygen consumption rate (OCR, pmol O_2/min) as a readout of mitochondrial respiration to be measured following the sequential addition of various mitochondrial inhibitors/uncouplers. The basal respiration was first measured, prior to the addition of the ATP synthase inhibitor oligomycin, followed by the mitochondrial membrane potential uncoupler FCCP (carbonyl cyanide-p-trifluoromethoxyphenylhydrazone) and then finally the ETC (electron transport chain) inhibitors antimycin A/rotenone. FCCP is an ionophore which facilitates the movement of H^+ ions across the inner mitochondrial membrane, thus disintegrating the proton gradient which usually exists across the membrane and drives ATP synthesis. The loss of the proton gradient forces the ETC to function at maximum capacity to try and restore the gradient, thus allowing maximal respiration to be quantified i.e. the full capacity of the mitochondria when working flat out. The difference in the OCR for the basal respiration and the maximal respiration then allows the spare capacity to be deduced – i.e. how much capability the mitochondria have left in reserve when not forced to work maximally. Following these measurements the total protein in each assay well is quantified such that the values are then expressed as OCR/ug protein.

There was no significant difference in the basal respiration for WT and miR-155KO cells (WT 11.83 OCR/ug protein vs miR-155KO 12.27 OCR/ug protein) (Figure 4.8.2 A). The maximal respiration and spare capacity was significantly higher in the miR-155KO cells however, indicating they have a higher mitochondrial capacity – i.e. healthier and thus better functioning mitochondria or a greater mitochondrial density.

It's important to note that due to the disparity in proliferation rates between the miR-155KO and WT cells the passage number of the cells used for these mitochondrial stress assays varied, with an average passage number of 15 for the miR-155KO MDFs and 12 for the WT MDFs. To assess the effect of increased passage number on mitochondrial function, the mitochondrial stress assays were repeated for miR-155KO MDFs with an average passage number of 26 and WTs with an average of 19 (Figure 4.8.2 B). In contrast to the measurements taken at lower passage numbers, the basal respiration was significantly higher in the miR-155KOs (WT 8.07 OCR/ug protein vs miR-155KO 14.67 OCR/ug protein). Maximal respiration was once again significantly increased in the miR-155KO compared to WT cells, however it was 111% higher at high passage compared to 46% higher at low passage (average passage number of 15 for miR-155KO, 12 for WT). The spare capacity advantage of the miR-155KOs was also enhanced at the higher passages where it was 150% greater than the WT, compared to 107% at low passage.

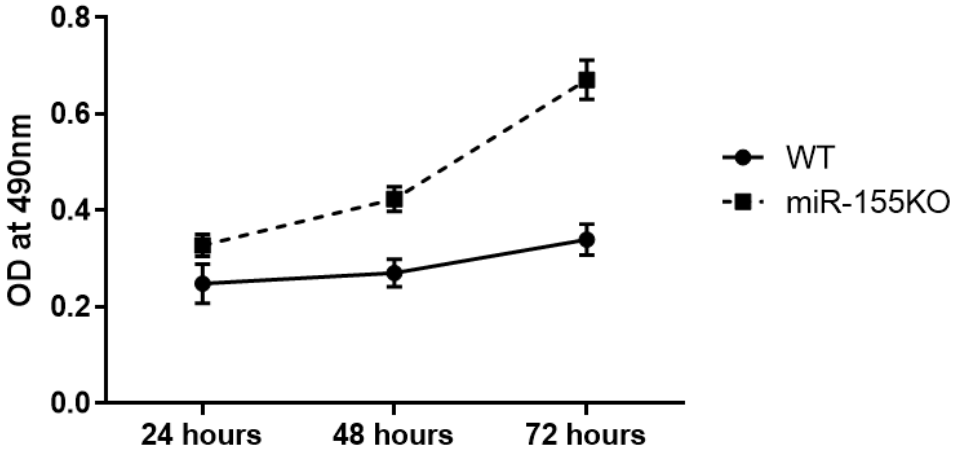

Figure 4.8.1 Proliferation rate of miR-155KO and WT MDFs.
The proliferation rate of miR-155KO and WT MDFs for 24, 48 and 72-hours post-seeding was measured using an XTT assay (n=4 biological replicates for all conditions). After seeding down, the cells were treated with 300ug/ml XTT and 20ug/ml PMS, with absorbance then measured at an optical density of 490nM after 24, 48 and 72-hour incubations. Data is shown as the absorbance at 490nm, error bars represent +/-SD. The data is representative of 3 separate biological experiments.

This suggests that the miR-155KO cells are intrinsically protected against replication induced senescence or impaired cellular function. This was very surprising given miR-155 has been widely described as having pro-tumourigenic effects [395-397], thus it was unexpected to discover that its loss induced a replicative phenotype more typical of cancer cells. There have been other studies which have identified lowered miR-155 levels as an important feature in mouse and in vitro models of malignant melanoma however [398, 399], consistent with these findings. Interestingly, these metabolic features and enhanced proliferation rate, were absent in miR-155KO MLFs derived from

the same animals (data not shown). Hence, it's important to note that the effects of absent miR-155 signalling on *in vitro* cultures appears to be highly dependent on the tissue cells are derived from.

A 72-hour pre-treatment with 50nM miR-155 mimic or 75nM *Bmal1* siRNA was once again used to see if the different mitochondrial phenotype of the miR-155KO cells relative to the WTs could be attenuated by either of these treatments, however no significant differences were observed (Figure 4.8.3 B and D). Similarly, WT MDFs also treated with the miR-155 mimic and *Bmal1* siRNA showed no significant changes to the parameters of mitochondrial function (Figure 4.8.3 A and C). Hence, transient increases in miR-155 or reduced *Bmal1* expression are unable to alter mitochondrial function, implying that the different mitochondrial phenotype of miR-155KO is an inherent feature which may have been acquired due to epigenetic or some other changes that are no longer attenuable.

As already mentioned, the interplay between OXPHOS and glycolysis is the dominant regulator of cellular NAD^+ levels, hence the glycolytic function of the WT and miR-155KO cells was next measured to test the hypothesis that enhanced glycolysis accounts for the reduced NAD^+ titres in miR-155KO compared to WT MDFs. To probe this, a 'Seahorse XF glycolysis stress test' was performed whereby the ECAR (extracellular acidification rate, mpH/min) is measured before and after the sequential additions of glucose, oligomycin and 2-DG (2-deoxyglucose) to the cells undergoing the assay. The initial stimulus of glucose activates glycolysis allowing measurement of basal levels, after which OXPHOS is inhibited by the addition of the ATP synthase inhibitor oligomycin. Inhibiting OXPHOS forces the cells to only use glycolysis for ATP production, thus the ECAR under these conditions provides a readout for maximal glycolysis. By subtracting the basal glycolysis values from the maximal glycolysis values also allows the glycolytic capacity to be determined from these measurements. Finally, adding 2-DG to the media blocks the first catalytic step in glycolysis, giving a value for non-glycolytic ECAR. Similar to the mitochondrial stress assay, total protein is quantified following the assay such that the data is presented as ECAR/ug protein.

All 3 parameters were higher in the miR-155KO cells, however the only significant difference was for the basal levels of glycolysis (WT 4.88 ECAR/ug protein vs miR-155KO 6.4 ECAR/ug protein, $p<0.05$) (Figure 4.8.4). The increased basal glycolysis combined with the enhanced maximal respiration previously measured suggests that the loss of miR-155 induces a shift toward glycolytic function, notably a hallmark of cancer cells.

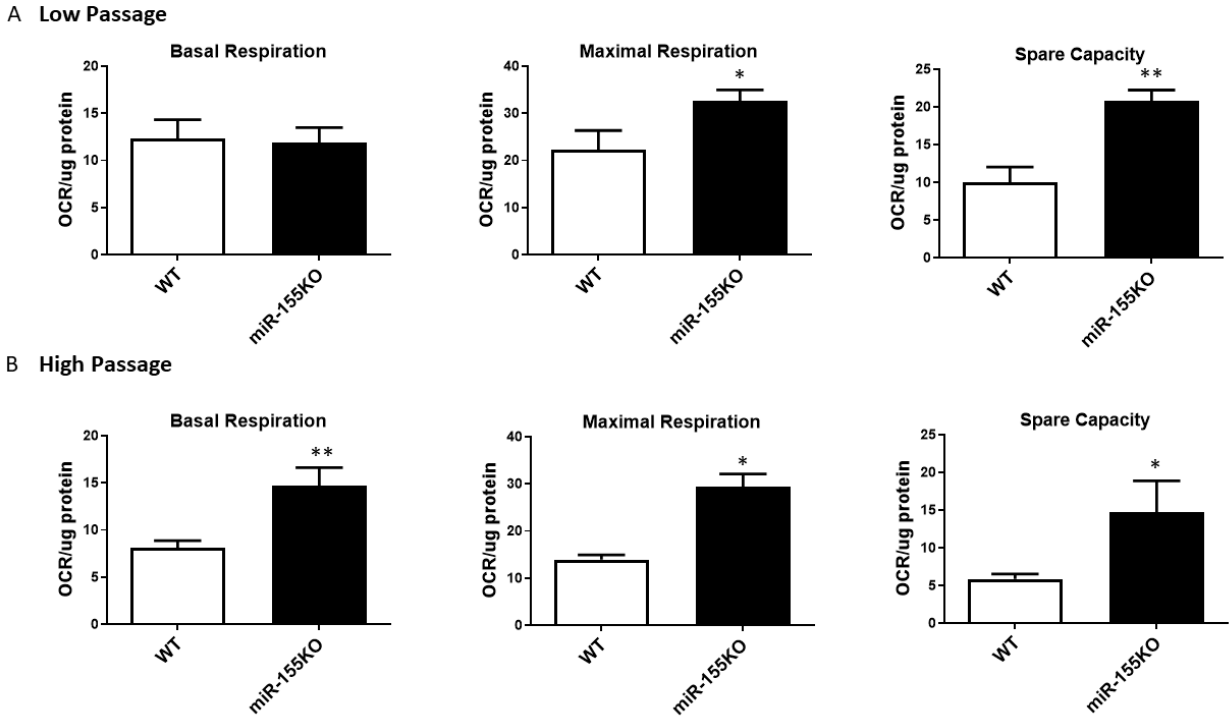

Figure 4.8.2 Mitochondrial function in low and high passage WT and miR-155KO MDFs.
Oxygen consumption rates (OCR, pmol O_2/min) as a readout for mitochondrial function were measured for miR-155KO and WT MDFs (n=3 biological replicates) at low (A) and high (B) passage following the sequential additions of oligomycin, FCCP and rotenone/antimycin A using the Seahorse XFp Analyser. Total protein for each assay plate well was then quantified by a BCA assay, allowing OCR to be normalised to protein levels. The data is shown as mean OCR/ug protein +/- SD. Significant differences between WT and miR-155KO for each parameter was tested for using an unpaired Student's t-test. *p<0.05, ** p<0.01. The data shown is representative of 2 separate biological experiments.

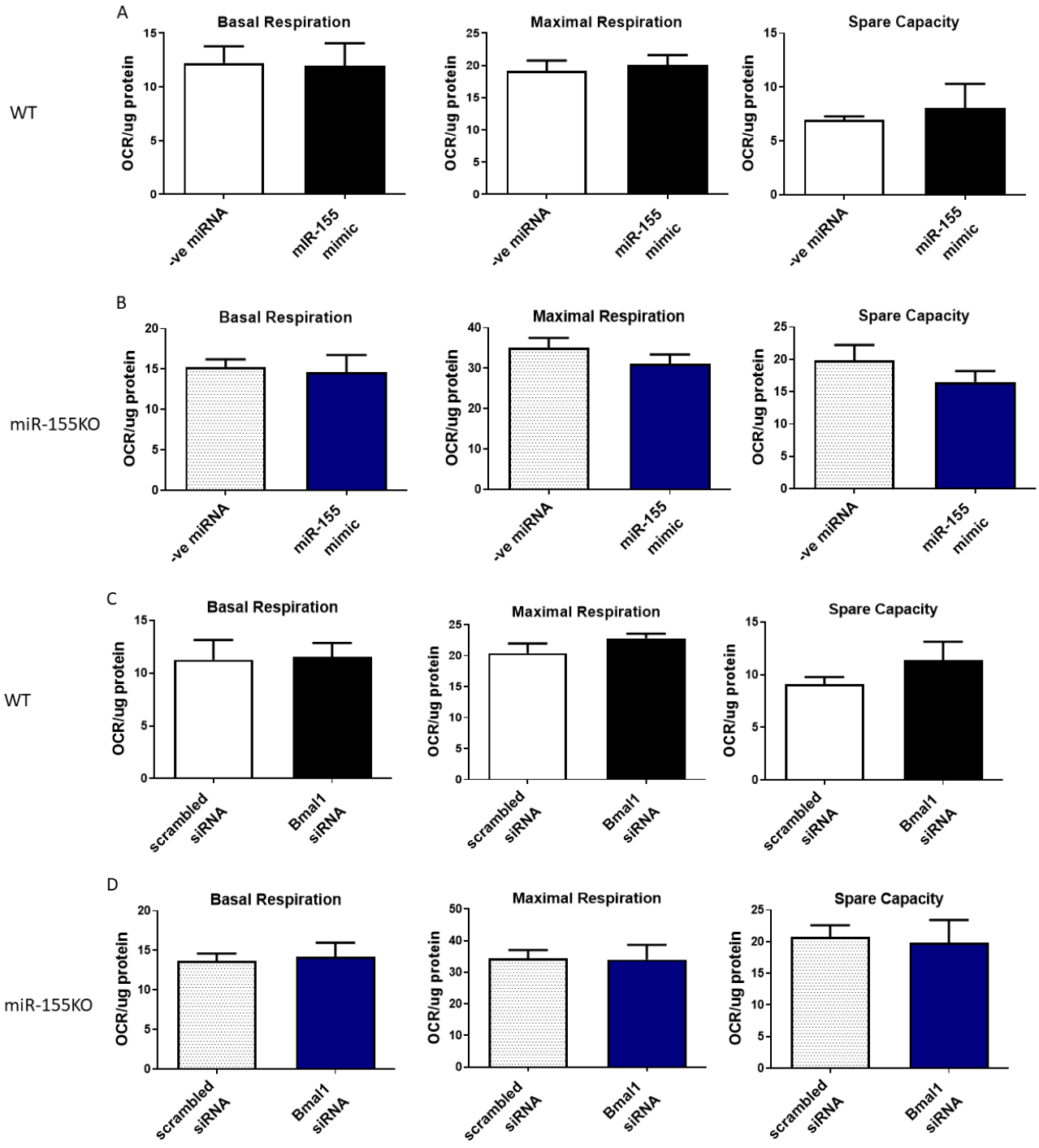

Figure 4.8.3 Mitochondrial function in WT and miR-155KO MDFs transfected with a miR-155 mimic or *Bmal1* siRNA.

(A) WT and (B) miR-155KO MDFs were transfected with 50nM miR-155 mimic or 50nM negative control miRNA for 72 hours. Additionally, (C) WT and (D) miR-155KO MDFs were treated for 72 hours with 75nM *Bmal1* siRNA or 75nM scrambled siRNA (n=3 biological replicates for all conditions). Oxygen consumption rates (OCR, pmol O_2/min) to quantify mitochondrial activity were then measured following the sequential additions of oligomycin, FCCP and rotenone/antimycin A using the Seahorse XFp Analyser. Total protein for each assay plate well was then quantified by a BCA assay, allowing OCR to be normalised to protein levels. The data is shown as mean OCR/ug protein +/- SD. Significant differences between the miR-155 mimic vs negative control miRNA and *Bmal1* siRNA vs scrambled siRNA for each parameter was tested for using an unpaired Student's t-test. Data is representative of 2 separate biological experiments.

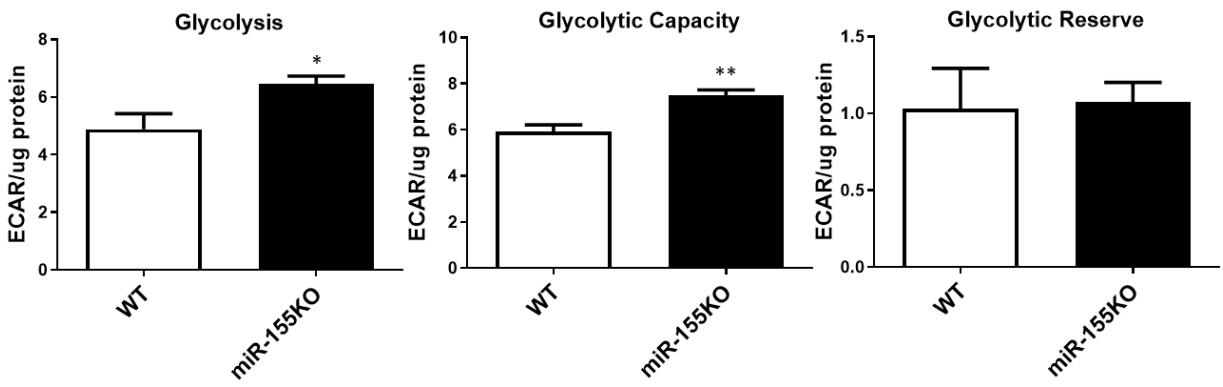

Figure 4.8.4 Glycolytic parameters of miR-155KO and WT MDFs.
Extracellular acidification rates (ECAR, mpH/min) were measured as a readout for glycolytic function in miR-155KO and WT MDFs (n=3 biological replicates for both genotypes) following the sequential additions of glucose, oligomycin and 2-DG using the Seahorse XFp Analyser. Total protein for each assay plate well was then quantified by a BCA assay, allowing ECAR to be normalised to protein levels. The data is shown as mean ECAR/ug protein, error bars represent +/- SD. Significant differences between WT and miR-155KOs for each parameter was tested for using an unpaired Student's t-test. *p<0.05, **p<0.01. The data shown is representative of two separate biological experiments.

4.9 miR-155KO MDFs Exhibit Enhanced Protection Against Oxidative Stress

To further characterise the phenotype of the miR-155KO MDFs, their viability in response to the oxidative stress inducer tbh7ox (tert-butyl hydroperoxide) was assessed. Tbh7ox functions similar to the classical oxidative stress inducer H_2O_2, inducing oxidative stress due to the high oxidising potential of the peroxide group whilst also having a higher stability than H_2O_2 – hence it's choice as the oxidative insult within this work.

Viability for miR-155KO and WT cells was expressed as % viability of the non tbh7ox treated cells, with viability measured by the fluorescence emitted in assay plate wells following a 4-hour incubation in 0.02% alamar blue media. 22 hours prior to the incubation in alamar blue, the treated cells were exposed for 2 hours to varying concentrations of tbh7ox (20 – 100uM).

The lowest dose (20uM tbh7ox) caused a 56% decrease in viability to the WTs, with no loss of viability for the miR-155KOs (Figure 4.9.1 B). Up until the 100uM tbh7ox dose the miR-155KO cells consistently displayed enhanced viability (tested for by 2-way ANOVA), with the CC50 of tbh7ox 40.0, 95% CI (31.9 – 50.3) for the miR-155KOs and 17.3, 95% CI (0.29, 1138) for the WT MDFs - suggesting the miR-155KOs possess a more potent antioxidant capacity. A possible explanation is their elevated levels of SIRT1 (Figure 4.9.1 A) which is a known activator of antioxidant pathways [176, 400, 401].

miR-155 regulation of SIRT1 levels have yet to demonstrated elsewhere in the literature, however its ability to upregulate the pro-inflammatory Wnt/β-catenin pathway is well established [402-404]. Hence, protein expression of β-catenin was also measured by western blotting to determine if miR-155 ablation had the expected outcome of reduced β-catenin levels (Figure 4.9.1 A). The clear downregulation of β-catenin observed in the miR-155KO MDFs confirms that the Wnt/β-catenin pathway is less active under basal conditions in the absence of miR-155. Consequently, in addition to protecting against oxidative stress, it is likely miR-155 knockout in MDFs mediates anti-inflammatory effects via suppression of Wnt/β-catenin signalling.

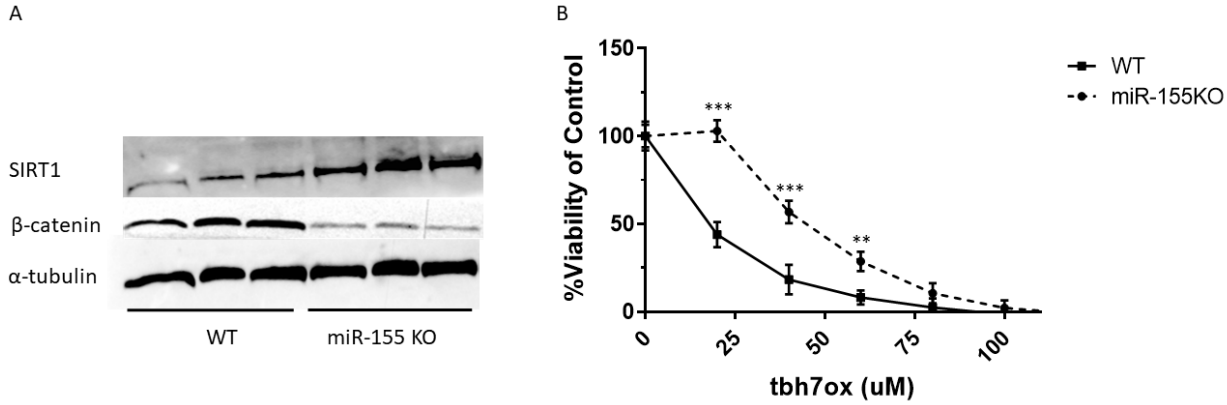

Figure 4.9.1 Antioxidant and anti-inflammatory features of miR-155KO MDFs.
(A) Sirt1, β-catenin and α-tubulin protein levels were measured in WT and miR-155KO MDFs (n=3 mice samples were derived from) by western blotting, with α-tubulin expression used as a loading control. The blot shown here is representative of 3 individual experiments. (B) WT and miR-155KO MDFs (n=4 mice samples were derived from for both genotypes) were treated with doses of 20, 40, 60, 80 or 100uM tbh7ox for 2 hours, before being returned to normal media lacking tbh7ox. 24 hours later viability was assessed following a 4-hour incubation of all assay plate wells in 0.02% alamar blue. The relative fluorescence (RFU) of all tbh7ox treated wells was expressed as a % of the RFU for the untreated WT or miR-155KO wells. The data in the graph is shown as mean % viability of the untreated control for 2 separate biological experiments, where error bars represent +/- SD.

4.10 *Bmal1*KO MLFs Exhibit Enhanced Proliferation but a Lowered Resistance to Oxidative Stress

Given the protection offered by the loss of miR-155 in the enhanced *Bmal1* expressing MDFs against oxidative stress, the effect of the loss of Bmal1 on cell viability in response to tbh7ox was next investigated using the *Bmal1*KO MLFs. An XTT assay was first performed to compare the proliferation rates of *Bmal1*KO and WT MLFs over a 72-hour period under normal growth conditions, with the surprising finding that the proliferation rate was higher in the *Bmal1*KOs.

To assess the effect of *Bmal1* knockout on the intracellular antioxidant capacity, the KO and WTs were treated with varying doses of the oxidative stress inducer tbh7ox and viability was assessed using alamar blue as done previously. 20uM and 40uM doses induced a 9% and 53% decrease in WT viability, whilst the same doses induced a 21% and 71% decrease for the *Bmal1*KOs, whereby this

difference in viability was found to be statistically different for both doses via 2-way ANOVA ($p<0.05$ for 20uM and $p<0.001$ for 40uM). Furthermore, the CC50 of tbh7ox was 40.7, 95% CI (38.9, 42.4) for the *Bmal1*KO MDFs and 34.6, 95% CI (23.2, 37.9) for the WTs. Hence, complete loss of *Bmal1* has the opposite effect of miR-155 knockout with regards to protection against oxidative stress – suggesting Bmal1 may be relevant to the protective phenotype in the miR-155KOs.

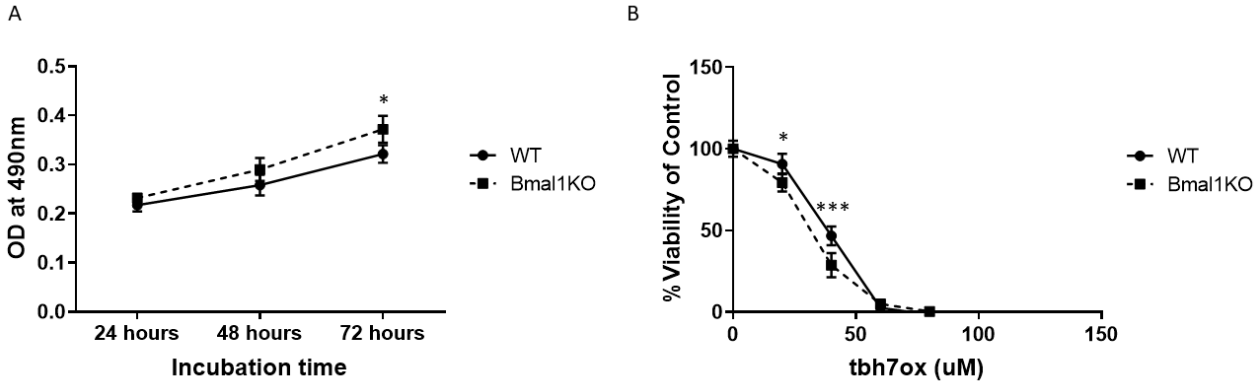

Figure 4.10.1 Proliferation and oxidative stress resistance in WT and *Bmal1*KO MLFs.
(A) Proliferation was assessed for 24, 48 and 72 hours post seeding by adding 300ug/ml XTT and 20ug/ml PMS to WT and *Bmal1*KO MLFs (n=2 biological replicates for all conditions) for the incubation times indicated. The optical density at a wavelength of 490nm was measured, indicating the extent of proliferation that occurred during the incubation period. (B) Cell viability in response to a 2-hour incubation with 20, 40, 60, 80 and 100uM concentrations of tbh7ox was quantified (n=2 biological replicates for all conditions). 20 hours after the oxidative insult, the cells were treated with 0.02% alamar blue for 4 hours and the relative fluorescence units (RFU) was then measured as a readout of cell viability. RFU values for each assay well were then expressed as a % of the untreated control. Data is shown as mean optical density or % viability +/- SD. The data is the average of the means from two separate biological experiments.

4.11 Discussion

Although circadian rhythms are a well-established biological mechanism thought to be conserved across many multicellular organisms, it is unclear the extent to which cellular processes are under their control and how it varies between cell and tissue types. BMAL1 is regarded as a 'master regulator' of circadian rhythms as well as a transcriptional activator of NAMPT expression, hence it was sought to determine whether NAD^+ levels exhibit any circadian rhythmicity and if so, whether alteration of BMAL1 levels could modulate NAD^+.

NHDFs, MDFs and MLFs all exhibit what appears to be circadian rhythmicity of their NAD^+ levels, showing the same general trend of levels starting low and gradually rising over the duration of a 24-hour timecourse. Of course, it is necessary to acknowledge the limitation of measuring mammalian circadian rhythms using an *in vitro* model: not only do these lack the hormonal input that occurs via the SCN *in vivo*, but they require circadian rhythm to be artificially induced. For this purpose, the

common approach of a short incubation in dexamethasone was used, however as a corticosteroid it is likely to have many off target effects which may influence the timecourse data. Furthermore, it is important to stress that this is a crude approach and a poor surrogate for the circadian rhythms that occur under physiological conditions, however it does establish rhythmic expression of circadian genes - it can be used probe whether other processes are under control of the intracellular circadian network.

Nonetheless, the dexamethasone pre-treatment induced an oscillation of *Bmal1* mRNA levels in MDFs, hence effectively creating a system of circadian rhythmicity even if not reflecting the exact nature of the rhythms that occur *in vivo*. Importantly, the altered NAD^+ profile in NHDFs synchronised with dexamethasone and treated with BMAL1 siRNA emphasises a prominent role for BMAL1 in the regulation of NAD^+. Furthermore, the BMAL1 siRNA failed to induce any significant change in NHDF NAD^+ under non-circadian synchronised conditions, suggesting BMAL1's regulation of NAD^+ is part of a complex network requiring the establishment of a circadian rhythm.

The mechanism by which BMAL1 regulates NAD^+ remains unclear however given siRNA induced *BMAL1* knockdown failed to reduce NAMPT protein levels - in contrast to be what had been hypothesised on the basis of previous studies describing BMAL1 mediated transcriptional control of NAMPT [234]. It would therefore be of interest to determine if the ability of *BMAL1* siRNA to alter NAD^+ following dexamethasone treatment corresponds to a change in NAMPT levels. When comparing *Bmal1* mRNA and NAD^+ levels over the 24-hour timecourse for the WT and miR-155KO MDFs there is no apparent correlation, therefore the circadian regulation of NAD^+ is more complex than the simplistic prediction that increased BMAL1 upregulates NAMPT which in turn increases NAD^+ synthesis and vice versa.

The complex relationship between BMAL1 and NAD^+ is further emphasised by the comparison of NAD^+ in WT and *Bmal1*KO MLFs, with NAD^+ found to be significantly lower in the *Bmal1*KO under non-synchronised conditions. However, the lack of any NAD^+ rhythmicity in the *Bmal1*KO cells in contrast to the WTs following dexamethasone treatment suggests BMAL1 is perhaps more important for the establishment of rhythmicity, rather than directly increasing or decreasing NAD^+ levels per se.

To investigate the effect of Bmal1 overexpression on NAD^+ and metabolism, miR-155KO and WT MDFs were used due to the upregulation of Bmal1 in the miR-155KO cells, a consequence of their lack of miR-155 which functions as an epigenetic repressor of *Bmal1*. In addition to increased basal Bmal1 protein expression, the *Bmal1* mRNA is also higher in the miR-155KO MDFs under synchronised conditions, which interestingly display a similar pattern to the WTs but with a phase

shift to the right. Despite the higher BMAL1 however, under non-synchronised conditions the NAD^+ is significantly lower in the miR-155KO MDFs - once again reinforcing the notion of the relationship between BMAL1 and NAD^+ being highly complex.

An interesting feature of the NAD^+ profile in dexamethasone synchronised miR-155KOs was a profound and transient peak at the 4-hour timepoint. This was absent in the WT cells, hence it may be that miR-155 plays a specific role in supressing NAD^+ early in the timecourse.

Due to the financial cost of running the NAD^+ assays, the experiments measuring NAD^+ in this chapter were only performed twice, going against standard experimental protocol of conducting all experiments at least 3 times. Hence, this has to be noted as a serious limitation of the work. Although preventing robust conclusions, the data generated is still informative and creates a foundation on which further work investigating the relationship between circadian rhythms, miR-155 and NAD^+ can be built.

It is also essential to acknowledge that miR-155KO cells in no way represent a bona fide model of enhanced BMAL1 levels despite their characteristically high expression. MiR-155 is a notably promiscuous miRNA which has the ability to repress many target genes, thus its knockout will affect a wide range of pathways. Indeed, in mice TargetScan identifies 3188 possible transcripts to which miR-155 could putatively bind (although in reality, it is unlikely to bind the majority).

Indeed, the multi-functional role of miR-155 is illustrated by the very different proliferative and metabolic phenotypes of the miR-155KO cells. The enhanced proliferation and basal levels of glycolysis could explain their significantly lower NAD^+ levels given a net increase in glycolysis shifts the redox balance between NAD^+ and NADH towards the reduced form. Additionally, the miR-155KO MDFs exhibit increased SIRT1 protein levels, which may also account for reduced NAD^+ if SIRT1 activity is also increased.

From a non-NAD^+ ageing perspective, the effects of miR-155 knockout merit further investigation. As well as increased SIRT1, the miR155KO cells showed strengthened resistance against the oxidative stress inducer tbh7ox, whilst their mitochondrial function was less affected by increased replication. The latter is particularly interesting, suggesting the potential presence of an anti-senescence mechanism in the absence of miR-155, however a common drawback of anti-senescent pathways is that they can also be pro-tumourigenic. Hence, it would be of use to the biogerontology field to further investigate miR-155 and the potential role of other miRNAs in ageing, given their ability to exert post-transcriptional control of many genes.

It cannot be ruled out that the different metabolic phenotype of the miR-155KO MDFs could be due to the immortalisation that mouse cells can spontaneously undergo under normoxic oxygen conditions (as opposed to physiological oxygen). The miR-155KO MDFs were noted for their which higher replication rate even at lower passages (<10), which combined with the similar phenotype in all the MDFs from 4 different animals however does suggest that this is unlikely, however the possibility should still be acknowledged.

To follow up the findings reported within this chapter, it would be of interest to use the miR-155KO mouse model for *in vivo* studies on lifespan, healthspan and response to senescent/other pro-ageing stimuli. With regards to BMAL1 and NAD^+, the *Bmal1*KO mice could also be used for further analysis to determine if NAD^+ titres within different tissues are affected by loss of *Bmal*1, which could also be performed over a 24-hour timecourse. Finally, to better understand the effect of sleep/wake cycles on NAD^+ levels, this could be assessed in rodent models or possibly in humans by obtaining blood samples from shift workers when working different rotas. Although this work establishes a tentative link between miR-155, BMAL1 and NAD^+, the aforementioned *in vivo* studies would be necessary to identify any physiological relevance regarding this interaction.

Chapter 5. Interventions to Enhance Human PBMC NAD^+ Levels *In Vivo*

5.1 Introduction

Given the recent emergence of NAD^+ as a potentially key molecule in physiological ageing, there is an intense interest in approaches to reverse the decline in NAD^+ levels suspected to occur with increasing age. A demonstration of this age-related decline was first provided by Massudi *et al.* [70], who found that in pelvic skin samples there was a linear relationship between increasing age and declining NAD^+ over a 0 – 80 years age range.

There is also evidence for an age-related NAD^+ decline in the liver, with non-pathological liver tissue obtained by hepatectomy from patients >65 years old exhibiting NAD^+ levels approximately 30% lower than that of non-pathological liver tissue from patients <45 years old (2). Furthermore, using MRI Zhu *et al.* found that brain concentrations of NAD^+ declined in a linear fashion over a 21 – 68 year-old age range (3), hence it appears NAD^+ is depleted in multiple tissues with increasing age. It is important to consider however, that the large variability in the metabolic phenotype of different tissues implies it is likely that certain cell types/tissues will be more susceptible to age-related NAD^+ decline. In particular, tissues with a high demand for ATP via OXPHOS would be more likely to see a reduction in the NAD^+/NADH ratio with increasing age due to higher rates of mitochondrial turnover and accumulation of mitochondrial oxidative damage. Consequently, this would impair electron transport chain function and the resulting oxidation of NADH to NAD^+.

Age-related changes in NAD^+ have yet to be investigated for PBMCs, however an effective NAD^+ enhancing intervention would need to work in multiple tissues, therefore PBMCs were chosen as the sample type for the work presented herein – primarily due to the ease of collecting these cells from human participants.

At present, the most common approach to increase NAD^+ *in vivo* is by oral ingestion of the NAD^+ precursor nicotinamide riboside (NR), currently marketed worldwide as a supplement to enhance NAD^+. A number of studies (Table 5.1.1) have recorded notable success at increasing NAD^+ using NR [310, 311, 405], with the largest increases reported being 129% following 21 days of NR supplementation in a 70-80 year-old male cohort [310] and 217% for a single individual after 7 days of consumption [152]. No data has been published investigating whether there is a difference in the efficacy of NR or NR containing combinations for different age groups – a feature which would help identify whether a ceiling effect exists, whereby such treatments are more effective with increasing age due to greater 'room' for NAD^+ enhancement.

It stands to reason that NAD^+ enhancement greater than that reported for NR thus far would indeed be possible, mainly given NR is an input into just a single arm of the complex network of enzymes and cellular processes that regulate intracellular NAD^+. A more tailored approach that targets inefficient enzymes that utilise NAD^+ and increases the re-cycling of NAD^+ metabolites back into the NAD^+ salvage pathway, in addition to providing precursors for NAD^+ synthesis has the advantage of targeting numerous mechanisms which regulate NAD^+ levels. To this end, many of the enzymes fulfilling these roles are known targets of various polyphenols (Table 5.1.2), thus opening the possibility to modulate them via dietary based interventions.

To test this theory, supplement cocktails containing multiple compounds targeting key enzymes involved in NAD^+ metabolism were given to 2 participants as part of a pilot study. The cocktails were conceived and developed by an enterprise specialising in network pharmacology, thus were designed with the intent to achieve maximal enhancement of NAD^+. The participant NAD^+ levels were specifically measured in PBMCs rather than whole blood due to the particular interest in enhancing NAD^+ as a means to promote SIRT1/PARP1 activity, which given the nuclear localisation of these two enzymes would be irrelevant in erythrocytes (the most abundant cell type in blood) which lack nuclei and mitochondria. It is of course necessary to note that the experimental design is limited by the use of only 2 participants, however as a pilot study it is still informative given the lack of data available regarding the implementation of multi-targeted approach to enhance NAD^+ titres *in vivo*.

5.2 Aims

The primary aim was to determine whether combinations of different compounds targeting NAD^+ related pathways were effective at raising NAD^+ levels in human PBMCs and how this compares with a precursor only approach.

5.3 Hypothesis

It was hypothesised that the supplement cocktails would significantly increase participant NAD^+ levels, with greater increases than those reported for studies using only using precursors such as NR. The cocktail versions with more targets in the NAD^+ degradation/recycling pathways should exhibit superior enhancement compared to the more simplified versions.

Table 5.1.1 Studies using precursors to enhance human NAD⁺.

Study Design	Cohort	Daily Dosage	Treatment Duration	Sample Type	Results
1 group receiving **NAM.** [150]	1 MELAS patient	4g **NAM** (4x 1g doses).	5 months	Whole blood	Max ↑ **NAD+ of 2400%** after 6 weeks of treatment. Declined to **600% ↑ NAD⁺** after 5 months.
1 group receiving **NA**. [148]	Healthy adults (n=2)	100mg **NA.**	56 days.	PBMCs	↑ **NAD⁺** for all weeks measured. Max increase **on week 8 of almost 5-fold** (raw values not given).
4 groups: 25mg **NA**, 50mg **NA**, 100mg **NA**, placebo. [149, 406]	Healthy male smokers (n=21)	25mg **NA**, 50mg **NA**, 100mg **NA**, placebo.	98 days.	PBMCs	Significant ↑ **NAD⁺** only for group consuming **50mg niacin**. Raw values/% changes not given.
2 groups: Patients, age/sex-matched controls. [140, 151]	5 MM patients and 10 age-matched healthy controls.	1st month – 250mg **NA**, 2nd month – 500mg **NA**, 3rd month – 750mg **NA**, 4th month – 100mg **NA**.	4 months controls, 10 months patients.	Whole blood, skeletal muscle	At 4 months: **610% ↑ NAD⁺** for patient blood samples and a **470% ↑ NAD⁺** for controls. 30% ↑ **NAD⁺** patient muscle NAD+, no change for controls. At 10 months: **720% ↑ NAD⁺** for patient blood samples and a **130% ↑ NAD⁺** patient muscle NAD+.
1 participant receiving **NR**. (9)	A 52 year-old male.	1000mg **NR**.	7 days.	PBMCs	After 1 day **167% ↑ NAD⁺**, after 7 days **217% ↑ NAD⁺.**
3 treatment arms: 1x NRPT, 2x NRPT, placebo. (6)	Healthy adults aged 60-80 (n=120).	1x NRPT – 250mg **NR** + 50mg **pterostilbene**. 2x NRPT – 500mg **NR** + 100mg **pterostilbene.**	60 days (blood taken at baseline, day 30 and day 60).	Whole blood	1x NPRT: **40% ↑ NAD⁺** at day 30 and day 60. 2x NPRT: **90% ↑ NAD⁺** at day 30 and **55% ↑** day 60.
Crossover: **NR** and placebo. [407]	Healthy adults aged 55-79 (n=60).	1000mg **NR** (500mg 2x daily).	42 days.	PBMCs	**60% ↑ NAD⁺** after 6 weeks NR compared to placebo.
Crossover: **NR** and placebo. (8)	12 male adults (median age 75).	1000mg **NR.**	21 days.	Whole blood, skeletal muscle	**129% ↑ whole blood NAD⁺** after 21 days NR compared to placebo. **No significant change in skeletal muscle NAD⁺.**
4 treatment groups: 100mg **NR**, 300mg **NR**, 1000mg **NR**, placebo. [408]	Healthy adults aged 40-60 (n=140).	100mg **NR**, 300mg **NR**, 1000mg **NR** or placebo.	56 days.	Whole blood	After 14 days: **100mg – 22%, 300mg – 51%, 1000mg – 142% ↑ NAD⁺.** After 56 days: **100mg – 10%, 300mg – 48%, 1000mg – 139% ↑ NAD⁺.**
Crossover: **NR** and placebo. [409]	13 healthy or overweight adults (n-13).	1000mg **NR**.	42 days.	Skeletal muscle (collected day 37)	**No significant change in NAD⁺.** 677% ↑ NAAD, 62% ↑ meNAM.

Abbreviations: NAM – nicotinamide, NRPT – nicotinamide riboside + pterostilbene, NR – nioctinamide riboside, MM – mitochondrial myopathy, MELAS - Mitochondrial encephalopathy, lactic acidosis, and stroke-like episodes.

Table 5.1.2 Key enzymes in NAD^+ synthesis and degradation pathways.

Enzyme	Mechanism	In vivo	In vitro	Activators	Inhibitors
AMPK	Upregulates NAMPT expression	↑ NAMPT protein levels [410] ↑ NAD^+ [411]	↑ NAD^+ via ↑ β-oxidation [411]	Berberine [412] **Alpha lipoic acid** [324] **Rutin** [413] Curcumin [414, 415] Metformin [416]	Dorsomorphin [417]
NAMPT	Conversion of NAM to NAD^+	↑ NAD^+ [418-420]	↑ NAD^+ [418, 420, 421]	SBI-797812 [418, 422] **Rutin** [423]	GMX1778 [424] FK866 [345]
NQO1	Converts NADH to NAD^+ during reduction of quinones	↑ NAD^+ [425, 426]	↑ NAD^+ [146]	**Alpha-lipoic acid** [427] **Apigenin** [428] B-lacaphone [426] Curcumin [429]	ES936 [430] Coumarin based compounds [431]
NRK 1/2	Phosphorylates NR to produce NMN within salvage pathway	↑ NAD^+ [181, 432]	↑ NAD^+ [146],[432, 433]	**Resveratrol** [433, 434]	-
NMNAT	Converts NMN to NAD^+	↑ NAD^+ [181]	↑ NAD^+ [435],[436]	**Resveratrol** [434]	Gallotanin [437] 6-MPRT [438]
NNMT	Methylates NAM, removing it from salvage pathway	↓ NAD^+ [406, 439]	-	-	BSNF-000088 [440]
CD38	Hydrolyses ADPR/cADPR via an NAD^+ dependent reaction	↓ NAD^+ [141, 418, 441-443]	↓ NAD^+ [444, 445]	-	**Apigenin** [156] 78c [422, 446]

*Ingredients used in NCD cocktails are highlighted in bold.

5.4 Enhancement of Human PBMC NAD^+ Using NR

A recent study brought into question the bioavailability of NR by showing that in mice, orally delivered NR that was isotopically labelled was almost entirely converted to NAM (nicotinamide) [447], an issue overcome if instead delivered intravenously. The conversion of NR to NAM may not be an issue if this NAM itself is subsequently converted to NAD^+, which is likely given the many studies showing the ability of oral NR to enhance blood NAD^+ [152, 311, 407]. Nonetheless, it was sought to verify whether NR was effective at increasing NAD^+ titres in a small human cohort (n=5).

Given a circadian oscillation of NAD^+ has already been characterised in liver tissue of mice [448-450] and *in vitro* within this thesis (Chapter 3) and other studies [234], it was deemed essential that samples would always be collected at the same timepoint on all study days, hence controlling for circadian rhythms. Participants were also told to keep sleep/wake times consistent for the duration of the study, once again to control for circadian rhythms which are strongly influenced by sleep patterns. Likewise, the potential effect of diet and time of feeding was controlled for by asking participants to keep a food diary and replicate this for both study weeks. 3 baseline blood samples were taken on 3 different days (days 1, 3 and 5) during the same week and compared to samples collected on days 1, 3 and 5 of the following week in which 500mg NR (Niagen) was taken at the same time with breakfast every morning for 5 days.

4 out of the 5 participants showed an increase in NAD^+ levels when comparing the treatment week average to the baseline week average (Figure 5.4.1 A), although a statistically significant difference wasn't observed for any of them. Looking at the NAD^+ titres for the individual treatment days on which samples were collected, 3 out of the 5 participants had a >90% increase in NAD^+ compared to the baseline average on day three, however for female 1 and 2 the NAD^+ returned close to baseline levels on day 5 (Figure 5.4.1 B). This is the first time NAD^+ levels in response to NR ingestion has been monitored on multiple days throughout the same week, indicating that its efficacy is highly variable on different days – likely due to a variety of other physiological factors that interact with NAD^+ regulating pathways.

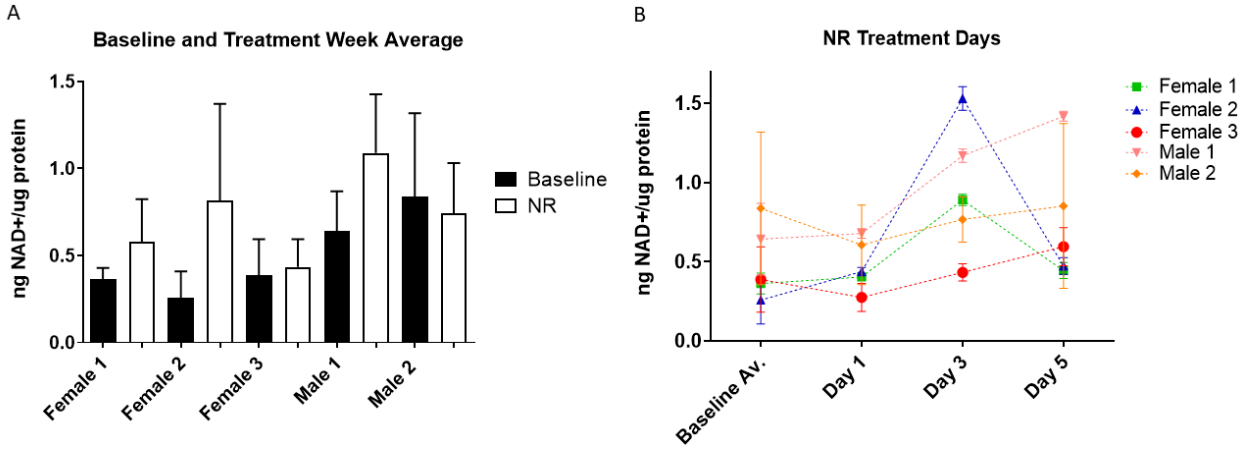

Figure 5.4.1 PBMC NAD⁺ levels during 5 days of NR supplementation.
Blood samples were collected at the same timepoint on days 1, 3 and 5 during a week in which the 5 participants didn't consume NR. The following week all participants consumed 500mg of NR at the same time every morning for 5 days and blood samples were once again collected on days 1, 3 and 5 at the same timepoint as for the previous week. PBMCs were isolated following each blood collection and immediately stored at -150°C. NAD⁺ levels were measured using an NAD⁺ cycling assay, before being normalised to protein concentration for each sample by performing a BCA assay. (A) The average ng NAD⁺/ug protein for the baseline week (n=3 separate biological samples) and NR treatment week (n=3 separate biological samples) for each participant is shown as mean +/- SD. Statistically significant differences between the baseline and treatment average for each participant was tested for using a paired Student's t-test. (B) The baseline average (n=3) and NAD⁺/ug protein for the individual treatment days (n=1) is shown. Error bars represent +/- SD of the two technical replicates for each treatment day sample.

5.5 A Multi-Targeted Approach to Enhancing Human NAD⁺ Titres

5.5.1 Human PBMC NAD⁺ Exhibits a Circadian Rhythm

To test the hypothesis that a more sophisticated multi-targeted approach would yield improved enhancement of NAD⁺ levels *in vivo* compared to NR, the efficacy of the supplement cocktails NCD201.1, NCD201.2, NCC202, NCD203 and NCD205 at enhancing NAD⁺ was assessed. All these cocktails contain multiple compounds with different targets within the NAD⁺ network. Given the existence of a circadian rhythm of NAD⁺ and also the possibility that there may be an upper limit to physiologically achievable NAD⁺ levels, whether the cocktails were more efficient at timepoints where NAD⁺ hits a daily nadir was of particular interest. Furthermore, the need for increased NAD⁺ would be most relevant at daily timepoints where an individual experiences a daily low. Thus, for both volunteers recruited for the pilot study (52 year-old male and 37-year old female) NAD⁺ was measured over the same 12-hour time period (8am – 8pm) to try and identify any individual peaks and troughs and to determine if their NAD⁺ levels followed a discernible diurnal pattern as predicted.

For the male two noticeable troughs were identified at 10am (day 1 - 0.23ng NAD^+/ug protein, day 2 - 0.20ng NAD^+/ug protein) and 2pm (day 1 – 0.43ng NAD^+/ug protein, day 2 – 0.14ng NAD^+/ug protein, day 3 – 0.21ng NAD^+/ug protein), with a noticeable peak at 12pm (day - 1.04ng NAD+/ug protein, day 2 – 0.97ng NAD^+/ug protein). Although the original intention was to obtain a complete profile of the NAD^+ fluctuations on 3 different days, only the 10am, 2pm and 6pm timepoints were collected on the third baseline day due to cannulation issues. Both days on which all samples were collected showed similarity however in that NAD^+ levels began low, before a sharp rise at 12pm and then a sudden drop at 2pm, after which they continued rising throughout the rest of the day. This was also somewhat resembled on baseline day 3, with the 2pm NAD^+ representing a low point before rising to a peak at 6pm.

Likewise, for the female there was variability across the 3 baseline days but a general trend was observed. The 8am levels were also low, however sharply rose at 10am (day 1 – 0.46ng NAD^+/ug protein, day 2 – 0.31ng NAD^+/ug protein, day 3 – 0.64ng NAD^+/ug protein) resembling the peak seen for the male at 12pm. This was also then followed by a drop in NAD^+, however this was less steep and more prolonged, lasting until 4pm before rising again.

The large variability between the different baseline days is emphasised by a 2-way ANOVA analysis, whereby there was a significant difference between all the baseline days for the female ($p<0.001$) and baseline days 1 and 2 for the male ($p<0.01$). This suggests that in addition to varying within the same day, PBMC NAD^+ levels show very high day to day variability over the course of the same week.

It's important to note that consistent blood drawing and processing is imperative when measuring NAD^+ given its labile nature and the likelihood that RBCs (due to their lack of nuclei/mitochondria and thus unique NAD^+ metabolism) possess a very different NAD^+ profile to PBMCs - hence their contamination must be kept to an absolute minimum when isolating the PBMCs from whole blood.

For this reason, when it came to calculating the average baseline values for each participant the 2pm baseline day 2 value for the male participant was disregarded due to high levels of RBC contamination (visually noticeable within the PBMC pellet), whilst the entirety of day 2 was excluded for the female due to problems with cannula insertion and the resulting concerns over excessive RBC contamination within the PBMC fraction due to clotting. Indeed, this is reflected in the results, with the male participant's baseline day 2 2pm value and the majority of baseline day 2 for the female appearing considerably lower than for the other days. Therefore in hindsight, the use of a RBC lysis buffer may have overcome these issues. Cell sorting is another method that could used separate

different blood cell types, however given the need to isolate PBMCs at cool temperature and as quickly as possibly, wouldn't be appropriate for this work.

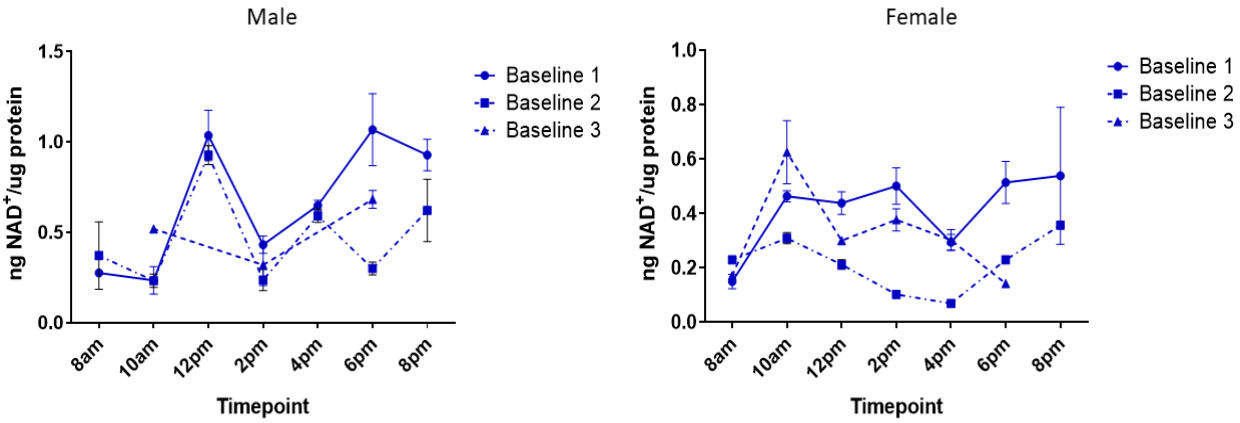

Figure 5.5.1.1 PBMC NAD^+ levels fluctuate over a 12-hour timecourse.
The daily fluctuation of NAD^+ levels on three separate days is shown for a male and a female participant. Blood samples were collected by cannulation at 2-hour intervals between 8am and 8pm (n=1 biological sample for each timepoint) and the PBMCs isolated by density centrifugation prior to freezing at -150°C. Upon thawing NAD^+ levels were measured by performing an NAD^+ cycling assay before being normalised to protein levels using a BCA assay. NAD^+ levels are therefore shown as mean ng NAD^+/ug protein. Error bars represent +/- SD of the two technical replicates for each treatment day sample.

Table 5.5.1.2 Dietary compounds targeting NAD⁺ related enzymes and in vivo anti-ageing evidence.

	NAD⁺ related enzymes	Dietary sources (mg/100g)	*In vivo* anti-ageing evidence
alpha-lipoic acid	↑NQO1 [427, 451] ↑AMPK [324, 452] ↑ SIRT1 [324]	Animal kidney – 260 [453] Animal heart – 150 [453]	Improves memory and reduces oxidative damage, but decreased lifespan in an Azheimer's disease mouse model. [454] Increases lifespan in *C. elegans*. [455]
apigenin	↑ NQO1 [428] ↓ CD38 [156, 456]	Dried parsley – 4504 gov [457] Fresh parsley – 216 [458]	Extends lifespan and improves motor function *D. melanogaster* model of Parkinson's disease. [459] Reduces oxidative stress, improves learning and motor function in D-galactose induced aged mice. [460]
rutin	↑ NAMPT [423] ↑ AMPK [413, 461, 462]	Buckwheat flower tea – 396 [463]	Extends lifespan in *D. melanogaster* [464] Reduces age-related pathology in ageing mouse model. [465]
resveratrol	↑ NRK1/2 [434] ↑ SIRT1 [466] ↑ NMNAT1 [315]	*Fallopia Japonica* – 2.1 [467] Itadori tea – 0.97 [468] Red wine – 0.85 [468]	Increased lifespan in Alzheimer's mouse model. [314] Improves cognition in aged and senescence-accelerated mice. [313, 469]
quercetin	↑ CD73 [470]	Capers – 234 [471] Lovage - 170 [458] Dock leaves - 86 [472]	Decreases disease pathology and improves cognitive function in Alzheimer's mouse model. [473] Extends lifespan in *C. elegans*. [474]
EGCG	↓ PARP1 [475]	Green Tea (dried leaf) - [476] Carob flour – 109 [477]	Extends lifespan and prevents age related mitochondrial decline in *C. elegans*. [478] Extends lifespan and reduces age-related increase in oxidative stress/inflammation in rats. [479]
curcumin	↑ NQO1 [429] ↑ AMPK [414, 415]	Curcuma roots (turmeric) – 8-125 [480]	Extends lifespan in mice [481] and reduces age-related brain pathology. [482]
fisetin	↑ SIRT1 [483, 484]	Freeze dried strawberries – 16 [485]	Extends lifespan, reduces age-related pathology in aged mice. [486] Improves cognition in rapid ageing mouse model. [487]
luteolin	↑ NAMPT [488]	Dried oregano – 1029 [489] Celery seed – 762	Reduces neuroinflammation and improves learning and memory in aged mice. [490, 491]

5.5.2 NCD201 Enhances PBMC NAD^+ Levels During a 16-day Treatment Phase

The first supplement cocktail (named NCD201) tested for its efficacy at enhancing NAD^+ levels contained 1000mg NR, 1125mg quercetin, 450mg resveratrol, 600mg alpha-lipoic acid and 600mg apigenin. The 1000mg represents the largest dose of NR used over a prolonged treatment period thus far in clinical studies, previously shown to increase NAD^+ up to 217% in PBMCs [152]. The components additional to NR within this cocktail were selected for their ability to modulate the activity or expression of targets involved in NAD^+ metabolism (Table 5.5.1.2).

Both participants began the consumption of NCD201 3 days after the completion of their baseline measurements, consuming it at the same time every morning for 16 consecutive days (no placebo or blinding in place). During this time, blood samples were collected for PBMC isolation every 2 or 3 days at the 2pm timepoint for the male and 4pm for the female. The 2pm timepoint was chosen for the male participant due to it giving consistent NAD^+ levels across the 3 baseline days, thus suggesting this low-point is a reliable feature of his NAD^+ profile. Furthermore, as it is of particular interest to enhance NAD^+ during daily nadirs when an enhancement of NAD^+ would be most necessary, this reinforced the decision that this was the appropriate timepoint to select. Likewise, for the female the 4pm timepoint was a consistent point at which NAD^+ levels dipped, hence it was chosen for her blood draws during the treatment period.

For the male participant the average increase of NAD^+ at the 2pm timepoint during the 16-day NCD201 treatment phase was 301% with a maximum increase of 821% (treatment day 11) and a minimum increase of 7.9% (treatment day 3) (Figure 5.5.2.1 A). This average of 301% is well above the largest previously reported increases for human studies using NR (Table 5.5.1), although this data is very preliminary given it is n=1 and cannot undergo statistical analysis. Interestingly, the largest increases were on days 11 and 14 before dropping off on day 16, perhaps suggesting there was some sensitisation to the cocktail by day 16 - thus raising the question as to what length of time the cocktail can maintain enhanced NAD^+ without the levels returning to baseline.

Furthermore, on treatment days 1 and 16 sampling was performed at multiple timepoints for the male (Figure 5.5.2.1 B). Samples were successfully obtained for all timepoints on day 16, however for treatment day 1 only the 10am, 12pm and 2pm samples were collected due to cannulation issues and concerns about the potential damage this would do to the participants' veins with numerous testing days still ahead. Hence, it was decided to obtain the full NAD^+ profile on only a single day and to save this for the last study visit. For treatment day 1, whilst the 2pm NAD^+ measurement was significantly higher than the baseline average, there was only a small increase at 10am (19.6%) and

12pm (6.5%). Given the participant consumed the cocktail at 8.30 am, this suggests it takes NCD201 >3.5hrs to be effective on the first day of consumption.

In addition to the 2pm timepoint, on treatment day 16 there was also notably large increases in NAD^+ levels when compared to the corresponding baseline average timepoint at 8am (210%), 10am (316%) and 4pm (192%). Overall, when compared to the baseline mean the day 16 NAD^+ levels were on average 122% higher and indeed elevated at every timepoint, with a maximum increase of 316% (10am) and a minimum of 33% (8pm). Therefore, even after 16 days of daily consumption the cocktail still maintains its ability to enhance NAD^+, although the absence of data for all the timepoints on the previous treatment days means it's unknown whether, as for 2pm, the enhancement at these timepoints is also on a downward trend.

Due to the constraints of the female participant having only one viable vein to use over the course of the study, a full day of NAD^+ measurements from 8am to 8pm whilst on the treatment wasn't attempted. However for the 4pm blood draws, a similar trend to that of the male participant was observed with the largest increases occurring on treatment days 10 (217% increase) and 11 (174% increase) before slightly tailing off on day 16 (150% increase) (Figure 5.5.2.1 C). It is interesting to note that in contrast to the male, NAD^+ was still substantially higher than the baseline on day 16. The average increase across the treatment period for the female 147%, with a maximum of 258% and minimum of 79%, thus NCD201 induced a lower increase in NAD^+ for the female although the increases recorded were much more consistent across the treatment days, as evidenced by the lower SD (305% for the male vs 48% for the female).

For the male participant, two further measurements of PBMC NAD^+ levels were made at 5 days (washout 1) and 9 days (washout 2) following completion of the treatment phase (Figure 5.5.2.1 D). This was done to check whether NAD^+ levels returned to the baseline values following a short period of supplement abstinence. Surprisingly, the 2pm NAD^+ levels on washout days 1 and 2 were higher than the baseline average (increases of 79% and 54% respectively). It is not clear whether this increase is due to long-lasting effects of the cocktail or possibly an unrelated physiological change within the participant.

On both these washout days, in addition to the 2pm timepoint blood was also collected at 2-hour intervals from 8am to 8pm so that the 12-hour profile could be compared to that of the baseline days. Aside from 2pm, the only other timepoint at which the washout and baseline averages were notably different was 8am, with washout 1 182% higher than the baseline average and washout 2 127% higher. The reason for the prominent change at this particular timepoint isn't obvious,

however given it's the earliest point measured it may be much more susceptible to the effects of sleep quality, which is known to influence circadian rhythms.

Including all the daily timepoints NAD^+ was measured at, on average NAD^+ levels on washout day 1 were 54% higher than the baseline average, whilst on baseline day 2 the average was only 16% higher.

When comparing the day 16 profile to the profiles taken on the two washout days (5 days and 9 days later), the day 16 NAD^+ is on average 64% greater, with statistically significantly higher levels at 12pm, 4pm and 6pm. As already discussed, it may be some lasting effects of the cocktail or an unrelated physiological change which accounts for the higher washout NAD^+ compared to the baselines, however aside from 8am, the day 16 spikes in NAD^+ are absent during the washout days.

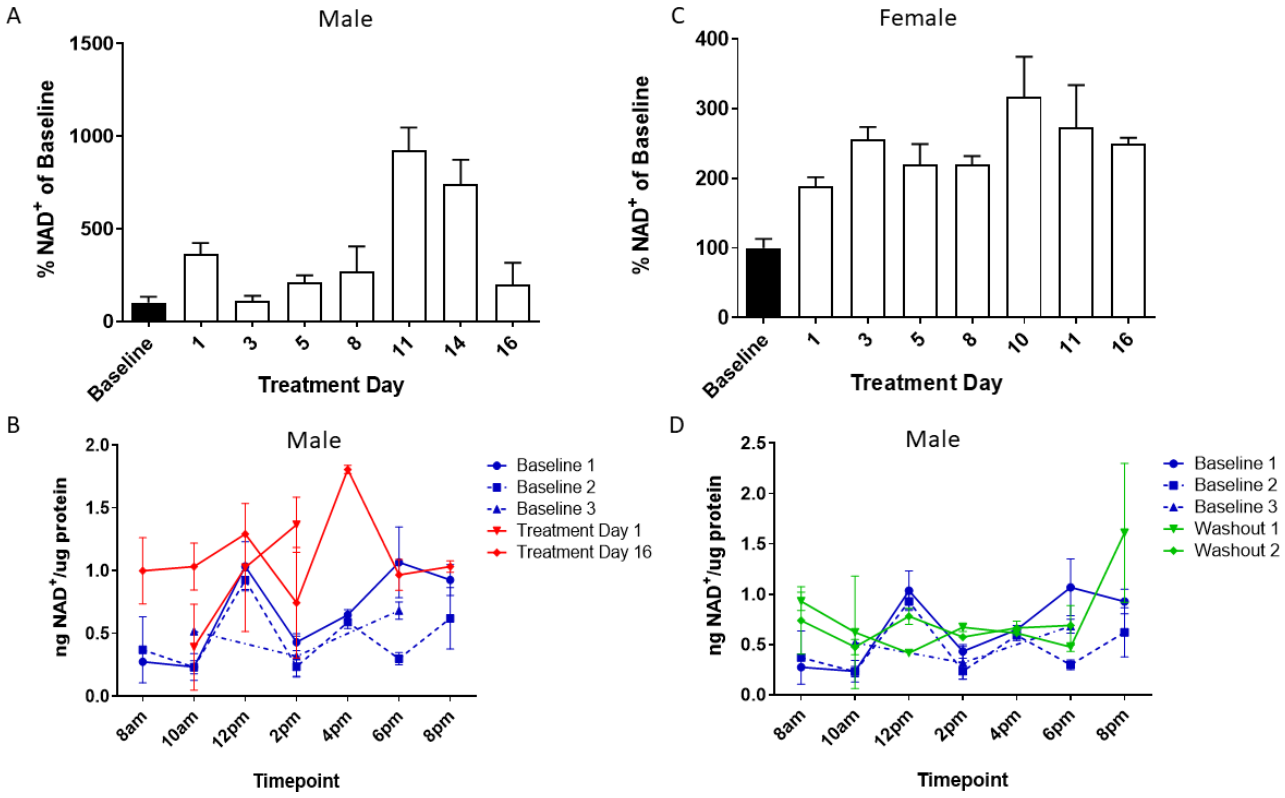

Figure 5.5.2.1 NAD^+ titres in the PBMCs of two volunteers after 16 days consumption of NCD201.1.
(A) The average NAD^+ levels measured at 2pm during the pre-treatment baseline week (n=3 biological samples) is compared to the NAD^+ levels at 2pm (n=1 biological sample for each treatment day) on the days indicated during a 16-day treatment period of NCD201 consumption for the male participant. Values are expressed as % ng NAD^+/ug protein of the baseline 2pm average for the 2 technical replicates. (B) The average NAD^+ levels measured at 4pm during the pre-treatment baseline week (n=3) is compared to the NAD^+ levels at 4pm on the days indicated (n=1) during a 16-day treatment period of NCD201 consumption for the female participant. Values are expressed as % ng NAD^+/ug protein of the baseline 4pm average for the 2 technical replicates. (C) The NAD^+ levels at the timepoints indicated are shown for the male participant on the pre-treatment baseline days (n=3) and on days 1 and 16 of the treatment period (n=1). Values are shown as ng NAD^+/ug protein of 2 technical replicates. (D) The NAD^+ levels at the timepoints indicated are shown for the male participant on the 3 pre-treatment baseline days and on washout days 1 and 2 (n=1), which were 5 and 9 days after the treatment phase ended. Values for the timepoints are shown as ng NAD^+/ug protein. Error bars represent +/- SD of the two technical replicates for each treatment day sample.

5.5.3 NCD201.2 Enhances NAD^+ But to a Lesser Extent Than NCD201

On the Monday of the week following the washout measurements (12 days after finishing the NCD201 treatment period), the male participant began an 8-day treatment phase of NCD201.2 - a cocktail containing the same ingredients as NCD201.1 but from different manufacturers and at different quantities. For this treatment phase blood samples were taken at both the 2pm and 4pm timepoints, testing the hypothesis that any changes induced by the cocktail would be greater at the timepoint associated with the daily nadir (2pm) compared to a timepoint in which the NAD^+ appeared to be rising (4pm). Although 4pm wasn't the point of peak NAD^+ during the baseline measurements, it was chosen due to the combination of it being a timepoint of rising NAD^+ and the consistent values across the different baseline and washout days. Because the washout week preceded this treatment, the NAD^+ averages for the timepoints on the two washout days were taken as the new baseline.

Given the expectation that the effects of the cocktail would be more pronounced at the nadir timepoint, it was surprising to find that 4pm showed a significant increase in NAD^+ levels on more days during the treatment phase (days 3, 6, 7 and 8) compared to 2pm (days 3 and 8) (Figure 5.5.3.1 A). The average increase across the treatment phase was however greater at 2pm (79% vs 55%), as was the maximum increase recorded (2pm day 8 - 176% vs 4pm day 7 - 108%).

It is therefore possible that the cocktail may simply be having a similar additive effect at all timepoints rather than preferentially enhancing at the timepoints associated with a daily low in NAD^+ levels. Alternatively, the length of time it takes the compounds to be metabolised and subsequently interact with their targets may make the cocktail more effective at later daily timepoints. It is also important to note that during the washout phase the 2pm NAD^+ levels were no longer a nadir, which provides another explanation for these results.

By comparison, the first 8 days for the NCD201.1 treatment caused an average NAD^+ increase of 137% for the 2pm timepoint (Figure 5.5.3.1 B), with the only day it was significantly increased being treatment day 1 (264%, $p<0.01$). Hence the average increase was lower for NCD201.2 (79%), although the lack of treatment days beyond day 8 prevents a more robust comparison between the two cocktails.

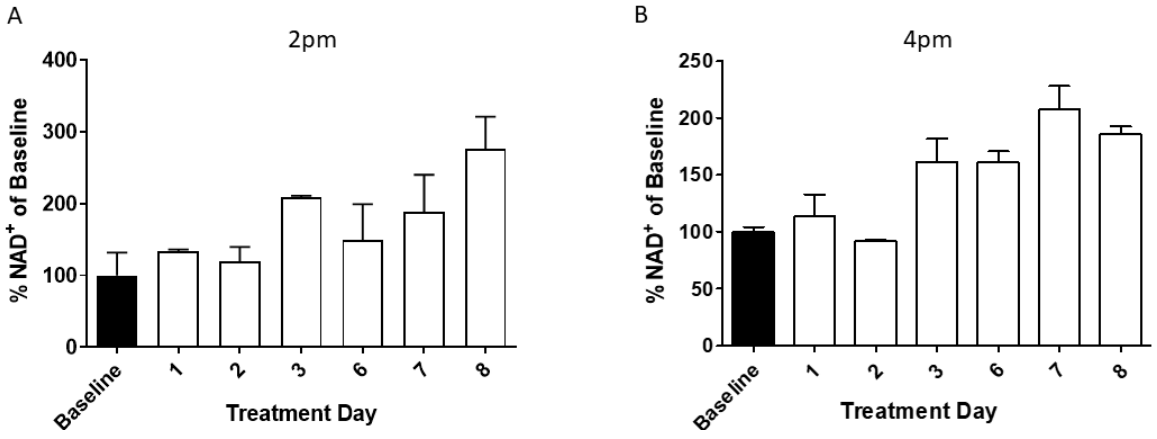

Figure 5.5.3.1 NCD201.2 increases PBMC NAD$^+$ levels.
Blood samples were collected and the PBMCs isolated at 2pm and 4pm (n=1 biological sample each treatment day, n=2 biological samples baseline) on the days indicated during an 8-day period consuming the supplement cocktail NCD201.2 for the male participant. NAD$^+$ levels were measured using an NAD$^+$ cycling assay and normalised to protein concentration quantified by a BCA assay. The NAD$^+$ levels were then expressed as a percentage of the baseline average (n=2), which was measured at 2pm and 4pm on two different days during the week prior to the initiation of treatment consumption. Data is shown as % NAD$^+$ of the baseline. Error bars represent +/- SD of the two technical replicates for each treatment day sample and +/- SD of the biological replicates for the baseline.

5.5.4 Removal of Precursor in the NCD202.1 and NCD202.2 Cocktails Reduces NAD$^+$ Enhancing Efficacy

NCD202.1 was the next cocktail to be tested, which differed from the NCD201 iterations in that it lacked the precursor (1000mg nicotinamide riboside) and also had the addition of an NNMT inhibitor. NNMT methylates NAM, which signals for it to be excreted from the cell and eventually metabolised by the liver. Theoretically, if NNMT is inhibited this will increase cellular NAM, which if combined with a NAMPT activator (e.g. resveratrol or quercetin) will allow the increased levels of NAM to be converted into NAD$^+$ by providing more substrate for NAMPT. Hence, by removing the precursor, it was hypothesised that this cocktail would enhance NAD$^+$ levels simply by modulating targets in the NAD$^+$ salvage pathway without the need for precursor, although likely to a lesser extent than NCD201. Different forms of NAD$^+$ precursors are found in foods typically consumed as part of a daily diet, thus it was anticipated that there would still be an adequate input for the de novo NAD$^+$ synthesis pathway to work in tandem with the NAD$^+$ salvage pathway.

The protocol for supplement consumption and blood collection was kept consistent with the NCD201 treatment phase. However, due to issues regarding participant availability, this cocktail was only tested for the male participant. After day 5 of consuming NCD202.1 the participant took a 2-day break from consumption, before replacing NCD202.1 with NCC202.2 which was consumed for a

further 5 days. The only variation between NCD202.1 and NCD202.2 was the use of a different NNMT inhibitor.

Over the 5-day treatment period NCD202.1 was much less effective than NCD201.1 and NCD201.2, inducing an average NAD^+ increase of 64%, with a maximum increase of 140% (day 4) and an 12% decrease as the minimum (day 5).

For the 5-day NCD202.2 treatment phase the average increase in NAD^+ was reduced to 32%, with a maximum increase of 80% (day 5) and a minimum on day 1 that was 7% less than the baseline average. Importantly, both NCD202 versions highlight the negative impact of precursor removal and suggest that to achieve maximal enhancements in human NAD^+, targeting the key regulators in NAD^+ metabolism needs to be combined with precursor supplementation.

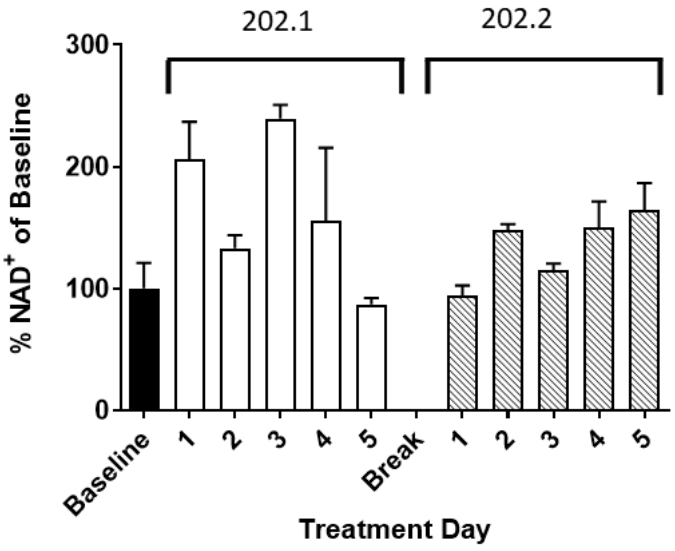

Figure 5.5.4.1 PBMC NAD^+ levels following consumption of NCD202.1 and NCD202.2.
PBMC NAD^+ levels are shown for blood samples taken at 2pm during a pre-treatment baseline week (n=3 baseline days), 1-week consuming NCD202.1 (n=1 biological sample for each treatment day) and also at 2pm for the following week consuming NCD202.2 (n=1 biological sample for each treatment day) in a male subject. NAD^+ levels were measured for the isolated PBMCs using an NAD^+ cycling assay and normalised to protein concentration quantified by a BCA assay. The NAD^+ levels were then expressed as % ng NAD^+/ug protein of the baseline average. Error bars represent +/- SD of the two technical replicates for each treatment day sample and +/- SD of the biological replicates for the baseline.

5.5.5 NCD203: Substituting NR with NAM Maintains Cocktail Efficacy

The next cocktail to be tested was NCD203: which had the same formula as NCD201.2 but with the addition of the NNMT inhibitor included for NCD202.1 whilst also using a different precursor (500mg NAM instead of 1000mg NR). NR was replaced with NAM on the rationale that supplementation with

NAM yielded the largest recorded human NAD^+ enhancement [150], in addition to the recent evidence that NR is metabolised to NAM following oral ingestion [447]. Furthermore, due to the intention of the supplier to eventually make the cocktail available commercially, NCD203 was designed to satisfy various manufacturing and regulatory restraints. As a result, some of the same compounds previously used in NCD201 were now in the form of a herbal extract, for example apigenin was included as parsley leaf extract rather than pure apigenin.

NCD203 was only tested in the female participant and was consumed following the same protocol as for previous versions. Blood samples were once again collected at the 4pm timepoint, this time on days 1, 2, 4, 8, 10 and 14 over a 14-day treatment phase. On average, the NAD^+ levels were 76% higher than compared to the baseline, with a maximum increase of 134% on day 10 and a minimum of 53% on day 4 (Figure 5.5.6.1 A).

The occurrence of enhanced NAD^+ elevation during the second week of consumption reflects what was also seen in the previous versions of the cocktails, suggesting consumption on consecutive days begins to have a cumulative effect during the second week of consumption. This may be due to the key components or their metabolites persisting longer than 24 hours in the body and hence building up over time, as has previously been documented for apigenin in rats [492].

Despite the enhancement of NAD^+ that occurs in response to NCD203 consumption, when compared vs NCD201.1 it is notably less effective: with an average increase of 76% vs 147%, maximum increase of 134% vs 276% and minimum increase of 53% vs 79%.

Consequently, this also infers that using herbal extracts as a source for the NAD^+ targeting compounds may be a less effective approach than using the extracted/synthesised compounds themselves. Even in lieu of these findings, using the extracts introduces the problem of accurately predicting the dosage, given different extract harvests will vary in their polyphenol concentration etc. Moreover, there may be additional compounds in the extracts interacting with the NAD^+ related pathways which may also explain the reduced efficacy at increasing NAD^+. Of course, one could argue that the additional compounds and nutrients contained within the extracts may offer wider health benefits given the health promoting effects of parsley leaf and green tea extract are well-documented, however from a solely NAD^+ enhancing perspective the ambiguity with regards to the dosage isn't ideal.

5.5.6 NCD205 Failed to Effectively Enhance NAD^+ in a Female Participant

The final cocktail (NCD205) tested was a further modification of NCD203 in which some ingredients from the previous versions were excluded so that the supplement could be administered in capsule

format rather than as a mix of powders. Each daily dosage contained: 500mg nicotinamide, 660mg green tea leaf extract, 632mg parsley leaf powder, 600mg rutin extract, 600mg black pepper fruit extract, 10mg zinc and 20mg vitamin C. Within this version, the green tea leaf extract provided the EGCG and the parsley leaf powder the apigenin, whilst black pepper extract was included to improve absorption of the compounds within the GI tract.

The protocol for consumption was slightly altered such that half the daily dose (3x capsules) was to be consumed with breakfast and the other half consumed with lunch. This was to ease potential issues regarding indigestion and heartburn with the cocktail now in capsule format. Baseline blood samples were taken at 2pm on two different days during the week prior to supplement consumption. During the 11-day treatment phase, samples were collected on days 1, 3, 5, 8 and 11 however a technical error meant the day 8 results needed to be excluded from the final analysis.

Over the treatment period the average change in NAD^+ recorded was a 0.3% increase, with a maximum increase of 20% (day 1) and the lowest recorded value a decrease of 40% (day 11) (Figure 5.5.6.1 B). Therefore, unlike its predecessors, NCD205 appeared ineffective at enhancing PBMC NAD^+.

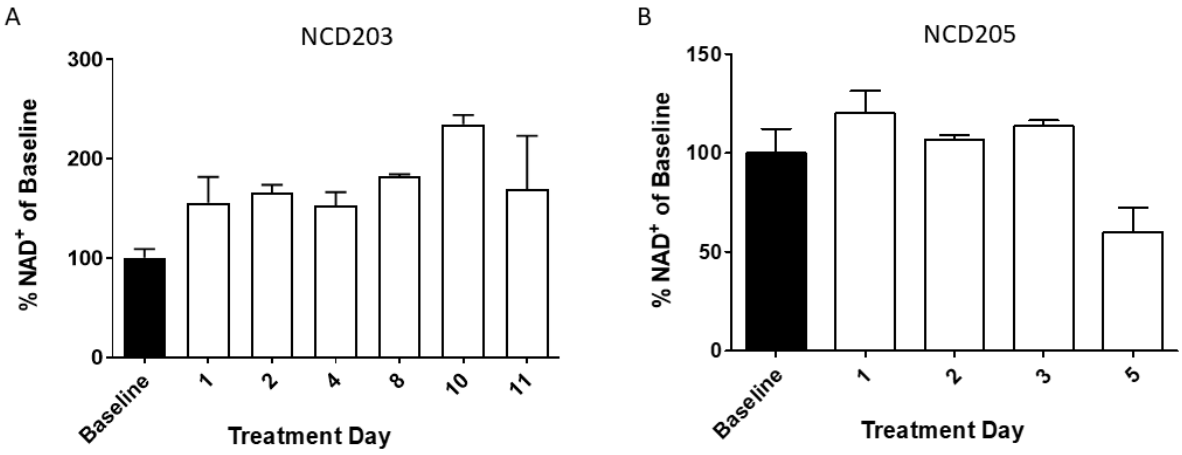

Figure 5.5.6.1 NAD^+ titres in a female participant in response to the NCD203 and NCD205 supplement cocktails.
PBMC NAD^+ levels are shown as a % of the untreated baseline average (n=3 biological samples) for blood samples taken at 4pm on the treatment days indicated for a female volunteer consuming NCD203 and NCD205 for 11 and 5 days respectively (n=1 biological sample for all treatment days). The untreated baseline blood samples were taken on 3 different days the week prior to beginning supplement consumption. NAD^+ levels were measured for the isolated PBMCs using an NAD^+ cycling assay and normalised to total protein quantified by a BCA assay. The NAD^+ levels were then expressed as a percentage of the baseline average, with error bars representing +/- SD of the two technical replicates for each treatment day sample and +/- SD of the biological replicates for the baseline.

5.6 Variability in NAD^+ Across Different Baselines – A Notable Caveat

It should be noted that there were significant variations in the average baseline NAD^+ levels measured for the female participant during the different baseline weeks. Unexpectedly, the trend showed a chronological increase in average baseline NAD^+ levels. As already mentioned, NAD^+ levels would be expected to decrease with age, however over a short timeframe (19 months) no significant differences would be expected to occur as a consequence of physiological ageing. The 3.1-fold increase in NAD^+ levels for the September 2019 baseline compared to the April 2018 baseline suggests that basal NAD^+ levels can potentially be drastically altered by nutritional, lifestyle or environmental factors. Alternatively, this variation may be a reflection of the high variability in running the NAD^+ assay on different days, perhaps due to the use of different freshly prepared standards for each of the baseline dates. Hence, no conclusions can be drawn from this data, however it would be of interest to profile an individual's NAD^+ levels over a >1 year timeframe in the future.

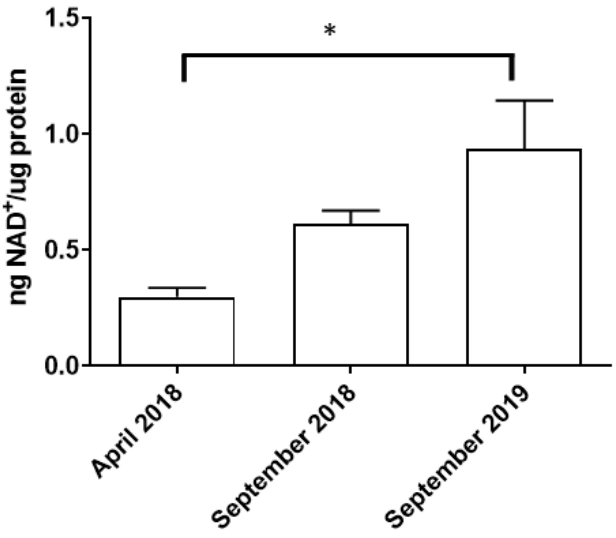

Figure 5.6.1 Average NAD^+ levels on 3 different baseline weeks for female participant.
Baseline NAD^+ levels were measured on 3 different days during 3 different weeks for the female participant, corresponding to the baselines for each of the three compound cocktails consumed. The average ng NAD^+/ug protein for each baseline week is shown (n=2 August 2018, n=3 September 2018 and 2019), with error bars representing +/- SD. Significance was tested for using 1-way repeated measures ANOVA and a Tukey's post hoc test. *$p<0.01$.

5.7 Measuring NAD^+ in PBMCs, Erythrocytes, Whole Blood and Plasma Samples

After testing all the versions of the cocktails, plans were put in place to begin a 30-person intervention study using a commercially viable cocktail based on the NCD formulations, named Time+. Although NAD^+ levels in PBMCs was the focus of the work discussed thus far, whole blood is

the most common sample type used in recent studies investigating potential NAD^+ enhancers in human studies. Therefore, it was deemed necessary to measure NAD^+ in whole blood in addition to PBMCs for the purpose of this intervention study. Hence as preparation for the study, NAD^+ was measured in PBMCs, erythrocytes, plasma and whole blood to determine the feasibility of measuring all 4 and also to understand how NAD^+ levels vary across the different blood fractions. 2 blood samples were collected at the same time from 3 healthy individuals by venepuncture, with 500ul immediately frozen at -150ºC before the rest of the blood was separated into the individual fractions as done previously by density centrifugation and also stored at -150ºC.

NAD^+ levels were measured following the standard NAD^+ cycling assay protocol, however quantification of protein concentration in the diluted whole blood and red blood cell fractions was problematic. Haemoglobin, the main constituent of red blood cells, absorbs strongly at 562nm which is the absorbance used for measuring protein concentration as part of the BCA assay. The lower sensitivity of measuring protein concentration at an absorbance of 280nm using a nanodrop proved an unreliable alternative due to the low protein concentration of the diluted PBMC, whole blood and erythrocyte samples used for the NAD^+ assay, resulting in very high standard error. Additionally, haemoglobin has a very low molar extinction coefficient due to its lack of tryptophan residues, and as the major protein present in whole blood and red blood cell samples this affected the absorbance at 280nm when less dilute samples were used. Thus, it was realised that NAD^+ levels in whole blood and erythrocytes should be expressed in units of molarity (uM) or as ng/ml, given normalisation to total protein couldn't be performed accurately.

Surprisingly, NAD^+ was undetectable in all of the plasma samples (<5nM). Consequently, it appears that enzymatic cycling assays aren't sensitive enough to measure plasma NAD^+ and therefore this would need to be done by the higher sensitivity mass spectrometry-based techniques. The whole blood NAD^+ measured was consistent across the participants, ranging from 18-26uM, whilst the erythrocyte fraction NAD^+ ranged from 25–34uM.

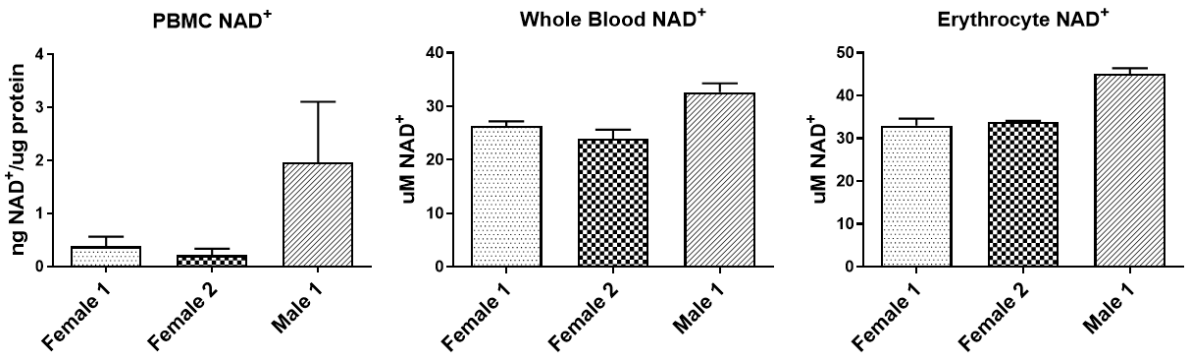

Figure 5.7.1 NAD$^+$ levels in different blood fractions.
2 blood samples were collected at the same time from 3 individuals and separated into whole blood, PBMC and erythrocyte fractions by density centrifugation (n=2 technical replicates for each participant). NAD$^+$ was then quantified using an NAD$^+$ cycling assay. NAD$^+$ levels were then normalised to protein levels via a BCA assay and expressed as ng NAD$^+$/ug protein for the PBMCs, whereas they were expressed in units of molarity (uM) for whole blood and the erythrocytes. Error bars represent +/- SD.

5.8 NAD$^+$ Degradation in Whole Blood and PBMCs Following Venepuncture

NAD$^+$ is known to be a highly labile molecule which rapidly degrades when stored in solution [493]. Thus, given the need to accurately quantify cellular NAD$^+$, the effect of different incubation times on NAD$^+$ titres in blood kept on wet ice (0ºC) was assessed. Approximately 30ml of blood was drawn into 3x 10ml vacutainers from one person and immediately placed on ice. At 5 minutes, 10 minutes, 20 minutes, 30 minutes, 40 minutes, 50 minutes and 60 minutes post blood draw 0.4ml from one of the 10ml tubes was added to two cryovials and immediately frozen at -80ºC. The rest of the blood was then used to isolate PBMCs at 10 minutes, 40 minutes, 70 minutes and 110 minutes post draw (in duplicate). The time it took to complete the PBMC isolation process means that these PBMCs were frozen down on average 53 minutes, 87 minutes, 114 minutes and 157 minutes after the blood was drawn from the participant.

The NAD^+ levels were then measured to assess the effect of different incubation times at 0°C (Figure 5.8.1). For the whole blood, NAD^+ levels only declined by 13% between 5 minutes and 60 minutes post blood draw, with none of the incubation times during this interval achieving a statistically significant difference compared to the 5-minute sample. For PBMCs, there was a 20% decrease in NAD^+ measured for the cells frozen down 157 minutes post blood draw compared to those frozen down after 53 minutes. As for the whole blood, there was no statistically significant differences between the different incubation times. Furthermore, for both PBMCs and whole blood there was no inverse correlation between time on wet ice and NAD^+ levels as one might expect given the labile nature of NAD^+. The lines of best fit for PBMC and whole blood NAD^+ levels against incubation time emphasise this, giving r^2 values of 0.32 and 0.12 respectively.

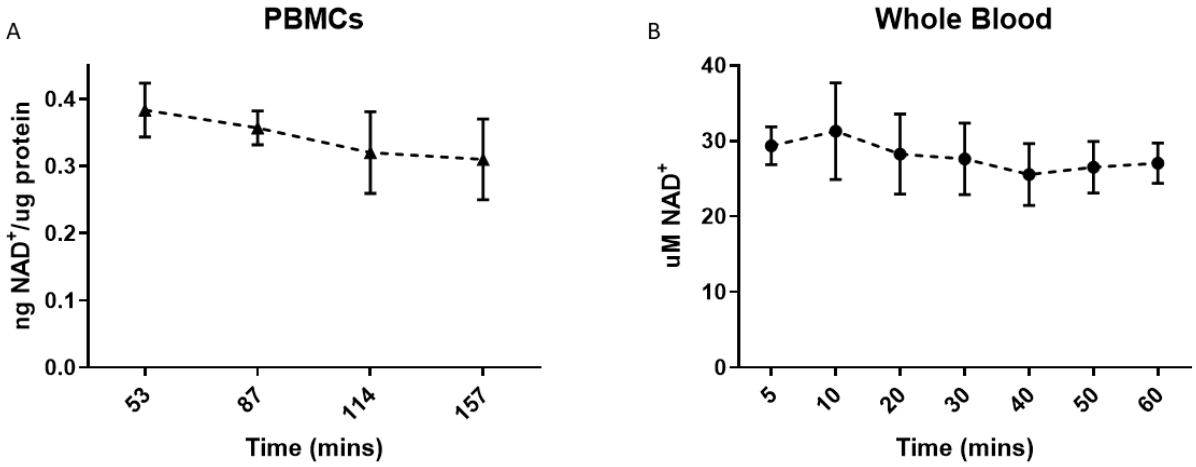

Figure 5.8.1 Degradation of NAD^+ in PBMCs and whole blood stored on ice.
(A) 2 blood samples from 1 individual were simultaneously collected by venepuncture and then incubated on ice for varying lengths of time (n=2 technical replicates for all timepoints). The time at which the subsequently isolated PBMCs were frozen down post isolation and their corresponding NAD^+ levels is shown. NAD^+ was measured by an NAD^+ cycling assay and then normalised to protein levels quantified via a BCA assay. (B) Whole blood was incubated on ice post-venepuncture for the times indicated and NAD^+ levels were measured by an NAD^+ cycling assay, expressed here as molarity (uM). Data shown is the mean of two blood samples from 1 person, error bars represent +/- SD. Statistical significance was tested for by 1-way ANOVA.

5.9 Ongoing Time+ Intervention Study

Following on from the work presented within this chapter, an intervention study using the Time+ cocktail was initiated and at present is still ongoing, with all sample collection completed and analysis in progress. The study design is a randomised, double-blinded, placebo-controlled crossover in which participants consume Time+ or placebo for 4 weeks, undergo a 4-week washout phase, then for another 4 weeks consume the treatment they didn't consume during the first arm (Figure 5.9.1). Study visits were once a week during the two treatment phases (always the same day), with two separate visits to measure baseline NAD^+ levels also taken the week prior to each treatment arm. To control for daily oscillations of NAD^+, time of study visit was kept constant for each participant

throughout. Additionally, participants were also requested to keep their weekly diet and sleep patterns as constant as possible and to avoid any drinks or supplements containing niacin, nicotinamide or nicotinamide riboside. Consumption of the treatment (placebo or Time+) was every day, keeping the time of consumption the same for all study day visits as well as for the day prior to each visit.

For the 28 participants that completed the study, the most commonly reported adverse side-effect was indigestion following capsule consumption (n=3), with impaired sleep (n=2) and excessive restlessness (n=1) also noted. Beneficial effects included improved sleep quality (n=4) and enhanced energy (n=3). Laboratory testing is currently underway to measure NAD^+ levels for all the study visits so that placebo and Time+ NAD^+ levels can be compared for each participant. Markers of NAD^+ metabolism (Figure 5.9.2) are also being measured by LC-MS (liquid chromatography-mass spectrometry) to gain an insight into how the cocktail may be influencing the wider NAD^+ metabolome.

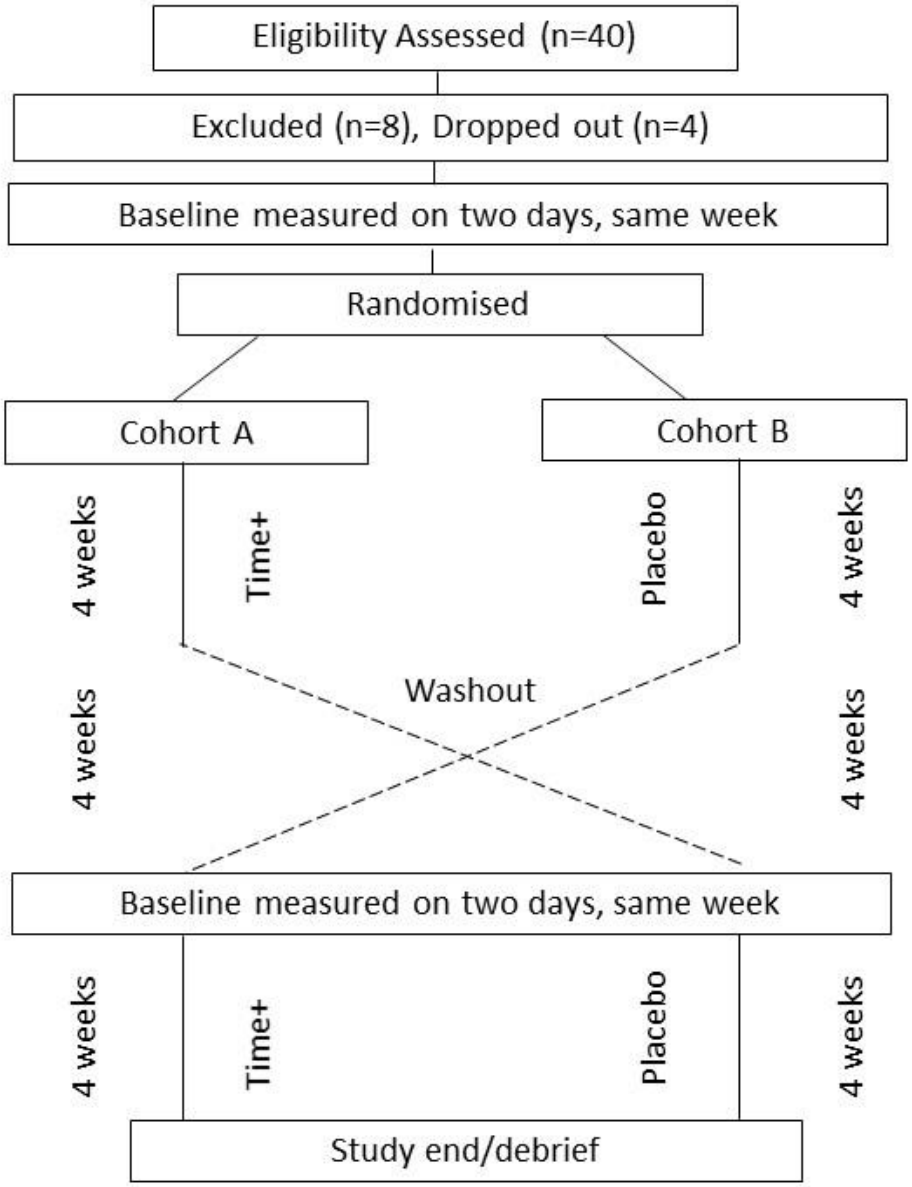

Figure 5.9.1 Time+ intervention study design.
A randomised, double-blinded, placebo-controlled crossover study testing Time+ for its ability to enhance NAD^+ in a human cohort is currently ongoing.

Table 5.9.2 Metabolites of mammalian NAD^+ metabolism.

Metabolite	Producers	Consumers
NAD^+	NMNAT1-3, NADSYN, NQO1, NADH dehydrogenase, $NADP^+$ phosphatase.	NADK, SIRT1-7, PARP1, CD38, CD157, tankyrase -1/2, Malate dehydrogenase, OGDC, IDH
NADH	SAM hydrolase, Malate dehydrogenase, OGDC, IDH	NADH dehydrogenase, NQO1
NAM	SIRT1-7, PARP1, CD38, CD157, tankyrase -1/2, PNP	NAMPT
meNAM	NMNT	Aldehyde oxidase
NMN	NRK, NAMPT	NMNAT, CD73
NR	CD73	NRK, PNP
$NADP^+$	NADK, HMG-CoA Reductase, Nocturnin, NQO1	IDH, GLDH, NADP-ME, G6PDH, $NADP^+$ Phosphatase
NADPH	IDH, GLDH, NADP-ME, G6PDH, $NADP^+$ Phosphatase,	NADPH Oxidase, HMG-CoA Reductase, Nocturnin, NQO1
NAAD	NMNAT1-3	NADSYN
NAMN	NAPRT, NRK, QPRT	NMNAT1-3,
cADPR/ADPR	CD38	-
NA	-	NAPRT, glycine N-acyltransferase
NAR	-	NRK, QPRT
2PY	Aldehyde oxidase	-
NUA	glycine N-acyltransferase	-

Table abbreviations:
Enzymes:
IDH - Isocitrate dehydrogenase, GLDH – glutamate dehydrogenase, NADP-ME – NADP malate dehydrogenase, G6PDH – glyceraldehyde-6-phosphate dehydrogenase, NADSYN - Glutamine-dependent NAD^+ synthetase, NMNT – nicotinamide-N-methyltransferase, NMNAT1-3 – nicotinamide adenylyltransferase 1-3, PNP – purine nucleoside phosphorylase, NAPRT – nicotinate phosphoribosyltransferase, NAMPT – nicotinamide phosphoribosyltransferase, NRK – nicotinamide riboside kinase, NADK – NAD^+ kinase, OGDC - oxoglutarate dehydrogenase complex, QPRT - quinolinate phosphoribosyl transferase.
Metabolites:
NUA – nicotinuric acid, NAR – nicotinic acid riboside, 2PY - N-methyl-2-pyridone-5-carboxamide, NA – nicotinic acid, cADPR – cyclic adenosine diphosphate ribose, NAMN – nicotinic acid mononucleotide, NAAD – nicotinic acid adenine dinucleotide, NADP – nicotinamide adenine dinucleotide phosphate, NAM – nicotinamide, meNAM – methylated nicotinamide.

5.10 Discussion

There is a growing interest in identifying effective interventions to enhance human NAD^+ levels, driven by the widespread belief that declining NAD^+ levels contribute to age-related physiological decline and increase the risk for age-associated morbidities. Currently, NR supplementation is the most commonly endorsed method to increase NAD^+, with its efficacy supported by a number of clinical studies [310, 311, 405, 407]. Within this chapter it's shown that NR does enhance PBMC NAD^+ levels in a small cohort (n=5), however its effectiveness was highly variable day-to-day within the same week, something yet to be investigated in other studies. Therefore, it's likely that a number of external factors may influence the efficacy of NR with variables such as sleep, diet, exercise and environmental temperature all possible contributors. To this end, it would've been much more revealing if other NAD^+ related metabolites (Table 5.9.2) had also been measured, thus identifying whether the variation was due to increased breakdown of NAD^+ or less efficient conversion of NR to NAD^+. The average increase in NAD^+ of 52% across the 5 participants was less than has been typically observed in previous human studies using NR (Table 5.3.1), however the dose here was 500mg/day opposed to the 1000mg/day used in most of the aforementioned studies.

Indeed, variation across different days was also observed when measuring daily NAD^+ fluctuations in the male and female participant PBMCs during their baseline weeks. Despite changes in the mean NAD^+ measured on different baseline days, the profile of NAD^+ during the 8am to 8pm timecourse was characterised by the presence of peaks and troughs that were generally consistent for both participants throughout the week. Importantly, this suggests that NAD^+ levels in human PBMCs do indeed follow a circadian rhythm, something which has yet to be verified in the literature.

Interestingly, there is one study which identified a circadian rhythm of NAD^+ levels in whole blood [388], however the NAD^+ displayed a pattern very different to what was shown here for the PBMCs, with the whole blood NAD^+ steadily decreasing from 8am to 8pm. This difference may be due to the very unique NAD^+ metabolism in erythrocytes (the most abundant cell type in blood) which lack mitochondria and nuclei. Consequently, unlike PBMCs, there is no expression of the circadian rhythm controlling genes which would suggest the circadian NAD^+ pattern in erythrocytes is regulated by hormones or some other external biomolecules. It's likely however for PBMCs that the circadian regulation of NAD^+ is regulated by the interaction between both hormones (e.g. melatonin) and the expression of endogenous circadian genes such as BMAL1, CLOCK, PER1-2 etc., thus possibly explaining the very different diurnal pattern.

From a therapeutic perspective, understanding the diurnal variation of an individual's NAD^+ levels would be useful to help identify the optimal time of day at which to consume NAD^+ enhancing

supplements. Of course, it is possible that the circadian profile varies between the different blood cell types and possibly different tissue types too, hence the regimens may need to be optimised for specific physiological needs. Another important point raised by the diurnal variation in NAD^+ is the need to keep the time of day at which samples are taken consistent for any clinical/intervention study. Hitherto, no studies in the literature mention whether time of day for participant study visits has been kept constant, however the data presented here suggests this should be an essential feature of any study testing NAD^+ boosting interventions.

To explore whether an approach combining NAD^+ precursors with compounds targeting NAD^+ metabolism could yield superior alternatives to NR, various 'cocktails' developed for this purpose by Nuchido Ltd. were tested. The first cocktail (NCD201) was tested on 2 participants, with NAD^+ levels measured on multiple days over a 16-day period - another important aspect of this work given all previous studies have only measured NAD^+ changes on one or two treatment days. Similar to NR, a large variation across the NAD^+ measurements on the different days was observed, further supporting the belief that NAD^+ levels are highly susceptible to multiple external factors. This further reinforces the need for clinical studies to measure the efficacy of any NAD^+ enhancing interventions on multiple treatment days and to take robust approaches to limit the influence of environmental variables.

For NCD201, the average increase in NAD^+ levels across the 16-day period was 301% for the male and 147% for the female, both larger than the reported increases in NAD^+ for 2-3 weeks of NR consumption [310, 408]. The most striking finding however was the massive increase in NAD^+ on days 11 (841%) and 14 (640%) for the male. Surprisingly, for the male there was a significant increase in NAD^+ on day 1 of treatment consumption but out of the 7 treatment days blood was taken the only other significant increases recorded were on days 11 and 14. This finding, along with the wide range in NAD^+ values recorded across the different treatment days (ranging from an 8% increase to 821% increase) emphasises the variable day to day efficacy of the cocktail.

The variation in values across the treatment period was much smaller for the female however, ranging from an 89% increase to a 217% increase. Despite the lower treatment average compared to the male participant, the consistently high elevation of NAD^+ yielded a statistically significant increase on all testing days for the female. This stark contrast to the large fluctuations in NAD^+ across the treatment phase for the male highlights the possibility that the effects of the cocktail will vary widely between individuals, although this hypothesis would need to be tested within a much larger cohort. Likewise, for both participants the NAD^+ levels reached a peak on day 11/14 before partially tapering off on day 16, hence it's essential to determine whether this is an authentic trend that

continues beyond day 16 – something that is being tested for in the ongoing study. It is possible that some unknown feedback mechanisms may be present which sense the increase in NAD^+ and consequently over time reduce the expression of enzymes in the NAD^+ salvage/synthesis pathways, thus dampening the effectiveness of the cocktail. However, supplementation with NR has been shown to be effective after a 60 day treatment phase in a large human cohort [405], suggesting that increased NAD^+ levels can be maintained long-term via dietary supplementation.

Indeed, the increased NAD^+ levels compared to the baseline that were measured for the male 5 days after finishing the NCD201 treatment regime hints that there may be a residual effect even once supplementation is ended. That said, after 9 days post-study completion the average increase in NAD^+ across all the daily timepoints measured compared to the baseline had dropped to 16%, suggesting that by this time the effects of the cocktail on NAD^+ levels had worn off.

To test whether the components of the cocktail specifically targeting the NAD^+ salvage pathway were indeed having the desired effect, the male participant consumed the cocktails NCD202.1 and NCD202.2, both of which had the same recipe as NCD201 but without the nicotinamide riboside precursor. Furthermore, NCD202.1 and NCD202.2 both had an NNMT inhibitor added, although the specific compound fulfilling this role varied between the two versions. NNMT methylates NAM, which signals for it to be excreted from the cell and eventually metabolised by the liver, thus by inhibiting NNMT this in theory would allow more NAM (a by-product of many NAD^+-dependent reactions) to be recycled by shuttling it back into the salvage pathway, subsequently yielding more NAD^+.

Over the course of the 5-day treatment periods for NCD202.1 and NCD202.2, on average the NAD^+ levels increased by 62% and 32% respectively, suggesting that the combination of compounds targeting NAD^+ degradation/synthesis pathways is effective at increasing NAD^+. The smaller enhancement of NAD^+ without the precursor was expected, given that the increased NAD^+ synthesis resulting from enhanced NAMPT activity also depends on precursor availability. Implementing a precursor-free approach to boosting NAD^+ using NCD202.1/NCD202.2 would therefore be highly dependent on the amount of nicotinamide/nicotinic acid/nicotinamide riboside ingested via the diet.

In order to delve deeper into the mechanics of how NAD^+-targeting therapeutics modulate NAD^+ homeostasis a wider look into the NAD^+ metabolome should be employed. This would be particularly pertinent for interventions such as the NCD cocktails which target multiple steps in NAD^+ synthesis/degradation pathways, allowing verification of whether the compounds are working through their expected mechanisms. For example, if NAMPT activity - a key purported target of the

cocktail - is upregulated then this would increase levels of NMN, the product of NAMPT catalysis. Similarly, measuring the levels of the substrate of NAMPT, NAM, would also give an indication of NAMPT activity. This overcomes the key limitation in measuring protein expression of the supplement targets which doesn't specifically inform of their enzymatic activity. By contrast, a wider metabolomics approach would tackle this problem, although some NAD^+ related metabolites are the product of multiple enzymatic reactions (Table 5.9.2), hence proteomic data could potentially corroborate the metabolomics findings by identifying which enzymes are responsible for specific metabolite changes. Specifically combining the metabolomics with a targeted proteomics approach using LC-MS would also give a much more comprehensive picture of the protein changes induced by the cocktail. Given some of the compounds have numerous predicted targets and NAD^+ changes can affect many pathways, it's expected the cocktail would induce extensive changes to the proteome.

Additionally, to better understand the variables that could contribute to changes in blood NAD^+ regardless of supplementation, determining NAD^+ levels within the different PBMC sub-populations is of great interest. A number of factors can alter the circulating levels of different lymphocyte subtypes (e.g. CD4+ T cells, CD8+ T cells, NK cells etc.) which could have an impact on the NAD^+ levels measured in PBMC fractions, particularly if certain subtypes are associated with NAD^+ levels significantly different to the PBMC average. A cell sorting approach could be employed to separate out PBMC fractions into their different populations and characterise their respective NAD^+ and NAD^+-related metabolite profile. This would also shed light on whether infection and the subsequent increase in specific lymphocyte populations would be expected to alter the NAD^+ titre within the PBMC blood fraction – another important consideration for intervention studies.

Future work to supplement the findings reported here should also include characterisation of the relationship between age and blood NAD^+ levels, which is especially relevant given the literature regarding this is still fairly thin. Although Massudi *et al.* found a significant inverse correlation between NAD^+ levels and age, for such a wide age range the cohort was small (n=49) and the only tissue used was skin [70]. One approach to determine if a similar relationship exists in blood/PBMCs would be to measure the NAD^+ levels for >100 individuals in the 0 - 80 age range. Although this should provide greater insight into the relationship between NAD^+ levels and age, the optimal approach would be to measure the entire NAD^+ metabolome in multiple tissues of young and old mice, identifying whether mammalian age-related NAD^+ decline is systemic and if specific tissues are especially susceptible. Moreover, by measuring the entire NAD^+ metabolome this could potentially identify the mechanisms driving age-related changes in NAD^+.

The findings within this chapter also emphasise the requirement for a clear consensus on how to measure NAD^+ levels from blood samples. Within this work all NAD^+ measurements were made using an enzymatic cycling assay, which reduces the complexity and costs associated with measurements made via LC-MS. Most recent studies assessing NAD^+ levels have opted for an LC-MS approach however, likely due to the higher sensitivity associated with this technique and the ability to measure multiple metabolites at once. Additionally, there is also large variation in blood processing methods across the literature, with different studies opting for whole blood, plasma or PBMCs. The rationale often cited for the use of whole blood is the ability to freeze it soon after collection, removing the need for centrifugation steps to separate the plasma and/or PBMCs. This is done on the basis that NAD^+ is highly labile and hence would be expected to quickly degrade in collected samples – hence the desire for minimal sample processing. When kept on ice however, it's shown here that the whole blood NAD^+ levels only decline by 12% over the course of an hour without any statistically significant changes detected, suggesting NAD^+ levels are much more stable in whole blood than previously thought. Similarly, increasing the length of time blood samples were incubated on ice for prior to PBMC isolation did reduce detectable NAD^+ levels, but again there were no significant differences between different incubation times across a 110-minute interval.

It is therefore likely that the assumption that cellular NAD^+ levels rapidly decline ex vivo are based on the instability of NAD^+ outside of the cell. Indeed, blood cells left incubated on ice are still completely viable and in a nutrient rich environment, hence NAD^+ homeostasis would continue within the cell similar to the blood cells circulating within the sample donor, aside from the slowing down of reactions and temperature stress induced by the storage on ice. With regards to sample processing, it would therefore seem the extra 45-50 minutes it takes to isolate PBMCs from whole blood will minimally reduce the NAD^+ levels provided samples are kept on ice/at $<4^oC$ throughout.

An important advantage of focusing on PBMCs identified in this work is the difficulty to accurately measure total protein concentration in whole blood (intracellular and extracellular). Consequently, this means NAD^+ levels in whole blood have to be expressed in units of molarity or ng/ml rather than ng NAD^+/ug protein. By not normalising to total protein levels, this means NAD^+ levels measured will be susceptible to changes in blood cell number – particularly problematic for a study collecting samples on multiple different days. Many illnesses in addition to nutritional and hormonal changes can increases or decrease blood cell levels, thus altering the whole blood uM NAD^+ by virtue of cell number rather than bona fide changes to NAD^+ metabolism.

Plasma NAD^+ levels have been successfully measured elsewhere in the literature [494, 495], however they were undetectable by the cycling assay (<5nM) within this work. By contrast, Clement *et al.*

[494] reported plasma NAD^+ levels in the 1-70nM range whilst another study detected them at <6nM concentrations [495], with both studies using an LC-MS approach. The inability to detect NAD^+ therefore may not entirely be due to the detection limit of the cycling assay but possibly other processing variables. Measuring plasma NAD^+ is of secondary importance however given the main biological role of NAD^+ occurs intracellularly. It's not clear if it serves a specific physiological function or where the plasma pool of NAD^+ is derived from, but its release from cells following lysis is a possible explanation.

Although measuring plasma NAD^+ may be of limited utility, the circulating levels of secreted NAD^+ breakdown products such as meNAM and 2PY would provide useful information on intracellular NAD^+ metabolism. Hence, when investigating the NAD^+ metabolome a focus on the changes in PBMCs and whole blood combined with plasma levels of meNAM and 2PY would appear the best approach.

In conclusion, it appears that a multi-targeted approach using dietary supplements in combination with precursors allows a greater enhancement of NAD^+ titres than NR. The analysis of NAD^+ targeting interventions however is complicated by the endogenous diurnal variations in PBMC NAD^+ as well as apparent day to day variability, important considerations for future NAD^+ intervention studies moving forward. Further work is required to verify the biological effects elicited by multi-targeting NAD^+ interventions, namely their effect on the entire NAD^+ metabolome.

Chapter 6. The Role of NAD^+ and SIRT1 in Skin Fibrosis

6.1 Introduction

Although enhancing NAD^+ would seem desirable in the context of an anti-ageing approach, there are other ailments in which it may have a negative effect. This is highlighted by a number of studies which have outlined a pro-tumorigenic effect of increasing NAD^+ (reviewed in [496, 497]). On one hand NAD^+ is essential for PARP1 activity and thus fulfils an anti-cancer role by maintaining genomic stability via PARP1, however NAD^+ is also an essential substrate for glycolysis and hence may facilitate the Warburg effect – the process by which cancer cells shift their energy metabolism towards glycolysis. Hence, it is possible that interventions that replenish NAD^+ in cancer cells simply fuel glycolysis, which would subsequently increase NADH levels rather than NAD^+.

It is therefore paramount to consider the possible adverse effects altering NAD^+ levels could have in diseases, particularly those defined by metabolic changes. One such disease is systemic sclerosis (SSc), a rare autoimmune disorder characterised by skin fibrosis (aka scleroderma) and often the gradual spread of fibrosis to other organs, eventually resulting in mortality. Although management of the symptoms has extended lifespan, patients still suffer from a poor quality of life with a curative treatment yet to be discovered. The potential role played by NAD^+ within SSc is unclear: both a pro and anti-fibrotic effect has been identified for SIRT1 [498-501], whilst another NAD^+-dependent enzyme, PARP1, has been implicated as anti-fibrotic [502].

Hence, it was sought to determine whether NAD^+ levels are relevant to the activation or inhibition of fibrotic pathways within an *in vitro* model of skin fibrosis. Similarly, the role of SIRT1 within these pathways was also investigated, allowing the contribution of the NAD^+/SIRT1 axis in fibrosis to be dissected.

As already mentioned, upregulated glycolysis is a key feature of cancer cells. Although the reason for cancer cells undergoing this metabolic re-modelling is controversial, one common theory is that glycolysis increases the production of biosynthetic intermediates which can then be used to support protein synthesis and cell proliferation. Interestingly, the requirement of enhanced protein synthesis and production of the same biosynthetic intermediates is a hallmark of fibrosis – which requires these intermediates as building blocks for increased ECM production. Indeed, an altered metabolic profile has already been observed in sera from SSc patients [503] and idiopathic pulmonary fibrosis (IPF) lung samples [504], hence it was theorised metabolic changes may be a key event in the development of skin fibrosis and thus would be detectable in pro-fibrotic dermal fibroblasts. Therefore, it was also of importance to identify any changes in the levels of glycolysis and OXPHOS

(regulators of the NAD^+/NADH redox balance) in pro-fibrotic fibroblasts to fully understand the role played by the NAD^+ axis within scleroderma.

TGF-β is a renowned activator of fibrotic genes and has been heavily implicated in the pathogenesis of SSc [505], making it a useful tool to model skin fibrosis *in vitro*. Thus, TGF-β treated NHDFs in addition to fibroblasts derived from SSc patient skin lesions were used within this chapter to investigate the role of NAD^+, SIRT1 and metabolic changes in skin fibrosis.

6.2 Aims

Understanding whether changes in NAD^+ levels can modulate fibrotic pathways, namely TGF-β signalling, was the key aim of this chapter. Additionally, identifying any changes to the activity of different energy metabolism pathways in TGF-β induced NHDFs was also of central importance to aid the understanding of the potential role played by NAD^+ in skin fibrosis.

6.3 Hypotheses

It was hypothesised that changes in energy metabolism would be observed in TGF-β induced NHDFs and SSc dermal lesion fibroblasts, likely to be an increase in glycolysis as seen in other autoimmune diseases. Thus, interventions that enhance NAD^+ would attenuate fibrotic markers under such conditions by shifting the energy metabolism equilibrium in the direction of OXPHOS at the expense of glycolysis.

6.4 TGF-β Upregulates Aerobic Glycolysis in NHDFs

To determine whether the pro-fibrotic activator TGF-β induced any metabolic changes in NHDFs, glycolysis and OXPHOS was measured using the Seahorse XFp Analyser for NHDFs treated for 48 hours with or without 10ng/ml TGF-β. By measuring subtle changes to the pH of the media in the assay plates the ECAR (extracellular acidification rate) is recorded, which changes in response to the protons released during glycolysis. As a result, glycolysis and specific features of glycolytic function can be analysed following the sequential addition of various chemicals to the assay plate wells. In total, 4 ECAR measurements are made: before glucose is added to the media, after 10mM glucose is added, after 1uM oligomycin is added and finally after 50mM 2-DG (2-deoxyglucose) is added. The ECAR recorded after adding glucose indicates basal glycolysis, whereas ECAR following oligomycin quantifies maximal glycolysis i.e. glycolytic capacity (due to oligomycin preventing any ATP production via OXPHOS and thus making the cells glycolysis dependent). The difference between the glycolytic capacity and basal glycolysis can then be calculated to deduce the glycolytic reserve.

In addition to ECAR, the oxygen consumption rate (OCR) is quantified by measuring changes in the oxygen concentration within the assay plate media – thus giving a readout of oxygen consumption by the mitochondrial electron transport chain (ETC). The consumption of oxygen to yield H_2O constitutes the final step in the ETC, therefore the OCR reflects the rate of OXPHOS.

Whilst there was no change in OXPHOS (Figure 6.4.1 B), basal glycolysis (1.26-fold, $p<0.05$), glycolytic capacity (1.34-fold, $p<0.05$) and glycolytic reserve (1.26-fold, $p<0.05$) were all significantly increased in the TGF-β treated cells (Figure 6.4.1 A). The lack of any change in OXPHOS suggests that the cells are still dependent on OXPHOS for ATP production following the induction of fibrosis, however the increase in all glycolytic parameters suggests these may be required for additional energy demands or possibly other byproducts of glycolysis.

Although there was upregulation of glycolysis following TGF-β stimulation, given TGF-β is a multi-functional cytokine it was sought to identify whether enhanced glycolysis was relevant to the pro-fibrotic phenotype or merely an unrelated downstream target of TGF-β signalling. To do this, NHDFs were treated with the prototypical glycolysis inhibitor 2-DG which inhibits the first step in the glycolytic chain. Highlighting the importance of glycolysis for the development of fibrosis, 2-DG was able to potently downregulate expression of the fibrotic marker collagen I in NHDFs co-treated with 10mM 2-DG and 10ng/ml TGF-β for 48 hours (Figure 6.4.1 C-D).

Densitometry analysis of western blots (n=3) for NHDFs treated with TGF-β and 2-DG reinforces the importance of glycolytic function for collagen synthesis, whereby the staining density of collagen I

relative to α-tubulin for each sample was expressed as a percentage of the untreated NHDF (control) average. TGF-β treatment increased collagen staining density by 88% compared to the control, whereas TGF-β and 2-DG reduced collagen staining density by 17%, with a statistically significant difference between the TGF-β and TGF-β with 2-DG conditions determined by an unpaired Student's t-test ($p<0.01$) (Figure 6.4.1 E) Treatment with just 2-DG reduced the collagen staining density by 51% compared to the control, thus 2-DG doesn't specifically inhibit TGF-β signalling, but rather collagen synthesis in general.

Within a therapeutic context however, complete inhibition of glycolysis would eventually have adverse consequences given its vital role in energy metabolism, hence an approach that downregulates rather than completely blocks glycolysis would be preferable. This was done using the glycolytic flux inhibitor 3PO (3-[3-pyridinyl]-1-[4-pyridinyl]-2-propen-1-one) which inhibits the cellular capacity to quickly upregulate glycolysis rather than directly inhibiting glycolysis per se [506]. Indeed, treatment with 3PO results in partial reduction of glycolysis without impairing cell viability at appropriate doses (Figure 6.4.3 C).

Importantly, 8uM 3PO was also able to partially attenuate the TGF-β driven increase of collagen I levels in NHDFs (Figure 6.4.1 D), the quintessential marker for fibrotic activity. Densitometry analysis of the blots found that the addition of 3PO reduced the collagen staining density in TGF-β treated NHDFs, however this difference failed to achieve statistical significance (Figure 6.4.1 F). Compared Consequently, these results suggest 3PO may represent a feasible alternative to 2-DG as a suppressor of glycolysis in the context of an anti-fibrotic treatment.

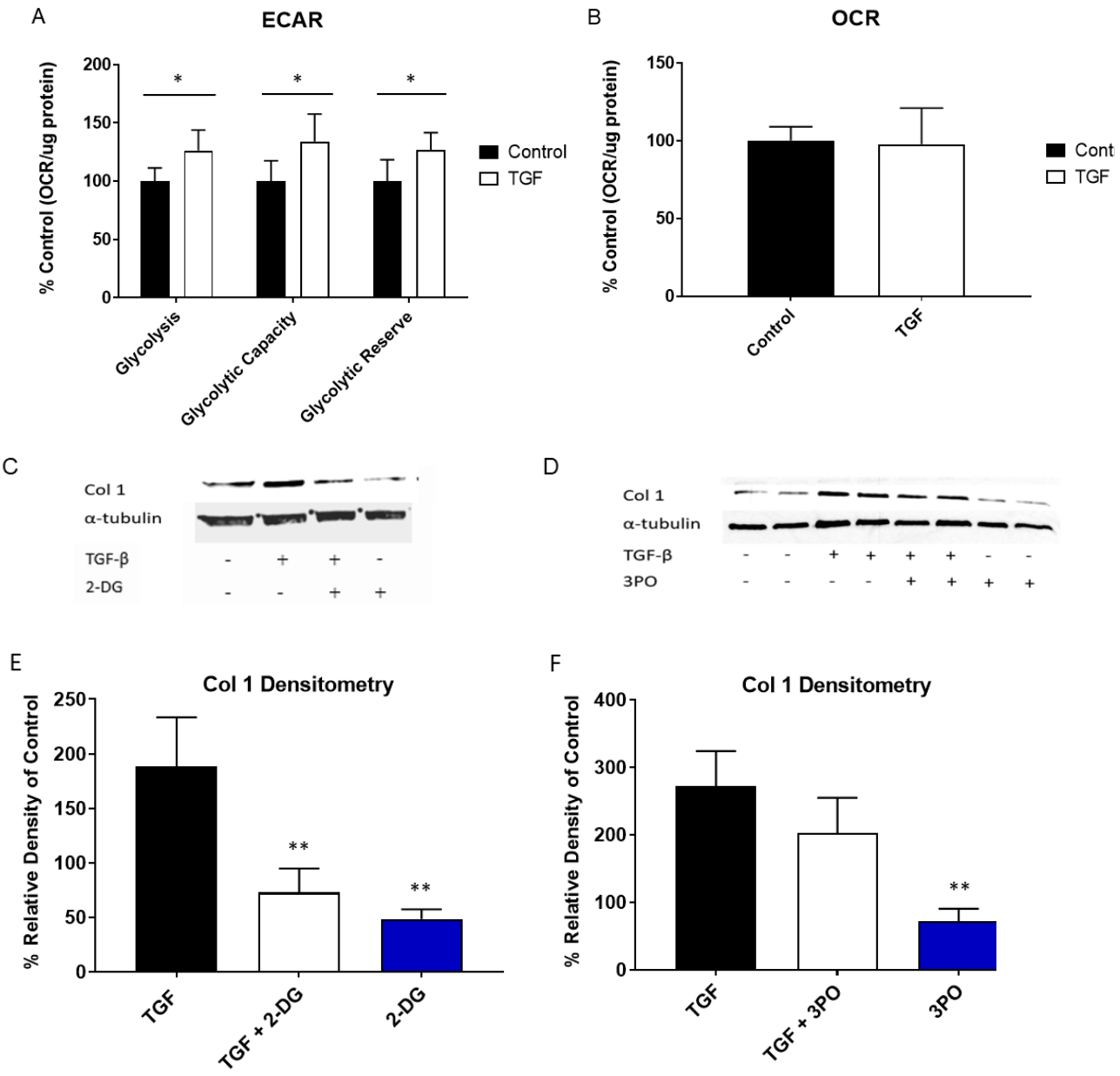

Figure 6.4.1 Glycolysis is an essential component of TGF-β induction of fibrotic proteins in NHDFs.
The glycolytic parameters of NHDFs treated with or without 10ng/ml TGF-β for 48 hours were quantified on a Seahorse XFp Analyser by performing a glycolysis stress test and measuring the ECAR (n=3 all conditions, 4 separate biological experiments). Afterwards a BCA assay was performed and ECAR values were then normalised to protein levels. The data is presented as the % ECAR/ug protein of the untreated NHDFs. (B) Basal OXPHOS was also assessed in NHDFs treated for 48 hours with or without 10ng/ml TGF-β by measuring OCR. Once again, a BCA assay was performed and OCR values normalised to protein levels. The data is presented as the % OCR/ug protein of the untreated NHDFs (n=3 all conditions, 4 separate biological experiments). (C) NHDFs were also treated with or without 10ng/ml TGF-β and/or the hexokinase II inhibitor 2-DG (10mM) for 48 hours, after which the proteins indicated were measured by western blotting. (D) Likewise, western blotting was used to observe specific protein changes in NHDFs treated for 48 hours with or without 10ng/ml TGF-β and the glycolytic flux inhibitor 3PO (8uM) or 0.02% DMSO. The blots in panels C and D are representative of 3 separate biological experiments. (E-F) Densitometry analysis was then performed on the blots in panels C and D (n=3) and the collagen I levels relative to α-tubulin expressed as a percentage of the untreated control. Statistical analysis was performed using 1-way ANOVA followed by a Dunnett's post hoc test whereby the TGF-β group was used as the control. A Student's t-test was used to test for significance in panel B and for each glycolytic parameter in panel A. Error bars represent +/-SD. Statistical significance between the treated and untreated NHDFs was tested for using an unpaired Student's unpaired t-test. *p<0.05.

The final step in glycolysis yields two molecules of pyruvate which then undergo one of two fates: fermentation into lactate (anaerobic glycolysis) or oxidative decarboxylation to produce acetyl CoA (aerobic glycolysis). The excessive production of lactate is synonymous with cancer cells [507], hence it was next investigated whether TGF-β induced glycolysis is predominantly anaerobic as in cancer or if it is occurring aerobically.

Given TGF-β increased glycolysis but had no impact on OXPHOS this would suggest that the glycolysis was occurring anaerobically, however the lactate levels secreted into the media by 10ng/ml TGF-β treated NHDFs failed to show any significant difference compared to untreated NHDFs over a 96-hour timecourse (Figure 6.4.2). One potential explanation is that whilst glycolysis is upregulated by TGF-β, the enhancement isn't as profound as seen in cancer, hence the failure to detect a significant increase in lactate secretion. Alternatively, it's possible that the pyruvate yielded in the final step of glycolysis is shuttled back into the TCA cycle however the cycle terminates early, hence the absence of any increase in OCR.

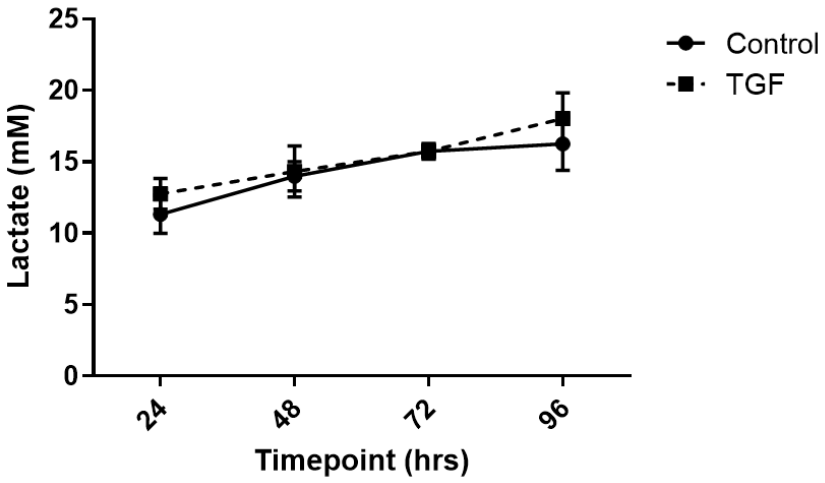

Figure 6.4.2 Lactate levels following TGF-β stimulation.
NHDFs were serum starved overnight and then treated with or without 10ng/ml TGF-β for 24, 48, 72 or 96 hours. The media was then removed at each of these timepoints and the lactate concentration (mM) within the media measured using an enzymatic assay kit (Sciencecell, Carlsbad, USA). Data is shown as the mean lactate concentration of two separate biological experiments, error bars represent +/-SD. Significance was tested for by 1-way ANOVA.

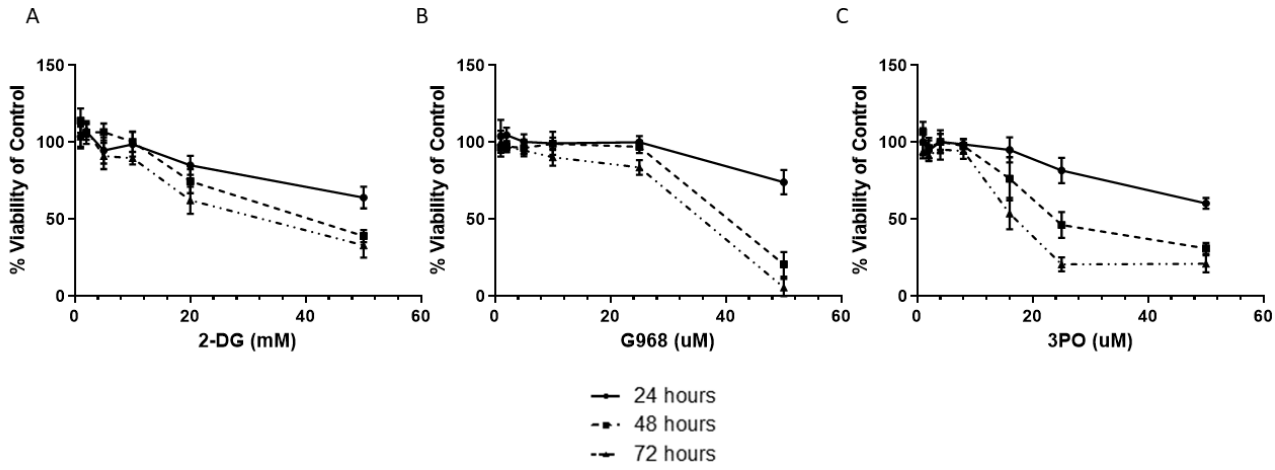

D

	24 hours	48 hours	72 hours
2-DG	**NA**	**22.7** 95% CI (14.4, 35.9)	**25.0** 95% CI (6.9, 91)
G968	**52.1** 95% CI (undefined)	**45.8** 95% CI (undefined)	**471.0** 95% CI (undefined)
3PO	**27.1** 95% CI (17.8, 36.3)	**18.8** 95% CI (16.2, 21.5)	**15.9** 95% CI (0.0, 94.1)

Figure 6.4.3 NHDF Viability in response to varying concentrations of 2-DG, G968 and 3PO.
NHDF viability assays were performed for the compounds indicated after 24, 48 and 72-hour incubations. At the end of the incubation period the culture media was replaced with media containing 0.02% alamar blue and the fluorescence for each well was measured 4 hours later using a fluorometric plate reader. Concentrations of (A) 0, 1, 2, 5, 10, 20 and 50mM were used for 2-DG, (B) 0, 1, 2, 5, 10, 25 and 50uM for G968 and (C) 0, 1, 2, 4, 8, 16, 25 and 50uM for 3PO. Viability is expressed as the % fluorescence of the untreated control for each timepoint, displayed here as the mean of two separate biological experiments, where error bars represent +/- SD. (D) The CC50 values (bold) and corresponding 95% CIs generated from the data in A-C is shown for each compound. Nonlinear regression analysis using a least squares fitting method within GraphPad prism software was performed to calculate the values shown.

6.5 Blocking NAMPT Prevents the Fibrotic Phenotype

Given the conversion of NAD^+ to NADH is a key step in glycolysis, NAD^+ is a limiting factor for glycolytic activity. As would be expected following increased glycolysis without any change in OXPHOS, NAD^+ levels in NHDFs are depleted following TGF-β stimulation (3.2-fold, $p<0.01$, Figure 6.5.1 A). Because of this dependency on NAD^+ availability, diminishing the cellular NAD^+ reserve by inhibiting NAMPT (the rate limiting enzyme in NAD^+ production via the NAD^+ salvage pathway) with the inhibitor FK866 causes a significant decrease in glycolysis (3.7-fold, $p<0.01$), glycolytic capacity (2.74-fold, $p<0.001$) and glycolytic reserve (455-fold, $p<0.0001$) (Figure 6.5.1 B). FK866 was added at a concentration of 10nM for 48 hours, conditions that were previously determined to deplete NAD^+ 5-fold without any loss of viability (Chapter 3, Figure 3.9.3). Additionally, FK866 also reduced collagen

I production in TGF-β treated NHDFs as shown by western blotting and densitometry analysis (Figure 6.5.1 C-D). Consequently, this implies that available NAD^+ is a requirement for TGF-β induced upregulation of fibrotic pathways, likely as an essential reducing agent for glycolysis.

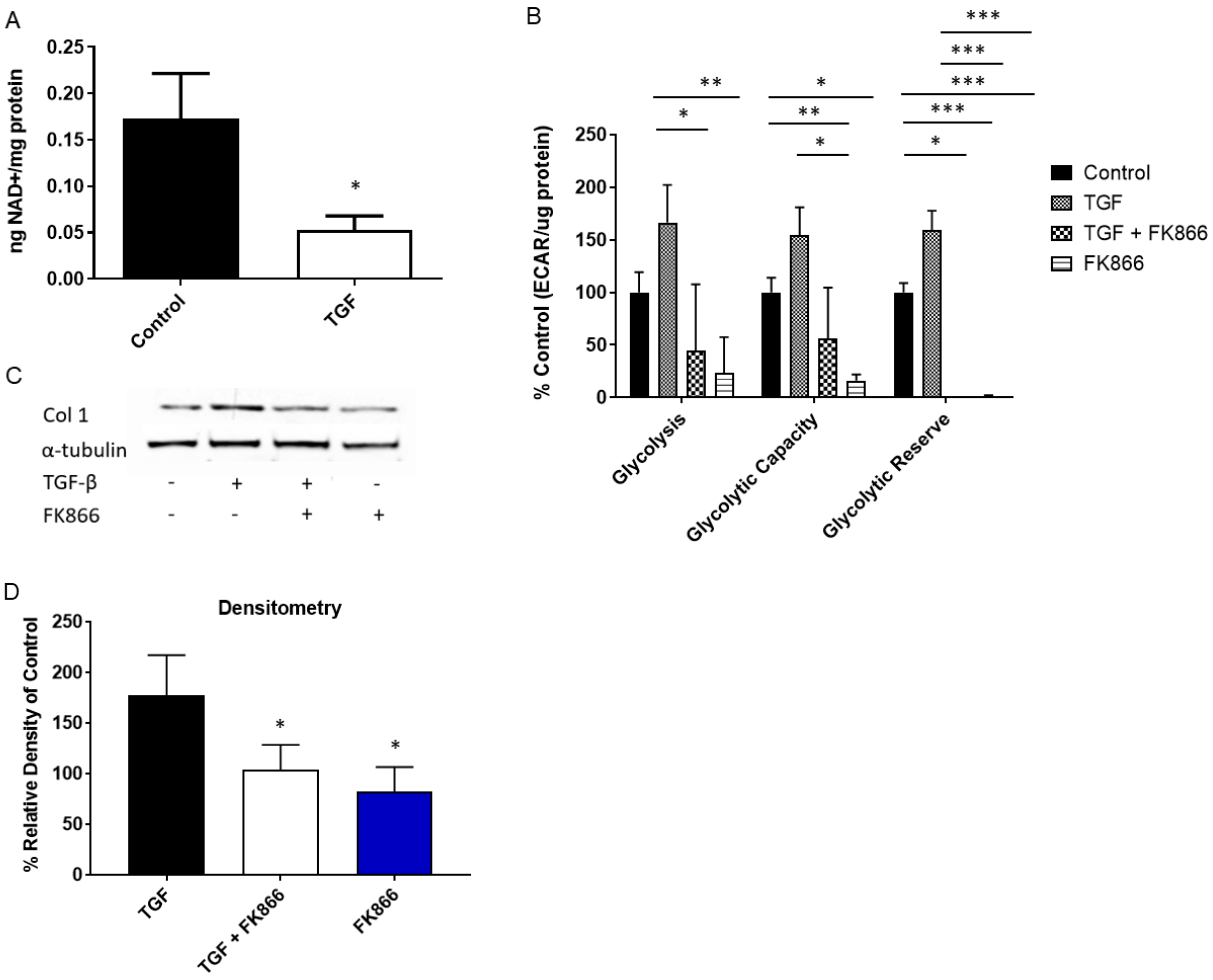

Figure 6.5.1 NAD^+ levels are key for glycolysis and fibrotic protein levels in TGF-β treated NHDFs.
(A) NAD^+ levels were measured using an NAD^+ cycling assay for NHDFs treated with or without 10ng/ml TGF-β for 48 hours (n=1 all conditions, 3 separate biological experiments). NAD^+ values was then normalised to protein levels following a BCA assay. Statistical significance was tested for using an unpaired Student's t-test. (B) The glycolytic parameters of NHDFs treated with or without 10ng/ml TGF-β and 10nM FK866 or 0.05% DMSO were measured on a Seahorse XFp Analyser by performing a glycolysis stress test (n=2 separate biological experiments). Statistical analysis was performed using 1-way ANOVA and significant differences between the treatments for each glycolytic parameter tested for using a Bonferroni post hoc test. (C) Protein levels of collagen I (Col I) and α-tubulin were measured by western blotting for NHDFs treated with or without 10ng/ml TGF-β and 10nM FK866 or 0.05% DMSO. The blot shown is representative of 3 separate biological experiments. (D) Densitometry analysis was then performed on the blots (n=3) and the collagen I levels relative to α-tubulin is expressed as a percentage of the untreated control. Statistical analysis was performed using 1-way ANOVA followed by a Dunnet's post hoc test whereby the TGF group was used as the control. Error bars represent +/- SD. *p<0.05, **p<0.01, ***p<0.0001.

6.6 Resveratrol Reduces TGF-β Upregulation of Collagen I

Given the accumulating evidence that SIRT1 may fulfil an anti-fibrotic role, NHDFs were treated with the prototypical SIRT1 activator resveratrol (RSV) to determine whether this could reverse TGF-β driven effects. Co-incubating 10ng/ml TGF-β treated NHDFs with 100uM RSV for 48 hours potently reversed the TGF-β induced increases in collagen I and α-SMA (Figure 6.6.1 B-C). Having already identified TGF-β driven upregulation of glycolysis, it was next investigated whether RSV could reverse this aspect of TGF-β signalling. Unlike for the fibrotic markers, 48 hours of 100uM RSV treatment was unable to induce any significant change to the glycolytic parameters (Figure 6.6.1 A), hence this highlights that RSV elicits an anti-fibrotic effect independent of glycolysis.

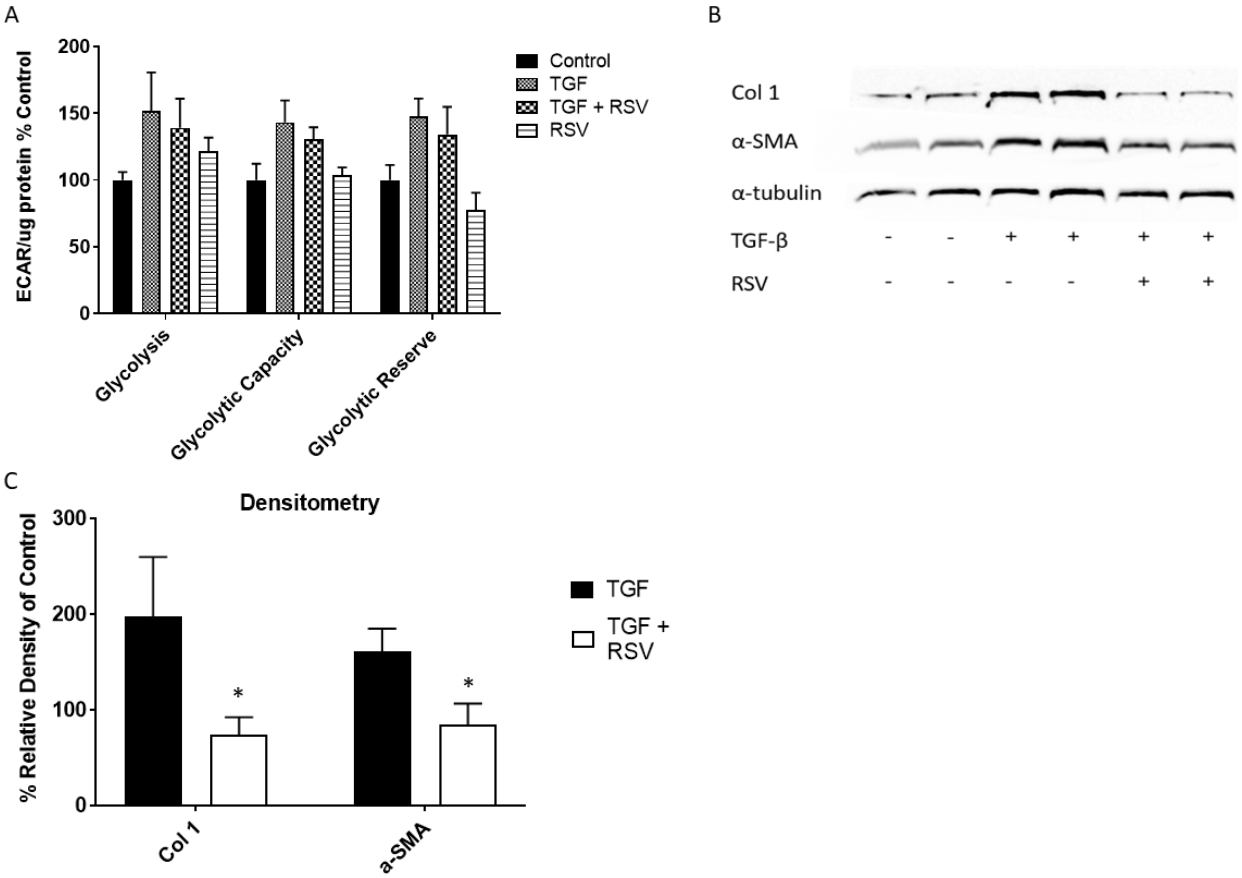

Figure 6.6.1 RSV reverses TGF-β upregulation of fibrotic markers but not glycolytic parameters.
NHDFs were treated for 48 hours with 10ng/ml TGF-β, 100uM RSV, 10ng/ml TGF-β and 100uM RSV or 0.1% DMSO (n=1 all conditions, 3 separate biological experiments). (A) Glycolytic parameters were assessed by performing a glycolysis stress test on the Seahorse XFp Analyser during which ECAR was measured. Afterwards, protein levels were measured by a BCA assay to allow normalisation of ECAR to protein. The data is shown as mean % ECAR/ug protein of the DMSO treated NHDF controls. (B) Additionally, the expression of the fibrotic markers collagen I (Col I) and α-SMA were measured by western blotting, with the loading control α-tubulin also probed to verify equal loading of protein lysates. The blot shown is representative of 3 separate biological experiments. **(**C) Densitometry analysis was then performed on the blots (n=3) and the collagen I and α-SMA levels relative to α-tubulin is expressed as a percentage of the untreated control. Error bars represent +/- SD. The statistical analysis for panel A was performed using 1-way ANOVA for each glycolytic parameter and significant differences between the treatments tested using a Bonferroni post hoc test. For panel C statistical significance was tested for using an unpaired Student's t-test for collagen I and α-SMA. *p<0.05.

6.7 NTC Suppress TGF-β Induction of Glycolysis but not Fibrotic Markers

NTC (Nuchido Time+ Cocktail) is a combination of naturally occurring compounds chosen for their ability to enhance NAD^+ levels by targeting pathways that regulate NAD^+ metabolism. The compounds were tested individually for any efficacy at reducing TGF-β induced collagen I synthesis by western blotting, however none showed any noticeable effect. Although the requirement of NAD^+ for glycolysis had been shown to be important for TGF-β driven effects, the anti-fibrotic role of SIRT1 suggests that increasing NAD^+ may not necessarily promote fibrosis if it fuels enhanced SIRT1 activity. Hence, to probe this TGF-β stimulated NHDFs were also co-treated with NTC for 48 hours to determine whether increasing NAD^+ via NTC inhibits/promotes fibrotic marker levels.

Surprisingly, NTC potently abrogated TGF-β upregulation of all glycolytic parameters (Figure 6.7.1 A). Despite this however, NTC was unable to reverse the enhanced levels of fibrotic markers (Figure 6.7.1 B). Whilst it was previously shown that inhibition of glycolysis prevented TGF-β induction of fibrotic markers (Figure 6.4.1 C), it appears that returning it to basal levels fails to have the same effect. This suggests that whilst TGF-β driven fibrosis is dependent on a fully functional glycolytic pathway, increasing its activity isn't necessary for the pro-fibrotic phenotype. Additionally, the data also suggests that targeting NAD^+ levels vis NTC isn't sufficient to inhibit TGF-β upregulation of collagen I via a predicted increase in SIRT1 activity.

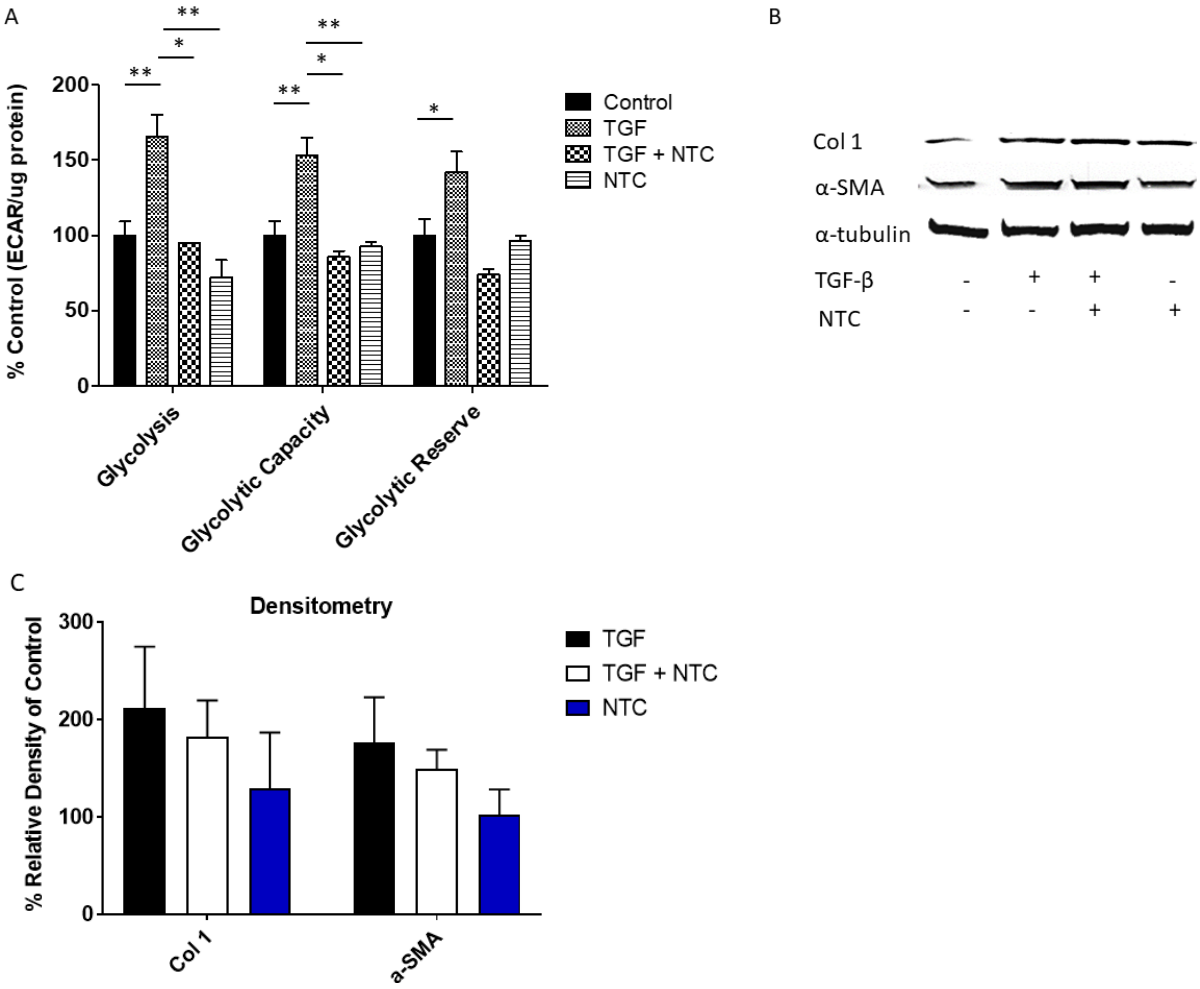

Figure 6.7.1 NTC attenuates TGF-β upregulation of glycolysis but not fibrotic marker levels.
NHDFs were treated for 48 hours with 10ng/ml TGF-β, NTC, 10ng/ml TGF-β and NTC or 0.26% DMSO (n=1 all conditions, 3 separate biological experiments). After 24 hours the media was replaced with fresh media also containing TGF-β, NTC and DMSO as before. (A) Glycolytic parameters were assessed by performing a glycolysis stress test on the Seahorse XFp Analyser during which ECAR was measured. Afterwards, protein levels were measured by a BCA assay to allow normalisation of ECAR to protein. The data is shown as mean % ECAR/ug protein of the DMSO treated NHDF controls. (B) Additionally, the expression of the fibrotic markers collagen I (Col I) and α-SMA were measured by western blotting, with the loading control α-tubulin used to verify equal loading of protein lysates. The blot shown is representative of 3 separate biological experiments**.** (C) Densitometry analysis was performed on these blots (n=3), whereby collagen I and α-SMA levels relative to α-tubulin is expressed as a percentage of the untreated control. Error bars represent +/- SD. For panel A statistical analysis was performed using 1-way ANOVA for each glycolytic parameter and significant differences between the treatments tested using a Bonferroni post hoc test. For panel C 1-way ANOVA was used for collagen I and α-SMA relative density separately, with a Dunnett's post hoc test to determine significant differences against the TGF-β treated group. *p<0.05, **p<0.01.

6.8 Glutaminolysis Is Essential For TGF-β Induced Fibrosis Independent of mTOR

Rapamycin, a compound which inhibits mTOR (mechanistic target of rapamycin), downregulates protein synthesis and other biosynthetic pathways which has stimulated interest around its potential as a novel anti-cancer agent [508-510]. mTOR primarily functions as a nutrient and energy sensor, whereby it upregulates cell growth and proliferation under conditions of adequate nutrient and energy availability. Hence, if biosynthetic intermediates from glycolysis or the TCA cycle are key for fibrosis, inhibition of mTOR should have an anti-fibrotic effect. To test this, NHDFs were stimulated with 10ng/ml TGF-β for 48 hours as done in previous experiments, along with the addition of 500nM rapamycin. Because rapamycin has been noted for its anti-glycolytic effects in other cell types [511], its effect on glycolysis in TGF-β treated NHDFs was first investigated by performing a glycolysis stress test. Treatment with rapamycin caused a small reduction in the levels of basal glycolysis, glycolytic capacity and glycolytic reserve in the TGF-β treated cells however these differences were statistically insignificant (Figure 6.8.1 A).

Under the same conditions, levels of the fibrotic markers collagen I and α-SMA were probed in TGF-β and rapamycin treated NHDFs by western blotting (Figure 6.8.1 C and F). The rapamycin failed to attenuate TGF-β enhancement of these markers, suggesting inhibition of mTOR fails to suppress induction of the pro-fibrotic phenotype in NHDFs.

To further test the theory that fibrotic cells modified their metabolic pathways to generate biosynthetic intermediates for ECM synthesis, the role of glutaminolysis was next investigated. The process of glutaminolysis involves two sequential steps whereby glutamine is first converted to glutamate, which is then converted to α-ketoglutarate. Subsequently, α-ketoglutarate can then feed into the TCA cycle, thus fuelling NADH production. Alternatively, α-ketoglutarate can also act as a cofactor for prolyl-4-hydroxylase, facilitating the hydroxylation of proline to yield hydroxyproline – the main constituent of collagen (Figure 6.10). Therefore, if an increase in the TCA cycle fuels ECM secretion following the upstream enhancement of glycolysis in the presence of TGF-β by yielding α-ketoglutarate, it is possible that glutaminolysis is also enhanced for the same purpose.

To determine whether glutamine is a key fuel source for enhanced collagen synthesis in pro-fibrotic fibroblasts, glutamine was added at different concentrations ranging from 0-8mM to NHDFs that were stimulated with or without 10ng/ml TGF-β. In addition to being serum starved prior to incubation with TGF-β, media without glutamine was used for 24 hours before adding the TGF-β and the varying concentrations of glutamine. 48 hours after treatment with glutamine and TGF-β the cells were lysed and the levels of collagen I, α-SMA and α-tubulin were then measured by western blotting.

Within the TGF-β treated cells there was no pattern of increasing collagen I levels with increasing glutamine concentration, (Figure 6.8.1 D and G) however for the NHDFs without TGF-β, collagen I production was impaired at the 0 and 1mM glutamine concentrations. Densitometry analysis of the blots was performed (Figure 6.8.1 F and G), with 2-way ANOVA finding that altering the glutamine concentration wasn't a significant source of variation in the relative density of collagen or α-SMA staining. Furthermore, 1-way ANOVA within both the TGF treated and untreated groups found no significant differences in collagen or α-SMA staining density. The 2-way ANOVA did find that TGF-β had a significant effect on collagen and α-SMA staining density (collagen $p<0.01$, α-SMA $p<0.001$), however multiple comparisons found no significant differences between the TGF-β and untreated groups for all glutamine concentrations, thus it is likely there was an issue with the TGF-β stock for this set of experiments.

Additionally, on review of the experimental setup, it is possible that the intracellular supply of glutamine/glutamate wasn't adequately depleted during the withdrawal of glutamine and thus limited the effect of altering glutamine concentration in the culture media. To address this, an inhibitor of glutaminase (which catalyses the first step in glutaminolysis) known as G968 (glutaminase inhibitor 968) was used. After characterising the relationship between G968 concentration and NHDF viability (Figure 6.4.3 B), 10uM was selected as an appropriate sub-cytotoxic dose for G968 and was added to NHDFs alongside 10ng/ml TGF-β for 48 hours before collagen I and α-tubulin were measured by western blotting (Figure 6.8.1 B). In contrast to glutamine withdrawal from the media, G968 appeared to lower collagen I levels in the TGF-β treated NHDFs, suggesting that glutaminolysis could be a key metabolic pathway in the development of a fibrotic phenotype *in vitro*.

Densitometry analysis of the blots found that TGF-β increased collagen staining density by 47% compared to the untreated control, whereas co-treatment with TGF-β and G968 reduced collagen staining density 1.5% compared to the untreated control (Figure 6.8.1 E). 1-way ANOVA comparing the TGF-β, TGF-β with G968 and G968 only found a statistically significant difference between the TGF-β and G968 groups however ($p<0.021$).

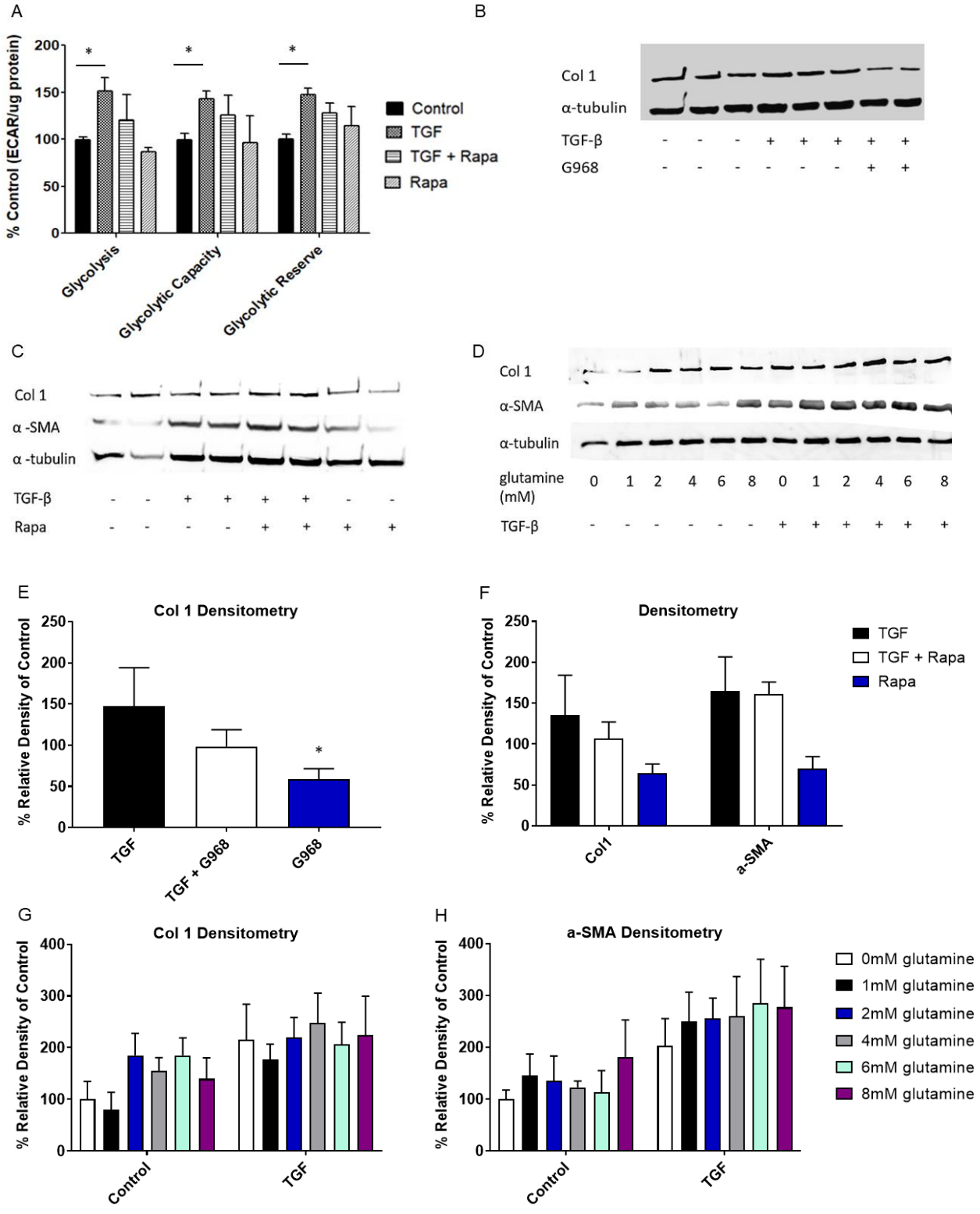
A
% Control (ECAR/ug protein)
200
150
100
50
0
*
*
*
Control
TGF
TGF + Rapa
Rapa
Glycolysis
Glycolytic Capacity
Glycolytic Reserve
B
Col 1
α-tubulin
TGF-β - - - + + + + +
G968 - - - - - - + +
C
Col 1
α -SMA
α -tubulin
TGF-β - - + + + + - -
Rapa - - - - + + + +
D
Col 1
α-SMA
α-tubulin
glutamine (mM) 0 1 2 4 6 8 0 1 2 4 6 8
TGF-β - - - - - - + + + + + +
E
Col 1 Densitometry
% Relative Density of Control
250
200
150
100
50
0
*
TGF
TGF + G968
G968
F
Densitometry
% Relative Density of Control
TGF
TGF + Rapa
Rapa
Col1
a-SMA
G
Col 1 Densitometry
% Relative Density of Control
400
300
200
100
0
Control
TGF
H
a-SMA Densitometry
% Relative Density of Control
0mM glutamine
1mM glutamine
2mM glutamine
4mM glutamine
6mM glutamine
8mM glutamine
Control
TGF

Figure 6.8.1 Glutaminase activity may contribute to TGF-β driven effects.
(A) The glycolytic parameters of NHDFs treated for 48 hours with 10ng/ml TGF-β, 500nM rapamycin (Rapa), 10ng/ml TGF-β and 500nM Rapa or 0.01% DMSO were measured on a Seahorse XFp Analyser by performing a glycolysis stress during which ECAR was measured (n=1 for all conditions, three separate biological experiments). The ECAR was then normalised to total protein and the ECAR/ug protein was subsequently expressed as a % of the untreated control. (B) Collagen I (Col I) and α-tubulin expression was assessed by western blotting for NHDFs treated with or without 10ng/ml TGF-β and the glutaminase inhibitor G968 (10uM) or 0.2% DMSO for 48 hours. (C) Expression of collagen I, α-SMA and α-tubulin were measured by western blotting for NHDFs treated 48 hours with 10ng/ml TGF-β, 500nM rapamycin (Rapa), 10ng/ml TGF-β and 500nM Rapa or 0.01% DMSO. (D) NHDFs were treated with or without 10ng/ml TGF-β and various concentrations of L-glutamine. Expression of collagen I, α-SMA and α-tubulin was again quantified by western blotting. (E-G) Densitometry analysis was performed for the western blots (n=3 separate biological experiments) from the experiments in panels B-D, whereby collagen I and α-SMA (F only) levels relative to α-tubulin is expressed as a percentage of the untreated control. Error bars represent +/- SD. For panel A the statistical analysis was performed using 1-way ANOVA for each glycolytic parameter and significant differences between the treatments tested using a Bonferroni post hoc test. For E-G 1-way ANOVA was used to analyse collagen I and α-SMA relative density separately, with a Dunnett's post hoc test to determine significant differences against the TGF-β treated group. *p<0.05.

6.9 Glutaminase But Not Collagen Is Enhanced in SSc Patient Fibroblasts

Although increased TGF-β signalling is a key driver of pathogenesis in fibrotic lesions of SSc patients, cultured fibroblasts derived from lesional tissue exhibit enhanced ECM production even without the presence of TGF-β in the culture media [512], suggesting endogenous mechanisms also contribute to fibrosis with epigenetic factors thought to be key. Hence, it was investigated whether glycolysis and glutaminolysis are altered in dermal fibroblasts derived from SSc patient skin lesions. The SSc fibroblasts were obtained from 4 different patients, whilst NHDFs were obtained from 3 age-matched controls and all experiments were performed with cells at passage ≤6. Due to the limited number of wells on a seahorse XFp miniplate, only 6 different samples can be assayed at once, hence it was decided to assay two sets of the control fibroblasts against the 4 different SSc fibroblasts. Initially, the 3 sets of control fibroblasts were assayed to determine which two should be chosen to assay alongside the SSc fibroblasts. Control 1 and 2 were selected given they had the highest and lowest ECAR/ug protein values for the glycolytic parameters, with a mean relatively close to the mean of control 3 (12% higher).

There was a high variability in the SSc cohort ECAR/ug protein values, which are expressed as a % of the control NHDFs' mean (Figure 6.9.1 A). For glycolysis, the % ECAR ug protein of the control for the SSc fibroblasts was: SSc 1 – 93%, SSc 2 – 80%, SSc 3 – 58% and SSc 4 – 151%. For glycolytic capacity the values were: SSc 1 – 93%, SSc 2 – 67%, SSc 3 – 41%, SSc 4 – 116% and for glycolytic reserve: SSc 1 – 114%, SSc 2 - 138%, SSc 3 – 163%, SSc 4 – 125%. Despite the variable values, there was no significant difference between any of the patient fibroblasts and the control mean.

To test for differences in the activity of glutaminolysis, levels of the enzyme glutaminase were analysed by western blotting performed on protein lysates from the 3 control and 4 patient fibroblasts (Figure 6.9.1 C). Glutaminase exists as 2 different isoforms, KGA (kidney-type glutaminase) and GAC (glutaminase C), thus produces two separate bands following immunoblotting at 65 kDa and 58 kDa respectively. Interestingly, KGA was elevated in all 4 patients compared to controls, with the GAC variant also elevated in patients 1 and 4, with this marker the only one showing a significant difference between the NHDF and SSc cohort (unpaired Student's t-test, $p=0.031$) - suggesting upregulated KGA may be a novel characteristic feature of SSc.

It should be noted that all protein makers measured were elevated (albeit only KGA significantly), which was surprising in the instance of SIRT1, which has been found to be antifibrotic in a number of studies. It was also surprising to find when comparing the collagen I levels of the controls and patients, that only patients 1 and 4 showed a noticeable increase compared to controls 2 and 3, hence the signature enhanced collagen production associated with SSc is absent *in vitro* – possibly due to the lack of circulating stimuli such as TGF-β and other *in vivo* mechanisms. The lack of increased collagen I levels does however question whether these SSc patient fibroblasts can be truly regarded as pro-fibrotic or representative of SSc pathogenesis under in vitro conditions.

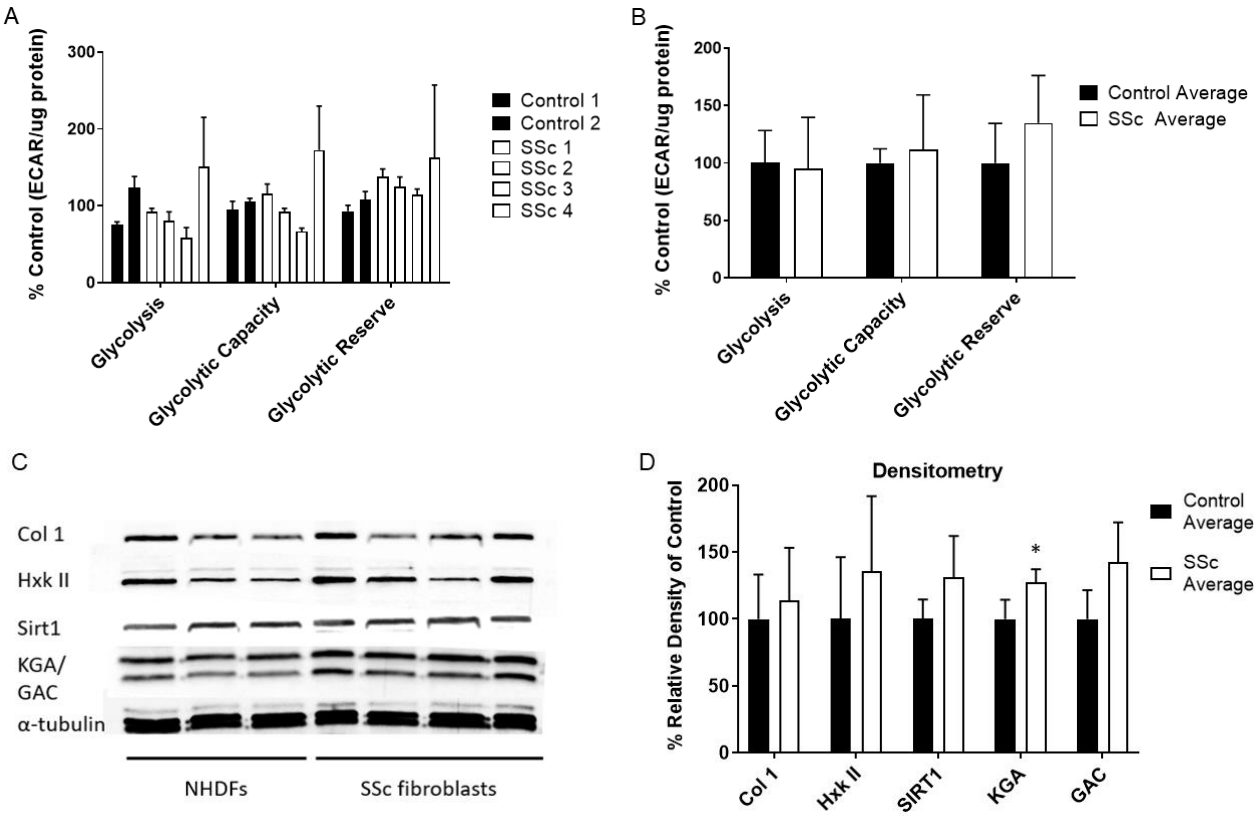

Figure 6.9.1 Glycolysis and glutaminase expression in SSc patient derived dermal fibroblasts.
Glycolytic parameters for NHDFs from healthy controls (n=2) and SSc patients (n=4) were assessed by measuring ECAR using a glycolysis stress test and then normalised to protein levels by performing a BCA assay. The ECAR/ug protein was then expressed as a % of the healthy control mean, presented here as the average of two separate biological experiments. (A) The data for both individual donor samples and (B) the SSc and control averages is shown. (C) Expression of glutaminase (KGA/GAC), hexokinase II (Hxk II), collagen I (Col I) and the loading control α-tubulin in SSc and the control NHDFs was analysed by western blotting. The blot shown is representative of 3 separate biological experiments. (D) Densitometry analysis was performed for these western blots (n=3), whereby the levels of all protein markers relative to α-tubulin is expressed as a percentage of the NHDF average. The data is shown as the combined average for the healthy controls (n=3) and SSc samples (n=4). The panel A statistical analysis was performed using 1-way ANOVA. For panel B significance was tested for each of the glycolytic parameters separately using an unpaired Student's t-test. Similarly, an unpaired Student's t-test was used to compare the relative density of the SSc average to the NHDF average separately for each protein marker measured. Error bars represent +/- SD.

6.10 Discussion

Metabolic re-programming is a well-established event in the development of tumourgenicity, however evidence is starting to accumulate that it is present in numerous other pathologies including fibrotic [513-515] and autoimmune diseases [516-518].

Eukaryotic energy metabolism consists of 3 core pathways: glycolysis, the TCA cycle and OXPHOS, with all 3 connecting to each other in that order (Figure 1.1.6.1) Glycolysis begins with one molecule of glucose which is metabolised to give a net yield of 2 ATP, 4 NADH and 2 pyruvate molecules. The pyruvate can then either be reduced to lactate or enter the TCA cycle after being converted to acetyl CoA, which will lead to a net gain of 1 ATP, 3 NADH and 1 $FADH_2$ per pyruvate molecule. Subsequently, the NADH and $FADH_2$ generated by glycolysis and the TCA cycle can fuel OXPHOS by donating their electrons, stimulating further ATP production via complex V. However, various steps such as the fermentation of pyruvate or the shuttling of TCA cycle intermediates into other pathways means that glycolysis and OXPHOS can become uncoupled – e.g. glycolysis levels can increase, accompanied by no change or even a decrease in OXPHOS.

Here it is shown that the pro-fibrotic stimulus TGF-β increases glycolysis in NHDFs, with no change in the levels of OXPHOS. This would suggest that the upregulation of glycolysis is culminating in increased lactate production, however the lactate levels in the media of TGF-β treated cells also showed no change compared to untreated NHDFs. It is therefore possible that TGF-β is increasing glycolysis which in turn increases the input of acetyl CoA into the TCA cycle, which is the point at which the uncoupling from OXPHOS occurs.

Indeed, one of the early intermediates within the TCA cycle is α-ketoglutarate, a precursor for hydroxyproline – the subunit required to assemble mature collagen. Given that inhibiting glycolysis using 2-DG or 3PO prevented TGF-β driven increases in collagen I, it was posited that the increased glycolysis was coupled to increased activity in the TCA cycle, from which α-ketoglutarate was then being removed to fuel collagen synthesis. This would stunt the TCA cycle beyond the point α-ketoglutarate is produced, hence the absence of any notable increase in OXPHOS.

In addition to the TCA cycle, the other main mechanism for cellular α-ketoglutarate production is glutaminolysis, a 2-step pathway in which glutamine is converted to a-ketoglutarate via a glutamate intermediate. Hence, if increased α-ketoglutarate is a key requirement for the development of fibrosis it was theorised that glutaminolysis may also be contributing to the fibrotic phenotype. Levels of glutaminolysis in NHDFs were altered by varying the concentration of glutamine in the media, however this had a minimal effect on the levels of fibrotic markers with or without TGF-β in

the media. Whether intracellular glutamine was adequately depleted for the changing media concentrations of glutamine to have an effect isn't clear however, hindered by the lack of robust methods to accurately measure glutaminolysis.

Inhibition of glutaminolysis using the glutaminase inhibitor G968 abrogated the increased production of collagen I in TGF-β treated NHDFs however, which suggests that glutaminolysis is an important pathway for fibrosis. Strikingly, the KGA isoform of glutaminase was ubiquitously elevated in fibroblasts obtained from the skin lesions of 4 SSc patients when compared to NHDFs from age-matched controls. In contrast, the different SSc fibroblasts showed high variation in their basal glycolysis, glycolytic capacity and glycolytic reserve suggesting that the involvement of glycolysis may be highly variable between different patients and heavily influenced by a number of disease independent factors.

Thus, combining the data from TGF-β induced NHDFs and the SSc fibroblasts depicts a possible scenario in SSc whereby circulating TGF-β stimulates increased glycolysis which synergises with endogenously enhanced glutaminolysis to ramp up α-ketoglutarate production. Subsequently, this increased α-ketoglutarate is used as a precursor for collagen synthesis and hence facilitates enhanced ECM secretion – the underlying hallmark of fibrosis.

Further work is required to test this theory, namely measuring the levels of succinate from TGF-β induced NHDFs and the SSc fibroblasts. Succinate is a downstream metabolite of α-ketoglutarate in the TCA cycle as well being a byproduct in the chain of reactions leading to collagen synthesis (Figure 3.11). However, it only exists as an intermediate which is subsequently converted to fumarate in the former, hence increased succinate levels along with enhanced glycolysis would be indicative of the latter – i.e. α-ketoglutarate being re-directed from the TCA cycle to fuel collagen production.

Ideally, a comprehensive omics approach would also be used to gain a more nuanced picture of the metabolic alterations occurring within skin fibrosis and their relevancy to the disease pathogenesis. Characterisation of the levels of the key enzymes involved in the energy pathways mentioned here along with those involved in lipid metabolism as well as nucleotide and protein synthesis via LC-MS based targeted proteomics would allow a deeper insight into the metabolic differences between SSc fibrotic lesion and non-lesion samples. Although LC-MS based proteomics have been performed on tissue samples from fibrotic mouse models [519-521], this approach has yet to be extended to SSc lesional tissue.

Furthermore, single cell RNA (scRNA) sequencing within fibrotic lesions could be performed for a similar purpose: identifying if there are differences in the expression of metabolic genes in normal

and fibrotic fibroblasts within lesional tissue. Indeed, laser microdissection has previously been used to select pro-fibrotic myofibroblasts in IPF fibrotic lung samples for a similar purpose [522].

Finally, the functional effects of modifying glycolytic and glutaminolytic activity performed within this work should be extended to *in vivo* models of skin fibrosis. There is already a precedence for the use of glycolysis and glutaminolysis inhibitors in various mouse models [523-525], hence inhibitors like 3PO and G968 could be trialled as therapeutics targeting bleomycin or TGF-β induced skin fibrosis in mice.

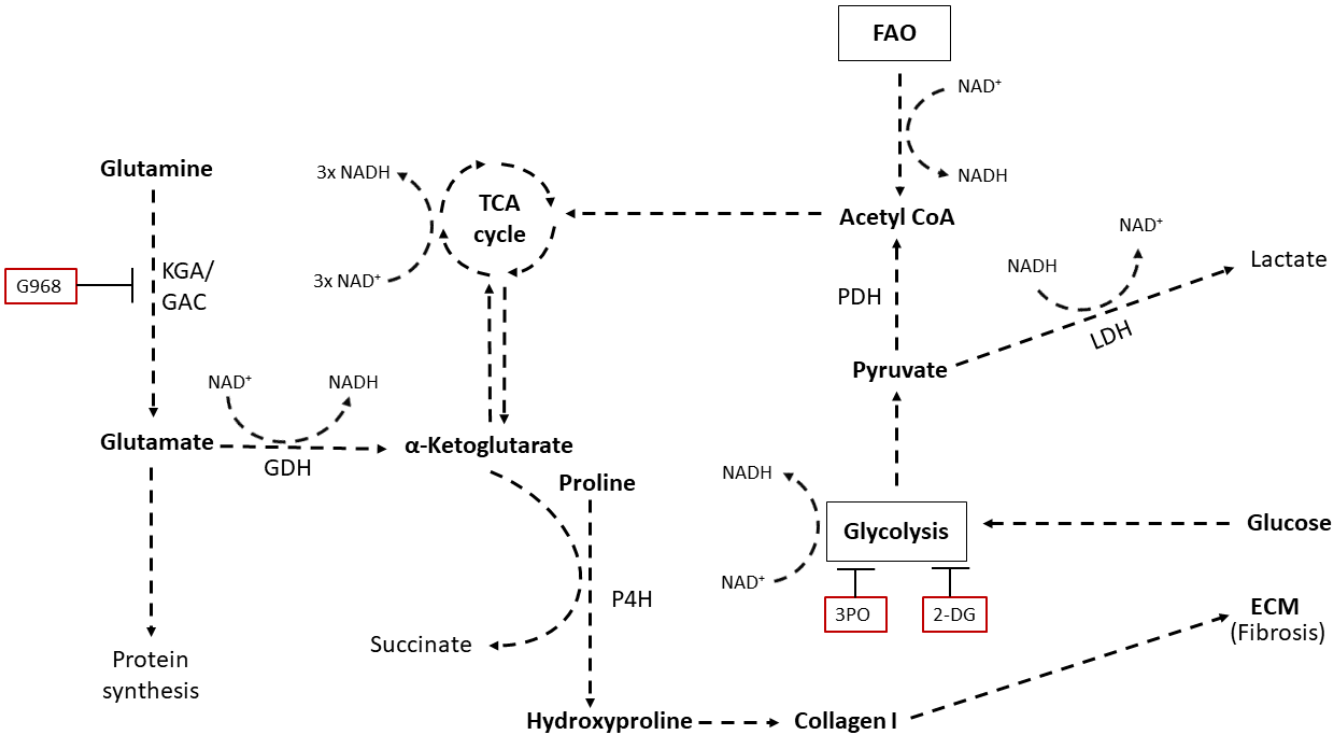

Figure 6.10.1 Interaction between energy metabolism pathways and collagen synthesis.
The mechanisms by which cellular energy metabolism pathways can fuel collagen synthesis is shown. Acetyl-CoA derived from either glycolysis or FAO is shuttled into the TCA cycle which yields α-ketoglutarate as an intermediate, which can also be synthesised from glutamine via glutaminolysis. Under fibrotic conditions, this α-ketoglutarate can be used as a co-substrate for hydroxyproline synthesis which is a building block for collagen – the main constituent of fibrotic lesions. Hypothetically, the use of inhibitors (G968, 3PO and 2-DG) targeting glycolysis and glutaminolysis could obstruct energy metabolism mediated upregulation of collagen production.
Abbreviations: KGA/GAC - kidney type glutaminase/glutaminase C, GDH - glutamate dehydrogenase, P4H - prolyl 4-hydroxylase, PDH - pyruvate dehydrogenase, LDH - lactate dehydrogenase, ECM - extracellular matrix, FAO - fatty acid oxidation.

Chapter 7. Concluding Remarks

As global life expectancy continues to rise, so does the incidence of highly debilitating age-related morbidities such as Alzheimer's disease, Parkinson's disease, various cancers and cardiovascular disease. This results in a low quality of life for those affected, as well as presenting an expanding economic and healthcare burden for society. Hence, this emphasises the pressing need to ensure human healthspan is also increased in tandem with lifespan, which has stimulated the quest for anti-ageing interventions.

With the goal of contributing towards this quest, the work within this thesis was undertaken with the primary intent of better understanding the mechanisms regulating NAD^+ levels and the subsequent implications altering NAD^+ has on aspects of cellular health – particularly in the context of pathways involved in ageing. Of particular note was the confirmation that NAD^+ levels exhibit circadian rhythmicity both *in vivo* and when pharmacologically induced *in vitro* – with BMAL1 functioning as a key mediator.

This raises important considerations for existing and prospective NAD^+ enhancing interventions, which would ideally be administered in a manner that targets the daily nadir in NAD^+ levels for maximal enhancement, given this is when cellular function is most susceptible to the adverse consequences of reduced NAD^+. Such an approach is hindered however by the likelihood that the circadian rhythmicity of NAD^+ varies between individuals, hence would require profiling prior to beginning an NAD^+- targeting regimens.

Given its apparent regulation by BMAL1, the circadian profile of NAD^+ may also be modulated upstream of BMAL1 by environmental factors such as sunlight exposure and sleep/wake patterns. Hence, future studies characterising the effects of these stimuli on the rhythmicity of NAD^+ and identifying any correlations may allow the circadian NAD^+ profile of an individual to be accurately predicted based on their environment and lifestyle traits – thus informing the optimal time to implement NAD^+ enhancing interventions.

Additionally, determining whether SIRT1 activity mirrors the circadian fluctuation in NAD^+ levels would also be a key follow on from the work presented within this thesis, providing clarity on the intimacy of the interaction that exists between SIRT1 and NAD^+ levels. Similarly, although the NTC *in vitro* and NCD201 *in vivo* interventions significantly increased NAD^+, it wasn't determined whether this translates to an increase in SIRT1 activity as predicted - which is another outstanding issue that needs addressed.

To this end, it should be noted that the measurement of SIRT1 activity is complicated given it shares many of its substrates with other enzymes, hence there is a lack of biomarkers which are exclusive for SIRT1. The acetylation status of P53 was initially measured by western blotting for this purpose, however it was found to be highly inconsistent in the presence of both the SIRT1 activator resveratrol and the inhibitor EX527, thus raising doubts over its validity as a bona fide marker of SIRT1 activity.

Indeed, this reinforces the need to go beyond molecular analyses and test the functional effects of the NCD cocktails using *in vivo* mammalian models. Recent studies have reported improvements in the exercise performance of elderly mice in response to NAD^+ precursor supplementation [180, 183], hence a deeper insight into the likely 'real world' utility of a multi-targeted NAD^+ intervention would be gained by replicating these studies using the multi-targeted approach. Moreover, this would also offer an improved characterisation of the widespread effects of the intervention by allowing analysis of the biochemical changes occurring across different tissues. Metabolomic and proteomic analysis of the changes induced by the multi-targeted approach would not only confirm whether it was working as intended, but could also identify off-target effects: good and bad.

This is especially pertinent given the polyphenolic compounds used within the multi-targeted approach are known to be able to influence numerous different pathways [526-529], depending on cell type and environmental factors. This is somewhat emphasised by the surprising discovery that the NTC *in vitro* supplement protected NHDFs against oxidative stress via an NAD^+-dependent but SIRT1/PARP1-independent mechanism.

Thus, for all future work involving NTC both *in vivo* and *in vitro*, a nicotinamide group (NTC without the polyphenols) should be included to determine the impact of the polyphenols, especially given nicotinamide itself already has been shown to enhance human NAD^+ levels [150] and improve health in a number of murine models of age-related disease [161, 166, 332, 343].

Similarly, a large-scale study directly pitting the multiple widely endorsed NAD^+ precursors against each other (nicotinamide, NR, NMN, NA) and testing their ability to enhance NAD^+ in a human cohort would clarify the optimal precursor for the purpose of human blood NAD^+ enhancement. Given the respective precursors are imported and metabolised by different enzymes, the reality may be that 'one precursor doesn't fit all' and specific precursors perform better for specific disease conditions (dependent on the tissues involved and molecular changes in the affected tissue). Again, large-scale studies using multiple precursors could determine if a superior precursor exists for specific diseases.

In summary, this work contributes to the wider efforts to understand and ultimately modify the cellular mechanisms implicated in ageing by identifying the presence of a circadian system regulating

NAD^+ levels, both in human PBMCs and cultured NHDFs. Furthermore, the combined use of dietary supplements targeting multiple facets of NAD^+ metabolism represents a novel approach to combat age-related NAD^+ decline, having demonstrated early promise both *in vitro* and in a 2-person pilot study.

References

1. Kenyon, C., et al., *A C. elegans mutant that lives twice as long as wild type.* Nature, 1993. **366**(6454): p. 461-4.
2. Tissenbaum, H.A. and L. Guarente, *Increased dosage of a sir-2 gene extends lifespan in Caenorhabditis elegans.* Nature, 2001. **410**(6825): p. 227-230.
3. Friedman, D.B. and T.E. Johnson, *A mutation in the age-1 gene in Caenorhabditis elegans lengthens life and reduces hermaphrodite fertility.* Genetics, 1988. **118**(1): p. 75.
4. Parkes, T.L., et al., *Extension of Drosophila lifespan by overexpression of human SOD1 in motorneurons.* Nature Genetics, 1998. **19**(2): p. 171-174.
5. Chavous, D.A., F.R. Jackson, and C.M. O'Connor, *Extension of the Drosophila lifespan by overexpression of a protein repair methyltransferase.* 2001. **98**(26): p. 14814-14818.
6. Johnson, T.E., *Increased life-span of age-1 mutants in Caenorhabditis elegans and lower Gompertz rate of aging.* Science, 1990. **249**(4971): p. 908-12.
7. Larsen, P.L., P.S. Albert, and D.L. Riddle, *Genes that regulate both development and longevity in Caenorhabditis elegans.* Genetics, 1995. **139**(4): p. 1567-83.
8. Ayyadevara, S., et al., *Remarkable longevity and stress resistance of nematode PI3K-null mutants.* Aging Cell, 2008. **7**(1): p. 13-22.
9. Hsin, H. and C. Kenyon, *Signals from the reproductive system regulate the lifespan of C. elegans.* Nature, 1999. **399**(6734): p. 362-6.
10. Clancy, D.J., et al., *Extension of life-span by loss of CHICO, a Drosophila insulin receptor substrate protein.* Science, 2001. **292**(5514): p. 104-6.
11. Tu, M.P., D. Epstein, and M. Tatar, *The demography of slow aging in male and female Drosophila mutant for the insulin-receptor substrate homologue chico.* Aging Cell, 2002. **1**(1): p. 75-80.
12. Tatar, M., et al., *A mutant Drosophila insulin receptor homolog that extends life-span and impairs neuroendocrine function.* Science, 2001. **292**(5514): p. 107-10.
13. Selman, C., et al., *Evidence for lifespan extension and delayed age–related biomarkers in insulin receptor substrate 1 null mice.* The FASEB Journal, 2008. **22**(3): p. 807-818.
14. Blüher, M., B.B. Kahn, and C.R. Kahn, *Extended longevity in mice lacking the insulin receptor in adipose tissue.* Science, 2003. **299**(5606): p. 572-4.
15. Kurosu, H., et al., *Suppression of aging in mice by the hormone Klotho.* Science (New York, N.Y.), 2005. **309**(5742): p. 1829-1833.
16. Lin, S.J., P.A. Defossez, and L. Guarente, *Requirement of NAD and SIR2 for life-span extension by calorie restriction in Saccharomyces cerevisiae.* Science, 2000. **289**(5487): p. 2126-8.
17. Kaeberlein, M., et al., *High osmolarity extends life span in Saccharomyces cerevisiae by a mechanism related to calorie restriction.* Mol Cell Biol, 2002. **22**(22): p. 8056-66.
18. Austad, S.N., *Life extension by dietary restriction in the bowl and doily spider, Frontinella pyramitela.* Exp Gerontol, 1989. **24**(1): p. 83-92.
19. Nusbaum, T.J. and M.R. Rose, *The effects of nutritional manipulation and laboratory selection on lifespan in Drosophila melanogaster.* J Gerontol A Biol Sci Med Sci, 1999. **54**(5): p. B192-8.
20. Marcellino, B.K., N. Ekasumara, and C.V. Mobbs, *Dietary Restriction and Glycolytic Inhibition Reduce Proteotoxicity and Extend Lifespan via NHR-49.* Current neurobiology, 2018. **9**(1): p. 1-7.
21. Sutphin, G.L. and M. Kaeberlein, *Dietary restriction by bacterial deprivation increases life span in wild-derived nematodes.* Exp Gerontol, 2008. **43**(3): p. 130-5.
22. Klass, M.R., *Aging in the nematode Caenorhabditis elegans: Major biological and environmental factors influencing life span.* Mechanisms of Ageing and Development, 1977. **6**: p. 413-429.
23. Weindruch, R., et al., *The retardation of aging in mice by dietary restriction: longevity, cancer, immunity and lifetime energy intake.* J Nutr, 1986. **116**(4): p. 641-54.

24. Fernandes, G., E.J. Yunis, and R.A. Good, *Influence of diet on survival of mice.* Proc Natl Acad Sci U S A, 1976. **73**(4): p. 1279-83.
25. Goodrick, C.L., et al., *Effects of intermittent feeding upon growth, activity, and lifespan in rats allowed voluntary exercise.* Exp Aging Res, 1983. **9**(3): p. 203-9.
26. Colman, R.J., et al., *Caloric restriction delays disease onset and mortality in rhesus monkeys.* Science, 2009. **325**(5937): p. 201-4.
27. Colman, R.J., et al., *Caloric restriction reduces age-related and all-cause mortality in rhesus monkeys.* Nat Commun, 2014. **5**: p. 3557.
28. Mattison, J.A., et al., *Impact of caloric restriction on health and survival in rhesus monkeys from the NIA study.* Nature, 2012. **489**(7415): p. 318-21.
29. Mattison, J.A., et al., *Caloric restriction improves health and survival of rhesus monkeys.* Nature Communications, 2017. **8**(1): p. 14063.
30. Le Bourg, E., *Does Calorie Restriction in Primates Increase Lifespan? Revisiting Studies on Macaques (Macaca mulatta) and Mouse Lemurs (Microcebus murinus).* Bioessays, 2018. **40**(10): p. e1800111.
31. Hatle, J.D., et al., *Calorie restriction and late-onset calorie restriction extend lifespan but do not alter protein storage in female grasshoppers.* Mechanisms of ageing and development, 2006. **127**(12): p. 883-891.
32. Wang, C., et al., *Adult-onset, short-term dietary restriction reduces cell senescence in mice.* Aging (Albany NY), 2010. **2**(9): p. 555-66.
33. Wang, X., et al., *Intermittent food restriction initiated late in life prolongs lifespan and retards the onset of age-related markers in the annual fish Nothobranchius guentheri.* Biogerontology, 2017. **18**(3): p. 383-396.
34. Singh, R., et al., *Late-onset intermittent fasting dietary restriction as a potential intervention to retard age-associated brain function impairments in male rats.* Age (Dordrecht, Netherlands), 2012. **34**(4): p. 917-933.
35. Correia-Melo, C., et al., *Mitochondria are required for pro-ageing features of the senescent phenotype.* Embo j, 2016. **35**(7): p. 724-42.
36. Ibebunjo, C., et al., *Genomic and proteomic profiling reveals reduced mitochondrial function and disruption of the neuromuscular junction driving rat sarcopenia.* Molecular and cellular biology, 2013. **33**(2): p. 194-212.
37. Li, F., et al., *Increased plaque burden in brains of APP mutant MnSOD heterozygous knockout mice.* J Neurochem, 2004. **89**(5): p. 1308-12.
38. Most, J. and L.M. Redman, *Impact of calorie restriction on energy metabolism in humans.* Exp Gerontol, 2020. **133**: p. 110875.
39. Ning, Y.-C., et al., *Short-term calorie restriction protects against renal senescence of aged rats by increasing autophagic activity and reducing oxidative damage.* Mechanisms of Ageing and Development, 2013. **134**(11): p. 570-579.
40. Mura, C.V., et al., *Effects of calorie restriction and aging on the expression of antioxidant enzymes and ubiquitin in the liver of Emory mice.* Mech Ageing Dev, 1996. **91**(2): p. 115-29.
41. Ma, L., et al., *Effect of caloric restriction on the SIRT1/mTOR signaling pathways in senile mice.* Brain Research Bulletin, 2015. **116**: p. 67-72.
42. Yang, F., et al., *mTOR and autophagy in normal brain aging and caloric restriction ameliorating age-related cognition deficits.* Behavioural Brain Research, 2014. **264**: p. 82-90.
43. Kirkwood, T.B. and R. Holliday, *The evolution of ageing and longevity.* Proc R Soc Lond B Biol Sci, 1979. **205**(1161): p. 531-46.
44. Dogan, S., et al., *Effects of Intermittent and Chronic Calorie Restriction on Mammalian Target of Rapamycin (mTOR) and IGF-I Signaling Pathways in Mammary Fat Pad Tissues and Mammary Tumors.* Nutrition and Cancer, 2011. **63**(3): p. 389-401.
45. Chen, C.-N., et al., *Age-dependent effects of caloric restriction on mTOR and ubiquitin-proteasome pathways in skeletal muscles.* GeroScience, 2019. **41**(6): p. 871-880.
46. Kapahi, P., et al., *Regulation of lifespan in Drosophila by modulation of genes in the TOR signaling pathway.* Curr Biol, 2004. **14**(10): p. 885-90.

47. Hansen, M., et al., *Lifespan extension by conditions that inhibit translation in Caenorhabditis elegans.* 2007. **6**(1): p. 95-110.
48. Harrison, D.E., et al., *Rapamycin fed late in life extends lifespan in genetically heterogeneous mice.* Nature, 2009. **460**(7253): p. 392-5.
49. Bitto, A., et al., *Transient rapamycin treatment can increase lifespan and healthspan in middle-aged mice.* Elife, 2016. **5**.
50. Baselga, J., et al., *Everolimus in Postmenopausal Hormone-Receptor–Positive Advanced Breast Cancer.* 2011. **366**(6): p. 520-529.
51. Gupta, A., et al., *Cyclosporin A, tacrolimus and sirolimus are potent inhibitors of the human breast cancer resistance protein (ABCG2) and reverse resistance to mitoxantrone and topotecan.* Cancer Chemotherapy and Pharmacology, 2006. **58**(3): p. 374-383.
52. Walters, H.E. and L.S. Cox, *mTORC Inhibitors as Broad-Spectrum Therapeutics for Age-Related Diseases.* Int J Mol Sci, 2018. **19**(8).
53. Moroz, N., et al., *Dietary restriction involves NAD$^+$ -dependent mechanisms and a shift toward oxidative metabolism.* Aging Cell, 2014. **13**(6): p. 1075-85.
54. Diaz-Ruiz, A., et al., *Overexpression of CYB5R3 and NQO1, two NAD(+) -producing enzymes, mimics aspects of caloric restriction.* Aging Cell, 2018. **17**(4): p. e12767.
55. Rogina, B. and S.L. Helfand, *Sir2 mediates longevity in the fly through a pathway related to calorie restriction.* 2004. **101**(45): p. 15998-16003.
56. Boily, G., et al., *SirT1 regulates energy metabolism and response to caloric restriction in mice.* PLoS One, 2008. **3**(3): p. e1759.
57. Bordone, L., et al., *SIRT1 transgenic mice show phenotypes resembling calorie restriction.* Aging Cell, 2007. **6**(6): p. 759-67.
58. Kaeberlein, M., M. McVey, and L. Guarente, *The SIR2/3/4 complex and SIR2 alone promote longevity in Saccharomyces cerevisiae by two different mechanisms.* Genes Dev, 1999. **13**(19): p. 2570-80.
59. Whitaker, R., et al., *Increased expression of Drosophila Sir2 extends life span in a dose-dependent manner.* Aging (Albany NY), 2013. **5**(9): p. 682-91.
60. Satoh, A., et al., *Sirt1 extends life span and delays aging in mice through the regulation of Nk2 homeobox 1 in the DMH and LH.* Cell metabolism, 2013. **18**(3): p. 416-430.
61. Mitchell, S.J., et al., *The SIRT1 activator SRT1720 extends lifespan and improves health of mice fed a standard diet.* Cell Rep, 2014. **6**(5): p. 836-43.
62. Fischer, N., et al., *The resveratrol derivatives trans-3,5-dimethoxy-4-fluoro-4'-hydroxystilbene and trans-2,4',5-trihydroxystilbene decrease oxidative stress and prolong lifespan in Caenorhabditis elegans.* J Pharm Pharmacol, 2017. **69**(1): p. 73-81.
63. Valenzano, D.R., et al., *Resveratrol prolongs lifespan and retards the onset of age-related markers in a short-lived vertebrate.* Curr Biol, 2006. **16**(3): p. 296-300.
64. Kayashima, Y., et al., *Alkylresorcinols activate SIRT1 and delay ageing in Drosophila melanogaster.* Sci Rep, 2017. **7**: p. 43679.
65. Burnett, C., et al., *Absence of effects of Sir2 overexpression on lifespan in C. elegans and Drosophila.* Nature, 2011. **477**(7365): p. 482-485.
66. Mercken, E.M., et al., *SIRT1 but not its increased expression is essential for lifespan extension in caloric-restricted mice.* Aging Cell, 2014. **13**(1): p. 193-6.
67. Newman, B.L., et al., *A Drosophila homologue of Sir2 modifies position-effect variegation but does not affect life span.* Genetics, 2002. **162**(4): p. 1675-85.
68. Hwang, E.S. and S.B. Song, *Nicotinamide is an inhibitor of SIRT1 in vitro, but can be a stimulator in cells.* Cellular and Molecular Life Sciences, 2017. **74**(18): p. 3347-3362.
69. Braidy, N., et al., *Age related changes in NAD+ metabolism oxidative stress and Sirt1 activity in wistar rats.* PloS one, 2011. **6**(4): p. e19194-e19194.
70. Massudi, H., et al., *Age-associated changes in oxidative stress and NAD+ metabolism in human tissue.* PloS one, 2012. **7**(7): p. e42357-e42357.
71. Rodgers, J.T., et al., *Nutrient control of glucose homeostasis through a complex of PGC-1α and SIRT1.* Nature, 2005. **434**(7029): p. 113-118.

72. Hallows, W.C., W. Yu, and J.M. Denu, *Regulation of glycolytic enzyme phosphoglycerate mutase-1 by Sirt1 protein-mediated deacetylation.* The Journal of biological chemistry, 2012. **287**(6): p. 3850-3858.
73. Gerhart-Hines, Z., et al., *Metabolic control of muscle mitochondrial function and fatty acid oxidation through SIRT1/PGC-1α.* The EMBO Journal, 2007. **26**(7): p. 1913-1923.
74. Vaquero, A., et al., *Human SirT1 interacts with histone H1 and promotes formation of facultative heterochromatin.* Mol Cell, 2004. **16**(1): p. 93-105.
75. Vaquero, A., R. Sternglanz, and D. Reinberg, *NAD+-dependent deacetylation of H4 lysine 16 by class III HDACs.* Oncogene, 2007. **26**(37): p. 5505-20.
76. Imai, S., et al., *Transcriptional silencing and longevity protein Sir2 is an NAD-dependent histone deacetylase.* Nature, 2000. **403**(6771): p. 795-800.
77. Shi, L. and B.P. Tu, *Acetyl-CoA and the regulation of metabolism: mechanisms and consequences.* Current opinion in cell biology, 2015. **33**: p. 125-131.
78. Dani, D., et al., *Modulation of oxidative phosphorylation machinery signifies a prime mode of anti-ageing mechanism of calorie restriction in male rat liver mitochondria.* Biogerontology, 2009. **11**: p. 321-34.
79. Yu, J. and J. Auwerx, *Protein deacetylation by SIRT1: An emerging key post-translational modification in metabolic regulation.* Pharmacological Research, 2010. **62**(1): p. 35-41.
80. Brunet, A., et al., *Stress-Dependent Regulation of FOXO Transcription Factors by the SIRT1 Deacetylase.* 2004. **303**(5666): p. 2011-2015.
81. Yeung, F., et al., *Modulation of NF-κB-dependent transcription and cell survival by the SIRT1 deacetylase.* The EMBO Journal, 2004. **23**(12): p. 2369-2380.
82. Reinhardt, H.C. and B. Schumacher, *The p53 network: cellular and systemic DNA damage responses in aging and cancer.* Trends in Genetics, 2012. **28**(3): p. 128-136.
83. Soussi, T. and C. Beroud, *Assessing TP53 status in human tumours to evaluate clinical outcome.* Nat Rev Cancer, 2001. **1**(3): p. 233-40.
84. Haupt, Y., et al., *Mdm2 promotes the rapid degradation of p53.* Nature, 1997. **387**(6630): p. 296-299.
85. Fuchs, S.Y., et al., *Mdm2 association with p53 targets its ubiquitination.* Oncogene, 1998. **17**(19): p. 2543-2547.
86. Gu, W. and R.G. Roeder, *Activation of p53 Sequence-Specific DNA Binding by Acetylation of the p53 C-Terminal Domain.* Cell, 1997. **90**(4): p. 595-606.
87. Tang, Y., et al., *Tip60-Dependent Acetylation of p53 Modulates the Decision between Cell-Cycle Arrest and Apoptosis.* Molecular Cell, 2006. **24**(6): p. 827-839.
88. Liu, L., et al., *p53 Sites Acetylated In Vitro by PCAF and p300 Are Acetylated In Vivo in Response to DNA Damage.* 1999. **19**(2): p. 1202-1209.
89. Cantó, C., et al., *The NAD(+) precursor nicotinamide riboside enhances oxidative metabolism and protects against high-fat diet-induced obesity.* Cell metabolism, 2012. **15**(6): p. 838-847.
90. Vaziri, H., et al., *hSIR2SIRT1 Functions as an NAD-Dependent p53 Deacetylase.* Cell, 2001. **107**(2): p. 149-159.
91. Luo, J., et al., *Negative control of p53 by Sir2alpha promotes cell survival under stress.* Cell, 2001. **107**(2): p. 137-48.
92. Luo, J., et al., *Deacetylation of p53 modulates its effect on cell growth and apoptosis.* Nature, 2000. **408**(6810): p. 377-381.
93. Han, M.-K., et al., *SIRT1 regulates apoptosis and Nanog expression in mouse embryonic stem cells by controlling p53 subcellular localization.* Cell stem cell, 2008. **2**(3): p. 241-251.
94. Huffman, D.M., et al., *SIRT1 Is Significantly Elevated in Mouse and Human Prostate Cancer.* 2007. **67**(14): p. 6612-6618.
95. Ford, J., M. Jiang, and J. Milner, *Cancer-Specific Functions of SIRT1 Enable Human Epithelial Cancer Cell Growth and Survival.* 2005. **65**(22): p. 10457-10463.
96. Bradbury, C.A., et al., *Histone deacetylases in acute myeloid leukaemia show a distinctive pattern of expression that changes selectively in response to deacetylase inhibitors.* Leukemia, 2005. **19**(10): p. 1751-1759.

97. Hida, Y., et al., *Hida Y, Kubo Y, Murao K, Arase S.. Strong expression of a longevity-related protein, SIRT1, in Bowen's disease. Arch Dermatol Res 299: 103-106.* Archives of dermatological research, 2007. **299**: p. 103-6.
98. Kozako, T., et al., *Novel small-molecule SIRT1 inhibitors induce cell death in adult T-cell leukaemia cells.* Scientific Reports, 2015. **5**: p. 11345.
99. He, M., et al., *SIRT1 and AMPK pathways are essential for the proliferation and survival of primary effusion lymphoma cells.* 2017. **242**(3): p. 309-321.
100. Ota, H., et al., *Sirt1 inhibitor, Sirtinol, induces senescence-like growth arrest with attenuated Ras–MAPK signaling in human cancer cells.* Oncogene, 2006. **25**(2): p. 176-185.
101. Wang, R.-H., et al., *Impaired DNA Damage Response, Genome Instability, and Tumorigenesis in SIRT1 Mutant Mice.* Cancer Cell, 2008. **14**(4): p. 312-323.
102. Wang, R.-H., et al., *Interplay among BRCA1, SIRT1, and Survivin during BRCA1-associated tumorigenesis.* Molecular cell, 2008. **32**(1): p. 11-20.
103. Hu, A., et al., *Curcumin as therapeutics for the treatment of head and neck squamous cell carcinoma by activating SIRT1.* Scientific Reports, 2015. **5**: p. 13429.
104. Firestein, R., et al., *The SIRT1 deacetylase suppresses intestinal tumorigenesis and colon cancer growth.* PloS one, 2008. **3**(4): p. e2020-e2020.
105. Asher, G., et al., *SIRT1 regulates circadian clock gene expression through PER2 deacetylation.* Cell, 2008. **134**(2): p. 317-28.
106. Cheng, Y., et al., *Sirtuin 1 attenuates oxidative stress via upregulation of superoxide dismutase 2 and catalase in astrocytes.* Journal of Neuroimmunology, 2014. **269**(1): p. 38-43.
107. Ma, L., et al., *Long-term caloric restriction activates the myocardial SIRT1/AMPK/PGC-1α pathway in C57BL/6J male mice.* Food Nutr Res, 2020. **64**.
108. Hirschey, M.D., et al., *SIRT1 and SIRT3 deacetylate homologous substrates: AceCS1,2 and HMGCS1,2.* Aging (Albany NY), 2011. **3**(6): p. 635-42.
109. Zhou, Y., et al., *SIRT1 suppresses adipogenesis by activating Wnt/β-catenin signaling in vivo and in vitro.* Oncotarget, 2016. **7**(47): p. 77707-77720.
110. Chen, G.D., W.D. Yu, and X.P. Chen, *SirT1 activator represses the transcription of TNF-α in THP-1 cells of a sepsis model via deacetylation of H4K16.* Mol Med Rep, 2016. **14**(6): p. 5544-5550.
111. Solomon, J.M., et al., *Inhibition of SIRT1 Catalytic Activity Increases p53 Acetylation but Does Not Alter Cell Survival following DNA Damage.* 2006. **26**(1): p. 28-38.
112. Dryden, S.C., et al., *Role for Human SIRT2 NAD-Dependent Deacetylase Activity in Control of Mitotic Exit in the Cell Cycle.* 2003. **23**(9): p. 3173-3185.
113. Watanabe, H., et al., *Sirt2 facilitates hepatic glucose uptake by deacetylating glucokinase regulatory protein.* Nature Communications, 2018. **9**(1): p. 30.
114. Ahn, B.H., et al., *A role for the mitochondrial deacetylase Sirt3 in regulating energy homeostasis.* Proc Natl Acad Sci U S A, 2008. **105**(38): p. 14447-52.
115. Someya, S., et al., *Sirt3 mediates reduction of oxidative damage and prevention of age-related hearing loss under caloric restriction.* Cell, 2010. **143**(5): p. 802-12.
116. Shimazu, T., et al., *SIRT3 deacetylates mitochondrial 3-hydroxy-3-methylglutaryl CoA synthase 2 and regulates ketone body production.* Cell Metab, 2010. **12**(6): p. 654-61.
117. Anderson, K.A., et al., *SIRT4 Is a Lysine Deacylase that Controls Leucine Metabolism and Insulin Secretion.* Cell metabolism, 2017. **25**(4): p. 838-855.e15.
118. Mathias, Rommel A., et al., *Sirtuin 4 Is a Lipoamidase Regulating Pyruvate Dehydrogenase Complex Activity.* Cell, 2014. **159**(7): p. 1615-1625.
119. Jeong, Seung M., et al., *SIRT4 Has Tumor-Suppressive Activity and Regulates the Cellular Metabolic Response to DNA Damage by Inhibiting Mitochondrial Glutamine Metabolism.* Cancer Cell, 2013. **23**(4): p. 450-463.
120. Du, J., et al., *Sirt5 is a NAD-dependent protein lysine demalonylase and desuccinylase.* Science, 2011. **334**(6057): p. 806-9.

121. Nakamura, Y., et al., *SIRT5 deacetylates and activates urate oxidase in liver mitochondria of mice.* FEBS Lett, 2012. **586**(23): p. 4076-81.
122. Bhardwaj, A. and S. Das, *SIRT6 deacetylates PKM2 to suppress its nuclear localization and oncogenic functions.* Proc Natl Acad Sci U S A, 2016. **113**(5): p. E538-47.
123. Zhong, L., et al., *The histone deacetylase Sirt6 regulates glucose homeostasis via Hif1alpha.* Cell, 2010. **140**(2): p. 280-93.
124. Zhang, N., et al., *Calorie restriction-induced SIRT6 activation delays aging by suppressing NF-κB signaling.* Cell Cycle, 2016. **15**(7): p. 1009-18.
125. Michishita, E., et al., *SIRT6 is a histone H3 lysine 9 deacetylase that modulates telomeric chromatin.* Nature, 2008. **452**(7186): p. 492-496.
126. Barber, M.F., et al., *SIRT7 links H3K18 deacetylation to maintenance of oncogenic transformation.* Nature, 2012. **487**(7405): p. 114-118.
127. Wang, W.W., et al., *A Click Chemistry Approach Reveals the Chromatin-Dependent Histone H3K36 Deacylase Nature of SIRT7.* Journal of the American Chemical Society, 2019. **141**(6): p. 2462-2473.
128. Tsai, Y.C., T.M. Greco, and I.M. Cristea, *Sirtuin 7 plays a role in ribosome biogenesis and protein synthesis.* Mol Cell Proteomics, 2014. **13**(1): p. 73-83.
129. Berger, N.A., *Poly(ADP-ribose) in the cellular response to DNA damage.* Radiat Res, 1985. **101**(1): p. 4-15.
130. Altmeyer, M., et al., *Molecular mechanism of poly(ADP-ribosyl)ation by PARP1 and identification of lysine residues as ADP-ribose acceptor sites.* Nucleic Acids Research, 2009. **37**(11): p. 3723-3738.
131. Farmer, H., et al., *Targeting the DNA repair defect in BRCA mutant cells as a therapeutic strategy.* Nature, 2005. **434**(7035): p. 917-921.
132. Eustermann, S., et al., *The DNA-Binding Domain of Human PARP-1 Interacts with DNA Single-Strand Breaks as a Monomer through Its Second Zinc Finger.* Journal of Molecular Biology, 2011. **407**(1): p. 149-170.
133. Slade, D., et al., *The structure and catalytic mechanism of a poly(ADP-ribose) glycohydrolase.* Nature, 2011. **477**(7366): p. 616-620.
134. Singh, N.P., et al., *Basal DNA damage in individual human lymphocytes with age.* Mutation Research/DNAging, 1991. **256**(1): p. 1-6.
135. Mecocci, P., et al., *Age-dependent increases in oxidative damage to DNA, lipids, and proteins in human skeletal muscle.* Free Radic Biol Med, 1999. **26**(3-4): p. 303-8.
136. Abdul Sani, N.F., et al., *DNA damage and protein oxidation associated with ageing correlate with cognitive dysfunction in a Malaysian population.* Free Radic Res, 2018. **52**(9): p. 1000-1009.
137. Fernandez, J.E., et al., *Analysis of the distribution of human CD38 and of its ligand CD31 in normal tissues.* Journal of biological regulators and homeostatic agents, 1998. **12**: p. 81-91.
138. Sauve, A.A., et al., *The Reaction Mechanism for CD38. A Single Intermediate Is Responsible for Cyclization, Hydrolysis, and Base-Exchange Chemistries.* Biochemistry, 1998. **37**(38): p. 13239-13249.
139. Chini, E.N., *CD38 as a regulator of cellular NAD: a novel potential pharmacological target for metabolic conditions.* Curr Pharm Des, 2009. **15**(1): p. 57-63.
140. Camacho-Pereira, J., et al., *CD38 Dictates Age-Related NAD Decline and Mitochondrial Dysfunction through an SIRT3-Dependent Mechanism.* Cell Metabolism, 2016. **23**(6): p. 1127-1139.
141. Tarragó, M.G., et al., *A Potent and Specific CD38 Inhibitor Ameliorates Age-Related Metabolic Dysfunction by Reversing Tissue NAD(+) Decline.* Cell metabolism, 2018. **27**(5): p. 1081-1095.e10.
142. Preugschat, F., et al., *A pre-steady state and steady state kinetic analysis of the N-ribosyl hydrolase activity of hCD157.* Archives of Biochemistry and Biophysics, 2014. **564**: p. 156-163.

143. Sato, A., et al., *Inhibitor peptide SNP-1 binds to a soluble form of BST-1/CD157 at a 2 : 2 stoichiometry.* European Journal of Biochemistry, 1999. **264**(2): p. 439-445.
144. Lesnefsky, E.J. and C.L. Hoppel, *Oxidative phosphorylation and aging.* Ageing Research Reviews, 2006. **5**(4): p. 402-433.
145. Roh, E., et al., *Exogenous nicotinamide adenine dinucleotide regulates energy metabolism via hypothalamic connexin 43.* Metabolism: clinical and experimental, 2018. **88**: p. 51-60.
146. Ratajczak, J., et al., *NRK1 controls nicotinamide mononucleotide and nicotinamide riboside metabolism in mammalian cells.* Nature Communications, 2016. **7**(1): p. 13103.
147. Grozio, A., et al., *Slc12a8 is a nicotinamide mononucleotide transporter.* Nature Metabolism, 2019. **1**(1): p. 47-57.
148. Weitberg, A.B., *Effect of nicotinic acid supplementation in vivo on oxygen radical-induced genetic damage in human lymphocytes.* Mutation Research/Environmental Mutagenesis and Related Subjects, 1989. **216**(4): p. 197-201.
149. Hageman, G.J., et al., *Nicotinic acid supplementation: effects on niacin status, cytogenetic damage, and poly(ADP-ribosylation) in lymphocytes of smokers.* Nutr Cancer, 1998. **32**(2): p. 113-20.
150. Majamaa, K., et al., *Increase of blood NAD+ and attenuation of lactacidemia during nicotinamide treatment of a patient with the melas syndrome.* Life Sciences, 1996. **58**(8): p. 691-699.
151. Pirinen, E., et al., *Niacin Cures Systemic NAD+ Deficiency and Improves Muscle Performance in Adult-Onset Mitochondrial Myopathy.* Cell Metabolism, 2020. **31**(6): p. 1078-1090.e5.
152. Trammell, S.A.J., et al., *Nicotinamide riboside is uniquely and orally bioavailable in mice and humans.* Nature communications, 2016. **7**: p. 12948-12948.
153. de Picciotto, N.E., et al., *Nicotinamide mononucleotide supplementation reverses vascular dysfunction and oxidative stress with aging in mice.* Aging cell, 2016. **15**(3): p. 522-530.
154. Yang, Y., et al., *Dihydronicotinamide riboside is a potent NAD(+) concentration enhancer in vitro and in vivo.* J Biol Chem, 2019. **294**(23): p. 9295-9307.
155. van de Weijer, T., et al., *Evidence for a Direct Effect of the NAD⁺ Precursor Acipimox on Muscle Mitochondrial Function in Humans.* Diabetes, 2015. **64**(4): p. 1193.
156. Escande, C., et al., *Flavonoid apigenin is an inhibitor of the NAD+ ase CD38: implications for cellular NAD+ metabolism, protein acetylation, and treatment of metabolic syndrome.* Diabetes, 2013. **62**(4): p. 1084-93.
157. Wang, X., et al., *Nicotinamide mononucleotide protects against β-amyloid oligomer-induced cognitive impairment and neuronal death.* Brain Res, 2016. **1643**: p. 1-9.
158. Brown, K.D., et al., *Activation of SIRT3 by the NAD⁺ precursor nicotinamide riboside protects from noise-induced hearing loss.* Cell Metab, 2014. **20**(6): p. 1059-68.
159. Hou, Y., et al., *NAD(+) supplementation normalizes key Alzheimer's features and DNA damage responses in a new AD mouse model with introduced DNA repair deficiency.* Proc Natl Acad Sci U S A, 2018. **115**(8): p. E1876-e1885.
160. De Jesús-Cortés, H., et al., *Neuroprotective efficacy of aminopropyl carbazoles in a mouse model of Parkinson disease.* Proc Natl Acad Sci U S A, 2012. **109**(42): p. 17010-5.
161. Jia, H., et al., *High doses of nicotinamide prevent oxidative mitochondrial dysfunction in a cellular model and improve motor deficit in a Drosophila model of Parkinson's disease.* Journal of Neuroscience Research, 2008. **86**(9): p. 2083-2090.
162. Yao, Z., et al., *Nicotinamide mononucleotide inhibits JNK activation to reverse Alzheimer disease.* Neurosci Lett, 2017. **647**: p. 133-140.
163. Conforti, L., et al., *Wld S protein requires Nmnat activity and a short N-terminal sequence to protect axons in mice.* The Journal of cell biology, 2009. **184**(4): p. 491-500.
164. Araki, T., Y. Sasaki, and J. Milbrandt, *Increased nuclear NAD biosynthesis and SIRT1 activation prevent axonal degeneration.* Science, 2004. **305**(5686): p. 1010-3.

165. Sasaki, Y., T. Araki, and J. Milbrandt, *Stimulation of nicotinamide adenine dinucleotide biosynthetic pathways delays axonal degeneration after axotomy.* J Neurosci, 2006. **26**(33): p. 8484-91.
166. Green, K.N., et al., *Nicotinamide Restores Cognition in Alzheimer's Disease Transgenic Mice via a Mechanism Involving Sirtuin Inhibition and Selective Reduction of Thr231-Phosphotau.* The Journal of Neuroscience, 2008. **28**(45): p. 11500.
167. Vakilinezhad, M.A., et al., *Nicotinamide loaded functionalized solid lipid nanoparticles improves cognition in Alzheimer's disease animal model by reducing Tau hyperphosphorylation.* Daru : journal of Faculty of Pharmacy, Tehran University of Medical Sciences, 2018. **26**(2): p. 165-177.
168. Ghosh, D., K.R. LeVault, and G.J. Brewer, *Dual-energy precursor and nuclear erythroid-related factor 2 activator treatment additively improve redox glutathione levels and neuron survival in aging and Alzheimer mouse neurons upstream of reactive oxygen species.* Neurobiology of aging, 2014. **35**(1): p. 179-190.
169. Long, A.N., et al., *Effect of nicotinamide mononucleotide on brain mitochondrial respiratory deficits in an Alzheimer's disease-relevant murine model.* BMC neurology, 2015. **15**: p. 19-19.
170. Gong, B., et al., *Nicotinamide riboside restores cognition through an upregulation of proliferator-activated receptor-γ coactivator 1α regulated β-secretase 1 degradation and mitochondrial gene expression in Alzheimer's mouse models.* Neurobiology of Aging, 2013. **34**(6): p. 1581-1588.
171. Lee, C.F., et al., *Targeting NAD+ Metabolism as Interventions for Mitochondrial Disease.* Scientific Reports, 2019. **9**(1): p. 3073.
172. Cerutti, R., et al., *NAD(+)-dependent activation of Sirt1 corrects the phenotype in a mouse model of mitochondrial disease.* Cell metabolism, 2014. **19**(6): p. 1042-1049.
173. Khan, N.A., et al., *Effective treatment of mitochondrial myopathy by nicotinamide riboside, a vitamin B3.* EMBO Mol Med, 2014. **6**(6): p. 721-31.
174. Sambeat, A., et al., *Endogenous nicotinamide riboside metabolism protects against diet-induced liver damage.* Nat Commun, 2019. **10**(1): p. 4291.
175. Pham, T.X., et al., *Nicotinamide riboside, an NAD+ precursor, attenuates the development of liver fibrosis in a diet-induced mouse model of liver fibrosis.* Biochimica et biophysica acta. Molecular basis of disease, 2019. **1865**(9): p. 2451-2463.
176. Wang, S., et al., *Nicotinamide riboside attenuates alcohol induced liver injuries via activation of SirT1/PGC-1α/mitochondrial biosynthesis pathway.* Redox biology, 2018. **17**: p. 89-98.
177. Han, X., et al., *Nicotinamide riboside exerts protective effect against aging-induced NAFLD-like hepatic dysfunction in mice.* PeerJ, 2019. **7**: p. e7568-e7568.
178. Balan, V., et al., *Life span extension and neuronal cell protection by Drosophila nicotinamidase.* J Biol Chem, 2008. **283**(41): p. 27810-9.
179. Mouchiroud, L., et al., *The NAD+/Sirtuin Pathway Modulates Longevity through Activation of Mitochondrial UPR and FOXO Signaling.* Cell, 2013. **154**(2): p. 430-441.
180. Zhang, H., et al., *NAD⁺ repletion improves mitochondrial and stem cell function and enhances life span in mice.* Science, 2016. **352**(6292): p. 1436-43.
181. Gomes, Ana P., et al., *Declining NAD+ Induces a Pseudohypoxic State Disrupting Nuclear-Mitochondrial Communication during Aging.* Cell, 2013. **155**(7): p. 1624-1638.
182. Mills, K.F., et al., *Long-Term Administration of Nicotinamide Mononucleotide Mitigates Age-Associated Physiological Decline in Mice.* Cell Metab, 2016. **24**(6): p. 795-806.
183. Das, A., et al., *Impairment of an Endothelial NAD(+)-H(2)S Signaling Network Is a Reversible Cause of Vascular Aging.* Cell, 2018. **173**(1): p. 74-89.e20.
184. Shiloh, Y. and H.M. Lederman, *Ataxia-telangiectasia (A-T): An emerging dimension of premature ageing.* Ageing Res Rev, 2017. **33**: p. 76-88.
185. Lautrup, S., et al., *Studying Werner syndrome to elucidate mechanisms and therapeutics of human aging and age-related diseases.* Biogerontology, 2019. **20**(3): p. 255-269.

186. Fang, E.F., et al., *NAD+ augmentation restores mitophagy and limits accelerated aging in Werner syndrome.* Nature Communications, 2019. **10**(1): p. 5284.
187. Fang, E.F., et al., *NAD(+) Replenishment Improves Lifespan and Healthspan in Ataxia Telangiectasia Models via Mitophagy and DNA Repair.* Cell metabolism, 2016. **24**(4): p. 566-581.
188. Taylor, A.M., *Ataxia telangiectasia genes and predisposition to leukaemia, lymphoma and breast cancer.* Br J Cancer, 1992. **66**(1): p. 5-9.
189. Ke, H.-L., et al., *High visfatin expression predicts poor prognosis of upper tract urothelial carcinoma patients.* American journal of cancer research, 2015. **5**(8): p. 2447-2454.
190. Maldi, E., et al., *Nicotinamide phosphoribosyltransferase (NAMPT) is over-expressed in melanoma lesions.* 2013. **26**(1): p. 144-146.
191. Zhou, T., T. Wang, and J.G.N. Garcia, *Expression of nicotinamide phosphoribosyltransferase-influenced genes predicts recurrence-free survival in lung and breast cancers.* Scientific reports, 2014. **4**: p. 6107-6107.
192. Sawicka-Gutaj, N., et al., *Nicotinamide phosphorybosiltransferase overexpression in thyroid malignancies and its correlation with tumor stage and with survivin/survivin DEx3 expression.* Tumour biology : the journal of the International Society for Oncodevelopmental Biology and Medicine, 2015. **36**(10): p. 7859-7863.
193. Nahimana, A., et al., *The NAD biosynthesis inhibitor APO866 has potent antitumor activity against hematologic malignancies.* Blood, 2009. **113**(14): p. 3276-86.
194. Zhang, L.-Y., et al., *Anti-proliferation effect of APO866 on C6 glioblastoma cells by inhibiting nicotinamide phosphoribosyltransferase.* European Journal of Pharmacology, 2012. **674**(2): p. 163-170.
195. Olesen, U.H., et al., *A Preclinical Study on the Rescue of Normal Tissue by Nicotinic Acid in High-Dose Treatment with APO866, a Specific Nicotinamide Phosphoribosyltransferase Inhibitor.* 2010. **9**(6): p. 1609-1617.
196. Zerp, S.F., et al., *NAD+ depletion by APO866 in combination with radiation in a prostate cancer model, results from an in vitro and in vivo study.* Radiotherapy and Oncology, 2014. **110**(2): p. 348-354.
197. Goldinger, S.M., et al., *Efficacy and Safety of APO866 in Patients With Refractory or Relapsed Cutaneous T-Cell Lymphoma: A Phase 2 Clinical Trial.* JAMA Dermatology, 2016. **152**(7): p. 837-839.
198. Gehrke, I., et al., *On-Target Effect of FK866, a Nicotinamide Phosphoribosyl Transferase Inhibitor, by Apoptosis-Mediated Death in Chronic Lymphocytic Leukemia Cells.* 2014. **20**(18): p. 4861-4872.
199. Sharif, T., et al., *The NAD(+) salvage pathway modulates cancer cell viability via p73.* Cell death and differentiation, 2016. **23**(4): p. 669-680.
200. Moore, Z., et al., *NAMPT inhibition sensitizes pancreatic adenocarcinoma cells to tumor-selective, PAR-independent metabolic catastrophe and cell death induced by β-lapachone.* Cell death & disease, 2015. **6**(1): p. e1599-e1599.
201. Son, M.J., et al., *Upregulation of mitochondrial NAD(+) levels impairs the clonogenicity of SSEA1(+) glioblastoma tumor-initiating cells.* Experimental & molecular medicine, 2017. **49**(6): p. e344-e344.
202. Nacarelli, T., et al., *NAD+ metabolism governs the proinflammatory senescence-associated secretome.* Nature Cell Biology, 2019. **21**(3): p. 397-407.
203. Villalobos, L.A., et al., *Visfatin/Nampt induces telomere damage and senescence in human endothelial cells.* Int J Cardiol, 2014. **175**(3): p. 573-5.
204. Ma, C., et al., *Nampt Expression Decreases Age-Related Senescence in Rat Bone Marrow Mesenchymal Stem Cells by Targeting Sirt1.* PLoS One, 2017. **12**(1): p. e0170930.
205. Pi, C., et al., *Nicotinamide phosphoribosyltransferase postpones rat bone marrow mesenchymal stem cell senescence by mediating NAD(+)-Sirt1 signaling.* Aging (Albany NY), 2019. **11**(11): p. 3505-3522.

206. van der Veer, E., et al., *Extension of human cell lifespan by nicotinamide phosphoribosyltransferase.* J Biol Chem, 2007. **282**(15): p. 10841-5.
207. Kourtzidis, I.A., et al., *The NAD(+) precursor nicotinamide riboside decreases exercise performance in rats.* J Int Soc Sports Nutr, 2016. **13**: p. 32.
208. Kourtzidis, I.A., et al., *Nicotinamide riboside supplementation dysregulates redox and energy metabolism in rats: Implications for exercise performance.* Exp Physiol, 2018. **103**(10): p. 1357-1366.
209. Selmaoui, B. and Y. Touitou, *Reproducibility of the circadian rhythms of serum cortisol and melatonin in healthy subjects: a study of three different 24-h cycles over six weeks.* Life Sciences, 2003. **73**(26): p. 3339-3349.
210. Kalsbeek, A., et al., *SCN Outputs and the Hypothalamic Balance of Life.* Journal of Biological Rhythms, 2006. **21**(6): p. 458-469.
211. Hamada, T., et al., *Expression of Period genes: rhythmic and nonrhythmic compartments of the suprachiasmatic nucleus pacemaker.* J Neurosci, 2001. **21**(19): p. 7742-50.
212. Horst, G.T.J.v.d., et al., *Mammalian Cry1 and Cry2 are essential for maintenance of circadian rhythms.* Nature, 1999. **398**(6728): p. 627-630.
213. Bugge, A., et al., *Rev-erbα and Rev-erbβ coordinately protect the circadian clock and normal metabolic function.* Genes Dev, 2012. **26**(7): p. 657-67.
214. Kondratov, R.V., et al., *Dual role of the CLOCK/BMAL1 circadian complex in transcriptional regulation.* 2006. **20**(3): p. 530-532.
215. Gekakis, N., et al., *Role of the CLOCK Protein in the Mammalian Circadian Mechanism.* 1998. **280**(5369): p. 1564-1569.
216. Yu, W., M. Nomura, and M. Ikeda, *Interactivating Feedback Loops within the Mammalian Clock: BMAL1 Is Negatively Autoregulated and Upregulated by CRY1, CRY2, and PER2.* Biochemical and Biophysical Research Communications, 2002. **290**(3): p. 933-941.
217. Duffy, J.F. and C.A. Czeisler, *Age-related change in the relationship between circadian period, circadian phase, and diurnal preference in humans.* Neuroscience Letters, 2002. **318**(3): p. 117-120.
218. Carrier, J., et al., *Sleep and morningness-eveningness in the 'middle' years of life (20-59 y).* J Sleep Res, 1997. **6**(4): p. 230-7.
219. Gubin, D.G., et al., *The Circadian Body Temperature Rhythm in the Elderly: Effect of Single Daily Melatonin Dosing.* Chronobiology International, 2006. **23**(3): p. 639-658.
220. Vitiello, M.V., et al., *Circadian temperature rhythms in young adult and aged men.* Neurobiology of Aging, 1986. **7**(2): p. 97-100.
221. Knight, M. and M. Mather, *Look out-it's your off-peak time of day! Time of day matters more for alerting than for orienting or executive attention.* Exp Aging Res, 2013. **39**(3): p. 305-21.
222. May, C.P., L. Hasher, and E.R. Stoltzfus, *Optimal Time of Day and the Magnitude of Age Differences in Memory.* Psychological Science, 1993. **4**(5): p. 326-330.
223. May, C.P., L. Hasher, and N. Foong, *Implicit memory, age, and time of day: paradoxical priming effects.* Psychol Sci, 2005. **16**(2): p. 96-100.
224. Van Cauter, E., R. Leproult, and D.J. Kupfer, *Effects of gender and age on the levels and circadian rhythmicity of plasma cortisol.* The Journal of Clinical Endocrinology & Metabolism, 1996. **81**(7): p. 2468-2473.
225. SHERMAN, B., W. WYSHAM, and B. PFOH, *Age-Related Changes in the Circadian Rhythm of Plasma Cortisol in Man*.* The Journal of Clinical Endocrinology & Metabolism, 1985. **61**(3): p. 439-443.
226. Kondratov, R.V., et al., *Early aging and age-related pathologies in mice deficient in BMAL1, the core componentof the circadian clock.* Genes Dev, 2006. **20**(14): p. 1868-73.
227. Antoch, M.P., et al., *Disruption of the circadian clock due to the Clock mutation has discrete effects on aging and carcinogenesis.* Cell Cycle, 2008. **7**(9): p. 1197-1204.
228. Pilorz, V. and S. Steinlechner, *Low reproductive success in Per1 and Per2 mutant mouse females due to accelerated ageing? %J REPRODUCTION.* 2008. **135**(4): p. 559.

229. Schernhammer, E.S., et al., *Night-Shift Work and Risk of Colorectal Cancer in the Nurses' Health Study.* JNCI: Journal of the National Cancer Institute, 2003. **95**(11): p. 825-828.
230. Conlon, M., N. Lightfoot, and N. Kreiger, *Rotating Shift Work and Risk of Prostate Cancer.* Epidemiology, 2007. **18**(1).
231. Viswanathan, A.N., S.E. Hankinson, and E.S. Schernhammer, *Night Shift Work and the Risk of Endometrial Cancer.* 2007. **67**(21): p. 10618-10622.
232. Bøggild, H. and A. Knutsson, *Shift work, risk factors and cardiovascular disease.* Scand J Work Environ Health, 1999. **25**(2): p. 85-99.
233. Nakahata, Y., et al., *Circadian control of the NAD+ salvage pathway by CLOCK-SIRT1.* Science (New York, N.Y.), 2009. **324**(5927): p. 654-657.
234. Ramsey, K.M., et al., *Circadian clock feedback cycle through NAMPT-mediated NAD+ biosynthesis.* Science (New York, N.Y.), 2009. **324**(5927): p. 651-654.
235. Ando, H., et al., *Influence of Age on Clock Gene Expression in Peripheral Blood Cells of Healthy Women.* The Journals of Gerontology: Series A, 2009. **65A**(1): p. 9-13.
236. Hofman, M.A. and D.F. Swaab, *Living by the clock: the circadian pacemaker in older people.* Ageing Res Rev, 2006. **5**(1): p. 33-51.
237. Emamgholipour, S., et al., *Evidence for possible role of melatonin in reducing oxidative stress in multiple sclerosis through its effect on SIRT1 and antioxidant enzymes.* Life Sciences, 2016. **145**: p. 34-41.
238. Gutierrez-Cuesta, J., et al., *Evaluation of potential pro-survival pathways regulated by melatonin in a murine senescence model.* J Pineal Res, 2008. **45**(4): p. 497-505.
239. Gregory, R.I., et al., *Human RISC couples microRNA biogenesis and posttranscriptional gene silencing.* Cell, 2005. **123**(4): p. 631-40.
240. Kluiver, J., et al., *BIC and miR-155 are highly expressed in Hodgkin, primary mediastinal and diffuse large B cell lymphomas.* J Pathol, 2005. **207**(2): p. 243-9.
241. Yanaihara, N., et al., *Unique microRNA molecular profiles in lung cancer diagnosis and prognosis.* Cancer Cell, 2006. **9**(3): p. 189-98.
242. Kong, W., et al., *Upregulation of miRNA-155 promotes tumour angiogenesis by targeting VHL and is associated with poor prognosis and triple-negative breast cancer.* Oncogene, 2014. **33**(6): p. 679-89.
243. Higgs, G. and F. Slack, *The multiple roles of microRNA-155 in oncogenesis.* Journal of Clinical Bioinformatics, 2013. **3**(1): p. 17.
244. Szűcs, D., et al., *Increased duodenal expression of miR-146a and -155 in pediatric Crohn's disease.* World journal of gastroenterology, 2016. **22**(26): p. 6027-6035.
245. Kurowska-Stolarska, M., et al., *MicroRNA-155 as a proinflammatory regulator in clinical and experimental arthritis.* Proc Natl Acad Sci U S A, 2011. **108**(27): p. 11193-8.
246. Mycko, M.P., et al., *miR-155-3p Drives the Development of Autoimmune Demyelination by Regulation of Heat Shock Protein 40.* J Neurosci, 2015. **35**(50): p. 16504-15.
247. O'Connell, R.M., et al., *MicroRNA-155 promotes autoimmune inflammation by enhancing inflammatory T cell development.* Immunity, 2010. **33**(4): p. 607-619.
248. Curtis, A.M., et al., *Circadian control of innate immunity in macrophages by miR-155 targeting Bmal1.* Proceedings of the National Academy of Sciences of the United States of America, 2015. **112**(23): p. 7231-7236.
249. Schlessinger, D. and G. Van Zant, *Does functional depletion of stem cells drive aging?* Mechanisms of Ageing and Development, 2001. **122**(14): p. 1537-1553.
250. Ovadya, Y. and V. Krizhanovsky, *Senescent cells: SASPected drivers of age-related pathologies.* Biogerontology, 2014. **15**(6): p. 627-642.
251. Rea, I.M., et al., *Age and Age-Related Diseases: Role of Inflammation Triggers and Cytokines.* 2018. **9**(586).
252. Neumann, T., et al., *Heart failure: the commonest reason for hospital admission in Germany: medical and economic perspectives.* Dtsch Arztebl Int, 2009. **106**(16): p. 269-75.
253. Fang, J., et al., *Heart Failure-Related Hospitalization in the U.S., 1979 to 2004.* 2008. **52**(6): p. 428-434.

254. Cowie, M.R., *The heart failure epidemic: a UK perspective %J Echo Research and Practice.* 2017. **4**(1): p. R15.
255. Alder, J.K., et al., *Short telomeres are a risk factor for idiopathic pulmonary fibrosis.* 2008. **105**(35): p. 13051-13056.
256. Selman, M., C. López-Otín, and A. Pardo, *Age-driven developmental drift in the pathogenesis of idiopathic pulmonary fibrosis.* 2016. **48**(2): p. 538-552.
257. Humphreys, B.D., *Mechanisms of Renal Fibrosis.* 2018. **80**(1): p. 309-326.
258. Poynard, T., et al., *Prevalence of liver fibrosis and risk factors in a general population using non-invasive biomarkers (FibroTest).* BMC Gastroenterol, 2010. **10**: p. 40.
259. Lafyatis, R., *Transforming growth factor β--at the centre of systemic sclerosis.* Nat Rev Rheumatol, 2014. **10**(12): p. 706-19.
260. Varga, J. and M.L. Whitfield, *Transforming growth factor-beta in systemic sclerosis (scleroderma).* Front Biosci (Schol Ed), 2009. **1**: p. 226-35.
261. Henderson, J., J. Distler, and S. O'Reilly, *The Role of Epigenetic Modifications in Systemic Sclerosis: A Druggable Target.* Trends Mol Med, 2019. **25**(5): p. 395-411.
262. Wilkes, M.C., et al., *Transforming Growth Factor-β Activation of Phosphatidylinositol 3-Kinase Is Independent of Smad2 and Smad3 and Regulates Fibroblast Responses via p21-Activated Kinase-2.* 2005. **65**(22): p. 10431-10440.
263. Ard, S., et al., *Sustained Smad2 Phosphorylation Is Required for Myofibroblast Transformation in Response to TGF-β.* 2019. **60**(3): p. 367-369.
264. Itoh, S., et al., *Signaling of transforming growth factor-beta family members through Smad proteins.* Eur J Biochem, 2000. **267**(24): p. 6954-67.
265. He, W. and C. Dai, *Key Fibrogenic Signaling.* Curr Pathobiol Rep, 2015. **3**(2): p. 183-192.
266. Meng, X.M., D.J. Nikolic-Paterson, and H.Y. Lan, *TGF-β: the master regulator of fibrosis.* Nat Rev Nephrol, 2016. **12**(6): p. 325-38.
267. Huang, N. and A. Perl, *Metabolism as a Target for Modulation in Autoimmune Diseases.* Trends Immunol, 2018. **39**(7): p. 562-576.
268. Vander Heiden, M.G. and R.J. DeBerardinis, *Understanding the Intersections between Metabolism and Cancer Biology.* Cell, 2017. **168**(4): p. 657-669.
269. Mobasheri, A., et al., *The role of metabolism in the pathogenesis of osteoarthritis.* Nat Rev Rheumatol, 2017. **13**(5): p. 302-311.
270. Bierhansl, L., et al., *Central Role of Metabolism in Endothelial Cell Function and Vascular Disease.* Physiology (Bethesda), 2017. **32**(2): p. 126-140.
271. Patel, K.P., et al., *The spectrum of pyruvate dehydrogenase complex deficiency: Clinical, biochemical and genetic features in 371 patients.* Molecular Genetics and Metabolism, 2012. **105**(1): p. 34-43.
272. Bricker, D.K., et al., *A mitochondrial pyruvate carrier required for pyruvate uptake in yeast, Drosophila, and humans.* Science, 2012. **337**(6090): p. 96-100.
273. Ostergaard, E., et al., *Novel Mutations in the PC Gene in Patients with Type B Pyruvate Carboxylase Deficiency.* JIMD reports, 2013. **9**: p. 1-5.
274. Saneto, R.P., *Genetics of Mitochondrial Disease.* Adv Genet, 2017. **98**: p. 63-116.
275. Warburg, O., F. Wind, and E. Negelein, *THE METABOLISM OF TUMORS IN THE BODY.* J Gen Physiol, 1927. **8**(6): p. 519-30.
276. Yu, L., et al., *Modeling the Genetic Regulation of Cancer Metabolism: Interplay between Glycolysis and Oxidative Phosphorylation.* Cancer Res, 2017. **77**(7): p. 1564-1574.
277. Yang, L., S. Venneti, and D. Nagrath, *Glutaminolysis: A Hallmark of Cancer Metabolism.* Annual Review of Biomedical Engineering, 2017. **19**(1): p. 163-194.
278. Carr, E.L., et al., *Glutamine Uptake and Metabolism Are Coordinately Regulated by ERK/MAPK during T Lymphocyte Activation.* The Journal of Immunology, 2010. **185**(2): p. 1037.
279. Nakaya, M., et al., *Inflammatory T Cell Responses Rely on Amino Acid Transporter ASCT2 Facilitation of Glutamine Uptake and mTORC1 Kinase Activation.* Immunity, 2014. **40**(5): p. 692-705.

280. Duran, R.V., et al., *Glutaminolysis activates Rag-mTORC1 signaling.* Mol Cell, 2012. **47**(3): p. 349-58.
281. Kim, J. and K.L. Guan, *mTOR as a central hub of nutrient signalling and cell growth.* Nat Cell Biol, 2019. **21**(1): p. 63-71.
282. Cheng, S.C., et al., *mTOR- and HIF-1α-mediated aerobic glycolysis as metabolic basis for trained immunity.* Science, 2014. **345**(6204): p. 1250684.
283. Wang, L. and R. Wang, *Effect of rapamycin (RAPA) on the growth of lung cancer and its mechanism in mice with A549.* Int J Clin Exp Pathol, 2015. **8**(8): p. 9208-13.
284. Yu, G., et al., *Metformin potentiates rapamycin and cisplatin in gastric cancer in mice.* Oncotarget, 2015. **6**(14): p. 12748-62.
285. Weber, H., et al., *Rapamycin and WYE-354 suppress human gallbladder cancer xenografts in mice.* Oncotarget, 2015. **6**(31): p. 31877-88.
286. Tai, W., et al., *Rapamycin attenuates the paraquat-induced pulmonary fibrosis through activating Nrf2 pathway.* Journal of Cellular Physiology, 2020. **235**(2): p. 1759-1768.
287. Liu, J., et al., *Rapamycin inhibits peritoneal fibrosis by modifying lipid homeostasis in the peritoneum.* American journal of translational research, 2019. **11**(3): p. 1473-1485.
288. Wang, W., et al., *Rapamycin ameliorates inflammation and fibrosis in the early phase of cirrhotic portal hypertension in rats through inhibition of mTORC1 but not mTORC2.* PloS one, 2014. **9**(1): p. e83908-e83908.
289. Yoshizaki, A., et al., *Treatment with rapamycin prevents fibrosis in tight-skin and bleomycin-induced mouse models of systemic sclerosis.* Arthritis Rheum, 2010. **62**(8): p. 2476-87.
290. Miquel, J., et al., *Mitochondrial role in cell aging.* Experimental Gerontology, 1980. **15**(6): p. 575-591.
291. Pérez, V.I., et al., *The overexpression of major antioxidant enzymes does not extend the lifespan of mice.* 2009. **8**(1): p. 73-75.
292. Remmen, H.V., et al., *Life-long reduction in MnSOD activity results in increased DNA damage and higher incidence of cancer but does not accelerate aging.* 2003. **16**(1): p. 29-37.
293. Wiley, Christopher D., et al., *Mitochondrial Dysfunction Induces Senescence with a Distinct Secretory Phenotype.* Cell Metabolism, 2016. **23**(2): p. 303-314.
294. Passos, J.F., et al., *Feedback between p21 and reactive oxygen production is necessary for cell senescence.* 2010. **6**(1): p. 347.
295. Ishikawa, H., Z. Ma, and G.N. Barber, *STING regulates intracellular DNA-mediated, type I interferon-dependent innate immunity.* Nature, 2009. **461**(7265): p. 788-792.
296. Zhou, R., et al., *A role for mitochondria in NLRP3 inflammasome activation.* Nature, 2011. **469**(7329): p. 221-225.
297. West, A.P., et al., *Mitochondrial DNA stress primes the antiviral innate immune response.* Nature, 2015. **520**(7548): p. 553-557.
298. Vizioli, M.G., et al., *Mitochondria-to-nucleus retrograde signaling drives formation of cytoplasmic chromatin and inflammation in senescence.* Genes Dev, 2020. **34**(5-6): p. 428-445.
299. Livak, K.J. and T.D. Schmittgen, *Analysis of Relative Gene Expression Data Using Real-Time Quantitative PCR and the 2−ΔΔCT Method.* Methods, 2001. **25**(4): p. 402-408.
300. Alcendor Ralph, R., et al., *Sirt1 Regulates Aging and Resistance to Oxidative Stress in the Heart.* Circulation Research, 2007. **100**(10): p. 1512-1521.
301. Wang, Y., et al., *Upregulation of SIRT1 by Kartogenin Enhances Antioxidant Functions and Promotes Osteogenesis in Human Mesenchymal Stem Cells.* Oxid Med Cell Longev, 2018. **2018**: p. 1368142.
302. Santini, S.J., et al., *SIRT1-Dependent Upregulation of Antiglycative Defense in HUVECs Is Essential for Resveratrol Protection against High Glucose Stress.* Antioxidants (Basel), 2019. **8**(9).
303. Gurd, B.J., et al., *Nuclear SIRT1 activity, but not protein content, regulates mitochondrial biogenesis in rat and human skeletal muscle.* American Journal of Physiology-Regulatory, Integrative and Comparative Physiology, 2011. **301**(1): p. R67-R75.

304. Li, Y.-g., et al., *Resveratrol protects cardiomyocytes from oxidative stress through SIRT1 and mitochondrial biogenesis signaling pathways.* Biochemical and Biophysical Research Communications, 2013. **438**(2): p. 270-276.
305. Gomes, A.P., et al., *Berberine protects against high fat diet-induced dysfunction in muscle mitochondria by inducing SIRT1-dependent mitochondrial biogenesis.* Biochimica et Biophysica Acta (BBA) - Molecular Basis of Disease, 2012. **1822**(2): p. 185-195.
306. Gillum, M.P., et al., *SirT1 Regulates Adipose Tissue Inflammation.* Diabetes, 2011. **60**(12): p. 3235.
307. Kauppinen, A., et al., *Antagonistic crosstalk between NF-κB and SIRT1 in the regulation of inflammation and metabolic disorders.* Cellular Signalling, 2013. **25**(10): p. 1939-1948.
308. Yoshizaki, T., et al., *SIRT1 inhibits inflammatory pathways in macrophages and modulates insulin sensitivity.* American Journal of Physiology-Endocrinology and Metabolism, 2009. **298**(3): p. E419-E428.
309. Ali, A.A.E., et al., *The zinc-finger domains of PARP1 cooperate to recognize DNA strand breaks.* Nat Struct Mol Biol, 2012. **19**(7): p. 685-692.
310. Elhassan, Y.S., et al., *Nicotinamide Riboside Augments the Aged Human Skeletal Muscle NAD(+) Metabolome and Induces Transcriptomic and Anti-inflammatory Signatures.* Cell reports, 2019. **28**(7): p. 1717-1728.e6.
311. Airhart, S.E., et al., *An open-label, non-randomized study of the pharmacokinetics of the nutritional supplement nicotinamide riboside (NR) and its effects on blood NAD+ levels in healthy volunteers.* PloS one, 2017. **12**(12): p. e0186459-e0186459.
312. Motulsky, H.J. and R.E. Brown, *Detecting outliers when fitting data with nonlinear regression – a new method based on robust nonlinear regression and the false discovery rate.* BMC Bioinformatics, 2006. **7**(1): p. 123.
313. Liu, G.-S., et al., *Resveratrol attenuates oxidative damage and ameliorates cognitive impairment in the brain of senescence-accelerated mice.* Life Sciences, 2012. **91**(17): p. 872-877.
314. Porquet, D., et al., *Dietary resveratrol prevents Alzheimer's markers and increases life span in SAMP8.* Age (Dordr), 2013. **35**(5): p. 1851-65.
315. Grant, R., *Resveratrol Increases Intracellular NAD+ Levels Through Up regulation of The NAD+ Synthetic Enzyme Nicotinamide Mononucleotide Adenylyltransferase.* Nature Precedings, 2010.
316. Kao, C.L., et al., *Resveratrol protects human endothelium from H(2)O(2)-induced oxidative stress and senescence via SirT1 activation.* J Atheroscler Thromb, 2010. **17**(9): p. 970-9.
317. Hou, X., et al., *Resveratrol serves as a protein-substrate interaction stabilizer in human SIRT1 activation.* Scientific Reports, 2016. **6**(1): p. 38186.
318. Polzonetti, V., et al., *Population variability in CD38 activity: Correlation with age and significant effect of TNF-α -308G>A and CD38 184C>G SNPs.* Molecular Genetics and Metabolism, 2012. **105**(3): p. 502-507.
319. Choi, S., et al., *Apigenin inhibits UVA-induced cytotoxicity in vitro and prevents signs of skin aging in vivo.* Int J Mol Med, 2016. **38**(2): p. 627-34.
320. Yoon, J.S., et al., *Cigarette smoke extract-induced adipogenesis in Graves' orbital fibroblasts is inhibited by quercetin via reduction in oxidative stress.* Journal of Endocrinology, 2013. **216**(2): p. 145-156.
321. Davis, G.D., et al., *Radioprotective effect of DL-alpha-lipoic acid on mice skin fibroblasts.* Cell Biol Toxicol, 2009. **25**(4): p. 331-40.
322. Rovito, H.A. and J.E. Oblong, *Nicotinamide preferentially protects glycolysis in dermal fibroblasts under oxidative stress conditions.* British Journal of Dermatology, 2013. **169**(s2): p. 15-24.
323. Hutchinson, S.M., *Exploring cellular actions and interactions of SIRT1 that may counteract ageing*. 2016.

324. Chen, W.L., et al., *α-Lipoic acid regulates lipid metabolism through induction of sirtuin 1 (SIRT1) and activation of AMP-activated protein kinase.* Diabetologia, 2012. **55**(6): p. 1824-1835.
325. Roy, S., et al., *Modulation of cellular reducing equivalent homeostasis by α-lipoic acid: Mechanisms and implications for diabetes and ischemic injury.* Biochemical Pharmacology, 1997. **53**(3): p. 393-399.
326. Buss, G.D., et al., *The action of quercetin on the mitochondrial NADH to NAD(+) ratio in the isolated perfused rat liver.* Planta Med, 2005. **71**(12): p. 1118-22.
327. Solmonson, A. and R.J. DeBerardinis, *Lipoic acid metabolism and mitochondrial redox regulation.* J Biol Chem, 2018. **293**(20): p. 7522-7530.
328. Suchankova, G., et al., *Concurrent regulation of AMP-activated protein kinase and SIRT1 in mammalian cells.* Biochem Biophys Res Commun, 2009. **378**(4): p. 836-41.
329. Braganhol, E., et al., *Ecto-5'-nucleotidase/CD73 inhibition by quercetin in the human U138MG glioma cell line.* Biochimica et Biophysica Acta (BBA) - General Subjects, 2007. **1770**(9): p. 1352-1359.
330. Drew, Y., et al., *Therapeutic Potential of Poly(ADP-ribose) Polymerase Inhibitor AG014699 in Human Cancers With Mutated or Methylated BRCA1 or BRCA2.* JNCI: Journal of the National Cancer Institute, 2010. **103**(4): p. 334-346.
331. Altman, S.A., et al., *tert.-Butyl hydroperoxide-mediated DNA base damage in cultured mammalian cells.* Mutation Research/Fundamental and Molecular Mechanisms of Mutagenesis, 1994. **306**(1): p. 35-44.
332. Klaidman, L.K., et al., *Nicotinamide as a precursor for NAD+ prevents apoptosis in the mouse brain induced by tertiary-butylhydroperoxide.* Neuroscience Letters, 1996. **206**(1): p. 5-8.
333. Jin, X., et al., *Amelioration of particulate matter-induced oxidative damage by vitamin c and quercetin in human bronchial epithelial cells.* Chemosphere, 2016. **144**: p. 459-66.
334. Ungvari, Z., et al., *Resveratrol attenuates mitochondrial oxidative stress in coronary arterial endothelial cells.* Am J Physiol Heart Circ Physiol, 2009. **297**(5): p. H1876-81.
335. Goralska, M., et al., *Alpha lipoic acid changes iron uptake and storage in lens epithelial cells.* Exp Eye Res, 2003. **76**(2): p. 241-8.
336. Sánchez-Marzo, N., et al., *Antioxidant and Photoprotective Activity of Apigenin and its Potassium Salt Derivative in Human Keratinocytes and Absorption in Caco-2 Cell Monolayers.* Int J Mol Sci, 2019. **20**(9).
337. Kwak, J.Y., et al., *Nicotinamide exerts antioxidative effects on senescent cells.* Mol Cells, 2015. **38**(3): p. 229-35.
338. Chen, B.H., et al., *Pretreated quercetin protects gerbil hippocampal CA1 pyramidal neurons from transient cerebral ischemic injury by increasing the expression of antioxidant enzymes.* Neural Regen Res, 2017. **12**(2): p. 220-227.
339. Adedara, I.A., et al., *Quercetin Improves Neurobehavioral Performance Through Restoration of Brain Antioxidant Status and Acetylcholinesterase Activity in Manganese-Treated Rats.* Neurochem Res, 2017. **42**(4): p. 1219-1229.
340. Yang, G., et al., *Resveratrol Alleviates Rheumatoid Arthritis via Reducing ROS and Inflammation, Inhibiting MAPK Signaling Pathways, and Suppressing Angiogenesis.* J Agric Food Chem, 2018. **66**(49): p. 12953-12960.
341. Hiller, S., et al., *α-Lipoic acid protects mitochondrial enzymes and attenuates lipopolysaccharide-induced hypothermia in mice.* Free Radic Biol Med, 2014. **71**: p. 362-367.
342. Telange, D.R., et al., *Formulation and characterization of an apigenin-phospholipid phytosome (APLC) for improved solubility, in vivo bioavailability, and antioxidant potential.* Eur J Pharm Sci, 2017. **108**: p. 36-49.
343. Sidhu, A., et al., *Nicotinamide reverses behavioral impairments and provides neuroprotection in 3-nitropropionic acid induced animal model ofHuntington's disease: implication of oxidative stress- poly(ADP- ribose) polymerase pathway.* Metab Brain Dis, 2018. **33**(6): p. 1911-1921.

344. Gertz, M., et al., *Ex-527 inhibits Sirtuins by exploiting their unique NAD⁺-dependent deacetylation mechanism.* 2013. **110**(30): p. E2772-E2781.
345. Hasmann, M. and I. Schemainda, *FK866, a Highly Specific Noncompetitive Inhibitor of Nicotinamide Phosphoribosyltransferase, Represents a Novel Mechanism for Induction of Tumor Cell Apoptosis.* 2003. **63**(21): p. 7436-7442.
346. Liang, X., et al., *Measuring NAD(+) levels in mouse blood and tissue samples via a surrogate matrix approach using LC-MS/MS.* Bioanalysis, 2014. **6**(11): p. 1445-57.
347. Dietrich, L.S., et al., *Nicotinamide Mononucleotide Pyrophosphorylase Activity in Animal Tissues.* Journal of Biological Chemistry, 1966. **241**(1): p. 188-191.
348. Colombo, I., S. Lheureux, and A.M. Oza, *Rucaparib: a novel PARP inhibitor for BRCA advanced ovarian cancer.* Drug Des Devel Ther, 2018. **12**: p. 605-617.
349. Knezevic, C.E., et al., *Proteome-wide Profiling of Clinical PARP Inhibitors Reveals Compound-Specific Secondary Targets.* Cell Chem Biol, 2016. **23**(12): p. 1490-1503.
350. Qiu, X., et al., *Calorie Restriction Reduces Oxidative Stress by SIRT3-Mediated SOD2 Activation.* Cell Metabolism, 2010. **12**(6): p. 662-667.
351. Signorile, A., et al., *Mitochondrial cAMP prevents apoptosis modulating Sirt3 protein level and OPA1 processing in cardiac myoblast cells.* Biochimica et Biophysica Acta (BBA) - Molecular Cell Research, 2017. **1864**(2): p. 355-366.
352. Liu, J., et al., *SIRT3 protects hepatocytes from oxidative injury by enhancing ROS scavenging and mitochondrial integrity.* Cell Death & Disease, 2017. **8**(10): p. e3158-e3158.
353. Patel, K., et al., *Discovery of SIRT3 Inhibitors Using SAMDI Mass Spectrometry.* Journal of Biomolecular Screening, 2015. **20**(7): p. 842-848.
354. Williams, T.I., et al., *Increased levels of 4-hydroxynonenal and acrolein, neurotoxic markers of lipid peroxidation, in the brain in Mild Cognitive Impairment and early Alzheimer's disease.* Neurobiol Aging, 2006. **27**(8): p. 1094-9.
355. Gabbita, S.P., M.A. Lovell, and W.R. Markesbery, *Increased Nuclear DNA Oxidation in the Brain in Alzheimer's Disease.* 1998. **71**(5): p. 2034-2040.
356. Kim, T.S., et al., *Decreased plasma antioxidants in patients with Alzheimer's disease.* Int J Geriatr Psychiatry, 2006. **21**(4): p. 344-8.
357. del Hoyo, P., et al., *Oxidative stress in skin fibroblasts cultures from patients with Parkinson's disease.* BMC Neurol, 2010. **10**: p. 95.
358. Junn, E. and M.M. Mouradian, *Human alpha-synuclein over-expression increases intracellular reactive oxygen species levels and susceptibility to dopamine.* Neurosci Lett, 2002. **320**(3): p. 146-50.
359. Béraud, D., et al., *Microglial activation and antioxidant responses induced by the Parkinson's disease protein α-synuclein.* J Neuroimmune Pharmacol, 2013. **8**(1): p. 94-117.
360. Keaney, J.F., Jr., et al., *Obesity and systemic oxidative stress: clinical correlates of oxidative stress in the Framingham Study.* Arterioscler Thromb Vasc Biol, 2003. **23**(3): p. 434-9.
361. Karakas, M., et al., *Myeloperoxidase is associated with incident coronary heart disease independently of traditional risk factors: results from the MONICA/KORA Augsburg study.* J Intern Med, 2012. **271**(1): p. 43-50.
362. Dikalova, A.E., et al., *Therapeutic targeting of mitochondrial superoxide in hypertension.* Circ Res, 2010. **107**(1): p. 106-16.
363. Miwa, S., et al., *Decreased mTOR signalling reduces mitochondrial ROS in brain via accumulation of the telomerase protein TERT within mitochondria.* Aging (Albany NY), 2016. **8**(10): p. 2551-2567.
364. Ishii, T., et al., *Endogenous reactive oxygen species cause astrocyte defects and neuronal dysfunctions in the hippocampus: a new model for aging brain.* Aging Cell, 2017. **16**(1): p. 39-51.
365. Yuan, Z.-p., et al., *Liposomal Quercetin Efficiently Suppresses Growth of Solid Tumors in Murine Models.* 2006. **12**(10): p. 3193-3199.
366. Li, H., et al., *Enhancement of gastrointestinal absorption of quercetin by solid lipid nanoparticles.* Journal of Controlled Release, 2009. **133**(3): p. 238-244.

367. Tan, Q., et al., *Preparation and evaluation of quercetin-loaded lecithin-chitosan nanoparticles for topical delivery.* International journal of nanomedicine, 2011. **6**: p. 1621-1630.
368. Priprem, A., et al., *Anxiety and cognitive effects of quercetin liposomes in rats.* Nanomedicine: Nanotechnology, Biology and Medicine, 2008. **4**(1): p. 70-78.
369. Hirayama, J., et al., *CLOCK-mediated acetylation of BMAL1 controls circadian function.* Nature, 2007. **450**(7172): p. 1086-90.
370. Sangoram, A.M., et al., *Mammalian circadian autoregulatory loop: a timeless ortholog and mPer1 interact and negatively regulate CLOCK-BMAL1-induced transcription.* Neuron, 1998. **21**(5): p. 1101-13.
371. Sakamoto, K., et al., *Multitissue circadian expression of rat period homolog (rPer2) mRNA is governed by the mammalian circadian clock, the suprachiasmatic nucleus in the brain.* J Biol Chem, 1998. **273**(42): p. 27039-42.
372. Zheng, B., et al., *The mPer2 gene encodes a functional component of the mammalian circadian clock.* Nature, 1999. **400**(6740): p. 169-73.
373. Qian, Y.X., et al., *Associations of sleep durations and sleep-related parameters with metabolic syndrome among older Chinese adults.* Endocrine, 2019. **66**(2): p. 240-248.
374. Costa, G., E. Haus, and R. Stevens, *Shift work and cancer - Considerations on rationale, mechanisms, and epidemiology.* Scandinavian journal of work, environment & health, 2010. **36**: p. 163-79.
375. Abu Farha, R. and E. Alefishat, *Shift Work and the Risk of Cardiovascular Diseases and Metabolic Syndrome Among Jordanian Employees.* Oman medical journal, 2018. **33**(3): p. 235-242.
376. Vetter, C., et al., *Night Shift Work, Genetic Risk, and Type 2 Diabetes in the UK Biobank.* Diabetes care, 2018. **41**(4): p. 762-769.
377. Havakuk, O., et al., *Shift Work and the Risk of Coronary Artery Disease: A Cardiac Computed Tomography Angiography Study.* Cardiology, 2018. **139**(1): p. 11-16.
378. Wright, M.C., et al., *Time of day effects on the incidence of anesthetic adverse events.* Quality & safety in health care, 2006. **15**(4): p. 258-263.
379. Duffy, J.F., D.W. Rimmer, and C.A. Czeisler, *Association of intrinsic circadian period with morningness–eveningness, usual wake time, and circadian phase.* Behavioral Neuroscience, 2001. **115**(4): p. 895-899.
380. Vink, J.M., et al., *Genetic analysis of morningness and eveningness.* Chronobiol Int, 2001. **18**(5): p. 809-22.
381. Klei, L., et al., *Heritability of morningness-eveningness and self-report sleep measures in a family-based sample of 521 hutterites.* Chronobiol Int, 2005. **22**(6): p. 1041-54.
382. Hur, Y.M., *Stability of genetic influence on morningness-eveningness: a cross-sectional examination of South Korean twins from preadolescence to young adulthood.* J Sleep Res, 2007. **16**(1): p. 17-23.
383. Natale, V., A. Adan, and M. Fabbri, *Season of Birth, Gender, and Social-Cultural Effects on Sleep Timing Preferences in Humans.* Sleep, 2009. **32**(3): p. 423-426.
384. Barclay, N.L., et al., *Monozygotic twin differences in non-shared environmental factors associated with chronotype.* J Biol Rhythms, 2013. **28**(1): p. 51-61.
385. Yoon, I.Y., et al., *Age-related changes of circadian rhythms and sleep-wake cycles.* J Am Geriatr Soc, 2003. **51**(8): p. 1085-91.
386. Khapre, R.V., et al., *BMAL1-dependent regulation of the mTOR signaling pathway delays aging.* Aging, 2014. **6**(1): p. 48-57.
387. Weichhart, T., *mTOR as Regulator of Lifespan, Aging, and Cellular Senescence: A Mini-Review.* Gerontology, 2018. **64**(2): p. 127-134.
388. Fukuwatari, T. and K. Shibata, *Consideration of diurnal variations in human blood NAD and NADP concentrations.* J Nutr Sci Vitaminol (Tokyo), 2009. **55**(3): p. 279-81.
389. Balsalobre, A., et al., *Resetting of circadian time in peripheral tissues by glucocorticoid signaling.* Science, 2000. **289**(5488): p. 2344-7.

390. Hida, A., et al., *In vitro circadian period is associated with circadian/sleep preference.* Scientific Reports, 2013. **3**(1): p. 2074.
391. Bieler, J., et al., *Robust synchronization of coupled circadian and cell cycle oscillators in single mammalian cells.* Mol Syst Biol, 2014. **10**(7): p. 739.
392. Woo, K.-C., et al., *Circadian Amplitude of Cryptochrome 1 Is Modulated by mRNA Stability Regulation via Cytoplasmic hnRNP D Oscillation.* Molecular and Cellular Biology, 2010. **30**(1): p. 197.
393. Friedman, R.C., et al., *Most mammalian mRNAs are conserved targets of microRNAs.* Genome Res, 2009. **19**(1): p. 92-105.
394. Agarwal, V., et al., *Predicting effective microRNA target sites in mammalian mRNAs.* Elife, 2015. **4**.
395. Tili, E., et al., *Mutator activity induced by microRNA-155 (miR-155) links inflammation and cancer.* Proceedings of the National Academy of Sciences, 2011. **108**(12): p. 4908.
396. Yang, M., et al., *High expression of miR-21 and miR-155 predicts recurrence and unfavourable survival in non-small cell lung cancer.* European Journal of Cancer, 2013. **49**(3): p. 604-615.
397. Tang, B., et al., *MicroRNA-155-3p promotes hepatocellular carcinoma formation by suppressing FBXW7 expression.* Journal of experimental & clinical cancer research : CR, 2016. **35**(1): p. 93-93.
398. DiSano, J.A., et al., *Loss of miR-155 upregulates WEE1 in metastatic melanoma.* Melanoma Res, 2019. **29**(2): p. 216-219.
399. Li, H., et al., *MiR-155 inhibits proliferation, invasion and migration of melanoma via targeting CBL.* Eur Rev Med Pharmacol Sci, 2019. **23**(21): p. 9525-9534.
400. Olmos, Y., et al., *SirT1 regulation of antioxidant genes is dependent on the formation of a FoxO3a/PGC-1α complex.* Antioxid Redox Signal, 2013. **19**(13): p. 1507-21.
401. Tamaki, N., et al., *Resveratrol improves oxidative stress and prevents the progression of periodontitis via the activation of the Sirt1/AMPK and the Nrf2/antioxidant defense pathways in a rat periodontitis model.* Free Radic Biol Med, 2014. **75**: p. 222-9.
402. Liu, N., et al., *MiRNA-155 promotes the invasion of colorectal cancer SW-480 cells through regulating the Wnt/β-catenin.* Eur Rev Med Pharmacol Sci, 2018. **22**(1): p. 101-109.
403. Dong, Z.C., et al., *MiR-155 affects proliferation and apoptosis of bladder cancer cells by regulating GSK-3β/β-catenin pathway.* Eur Rev Med Pharmacol Sci, 2019. **23**(13): p. 5682-5690.
404. Yan, Z., et al., *miR-155 contributes to the progression of glioma by enhancing Wnt/β-catenin pathway.* Tumour Biol, 2015. **36**(7): p. 5323-31.
405. Dellinger, R.W., et al., *Repeat dose NRPT (nicotinamide riboside and pterostilbene) increases NAD(+) levels in humans safely and sustainably: a randomized, double-blind, placebo-controlled study.* NPJ aging and mechanisms of disease, 2017. **3**: p. 17-17.
406. Kraus, D., et al., *Nicotinamide N-methyltransferase knockdown protects against diet-induced obesity.* Nature, 2014. **508**(7495): p. 258-262.
407. Martens, C.R., et al., *Chronic nicotinamide riboside supplementation is well-tolerated and elevates NAD(+) in healthy middle-aged and older adults.* Nature communications, 2018. **9**(1): p. 1286-1286.
408. Conze, D., C. Brenner, and C.L. Kruger, *Safety and Metabolism of Long-term Administration of NIAGEN (Nicotinamide Riboside Chloride) in a Randomized, Double-Blind, Placebo-controlled Clinical Trial of Healthy Overweight Adults.* Scientific Reports, 2019. **9**(1): p. 9772.
409. Remie, C.M.E., et al., *Nicotinamide riboside supplementation alters body composition and skeletal muscle acetylcarnitine concentrations in healthy obese humans.* The American Journal of Clinical Nutrition, 2020. **112**(2): p. 413-426.
410. Brandauer, J., et al., *AMP-activated protein kinase regulates nicotinamide phosphoribosyl transferase expression in skeletal muscle.* J Physiol, 2013. **591**(20): p. 5207-20.

411. Cantó, C., et al., *AMPK regulates energy expenditure by modulating NAD+ metabolism and SIRT1 activity.* Nature, 2009. **458**(7241): p. 1056-1060.
412. Jeong, H.W., et al., *Berberine suppresses proinflammatory responses through AMPK activation in macrophages.* 2009. **296**(4): p. E955-E964.
413. Cai, E.P. and J.K. Lin, *Epigallocatechin gallate (EGCG) and rutin suppress the glucotoxicity through activating IRS2 and AMPK signaling in rat pancreatic beta cells.* J Agric Food Chem, 2009. **57**(20): p. 9817-27.
414. Pu, Y., et al., *Dietary Curcumin Ameliorates Aging-Related Cerebrovascular Dysfunction through the AMPK/Uncoupling Protein 2 Pathway.* Cellular Physiology and Biochemistry, 2013. **32**(5): p. 1167-1177.
415. Soetikno, V., et al., *Curcumin decreases renal triglyceride accumulation through AMPK–SREBP signaling pathway in streptozotocin-induced type 1 diabetic rats.* The Journal of Nutritional Biochemistry, 2013. **24**(5): p. 796-802.
416. Hawley, S.A., et al., *The Antidiabetic Drug Metformin Activates the AMP-Activated Protein Kinase Cascade via an Adenine Nucleotide-Independent Mechanism.* 2002. **51**(8): p. 2420-2425.
417. Meley, D., et al., *AMP-activated protein kinase and the regulation of autophagic proteolysis.* J Biol Chem, 2006. **281**(46): p. 34870-9.
418. Gardell, S.J., et al., *Boosting NAD+ with a small molecule that activates NAMPT.* Nature Communications, 2019. **10**(1): p. 3241.
419. Skokowa, J., et al., *NAMPT is essential for the G-CSF-induced myeloid differentiation via a NAD(+)-sirtuin-1-dependent pathway.* Nat Med, 2009. **15**(2): p. 151-8.
420. Xiong, X., et al., *NAMPT overexpression alleviates alcohol-induced hepatic steatosis in mice.* PLoS One, 2019. **14**(2): p. e0212523.
421. Revollo, J.R., A.A. Grimm, and S. Imai, *The NAD biosynthesis pathway mediated by nicotinamide phosphoribosyltransferase regulates Sir2 activity in mammalian cells.* J Biol Chem, 2004. **279**(49): p. 50754-63.
422. Haffner, C.D., et al., *Discovery, Synthesis, and Biological Evaluation of Thiazoloquin(az)olin(on)es as Potent CD38 Inhibitors.* Journal of Medicinal Chemistry, 2015. **58**(8): p. 3548-3571.
423. Zhang, Z.-F., et al., *Troxerutin improves hepatic lipid homeostasis by restoring NAD+-depletion-mediated dysfunction of lipin 1 signaling in high-fat diet-treated mice.* Biochemical Pharmacology, 2014. **91**(1): p. 74-86.
424. Cerna, D., et al., *Inhibition of nicotinamide phosphoribosyltransferase (NAMPT) activity by small molecule GMX1778 regulates reactive oxygen species (ROS)-mediated cytotoxicity in a p53- and nicotinic acid phosphoribosyltransferase1 (NAPRT1)-dependent manner.* J Biol Chem, 2012. **287**(26): p. 22408-17.
425. Kim, H.-J., et al., *Augmentation of cellular NAD+ by NQO1 enzymatic action improves age-related hearing impairment.* 2019. **18**(5): p. e13016.
426. Oh, G.S., et al., *Pharmacological activation of NQO1 increases NAD^+ levels and attenuates cisplatin-mediated acute kidney injury in mice.* Kidney Int, 2014. **85**(3): p. 547-60.
427. Elangovan, S. and T.C. Hsieh, *Control of cellular redox status and upregulation of quinone reductase NQO1 via Nrf2 activation by alpha-lipoic acid in human leukemia HL-60 cells.* Int J Oncol, 2008. **33**(4): p. 833-8.
428. Sang, Y., et al., *Apigenin exhibits protective effects in a mouse model of d-galactose-induced aging via activating the Nrf2 pathway.* Food Funct, 2017. **8**(6): p. 2331-2340.
429. Wu, J., et al., *Neuroprotection by curcumin in ischemic brain injury involves the Akt/Nrf2 pathway.* PLoS One, 2013. **8**(3): p. e59843.
430. Dehn, D.L., et al., *Biochemical, cytotoxic, and genotoxic effects of ES936, a mechanism-based inhibitor of NAD(P)H:quinone oxidoreductase 1, in cellular systems.* Mol Pharmacol, 2003. **64**(3): p. 714-20.

431. Nolan, K.A., et al., *Pharmacological inhibitors of NAD(P)H quinone oxidoreductase, NQO1: Structure/activity relationships and functional activity in tumour cells.* Biochemical Pharmacology, 2010. **80**(7): p. 977-981.
432. Fan, R., et al., *Overexpression of NRK1 ameliorates diet- and age-induced hepatic steatosis and insulin resistance.* Biochemical and Biophysical Research Communications, 2018. **500**(2): p. 476-483.
433. Lee, W.J., et al., *α-Lipoic acid increases insulin sensitivity by activating AMPK in skeletal muscle.* Biochemical and Biophysical Research Communications, 2005. **332**(3): p. 885-891.
434. Hwang, D., et al., *Oxyresveratrol stimulates mucin production in an NAD+-dependent manner in human intestinal goblet cells.* Food and Chemical Toxicology, 2018. **118**: p. 880-888.
435. Zhang, T., et al., *Regulation of poly(ADP-ribose) polymerase-1-dependent gene expression through promoter-directed recruitment of a nuclear NAD+ synthase.* J Biol Chem, 2012. **287**(15): p. 12405-16.
436. Gomes, A.P., et al., *Declining NAD(+) induces a pseudohypoxic state disrupting nuclear-mitochondrial communication during aging.* Cell, 2013. **155**(7): p. 1624-38.
437. Berger, F., et al., *Subcellular Compartmentation and Differential Catalytic Properties of the Three Human Nicotinamide Mononucleotide Adenylyltransferase Isoforms.* The Journal of biological chemistry, 2005. **280**: p. 36334-41.
438. Sorci, L., et al., *Initial-Rate Kinetics of Human NMN-Adenylyltransferases: Substrate and Metal Ion Specificity, Inhibition by Products and Multisubstrate Analogues, and Isozyme Contributions to NAD + Biosynthesis †.* Biochemistry, 2007. **46**: p. 4912-22.
439. Komatsu, M., et al., *NNMT activation can contribute to the development of fatty liver disease by modulating the NAD (+) metabolism.* Scientific reports, 2018. **8**(1): p. 8637-8637.
440. Kannt, A., et al., *A small molecule inhibitor of Nicotinamide N-methyltransferase for the treatment of metabolic disorders.* Scientific Reports, 2018. **8**(1): p. 3660.
441. Aksoy, P., et al., *Regulation of intracellular levels of NAD: a novel role for CD38.* Biochem Biophys Res Commun, 2006. **345**(4): p. 1386-92.
442. Braidy, N., et al., *Mapping NAD+ metabolism in the brain of ageing Wistar rats: potential targets for influencing brain senescence.* Biogerontology, 2014. **15**(2): p. 177-198.
443. Hara, N., et al., *Quantitative analysis of the effects of nicotinamide phosphoribosyltransferase induction on the rates of NAD+ synthesis and breakdown in mammalian cells using stable isotope-labeling combined with mass spectrometry.* PLoS One, 2019. **14**(3): p. e0214000.
444. Chatterjee, S., et al., *CD38-NAD(+)Axis Regulates Immunotherapeutic Anti-Tumor T Cell Response.* Cell Metab, 2018. **27**(1): p. 85-100.e8.
445. Hu, Y., et al., *Overexpression of CD38 Decreases Cellular NAD Levels and Alters the Expression of Proteins Involved in Energy Metabolism and Antioxidant Defense.* Journal of Proteome Research, 2014. **13**(2): p. 786-795.
446. Dong, W., et al., *Curcumin plays neuroprotective roles against traumatic brain injury partly via Nrf2 signaling.* Toxicology and Applied Pharmacology, 2018. **346**: p. 28-36.
447. Liu, L., et al., *Quantitative Analysis of NAD Synthesis-Breakdown Fluxes.* Cell metabolism, 2018. **27**(5): p. 1067-1080.e5.
448. Sahar, S., et al., *Altered behavioral and metabolic circadian rhythms in mice with disrupted NAD+ oscillation.* Aging, 2011. **3**(8): p. 794-802.
449. Peek, C.B., et al., *Circadian clock NAD+ cycle drives mitochondrial oxidative metabolism in mice.* Science (New York, N.Y.), 2013. **342**(6158): p. 1243417-1243417.
450. Sato, S., et al., *Circadian Reprogramming in the Liver Identifies Metabolic Pathways of Aging.* Cell, 2017. **170**(4): p. 664-677.e11.
451. Xia, D., et al., *Alpha lipoic acid inhibits oxidative stress-induced apoptosis by modulating of Nrf2 signalling pathway after traumatic brain injury.* J Cell Mol Med, 2019. **23**(6): p. 4088-4096.
452. Wang, Y., et al., *alpha-Lipoic acid increases energy expenditure by enhancing adenosine monophosphate-activated protein kinase-peroxisome proliferator-activated receptor-*

gamma coactivator-1alpha signaling in the skeletal muscle of aged mice. Metabolism: clinical and experimental, 2010. **59**(7): p. 967-976.
453. Rochette, L., et al., *Alpha-lipoic acid: molecular mechanisms and therapeutic potential in diabetes.* Canadian Journal of Physiology and Pharmacology, 2015. **93**(12): p. 1021-1027.
454. Farr, S.A., et al., *Effect of alpha-lipoic acid on memory, oxidation, and lifespan in SAMP8 mice.* J Alzheimers Dis, 2012. **32**(2): p. 447-55.
455. Brown, M.K., J.L. Evans, and Y. Luo, *Beneficial effects of natural antioxidants EGCG and alpha-lipoic acid on life span and age-dependent behavioral declines in Caenorhabditis elegans.* Pharmacol Biochem Behav, 2006. **85**(3): p. 620-8.
456. Ogura, Y., et al., *CD38 inhibition by apigenin ameliorates mitochondrial oxidative stress through restoration of the intracellular NAD(+)/NADH ratio and Sirt3 activity in renal tubular cells in diabetic rats.* Aging (Albany NY), 2020. **12**(12): p. 11325-11336.
457. Mattila, P., J. Astola, and J. Kumpulainen, *Determination of Flavonoids in Plant Material by HPLC with Diode-Array and Electro-Array Detections.* Journal of Agricultural and Food Chemistry, 2000. **48**(12): p. 5834-5841.
458. Justesen, U. and P. Knuthsen, *Composition of flavonoids in fresh herbs and calculation of flavonoid intake by use of herbs in traditional Danish dishes.* Food Chemistry, 2001. **73**(2): p. 245-250.
459. Siddique, Y., et al., *Apigenin Extends Lifespan And Improves The Activity Pattern Of Parkinson's Disease Model Flies.* Journal of Neuropathology and Experimental Neurology, 2014. **73**: p. 598.
460. Oyebode, O.T., et al., *Apigenin ameliorates D-galactose-induced lifespan shortening effects via antioxidative activity and inhibition of mitochondrial-dependent apoptosis in Drosophila melanogaster.* Journal of Functional Foods, 2020. **69**: p. 103957.
461. Seo, S., et al., *Rutin Increases Muscle Mitochondrial Biogenesis with AMPK Activation in High-Fat Diet-Induced Obese Rats.* Nutrients, 2015. **7**(9): p. 8152-69.
462. Wu, C.H., et al., *Rutin inhibits oleic acid induced lipid accumulation via reducing lipogenesis and oxidative stress in hepatocarcinoma cells.* J Food Sci, 2011. **76**(2): p. T65-72.
463. Park, C., et al., *Rutin content in food products processed from groats, leaves, and flowers of buckwheat.* Fagopyrum, 2000. **17**: p. 63-66.
464. Chattopadhyay, D., et al., *Hormetic efficacy of rutin to promote longevity in Drosophila melanogaster.* Biogerontology, 2017. **18**(3): p. 397-411.
465. Sun, K., et al., *Anti-Ageing Effect of Physalis alkekengi Ethyl Acetate Layer on a d-galactose-Induced Mouse Model through the Reduction of Cellular Senescence and Oxidative Stress.* Int J Mol Sci, 2020. **21**(5).
466. Li, L., et al., *Overexpression of SIRT1 Induced by Resveratrol and Inhibitor of miR-204 Suppresses Activation and Proliferation of Microglia.* J Mol Neurosci, 2015. **56**(4): p. 858-867.
467. Chen, H., et al., *Quality Assessment of Japanese Knotweed (Fallopia japonica) Grown on Prince Edward Island as a Source of Resveratrol.* Journal of Agricultural and Food Chemistry, 2013. **61**(26): p. 6383-6392.
468. Zamora-Ros, R., et al., *Concentrations of resveratrol and derivatives in foods and estimation of dietary intake in a Spanish population: European Prospective Investigation into Cancer and Nutrition (EPIC)-Spain cohort.* British Journal of Nutrition, 2008. **100**(1): p. 188-196.
469. Li, X.M., et al., *Resveratrol pretreatment attenuates the isoflurane-induced cognitive impairment through its anti-inflammation and -apoptosis actions in aged mice.* J Mol Neurosci, 2014. **52**(2): p. 286-93.
470. Kavutcu, M. and M.F. Melzig, *In vitro effects of selected flavonoids on the 5'-nucleotidase activity.* Die Pharmazie, 1999. **54**(6): p. 457-459.
471. Giuffrida, D., et al., *Initial investigation on some chemical constituents of capers (Capparis spinosa L.) from the island of Salina.* Ital J food Sci, 2002. **14**: p. 25-33.
472. Trichopoulou, A., et al., *Nutritional composition and flavonoid content of edible wild greens and green pies: a potential rich source of antioxidant nutrients in the Mediterranean diet.* Food Chemistry, 2000. **70**(3): p. 319-323.

473. Sabogal-Guáqueta, A.M., et al., *The flavonoid quercetin ameliorates Alzheimer's disease pathology and protects cognitive and emotional function in aged triple transgenic Alzheimer's disease model mice.* Neuropharmacology, 2015. **93**: p. 134-145.
474. Kampkötter, A., et al., *Increase of stress resistance and lifespan of Caenorhabditis elegans by quercetin.* Comparative Biochemistry and Physiology Part B: Biochemistry and Molecular Biology, 2008. **149**(2): p. 314-323.
475. Braidy, N., et al., *Neuroprotective effects of naturally occurring polyphenols on quinolinic acid-induced excitotoxicity in human neurons.* The FEBS Journal, 2010. **277**(2): p. 368-382.
476. Prayonga, P., N. Weerapreeyakul, and B. Sripanidkulchai, *Validation of Isocratic Eluting and Stepwise Flow Rate Gradient for HPLC Determination of Catechins, Gallic Acid and Caffeine in Tea.* ScienceAsia, 2007. **33**: p. 113-117.
477. Sakakibara, H., et al., *Simultaneous Determination of All Polyphenols in Vegetables, Fruits, and Teas.* Journal of Agricultural and Food Chemistry, 2003. **51**(3): p. 571-581.
478. Xiong, L.-G., et al., *Epigallocatechin-3-gallate promotes healthy lifespan through mitohormesis during early-to-mid adulthood in Caenorhabditis elegans.* Redox biology, 2018. **14**: p. 305-315.
479. Niu, Y., et al., *The phytochemical, EGCG, extends lifespan by reducing liver and kidney function damage and improving age-associated inflammation and oxidative stress in healthy rats.* Aging Cell, 2013. **12**(6): p. 1041-9.
480. Dutta, B.J.J.o.M.P.S., *Study of secondary metabolite constituents and curcumin contents of six different species of genus Curcuma.* 2015. **3**: p. 116-119.
481. Kitani, K., T. Yokozawa, and T. Osawa, *Interventions in aging and age-associated pathologies by means of nutritional approaches.* Ann N Y Acad Sci, 2004. **1019**: p. 424-6.
482. Bala, K., B.C. Tripathy, and D. Sharma, *Neuroprotective and anti-ageing effects of curcumin in aged rat brain regions.* Biogerontology, 2006. **7**(2): p. 81-9.
483. Liou, C.J., et al., *Fisetin Protects Against Hepatic Steatosis Through Regulation of the Sirt1/AMPK and Fatty Acid β-Oxidation Signaling Pathway in High-Fat Diet-Induced Obese Mice.* Cell Physiol Biochem, 2018. **49**(5): p. 1870-1884.
484. Yang, W., et al., *Fisetin improves lead-induced neuroinflammation, apoptosis and synaptic dysfunction in mice associated with the AMPK/SIRT1 and autophagy pathway.* Food and Chemical Toxicology, 2019. **134**: p. 110824.
485. Arai, Y., et al., *Dietary intakes of flavonols, flavones and isoflavones by Japanese women and the inverse correlation between quercetin intake and plasma LDL cholesterol concentration.* J Nutr, 2000. **130**(9): p. 2243-50.
486. Yousefzadeh, M.J., et al., *Fisetin is a senotherapeutic that extends health and lifespan.* EBioMedicine, 2018. **36**: p. 18-28.
487. Currais, A., et al., *Fisetin Reduces the Impact of Aging on Behavior and Physiology in the Rapidly Aging SAMP8 Mouse.* J Gerontol A Biol Sci Med Sci, 2018. **73**(3): p. 299-307.
488. Zhu, Y., et al., *Combination of luteolin and lycopene effectively protect against the "two-hit" in NAFLD through Sirt1/AMPK signal pathway.* Life Sciences, 2020. **256**: p. 117990.
489. Lin, L.-Z., et al., *Identification and quantification of flavonoids of Mexican oregano (Lippia graveolens) by LC-DAD-ESI/MS analysis.* Journal of Food Composition and Analysis, 2007. **20**(5): p. 361-369.
490. Jang, S., R.N. Dilger, and R.W. Johnson, *Luteolin inhibits microglia and alters hippocampal-dependent spatial working memory in aged mice.* The Journal of nutrition, 2010. **140**(10): p. 1892-1898.
491. Burton, M.D., et al., *Dietary Luteolin Reduces Proinflammatory Microglia in the Brain of Senescent Mice.* Rejuvenation research, 2016. **19**(4): p. 286-292.
492. Gradolatto, A., et al., *Pharmacokinetics and metabolism of apigenin in female and male rats after a single oral administration.* Drug Metab Dispos, 2005. **33**(1): p. 49-54.
493. Biellmann, J.F., et al., *Structure of lactate dehydrogenase inhibitor generated from coenzyme.* Biochemistry, 1979. **18**(7): p. 1212-7.

494. Clement, J., et al., *The Plasma NAD(+) Metabolome Is Dysregulated in "Normal" Aging.* Rejuvenation Res, 2019. **22**(2): p. 121-130.
495. Seyedsadjadi, N., et al., *High protein intake is associated with low plasma NAD+ levels in a healthy human cohort.* PLOS ONE, 2018. **13**: p. e0201968.
496. Zhu, Y., et al., *Subcellular compartmentalization of NAD+ and its role in cancer: A sereNADe of metabolic melodies.* Pharmacology & Therapeutics, 2019. **200**: p. 27-41.
497. Audrito, V., et al., *NAD-Biosynthetic and Consuming Enzymes as Central Players of Metabolic Regulation of Innate and Adaptive Immune Responses in Cancer.* Frontiers in immunology, 2019. **10**: p. 1720-1720.
498. Chu, H., et al., *Sirtuin1 Protects against Systemic Sclerosis–related Pulmonary Fibrosis by Decreasing Proinflammatory and Profibrotic Processes.* 2018. **58**(1): p. 28-39.
499. Zhu, X., et al., *Sirt1 ameliorates systemic sclerosis by targeting the mTOR pathway.* J Dermatol Sci, 2017. **87**(2): p. 149-158.
500. Wei, J., et al., *The Histone Deacetylase Sirtuin 1 Is Reduced in Systemic Sclerosis and Abrogates Fibrotic Responses by Targeting Transforming Growth Factor β Signaling.* 2015. **67**(5): p. 1323-1334.
501. Zerr, P., et al., *Sirt1 regulates canonical TGF-β signalling to control fibroblast activation and tissue fibrosis.* Ann Rheum Dis, 2016. **75**(1): p. 226-33.
502. Zhang, Y., et al., *Poly(ADP-ribose) polymerase-1 regulates fibroblast activation in systemic sclerosis.* Ann Rheum Dis, 2018. **77**(5): p. 744-751.
503. Murgia, F., et al., *Metabolomic profile of systemic sclerosis patients.* Sci Rep, 2018. **8**(1): p. 7626.
504. Kang, Y.P., et al., *Metabolic Profiling Regarding Pathogenesis of Idiopathic Pulmonary Fibrosis.* J Proteome Res, 2016. **15**(5): p. 1717-24.
505. Lafyatis, R., *Transforming growth factor beta--at the centre of systemic sclerosis.* Nat Rev Rheumatol, 2014. **10**(12): p. 706-19.
506. Clem, B., et al., *Small-molecule inhibition of 6-phosphofructo-2-kinase activity suppresses glycolytic flux and tumor growth.* Mol Cancer Ther, 2008. **7**(1): p. 110-20.
507. Hirschhaeuser, F., U.G. Sattler, and W. Mueller-Klieser, *Lactate: a metabolic key player in cancer.* Cancer Res, 2011. **71**(22): p. 6921-5.
508. Xu, M., et al., *Rapamycin inhibits the proliferation of SW1990 pancreatic cancer cell.* Eur Rev Med Pharmacol Sci, 2015. **19**(16): p. 3072-9.
509. Comins, C., et al., *Synergistic antitumour effects of rapamycin and oncolytic reovirus.* Cancer Gene Ther, 2018. **25**(5-6): p. 148-160.
510. Burleigh, A., N. Kanigsberg, and J.M. Lam, *Topical rapamycin (sirolimus) for the treatment of uncomplicated tufted angiomas in two children and review of the literature.* Pediatr Dermatol, 2018. **35**(5): p. e286-e290.
511. Edinger, A., et al., *Differential Effects of Rapamycin on Mammalian Target of Rapamycin Signaling Functions in Mammalian Cells.* Cancer research, 2004. **63**: p. 8451-60.
512. Wang, Y., P.S. Fan, and B. Kahaleh, *Association between enhanced type I collagen expression and epigenetic repression of the FLI1 gene in scleroderma fibroblasts.* Arthritis Rheum, 2006. **54**(7): p. 2271-9.
513. Srivastava, S.P., et al., *SIRT3 deficiency leads to induction of abnormal glycolysis in diabetic kidney with fibrosis.* Cell Death Dis, 2018. **9**(10): p. 997.
514. Ding, H., et al., *Inhibiting aerobic glycolysis suppresses renal interstitial fibroblast activation and renal fibrosis.* Am J Physiol Renal Physiol, 2017. **313**(3): p. F561-f575.
515. Cho, S.J., et al., *GLUT1-dependent glycolysis regulates exacerbation of fibrosis via AIM2 inflammasome activation.* Thorax, 2020. **75**(3): p. 227-236.
516. Abboud, G., et al., *Inhibition of Glycolysis Reduces Disease Severity in an Autoimmune Model of Rheumatoid Arthritis.* Front Immunol, 2018. **9**: p. 1973.
517. Yin, Y., et al., *Normalization of CD4+ T cell metabolism reverses lupus.* Sci Transl Med, 2015. **7**(274): p. 274ra18.

518. Shi, L., et al., *HIF1alpha-dependent glycolytic pathway orchestrates a metabolic checkpoint for the differentiation of TH17 and Treg cells.* The Journal of experimental medicine, 2011. **208**: p. 1367-76.
519. Kulkarni, Y.M., et al., *A proteomics approach to identifying key protein targets involved in VEGF inhibitor mediated attenuation of bleomycin-induced pulmonary fibrosis.* Proteomics, 2016. **16**(1): p. 33-46.
520. Fukunaga, S., et al., *Integrative analyses of miRNA and proteomics identify potential biological pathways associated with onset of pulmonary fibrosis in the bleomycin rat model.* Toxicol Appl Pharmacol, 2015. **286**(3): p. 188-97.
521. Gouda, M.M., et al., *Proteomics Analysis Revealed the Importance of Inflammation-Mediated Downstream Pathways and the Protective Role of Curcumin in Bleomycin-Induced Pulmonary Fibrosis in C57BL/6 Mice.* J Proteome Res, 2020. **19**(8): p. 2950-2963.
522. Guillotin, D., et al., *Transcriptome analysis of IPF fibroblastic foci identifies key pathways involved in fibrogenesis.* Thorax, 2020.
523. Cui, H., et al., *Inhibition of Glutaminase 1 Attenuates Experimental Pulmonary Fibrosis.* Am J Respir Cell Mol Biol, 2019. **61**(4): p. 492-500.
524. Kono, M., et al., *Glutaminase 1 Inhibition Reduces Glycolysis and Ameliorates Lupus-like Disease in MRL/lpr Mice and Experimental Autoimmune Encephalomyelitis.* Arthritis Rheumatol, 2019. **71**(11): p. 1869-1878.
525. Perrotta, P., et al., *Partial Inhibition of Glycolysis Reduces Atherogenesis Independent of Intraplaque Neovascularization in Mice.* Arterioscler Thromb Vasc Biol, 2020. **40**(5): p. 1168-1181.
526. Carvalho, D., et al., *Structural evidence of quercetin multi-target bioactivity: A reverse virtual screening strategy.* European Journal of Pharmaceutical Sciences, 2017. **106**: p. 393-403.
527. Arango, D., et al., *Molecular basis for the action of a dietary flavonoid revealed by the comprehensive identification of apigenin human targets.* 2013. **110**(24): p. E2153-E2162.
528. Nouri, Z., et al., *Targeting Multiple Signaling Pathways in Cancer: The Rutin Therapeutic Approach.* 2020. **12**(8): p. 2276.
529. Kulkarni, S.S. and C. Cantó, *The molecular targets of resveratrol.* Biochimica et Biophysica Acta (BBA) - Molecular Basis of Disease, 2015. **1852**(6): p. 1114-1123.